Identification and functional characterization of relaxin-type and pedal peptide/orcokinin-type neuropeptides in the starfish *Asterias rubens*

Ming Lin

Submitted in partial fulfillment of the requirements of the Degree of Doctor of Philosophy

July 2017

Statement of originality

I, Ming Lin, confirm that the research included within this thesis is my own work or that where it has been carried out in collaboration with, or supported by others, that this is duly acknowledged below and my contribution indicated. Previously published material is also acknowledged below.

I attest that I have exercised reasonable care to ensure that the work is original, and does not to the best of my knowledge break any UK law, infringe any third party's copyright or other Intellectual Property Right, or contain any confidential material.

I accept that the College has the right to use plagiarism detection software to check the electronic version of the thesis.

I confirm that this thesis has not been previously submitted for the award of a degree by this or any other university.

Signature: Ming Lin

Date: September 2017

Details of collaboration and publications:

(1) Collaborations:

(1) Professor Masatoshi Mita

Department of Biology, Faculty of Education, Tokyo Gakugei University, Tokyo, Japan

Collaboration with Professor Masatoshi Mita for the comparison of the effects of synthetic AruRGP and PpeRGP on *A. rubens* ovarian fragments, as reported in chapter 2.

(2) Dr. Alexandra M. Jones and Dr. Cleidiane G. Zampronio

School of Life Sciences and Proteomics Research Technology Platform, University of Warwick, Coventry, UK

Collaboration with Dr. Alexandra M. Jones and Dr. Cleidiane G. Zampronio for mass spectrometric confirmation of neuropeptides (AruRGP, ArPPLN1s and ArPPLN2s) in extracts of *A. rubens* radial nerve cords, as reported in chapters 2, 3 and 4, respectively.

(2) Publications:

Lin M, Mita M, Egertova M, Zampronio CG, Jones AM, Elphick MR. 2017. Cellular localization of relaxin-like gonad-stimulating peptide expression in *Asterias rubens*: new insights into neurohormonal control of spawning in starfish. *J Comp Neurol* 525(7):1599-1617.

Lin M, Egertova M, Zampronio CG, Jones AM, Elphick MR. 2017. Pedal peptide/orcokinin-type neuropeptide signaling in a deuterostome: the anatomy and pharmacology of starfish myorelaxant peptide in *Asterias rubens*. *J Comp Neurol*.

Kim CH, Kim EJ, Go HJ, Oh HY, **Lin M**, Elphick MR, Park NG. 2016. Identification of a novel starfish neuropeptide that acts as a muscle relaxant. *J Neurochem* 137(1):33-45.

Abstract

Neuropeptides are neuronal signaling molecules that regulate many physiological and behavioural processes in vertebrates and invertebrates. Investigation of neuropeptide signaling in echinoderms (e.g. starfish) can provide insights into the evolution of neuropeptide systems because as deuterostomian invertebrates they occupy an "intermediate" phylogenetic position between vertebrates and protostomian invertebrates. Recent analysis of neural transcriptome data from the starfish *Asterias rubens* has identified 40 transcripts encoding neuropeptide precursors. Here the expression and function of neuropeptides derived from four of these precursors was investigated: relaxin-like gonad-stimulating peptide precursor (AruRGPP), relaxin-like peptide precursor 2 (AruRLPP2), pedal peptide-like neuropeptide precursors 1 and 2 (ArPPLNP1 and ArPPLNP2).

AruRGP induces spawning of ovarian fragments from *A. rubens*. Analysis of the expression of AruRGPP in *A. rubens* using mRNA *in situ* hybridization revealed expression by cells in the radial nerve cords, circumoral nerve ring and tube feet. Furthermore, a band of AruRGPP-expressing cells was also identified in the body wall epithelium lining the cavity that surrounds the sensory terminal tentacle and optic cushion at the tips of the arms. Discovery of these cells is important because they are candidate physiological mediators for hormonal control of starfish spawning in response to environmental cues. Interestingly, AruRLPP2 is also expressed in the same region of the arm tip as AruRGPP but the physiological role(s) of AruRLP2 is not yet known.

Analysis of the expression of ArPPLNP1 and ArPPLNP2 using mRNA *in situ* hybridization revealed a widespread pattern of expression in *A. rubens*. Furthermore, immunohistochemical localization of peptides derived from these precursors revealed

immunostaining in neuronal processes innervating muscles. Consistent with this pattern of expression, peptides derived from ArPPLNP1 and ArPPLNP2 act as muscle relaxants in starfish. Interestingly, this contrasts with previous findings from protostomian invertebrates, where pedal peptide/orcokinin-type neuropeptides act as muscle contractants.

Table of contents

Table of Figures

Abbreviations

ACh	acetylcholine
ADO	adambulacral ossicle
AM	apical muscle
Am	ampulla
AMO	ambulacral ossicle
ArPPLN	*Asterias rubens* pedal peptide-like neuropeptide
ArPPLNP	*Asterias rubens* pedal peptide-like neuropeptide precursor
AruRGP	*Asterias rubens* relaxin-like gonad-stimulating peptide
AruRGPP	*Asterias rubens* relaxin-like gonad-stimulating peptide precursor
AruRLP2	*Asterias rubens* relaxin-like peptide 2
AruRLPP2	*Asterias rubens* relaxin-like peptide precursor 2
ASW	artificial seawater
BNP	basiepithelial nerve plexus
BNR	basal nerve ring
BW	body wall
CBNP	coelomic basiepithelial nerve plexus
CCAP	crustacean-cardioactive peptide
CE	coelomic epithelium
CMLNP	circular muscle layer nerve plexus
CO	carinal ossicle
CONR	circumoral nerve ring
CPD	carboxypeptidase D
CPE	carboxypeptidase E
CS	cardiac stomach
CT	collagenous tissue
CuL	cuticular layer
DAB	diaminobenzidine
DIG	digoxygenin
DTT	dithiothreitol
Ec	ectoneural region
ELISA	Enzyme-Linked ImmunoSorbent Assays
Ep	epithelium
ER	endoplasmic reticulum
Es	esophagus
GnRH	gonadotropin- releasing hormone
GPCRs	G protein-coupled receptors
GSS	gonad-stimulating substance
Hy	hyponeural region
IGF	insulin-like growth factor
INSL	insulin-like
LL	lateral lappet
LSM	longitudinal supra-ambulacral muscle
Lu	lumen
MCH	melanin-concentrating hormone
ML	muscle layer
MO	marginal ossicles
Mo	mouth

Mu	mucosa
NPS	neuropeptide-S
NPY	neuropeptide-Y
OC	optic cushion
OD	optical density
OHR	oral hemal ring
OK	orcokinin
ORF	open read frame
Os	ossicle
PAM	peptidyl-alpha-amidating monooxygenase
Pa	papulae
PBS	Phosphate-buffered saline
PBST	PBS/0.1% Tween-20
PC	pyloric caeca
PC1	prohormone convertase 1
PD	pyloric duct
PDF	pigment dispersing hormone
Pe	pedicellariae
PM	peristomial membrane
PP	Pedal peptide
PS	pyloric stomach
RC	rectal caeca
Re	rectum
RHS	radial hemal strand
RLN	relaxin
RNC	radial nerve cord
RO	reticular ossicles
RSP	regulated secretory pathway
SMP	starfish myorelaxant peptide
SNP	sub-epithelial nerve plexus
Sp	spine
SpPPLNP	*Strongylocentrotus purpuratus* pedal peptide-like neuropeptide
Su	sucker
TB	Tiedemann's body
TF	tube feet
TIM	transverse infra-ambulacral muscle
TM	transmembrane
TRH	thyrotropin releasing hormone
TSM	transverse supra-ambulacral muscle
TT	terminal tentacle
VM	visceral muscle

1 General Introduction

1.1 What are neuropeptides?

Neuropeptides are small polypeptides ranging from 3 to 100 amino acid residues (Malenka, 2010) that are synthesized by the nervous system, endocrine system and gut, and are involved in regulation of many types of physiological and behavioral processes in vertebrates and invertebrates (Fricker, 2012). Bioactive neuropeptides are produced from their corresponding precursor proteins after a series of modifications. Neuropeptides are one of the largest groups of neurotransmitters and they mediate communication between neurons and other cells by binding to specific receptors (Fricker, 2012), which are typically G protein-coupled receptors (Gomes et al., 2013).

1.1.1 Neuropeptide precursor structural characteristics

A bioactive neuropeptide is not generated directly from mRNA but is derived from a larger specific precursor protein (Figure 1.1). Neuropeptide precursors contain a 20-30 amino acid residue N-terminal signal peptide, which is followed by one or more copies of physiologically active neuropeptides (Sossin et al., 1989). The signal peptides are comprised of three structurally dissimilar regions: N-terminal region (n-region), central hydrophobic region (h-region) and C-terminal region (c-region) (von Heijne, 1985). The n-region is variable both in length and amino acid composition, but it usually has a positive net charge, which is thought to interact with the "docking protein" catalyzed release of the "signal recognition particle (SRP)" induced block (Hall et al., 1983; Vlasuk et al., 1983; von Heijne, 1985). The h-region is a seven or eight-residue long sequence in the "minimal" signal peptide, sandwiched between the n-region and c-region, and is thought to be the target site of the SRP (von Heijne, 1985). The c-region

is consistent in length, 5 or 6 amino acid residues, and is a more polar region that determines the cleavage site (von Heijne, 1984). Online software is available now to predict the signal peptides of neuropeptide precursors (SignalP 4.1 Server, http://www.cbs.dtu.dk/services/SignalP/).

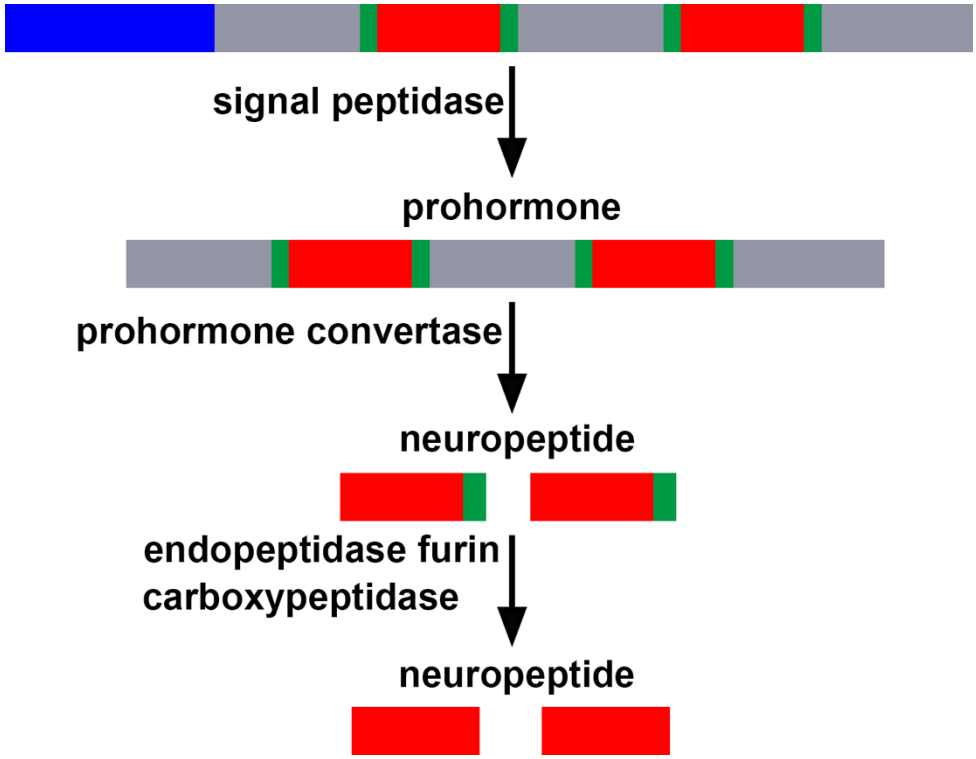

Figure 1.1 Processing of a neuropeptide precursor.
A signal peptidase cleaves the signal peptide from a preprohormone to generate a prohormone. Prohormone convertase cleaves at dibasic/monobasic cleavage sites to produce a peptide hormone (neuropeptide). Endopeptidase furin and carboxypeptidase cleave dibasic/monobasic cleavage sites, giving rise to a bioactive peptide hormone. The signal peptide is represented in blue, neuropeptides are represented in red and dibasic/monobasic cleavage sites are represented in green. Figure is based on Fricker (2012) and Semmens (2015).

The cleavage sites are usually composed of dibasic/monobasic amino acids lysine (K) and/or arginine (R), which are recognized by prohormone convertase cleaving enzymes (Rholam et al., 1995; Steiner, 1998; Veenstra, 2000; Southey et al., 2006). Rules have been proposed based on experimentally verified or published cleavage data to predict the cleavage sites in vertebrate neuropeptide precursors (Rholam et al., 1995; Rouille et al., 1995) and insect (Veenstra, 2000). In vertebrates,

pairs of basic residues, Lys-Arg or Arg-Arg, are generally used, although single Arg, dibasic Arg-Lys or Lys-Lys are also found to be processed (Rouille et al., 1995). There are differences in the cleavage sites between vertebrates and insects (Veenstra, 2000). There is more knowledge about the cleavage sites of insect neuropeptide precursors. Firstly, the cleavages of the Lys-Arg pairs in insects are not often followed by an aliphatic or basic amino acid residue. Moreover, Lys-Lys pairs are not frequently used for processing in insects. Thirdly, it is not clear whether Lys-Arg/Arg-Arg pairs followed by either an aliphatic or a basic amino acid residue are processed or not in insect neuropeptide precursors. Arg-Lys pair has not been reported as cleavage site so far in insects. But processing at single Arg residue occurs in insect under limited conditions, with an Arg, Lys or His residues being in the position -4, -6, or -8.

Several prohormone convertases, including furin, PC1/3, PC2, PC4, PACE4 and PC5, have been characterized for the proteolytic cleavage, which will be discussed in more detail below (Veenstra, 2000; Southey et al., 2006). The rules mentioned above are quite helpful to predict potential cleavage sites in neuropeptide precursors identified in genome/transcriptome sequences, but ambiguous processing sites still exist to allow differential cleavage of the same precursor to produce different peptides (Veenstra, 2000). Approaches used for prediction of cleavage sites in neuropeptide precursors have been developed based on reported cleavage motifs, for example NeuroPred (http://stagbeetle.animal.uiuc.edu/cgi-bin/neuropred.py) (Southey et al., 2006).

1.1.2 Neuropeptide biosynthesis, release and inactivation

Physiologically active neuropeptides are generated via a series of enzymatic cleavages of their precursor proteins within the regulated secretory pathway (RSP) (Figure 1.1, 1.2). Bioactive neuropeptides produced and secreted from neurons then

bind to receptor proteins before being removed from the extracellular space, as shown in Figure 1.2. After being directed into the lumen of the endoplasmic reticulum (ER) by the signal peptide, the first proteolytic cleavage of the prohormone occurs with a non-specific signal peptidase removing the signal peptide (Sossin et al., 1989; Fricker, 2012). Following the signal peptide cleavage, complex carbohydrate chains can be added to asparagine (N) residues (if present) located within N-linked glycosylation sequences (NxS/T, where x is any amino acid except Pro) in the ER (Schwarz and Aebi, 2011). Then the prohormones are transferred to the Golgi apparatus for further modification, such as the removal and addition of carbohydrate units, phosphorylation and sulfation (Sossin et al., 1989; Beisswanger et al., 1998; Fricker, 2012). In the late Golgi, known as the trans-Golgi network, the neuropeptides are sorted into so-called large dense core vesicles or secretory granules together with processing enzymes under low pH (Sossin et al., 1989; van den Pol, 2012). Neuropeptide proteolytic cleavages are performed by prohormone convertases, prohormone convertase 1 (PC1, also known as PC3, and often referred to as PC1/3) and prohormone convertase 2 (PC2), generating intermediates that contain basic residues (lysine (K) and arginine (R)), which are removed by carboxypeptidase E (CPE) (Sossin et al., 1989; Fricker, 2012). Some neuropeptide proteolytic cleavages are processed in the trans-Golgi network by furin. PC1/3 and PC2 are distributed within secretory granules throughout neurons and endocrine and neuroendocrine cells but absent from non-neuroendocrine tissues (Fricker, 2012). Both PC1/3 and 2 are able to cleave substrates at the following sites: XXKR, RXXR, and RXXXXR (Seidah, 2011; Hoshino and Lindberg, 2012). PC4, PACE4 and PC5 have restricted expression, with PC4 only in germ cells and PACE4 and PC5 in several tissues (Veenstra, 2000). Furin is broadly expressed among different tissues and is most localized in the trans-Golgi network (Fricker, 2012). The cleavage occurs after the last

Arg of the consensus site RXXR, especially a basic residue in the P2 position, such as RXK/RR (Nakayama, 1997; Thomas, 2002). Further neuropeptide proteolytic processing occuring in the trans-Golgi network is mediated by the exopeptidase carboxypeptidase D (CPD) or carboxypeptidase E (CPE) (Fricker, 2012). In some cases, additional enzymatic modifications of the final mature peptide occur to protect the peptide from exopeptidases. A common post-translational modification is C-terminal amidation, where a C-terminal glycine residue is converted to an amide group through the action of the enzyme known as peptidyl-alpha-amidating monooxygenase (PAM) (Fricker, 2012).

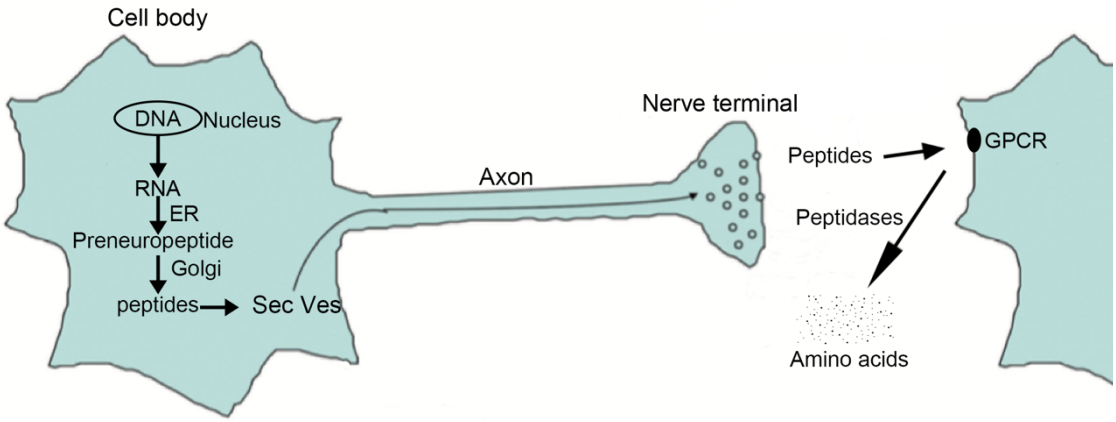

Figure 1.2 Neuropeptide biosynthesis, processing and degradation.
Neuropeptide precursors/preneuropeptides are synthesized on ribosomes in the rough endoplasmic reticulum (ER) and processed through the Golgi apparatus. Neuropeptides are packaged into secretory vesicles (Sec Ves), which are axonally transported to the site of release. Neuropeptides are degraded by extracellular peptidases to amino acids after activating the receptor, usually a G protein-coupled receptor (GPCR). Figure is modified from Fricker 2012.

Although the peptide synthesis can be regulated at several steps, the mature peptides are stored in secretory vesicles, which is the most important mechanism for regulation of the extracellular levels of the neuropeptides (Fricker, 2012).

Neuronal depolarization triggers fusion of secretory vesicles with the cell membrane to release the peptides into the extracellular environment to bind to a receptor protein to influence activity of other cells. An increase in cytoplasmic calcium

concentration induced by spike bursts is a key to the enhanced probability of neuropeptide release (Bondy et al., 1987; Jackson et al., 1991; Muschol and Salzberg, 2000; Tallent, 2008). Calcium is important as regulator of the release of both fast amino acid transmitters and peptides, but a greater increase in cytoplasmic calcium and neuronal activity is required for peptide release than amino acid secretion (Tallent, 2008). It has been reported that the increase in cytoplasmic calcium in axon terminals may enhance the probability of dense core vesicle exocytosis, which is induced by spike bursts (Bondy et al., 1987; Jackson et al., 1991; Muschol and Salzberg, 2000; van den Pol, 2012).

The sites of neuropeptide release, mostly from non-synaptic regions, are different from that of amino acid transmitter release. Thus, peptides typically diffuse over longer distances than amino acid transmitters to exert their effects, which are typically mediated by activation of G protein-coupled receptors (van den Pol, 2012). Finally, after increasing or decreasing the activity of other cells, neuropeptides are degraded by extracellular peptidases into amino acids.

1.1.3 G protein-coupled receptors (GPCRs) as mediators of the effects of neuropeptides

Neuropeptides exert their effects through the activation of corresponding receptors on the surface of nearby cells or, in the case of hormones, distant cells. Most neuropeptides bind to G protein-coupled receptors (GPCRs) that are responsible for converting these extracellular stimuli into intracellular responses (Gomes et al., 2013). GPCRs can be divided into three domains: an extracellular domain, a transmembrane (TM) core and an intracellular domain as shown in Figure 1.3 (Gomes et al., 2013). The extracellular domain contains the N-terminal tail and the extracellular loops (e1, e2, e3)

and this domain is involved in binding the neuropeptide, leading to activation of the receptor. The TM core comprises seven α-helical regions (TM1 to TM7), which convey conformational changes induced by ligand binding to the extracellular domain of the receptor to the intracellular domain of the receptor. Similar to the extracellular domain, the intracellular domain is formed by the C-terminal tail and the intracellular loops (i1, i2, i3) of the TM core.

When the association between intracellular domain and the TM core changes, affecting the G proteins – dissociated into α and β-γ, the signal is processed and amplified to elicit the intracellular response and exert the neuropeptide's physiological effect. G-proteins are trimeric protein complexes including an α, β, and γ subunit, which are used to modulate the activity of effectors, such as adenylyl cyclase or phospholipase (Fricker, 2012). Based on the type of α subunit, Gs, Gi, Go, and Gq, G proteins can be divided into different subfamilies.

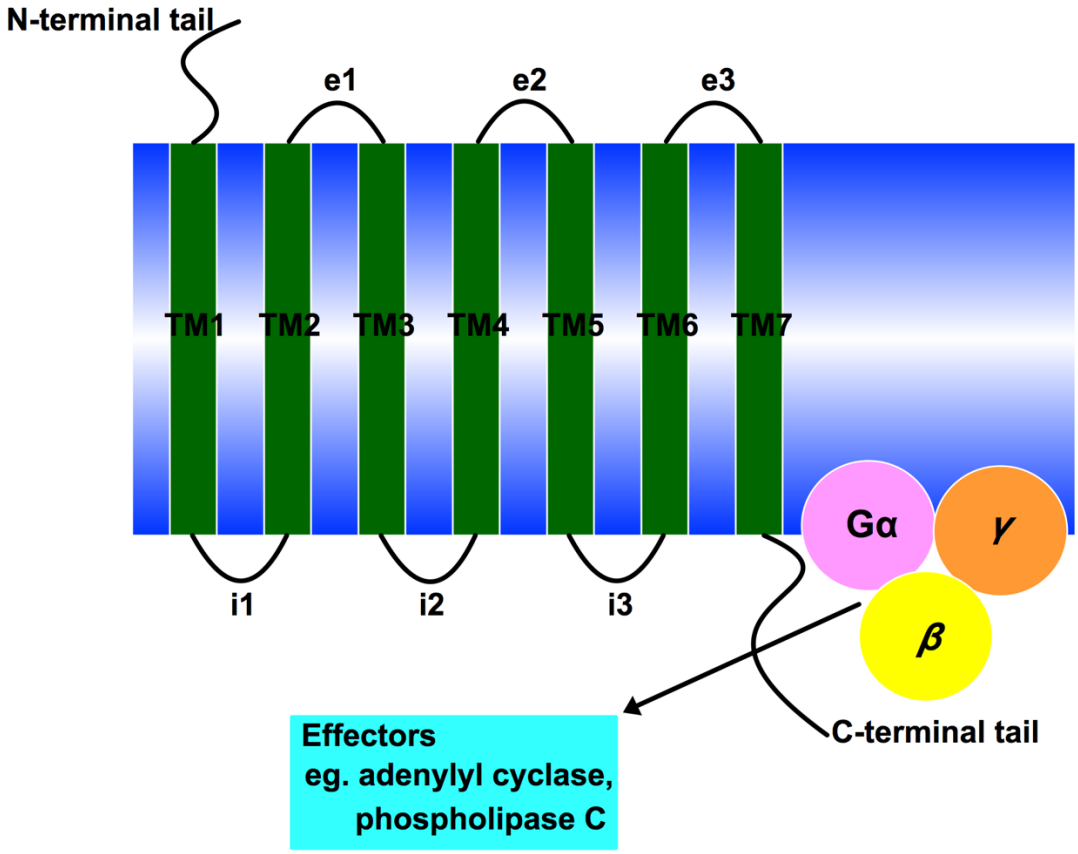

Figure 1.3 Characteristics of G protein-coupled receptors (GPCRs).
A GPCR includes extracellular, transmembrane (TM) and intracellular domains. The extracellular domain contains the N-terminal tail and the extracellular loops (e1, e2, e3). The TM core comprises seven α-helical regions (TM1 to TM7, shown in green). The intracellular domain is formed by the C-terminal tail and the intracellular loops (i1, i2, i3) of the TM core. G-proteins are made up of an α (pink), β (yellow), and γ (orange) subunit. Adenylyl cyclase and phospholipase are examples of G-protein effectors. Schematic diagram was prepared using Illustrator for Biological Sequences (IBS, version 1.0.3) software based on Gomes et al. (2013).

As highlighted above, neuropeptides play their roles in physiological processes via specific receptors. There are at least four patterns in the interaction between neuropeptides and receptors (Figure 1.4) (Fricker, 2012). The simplest is the classic "lock and key" model, in which one peptide binds to only one receptor (Gomes et al., 2013). But usually, one neuropeptide can bind to several receptors or different neuropeptides can activate the same receptor or a combination of these two patterns. The complicated interaction between neuropeptide and receptor makes it possible that one neuropeptide can have several functions (Fricker, 2012).

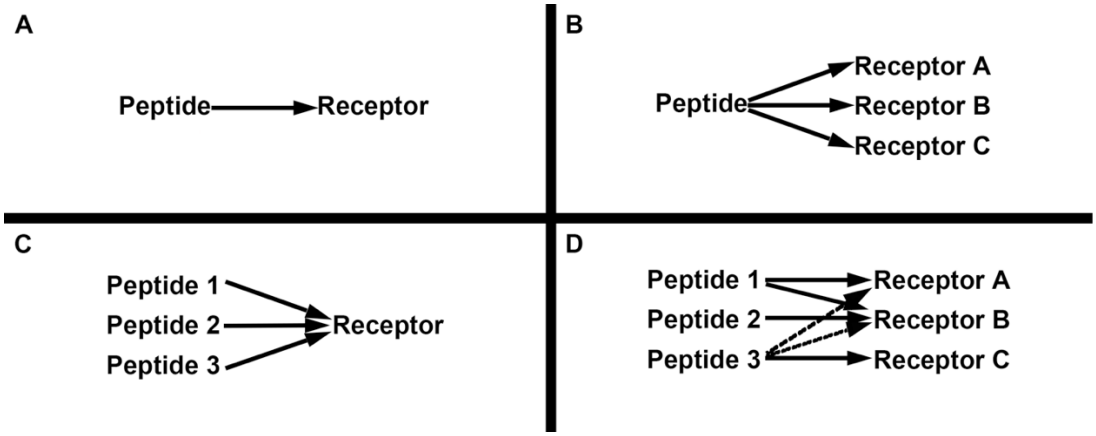

Figure 1.4 Diversity of peptide-receptor signaling.
The simplest model is that one peptide binds only to one receptor (**A**). But frequently, one peptide can bind to multiple receptors (**B**) or different peptides can bind to a single receptor (**C**), or a combination of these two patterns (**D**).

1.1.4 The physiological roles of neuropeptides

Neuropeptides are involved in the regulation of different types of physiological and behavioral processes in animals and a variety of methods have been developed to study the functions of neuropeptides. Initially, radioimmunoassay, immunohistochemistry, bioassays and electrophysiology were used, and later on modern molecular biological methods have contributed greatly to our knowledge of the diversity of neuropeptides (Hökfelt et al., 2000). Radioimmunoassay and immunohistochemistry are used to detect the expression of neuropeptides and receptors, which is helpful to predict their functions. An example is provided by research on neuropeptide-Y (NPY). Anatomical and physiological studies suggested a variety of functions of NPY in the mammalian nervous system (Gray and Morley, 1986). NPY immunoreactivity is detected widely in the central and peripheral nervous systems using radioimmunoassay. The increase in ingestive behaviors caused by NPY administration is related to the NPY-immunoreactivity in the hypothalamus. The effect of NPY in modulating luteinizing hormone release and sexual behavior is thought to be related to an NPY-immunoreactive pathway from the arcuate nucleus to the medial preoptic area.

The NPY-immunoreactivity in a dense plexus around cerebral vessels is consistent with NPY's effect in causing vasoconstriction of cerebral vessels.

In vitro and *in vivo* pharmacological techniques are the main methods for functional studies. The isolated hindgut preparation of the cockroach, *Leucophaea maderae*, has contributed a lot for the isolation and functional characterisation of many insect myotropic peptides (Holman et al., 1991); for example, the isolation and characterization of two novel tachykinin-related peptides from the crab *Cancer borealis* nervous system (Christie et al., 1997). The following reports about GnRH and PDF prove that *in vivo* methods are quite helpful for physiological study. Continuous low-dose administration of a GnRH analogue can produce reversible, long-term suppression of reproductive function of male and female domestic dogs (Trigg et al., 2001). PDF was found to serve as an output regulator of locomotor circadian rhythm in the German cockroach via RNAi, a kind of molecular biotechnique, to silence this gene (Lee et al., 2009).

Neuropeptides can be involved in more than one physiological process, and a behavioral change may not be caused by only one neuropeptide. Melanin-concentrating hormone (MCH) was initially found to induce body colour changes (Kawauchi et al., 1983). Subsequently, it was discovered that MCH also played key roles in feeding (Georgescu et al., 2005) and sleeping behaviour (Willie et al., 2008). Sulfakinin is another important neuropeptide to regulate food intake in multiple insect species (Wei et al., 2000).

1.1.5 Two approaches to neuropeptide discovery: function first or neuropeptide first

With the development of biological research techniques, more and more methods have been applied to identify new neuropeptides, which can be divided into two approaches, namely “function first” and “neuropeptide first”, respectively (Fricker, 2012). Neuropeptides were first discovered due to their physiological effects, and this bioassay method is still an important tool, with the bioactivity of a tissue extract being identified first and then the bioactive neuropeptide being purified later to determine its molecular structure. The discovery of substance P is a good example, with its effect in stimulating contraction of the intestinal smooth muscles and lowering blood pressure discovered in 1931 (Euler and Gaddum, 1931). But its sequence was not determined until 1971 (Chang et al., 1971).

The “neuropeptide first” approach starts with the application of techniques to identify the peptides or the genes encoding neuropeptide precursors. Once the existence of the predicted peptides has been confirmed, using techniques such as peptide sequencing and mass spectrometry, pharmacological tests are performed to determine the actions of the identified peptide(s). With the publication of genomic, transcriptomic and proteomic data, numerous putative neuropeptides have been identified based on the structural characteristics of neuropeptide precursors, such as the N-terminal signal peptide and specific cleavage sites (e.g. KR or RR). Rising numbers of neuropeptide precursors have been predicted via BLAST by using the homologues identified in other animals as queries. In model organisms, 32 *Caenorhabditis elegans* genes encoding neuropeptides were identified after searching its genome (Nathoo et al., 2001) and 119 neuropeptide genes have been predicted in *Drosophila melanogaster* (Clynen et al., 2010). Andrew E. Christie has contributed a lot to neuropeptide gene discovery by mining genome/transcriptome databased. For example, Andrew E. Christie has identified 39 ESTs encoding putative peptide precursors from four aphid species (14 in

Acyrthosiphon pisum, 4 in *Aphis gossypii*, 20 in *Myzus persicae* and 1 in *Toxoptera citricida*) (Christie, 2008).

The two main approaches to neuropeptide discovery take advantage of similar techniques but in different orders. There are some limitations for each method, so several techniques are applied together to confirm the finding. Since the first neuropeptide substance P was discovered by van Euler and Gaddum in 1931 (Euler and Gaddum, 1931) and sequenced in 1971 (Chang et al., 1971), 5949 non-redundant neuropeptide entries originating from 493 organisms belonging to 65 neuropeptide families have been identified, 3455 and 2406 in invertebrates and vertebrates, respectively, although the physicochemical properties of some peptides are still not clear (Wang et al., 2015).

1.1.6 Evolutionary relationships of neuropeptides in the animal kingdom

Neuropeptides and their receptors have a widespread phylogenetic distribution in the animal kingdom, ranging from cnidarians (e.g. *Hydra*), which have a very simple nervous system, to mammals. For many neuropeptide families, the members are highly diverse because of the relatively short sequences of the mature peptides, and it is common that the number of neuropeptide copies is not consistent between species (Jekely, 2013). But many neuropeptides belonging to the same neuropeptide family have been identified in different animal species, such as the FMRFamide family (Hökfelt et al., 2000).

Olivier Mirabeau assessed the evolutionary relationship between protostomian and deuterostomian peptidergic systems (PSs) by analyzing the sequences of rhodopsin and secretin-type G protein-coupled receptors of 15 bilaterian species (Mirabeau and Joly, 2013). In some cases, there is high conservation between the sequences of

invertebrate and vertebrate neuropeptides. The insulin/insulin-like growth factor (IGF)/relaxin superfamily is a good example, which contains a signature sequence of a cysteine motif "CCxxxCxxxxxxxxC" (Mita et al., 2009b). Analyzing the evolution of neuropeptides and receptors should be helpful to gain novel insights into neuropeptide function and to predict ancestral neuron types that were probably present in the last common bilaterian ancestor.

As discussed above, many neuropeptides have been identified but sequence similarity is often not satisfactory for phylogenetic analysis (Wang et al., 2015). However, most neuropeptides exert their effects via GPCRs, which are much more conserved among different animal species and could be useful for analyzing the evolutionary relationships of neuropeptides. The superfamily of GPCRs has been divided into five main families (glutamate, rhodopsin, adhesion, frizzled/taste2, and secretin) with phylogenetic analyses of 342 unique functional non-olfactory human GPCR sequences (Fredriksson et al., 2003). The rhodopsin family is the largest GPCRs family including four main groups ($\alpha, \beta, \gamma, \delta$) according to the analysis of Fredriksson et al (Fredriksson et al., 2003). Especially, the β group receptors all react with peptides, such as neuropeptide Y (NPY), thyrotropin releasing hormone (TRH), gonadotropin-releasing hormone (GnRH) receptors. Neuropeptides belonging to the same neuropeptide family interact with members of the same GPCR family, while different neuropeptide families can act via GPCRs belonging to different families (Mirabeau and Joly, 2013), for example, vasopressin receptors and corticoliberin receptors belonging to the rhodopsin and secretin families, respectively. The relationships of GPCRs can be helpful to investigate the evolutionary relationships of neuropeptides in the animal kingdom. For example, the receptors of protostomian allatotropin (p-AT)-type peptides and deuterostomian orexin-type peptides are closely related orthologs, indicating that

the neuropeptides that activate these receptors are also orthologous (Mirabeau and Joly, 2013). Furthermore, by identifying the receptor for a neuropeptide, potential roles of that neuropeptide can be predicted based on insights from orthologous neuropeptides in other phyla.

Neuropeptide signaling systems have been analyzed in great detail in vertebrates and in model invertebrates such as *Caenorhabditis elegans* and *Drosophila melanogaster* (Broeck, 2001). In *C. elegans*, over 250 signaling molecules are derived from neuropeptide precursor (Li et al., 1999; Nathoo et al., 2001; Pierce et al., 2001; Frooninckx et al., 2012). And more than 1100 GPCRs have been identified, in which approximately 100 thought to be specific for neuropeptides (Bargmann, 1998). In *D. melanogaster*, 119 neuropeptide genes being divided into 46 neuropeptide families have been predicted (Clynen et al., 2010). About 160 GPCRs were found in *D. melanogaster* (Hewes and Taghert, 2001). Most families of known neuropeptides have been matched to receptors in *D. melanogaster* (Hewes and Taghert, 2001; Johnson et al., 2003; Clynen et al., 2010). Research about *D. melanogaster* neuropeptide and GPCRs extends our understanding of certain neuropeptides physiological action (Bendena et al., 2012). For example, allatostatin-like peptides appear to influence foraging behavior in *D. melanogaster*. However, because vertebrates and *Drosophila* are evolutionarily distantly related, it can be difficult to identify relationships between their neuropeptide systems. Therefore, analysis of a phylum located "between" the vertebrates and the protostomian invertebrates in animal phylogeny could provide important insights into neuropeptide evolution and neuropeptide relationships, as discussed below with echinoderms as an example.

1.2 Echinoderms as model systems for neuropeptide research

The phylum Echinodermata is a group of marine invertebrates that include five extant classes: Asteroidea (starfish), Ophiuroidea (brittle stars), Echinoidea (sea urchins, sand dollars), Holothuroidea (sea cucumbers) and Crinoidea (feather stars and sea lilies) (Figure 1.5) (Peterson and Eernisse, 2016; Semmens et al., 2016). They are deuterostomian invertebrates, which occupy an "intermediate" position between the chordates, including vertebrates, and the protostomian invertebrates, such as Arthropoda (*Drosophila melanogaster*) and Nematoda (*Caenorhabditis elegans*) (Figure 1.6) (Turbeville et al., 1994; Lowe and Wray, 1997; Halanych, 2004).

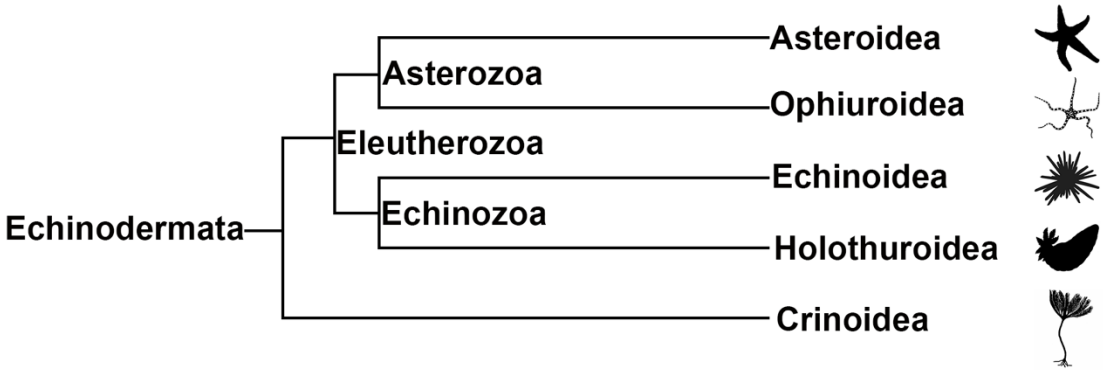

Figure 1.5 Phylogenetic tree showing relationships of the five extant echinoderm classes, based on Peterson and Eernisse (2016).
The Asteroidea (e.g. starfish) and Ophiuroidea (e.g. brittle stars) form the asterozoan clade. The Echinoidea (e.g. sea urchins) and holothuridea (e.g. sea cucumbers) form the echinozoan clade. The crinoidea (e.g. feather stars and sea lilies) are a sister group to the eleutherzoan clade that comprises echinozoans and asterozoans. Images of representative animals for Asteroidea, Ophiuroidea and Echinoidea are from http://phylopic.org. Images of representative animals for Holothuroidea and Crinoidea are produced by author of this thesis.

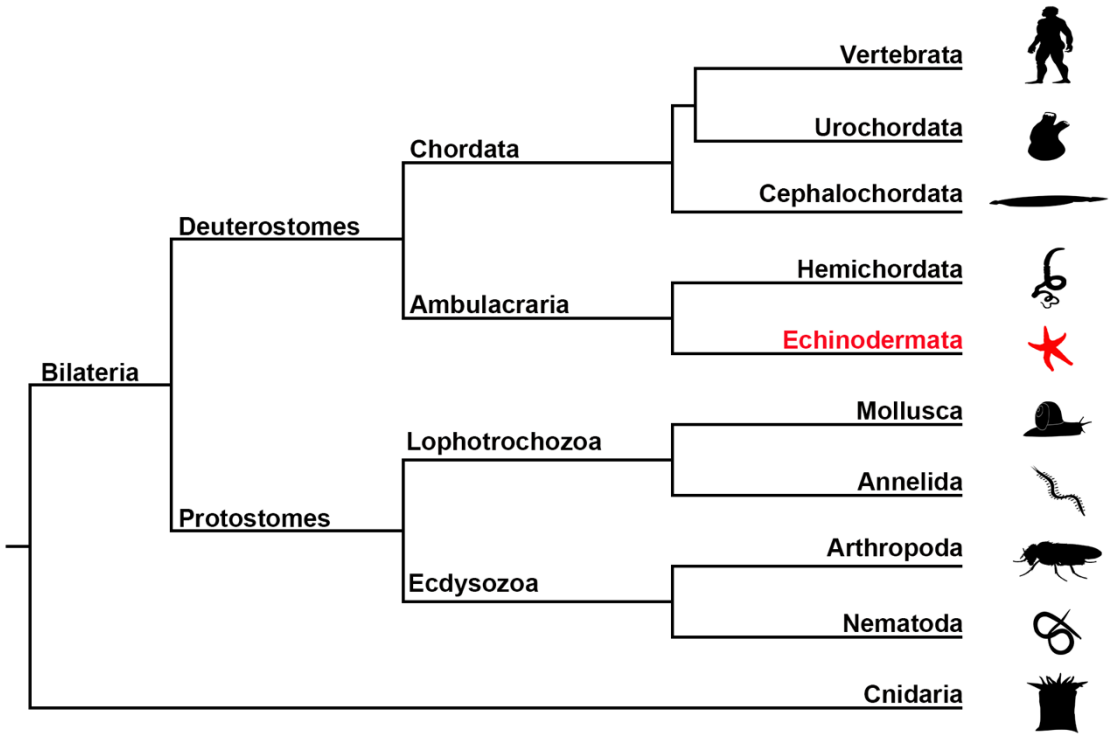

Figure 1.6 Animal phylogeny.
Phylogenetic diagram showing the position of the phylum Echinodermata (shown in red; e.g. starfish) in the deuterostomian branch of the animal kingdom. The Bilateria comprise two super-phyla, the deuterostomes and the protostomes. The deuterostomes comprise the chordates (vertebrates, urochordates and cephalochordates) and the ambulacrarians (hemichordates and echinoderms). The protostomes comprise the lophotrochozoans (molluscs and annelids) and the ecdysozoans (arthropods and nematodes). The Cnidaria (e.g. sea anemones) are basal to the Bilateria. Images of representative animals for each phylum were obtained from http://phylopic.org. This figure is modified from Semmens, Mirabeau et al. 2016.

Adult echinoderms are characterized by exhibiting pentaradial symmetry. By analyzing the expression pattern of three important developmental regulatory genes (*distal-less*, *engrailed* and *orthodenticle*) (Duboule, 1995), it has been demonstrated that the reorganization of echinoderm body architecture involved extensive changes in the deployment and roles of homeobox genes, which include modifications of expression domains and the evolution and loss of developmental roles of these genes (Lowe and Wray, 1997). These changes occurred at different time in the evolutionary history of echinoderms, leading to the current morphological characters of adult echinoderms. Other notable and distinct traits of echinoderms are their ability to autotomize and

regenerate body parts. Additionally, the mutability of their collagenous tissue, changing between stiff and soft states, is another unusual feature of echinoderms (Mo et al., 2016).

With the completion of genome and transcriptome data analysis, potential neuropeptide precursors have been identified in several echinoderm species. Matthew Rowe and Maurice Elphick (Rowe and Elphick, 2012) identified 28 cDNAs encoding neuropeptide precursors in the sea urchin *Strongylocentrotus purpuratus*, which provided new insights into neuropeptide evolution (Semmens and Elphick, 2017). For example, the *S. purpuratus* thyrotropin-releasing hormone-type precursor is the first one identified in invertebrate. Discovery of NG peptides in sea urchins bridged the gap between neuropeptide S in tetrapod vertebrates and crustacean cardioactive peptide in protostomes (Semmens et al., 2015). Later on, a total of 17 neuropeptide precursors have been identified in sea cucumber *Apostichopus japonicus* transcriptome sequence data by using homologs predicted in *Strongylocentrotus purpuratus* as queries for BLAST searches (Rowe et al., 2014). Recently, 40 transcripts encoding neuropeptide precursors were identified in the starfish *Asterias rubens* (Semmens et al., 2016). Transcriptome sequence data from three brittle star species, *Ophionotus victoriae*, *Amphiura filiformis* and *Ophiopsila aranea*, have also been analyzed to identify neuropeptide precursors (Zandawala et al., 2017).

1.3 The common European starfish *A. rubens*

Asterias rubens is one of the most abundant starfish species in the eastern and western regions of north Atlantic. It can be found throughout the coasts of the UK from intertidal rocky shores to deep water area. *A. rubens* on the south-west coast of Britain has a relatively clear annual reproductive cycle with the gonad growth in autumn and winter and spawning in spring to early summer after the gonad reaching full size

(Barker and Nichols, 1983). Fertilization occurs soon after spawning of eggs and sperm and the larval development of *A. rubens* takes about 87 days to 140 days, which provides enough time to allow for wide dispersal and geographical distribution before the larvae settle (Barker and Nichols, 1983). The growth of *A. rubens* larvae and juveniles is affected by water temperature, food abundance and other factors, but after the completion of metamorphosis, the juvenile *A. rubens* is free from the attachment and feed carnivorously on algae (Barnes and Powell, 1951; Barker and Nichols, 1983).

1.3.1 The anatomy of *A. rubens*

The adult *A. rubens* is a five-rayed starfish, with each arm radiating from the central disk region. The upper or aboral side is orange, purple or pale brown, depending on geographical location and/or environmental conditions. The aboral body wall has numerous appendages, including spines, pedicellariae and papulae (Figure 1.7). The spines and pedicellariae are mainly involved in the passive and active defense of starfish (Dubois and Ameye, 2001). The papulae have a respiratory function, enabling gas exchange between seawater externally and the coelomic fluid internally (Cobb, 1978). On the aboral surface of the central disk is the madreporite (Figure 1.7), a disc-like plate that connects the water vascular system to the external environment. On the lower or oral side of the central disk is located the mouth, surrounded by the peristomial membrane. On the oral side of each arm is the ambulacral groove, which comprises rows of tube feet extending from the peristome to the arm tips (Figure 1.7). Tube feet are fleshy, extendable and movable fluid-filled tubes with a disc-like sucker (Figure 1.7, 1.8) that have important roles in locomotion, attachment and feeding (Hennebert, 2010).

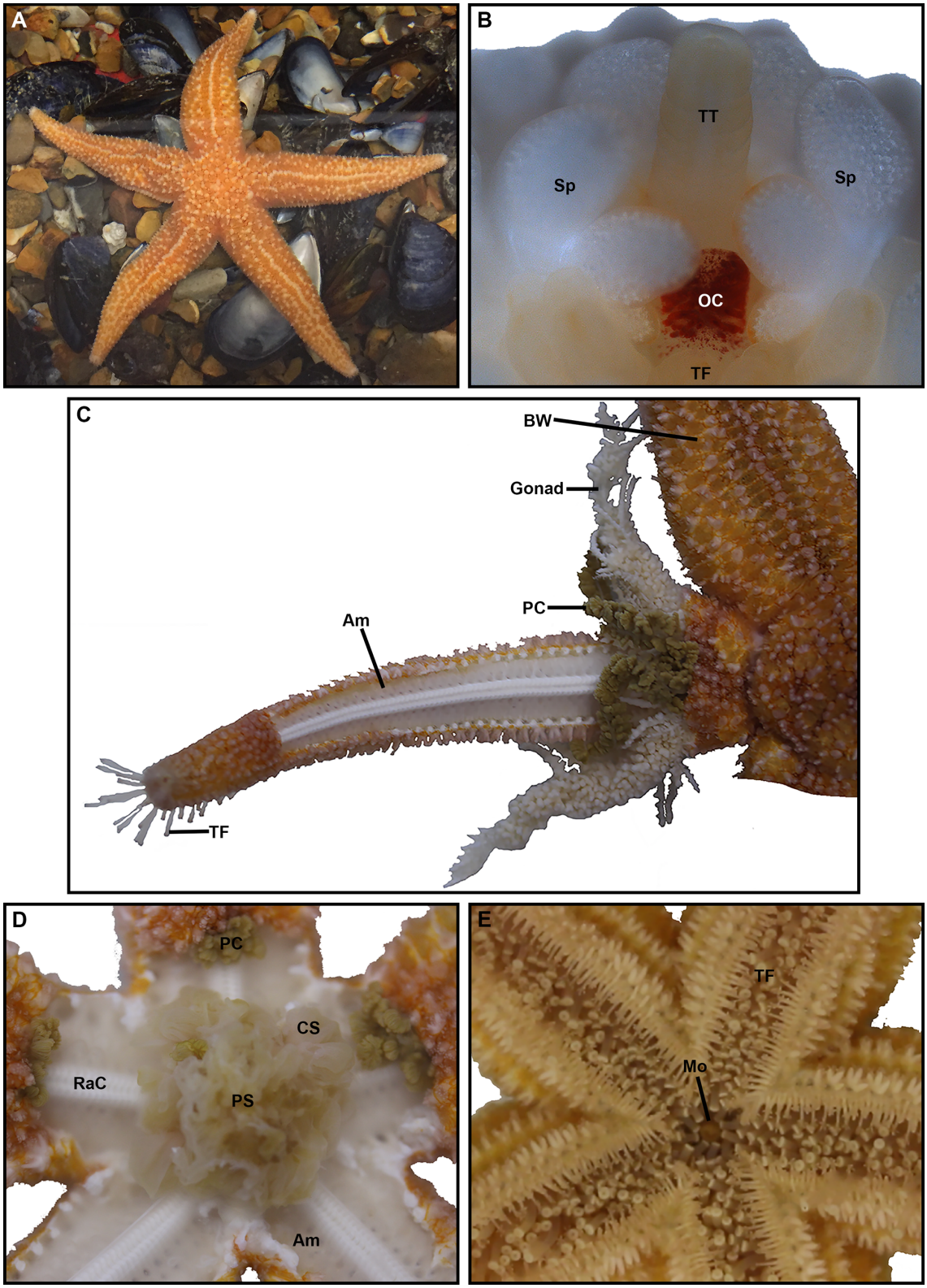

Figure 1.7 The anatomy of starfish *Asterias rubens*.
A: Photograph of five-rayed adult *A. rubens* with each arm radiating from the central disk region from the aboral side feeding on mussels (*Mytilus edulis*). **B:** Photograph of a living specimen of *A. rubens* showing the arm tip region viewed from the underside (oral) of the animal, taken using a Leica DFC420 C camera linked to a Leica S8 APO microscope. The most prominent feature is the pigmented optic cushion, which is located at the base of the terminal tentacle. The terminal tentacle and optic cushion are

bounded on each side by spines and rows of tube feet can be seen adjacent to the optic cushion. **C:** Photograph of a partially dissected starfish without the aboral body wall of the arm showing gonads (white), pyloric caeca (brown), radial canal (RaC), ampulla (Am) and tube feet (TF) from the aboral side. **D:** Photograph of *A. rubens* central disk without the aboral body wall showing the cardiac stomach (CS), pyloric stomach (PS), pyloric caeca (PC) and ampulla (Am) from the aboral side. **E:** Photograph of *A. rubens* showing mouth (Mo) in the middle of the central disk and rows of tube feet radiating from the central disk region from the oral side.

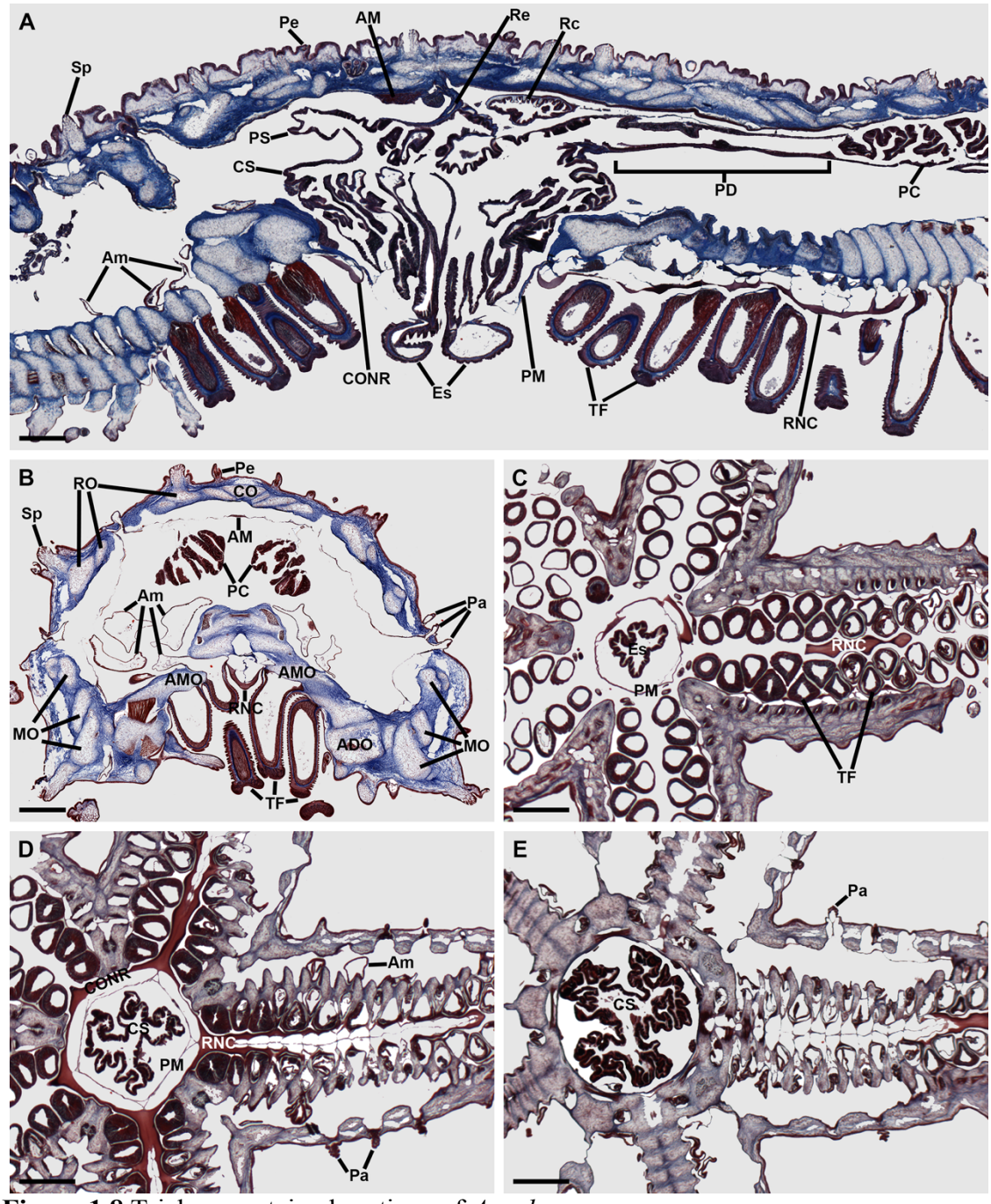

Figure 1.8 Trichrome stained sections of *A. rubens*.
A: This section runs transversely across the middle of the central disk region and parasagittally through two arms. **B**: Transverse section of an arm. **C-E**: Horizontal sections through the central disk and arms of a juvenile specimen, with C at the level of

the esophagus, D at the level of the circumoral nerve ring and E at the level of the highly-folded pouches of the cardiac stomach. ADO, adambulacral ossicle; AM, apical muscle; Am, ampulla; AMO, ambulacral ossicle; CE, coelomic epithelium; CO, carinal ossicle; CONR, circumoral nerve ring; CS, cardiac stomach; Es, esophagus; MO, marginal ossicles; Pa, papulae; PC, pyloric caeca; PD, pyloric duct; Pe, pedicellariae; PM, peristomial membrane; PS, pyloric stomach; RC, rectal caeca; Re, rectum; RNC, radial nerve cord; RO, reticular ossicles; Sp, spine; TF, tube feet. Scale bars: 500 μm in A, B; 200 μm in C, D, E.

The body wall of starfish consists of an external epithelial layer and an internal coelomic epithelium. Sandwiched between these epithelia calcareous ossicles (Figure 1.8) form an endoskeleton, with individual ossicles surrounded and/or linked by collagenous tissue composed of collagen fibers (dermis) and small bundles of muscle (myocytes) (Lawrence, 2013).

At the tip of each arm is the terminal tentacle and optic cushion (Figure 1.7), which have important sensory functions. The terminal tentacle is tube foot-like structure and it is involved in detecting environmental changes (Hennebert et al., 2013). The optic cushion (a red spot) is located at the oral base of the terminal tentacle and is composed of a cluster of pigment-cup ocelli that form a simple “eye”. Evidence has been obtained recently that the coral-reef-associated starfish *Linckia laevigata* optic cushions are involved in negative phototaxis (Garm and Nilsson, 2014).

When it comes to the internal anatomy of *A. rubens*, it can be divided into the nervous system, digestive system and circulatory system. The nervous system of *A. rubens* comprises radial nerve cords, which are located on the oral side of each arm with two rows of tube feet on either side (Figure 18B, C), and a circumoral nerve ring located in the central disk that links the five radial nerve cords (Figure 18A, D). Linked to each tube foot is an associated contractile ampulla that is located internal to the body wall (Figure 18A, B). The circumoral nerve ring is located at the periphery of the peristomial membrane (Figure 1.8). The V-shaped radial nerve cords in transverse

section (Figure 1.8B) run along with the length of each arm in the middle of the ambulacral groove, bordered on each side by two rows of tube feet (Moore and Thorndyke, 1993). Both the circumoral nerve ring and radial nerve cord are comprised of ectoneural and hyponeural regions. The ectoneural region occupies a superficial position in the oral epidermis and is the predominant part of the nervous system (Mashanov et al., 2016). It is continuous with the subepidermal plexus, which covers almost the whole body (Cobb, 1970). The ectoneural neurons are thought to comprise motoneurons, interneurons sensory neurons (Cobb, 1970; Cobb, 1987; Moore and Thorndyke, 1993). The hyponeural region is located at the aboral surface of the respective ectoneural cords as a thinner nervous tissue layer (Mashanov et al., 2016). Hyponeural neurons are thought to be motoneurons exclusively (Cobb, 1970; Cobb, 1987; Moore and Thorndyke, 1993).

The digestive system is a prominent part of the internal anatomy of *A. rubens*, including the mouth, cardiac stomach, pyloric stomach, pyloric duct, pyloric caeca, rectum and anus, as illustrated in Figure 1.7 and Figure 1.8. During the feeding processes, the mouth in the middle of central disc opens first, and the oral voluminous and foldable cardiac stomach is everted outside the mouth to surround digestible parts of prey (Figure 1.8A). Digestion occurs largely externally through the actions of enzymes secreted by the stomach. Then the cardiac stomach is retracted back and digested particles are transported to the smaller flattened aboral pyloric stomach and pyloric caeca through the pyloric ducts for further digestion, absorption and storage. Waste material is passed from the pyloric caeca to the rectum, via the pyloric duct, and expelled through the anus in the center of the aboral central disk (Ruppert et al., 2004).

The circulatory system of starfish is complex, including the coelom, the hemal system and the water vascular system. The coelom comprises a single cavity in the disc and five arm cavities, which are filled with circulating coelomic fluid. The hemal system is comprised of three pairs of hemal rings (hyponeural hemal ring, gastric hemal ring and genital hemal ring) and the connecting axial sinus located in the coelomic cavity of the disk (Broertjes and Posthuma, 1978; Beijnink and Voogt, 1986). A simple heart is located on top of the axial sinus, above the three hemal rings and the same side as the madreporite (Ruppert et al., 2004). The hemal system is mainly used for transporting nutrients derived from the digestive system. It is not clear whether the *A. rubens* hemal system is also responsible for the transportation of hormones (e.g. neuropeptides). The water vascular system, containing a ring canal, five radial canals and ampullae (Figure 1.8), is used to control the movement of fluid required for the hydraulic tube feet. External seawater enters the body wall to the stone canal via the madreporite and then fluid moves into the ring canal around the mouth and along the radial canals in each arm to reach the ampullae, which by contracting or relaxing control the extension or retraction of tube feet (Smith, 1950; Hennebert et al., 2013).

1.3.2 *A. rubens*: a model system for neuropeptide research

1.3.2.1 Identification of transcripts encoding neuropeptide precursors and neuropeptide receptors in the starfish *A. rubens*

Sequencing of the neural transcriptome of *A. rubens* has enabled the most comprehensive identification of neuropeptide precursor proteins in an echinoderm to date, with 40 transcripts encoding neuropeptide precursors identified (Semmens et al., 2016). Some of these neuropeptide precursors are the first to be discovered in a non-chordate species, such as kisspeptin-type and melanin-concentrating hormone-type

precursors. The starfish tachykinin-type, somatostatin-type, pigment-dispersing factor-type and corticotropin-releasing hormone-type precursors are the first to be identified in an echinoderm. *A. rubens* neuropeptide precursors that are homologues of neuropeptides identified in other animal types include vasopressin/oxytocin-type, gonadotropin-releasing hormone-type, thyrotropin-releasing hormone-type, calcitonin-type, cholecystokinin/gastrin-type, orexin-type, luqin-type, pedal peptide/orcokinin-type, glycoprotein hormone-type, bursicon-type, relaxin-type and insulin-like growth factor-type precursors (Semmens et al., 2016). Discovery of all these neuropeptide precursor transcripts has provided a basis for functional analysis of neuropeptides in *A. rubens*. However, more experimental work is now necessary to confirm the sequences of predicted peptides and to investigate their physiological roles.

1.3.2.2 Functional characterisation of neuropeptides in the starfish *A. rubens*

A. rubens has been a model system for functional characterisation of neuropeptides since the detection of FMRFamide-like immunoreactivity in the radial nerve and circumoral nerve ring (Elphick et al., 1989). Furthermore, the first neuropeptides to be identified in an echinoderm, the SALMFamides S1 (GFNSALMF-NH_2) and S2 (SGPYSFNSGLTF-NH_2), were isolated from *A. rubens* based on their cross-reactivity with antibodies to FMRFamide-like peptides (Elphick et al., 1991a). The expression of S1 and S2 in the radial nerve cords, the tube feet, apical muscle and cardiac stomach was visualised using specific antisera to S1 or S2, respectively (Elphick et al., 1991b; Elphick et al., 1995; Newman et al., 1995b). The function of S1 and S2 in starfish has been investigated using *in vitro* and *in vivo* pharmacological methods, revealing that both peptides cause relaxation of cardiac stomach, tube foot and apical muscle preparations *in vitro* (Elphick et al., 1995; Melarange et al., 1999; Melarange

and Elphick, 2003) and trigger cardiac stomach eversion *in vivo* (Elphick et al., 1995; Melarange et al., 1999).

RT-PCR and mRNA *in situ* hybridization have been used to investigate the expression of neuropeptide precursor transcripts; for example, transcripts encoding the precursor of relaxin-like gonad-stimulating peptide (RGP) in the starfish *Patiria pectinifera* (Mita et al., 2009a; Mita et al., 2009b). However, to obtain a detailed of knowledge of neuropeptide function in starfish, a range of approaches are required that combine anatomical studies employing mRNA *in situ* hybridization and immunohistochemistry with *in vitro* and *in vivo* pharmacological methods.

In addition to the above, there are several other reasons why *A. rubens* is a good experimental animal for neuropeptide research. Firstly, it is relatively easy to collect and maintain this species as it has a widespread distribution around the coast of the UK and Europe. Secondly, as a member of the starfish order Forcipulatida, which includes at least 5 starfish species (Janies, 2001), research about *A. rubens* (the most common and familiar starfish in the north-east Atlantic) is representative and can provide global interest. Thirdly, although starfish are sometimes eaten as a snack food (e.g. in China), they can also be harmful to marine resources by eating economical important shellfish or destroying coral reefs (Dare, 1982; Dolmer, 1998; Agüera et al., 2012; Magnesen and Redmond, 2012; Uthicke et al., 2015). Research on starfish neuropeptides, especially those involved in regulation of feeding and reproduction behavior, may be helpful for developing novel approaches to control starfish species that have negative impacts economically or ecologically.

1.4 Aims and objectives

The general aim of the work reported in this thesis was to investigate the expression and functions of neuropeptides derived from four predicted neuropeptide precursor proteins in *Asterias rubens*: relaxin-like gonad-stimulating peptide precursor (AruRGPP), relaxin-like peptide precursor 2 (AruRLPP2), pedal peptide-type neuropeptide precursors 1 and 2 (ArPPLNP1 and ArPPLNP2), respectively.

Chapter 2 reports experimental analysis of relaxin-like gonad-stimulating peptide precursor (AruRGPP) and relaxin-like peptide precursor 2 (AruRLPP2), which were originally identified by analysis of *A. rubens* radial nerve cord transcriptome sequence data (Semmens et al., 2016). The sequences of these two precursors are confirmed by cDNA cloning and sequencing and the structure of the neuropeptide derived from AruRGPP is characterized using mass spectrometry. The expression of both precursors in *A. rubens* are analysed using mRNA *in situ* hybridization and the physiological roles of AruRGP are investigated using an *in vitro* assay. Importantly, this is the first study to characterize in detail the expression patterns of relaxin-type peptides in an echinoderm.

Chapters 3 and 4 report experimental analysis of two pedal peptide-type neuropeptide precursors in *A. rubens*, ArPPLNP1 and ArPPLNP2. A partial sequence of ArPPLNP2 has been reported previously based on analysis of *A. rubens* radial nerve cord transcriptome sequence data (Semmens et al., 2016). Here full length cDNAs encoding ArPPLNP1 and ArPPLNP2 are cloned and sequenced, providing templates for production of probes that are used for analysis of their expression patterns in *A. rubens* using mRNA *in situ* hybridization. Mass spectrometry is used to determine the structures of peptides derived from ArPPLNP1 and ArPPLNP2. Then antibodies to

peptides derived from ArPPLNP1 and ArPPLNP2 are generated and characterized to enable analysis of the expression of these peptides in *A. rubens* using immunohistochemical techniques. Finally, *in vitro* and *in vivo* pharmacology methods are used to investigate the physiological roles in *A. rubens* of peptides derived from ArPPLNP1 and ArPPLNP2. Importantly, this is the first study to characterize the expression patterns of pedal peptide-type peptides in an echinoderm and to compare the pharmacological actions of peptides derived from different pedal peptide-type precursors in an echinoderm.

2 Cellular localization of the expression of two relaxin-type neuropeptide precursors in *Asterias rubens*: new insights into neurohormonal control of spawning in starfish *Asterias rubens*

2.1 Introduction

Relaxin-type peptides include relaxin and insulin/relaxin-like peptides, which belong to the insulin/IGF/relaxin superfamily. The insulin/IGF/relaxin superfamily includes insulin, IGFs, relaxin and insulin/relaxin-like peptides, which is divided into two subfamilies: the insulin and insulin-like growth factor (IGF) subfamily and the relaxin (RLN) and relaxin/insulin-like (INSL) subfamily based on evolutionary relationships that are reflected in precursor structure (Figure 2.1 A) (Steiner et al., 1985; Lu et al., 2005). The focus of the work reported in this chapter are two starfish neuropeptides that are relaxin-type neuropeptides (Semmens et al., 2016). Therefore, here relaxin-type peptides are introduced.

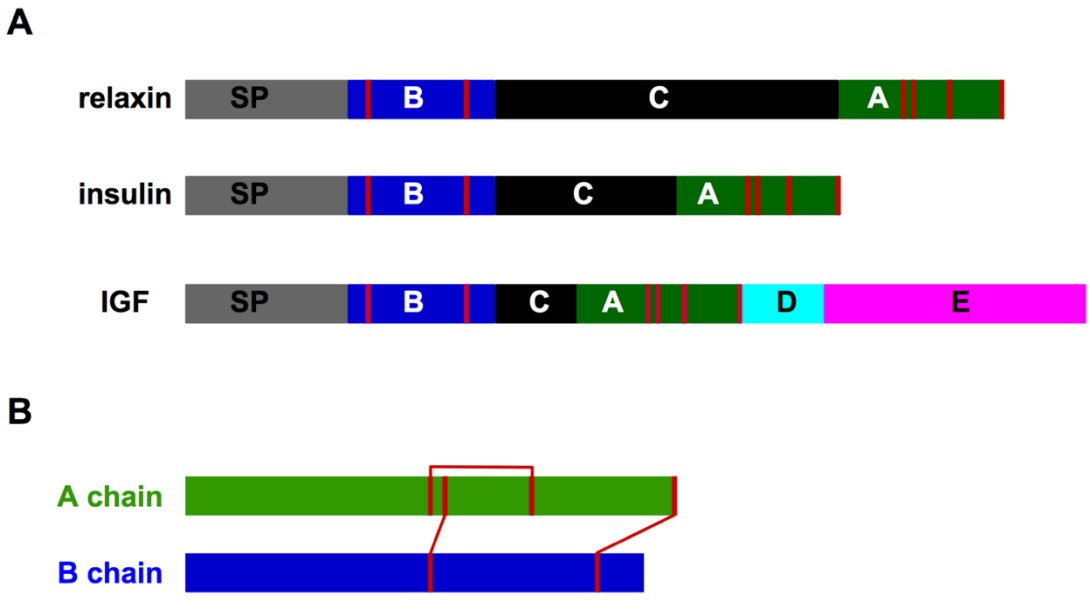

Figure 2.1 General structure of relaxin, insulin and IGF precursors (**A**) and predicted dimeric structure of relaxin/insulin (**B**).
The signal peptide (SP) is shown with a grey rectangle. A to E chains are shown in green, blue, black, turquoise and purple, respectively. Cysteines and disulfide bridges

are shown with red lines. Schematic diagrams were prepared using Illustrator for Biological Sequences (IBS, version 1.0.3) software.

All members in the relaxin subfamily are synthesized as an immature precursor with an N-terminal signal peptide and a B-C-A domain (Figure 2.1 A). The mature and bioactive peptide is produced after the cleavage of the signal peptide and C chain, and the formation of two disulfide bridges between A and B chains and one disulfide bridge within A chain (Steinetz et al., 2009) (Figure 2.1 B). Since the initial discovery of relaxin as a relaxant of pubic ligaments (Hisaw, 1926), it has been reported that relaxin-type peptides are involved in regulation of a variety of physiological processes. Consistent with the multiple functions of this neuropeptide family, relaxin-type peptides are detected not only in reproductive tissues but also in the nervous system and in other peripheral organs/tissues (Bathgate et al., 2013).

2.1.1 The relaxin-type neuropeptide family in vertebrates and the evolution of relaxin-type neuropeptides

2.1.1.1 Discovery and determination of the structure of relaxin

Relaxin was initially discovered in guinea pig due to its effect on the female reproductive system (Hisaw, 1926). It was purified and named as relaxin because it causes relaxation of interpubic ligaments (Fevold et al., 1930). The amino-acid sequences of relaxins were determined in more than twenty animal species between the 1970s and 1990s and the precursors of these peptides all have the signal peptide-B-C-A structure (Figure 2.1 A) (Schwabe et al., 1976; Schwabe and McDonald, 1977a; John et al., 1981; Hudson et al., 1984; Evans et al., 1993; Bryant-Greenwood and Schwabe, 1994; Bathgate et al., 2002). The tertiary structure of relaxin was investigated by X-ray crystallography in 1991 and its dimer structure was confirmed (Eigenbrot et al., 1991).

2.1.1.2 Evolution of relaxins in vertebrates

Rising numbers of relaxin or insulin/relaxin-like neuropeptide precursors have been identified in mammals and other vertebrates (Good-Avila et al., 2009; Hoffmann and Opazo, 2011), including INSL3 (Burkhardt et al., 1994a; Zimmermann et al., 1999), INSL4 (Chassin et al., 1995; Koman et al., 1996; Conklin et al., 1999), INSL5 (Conklin et al., 1999; Hsu, 1999), and INSL6 (Hsu, 1999; Kasik et al., 2000; Lok et al., 2000), since the initial discovery of relaxin in 1926 (Hisaw, 1926). Although these more recently identified peptides are named insulin/relaxin-like peptides (INSL), they are more closely related to relaxin from physiological and evolutionary perspectives, as discussed below. Genes encoding relaxin-type peptide precursors have a similar structure with two exons interrupted by an intron, which is situated in the middle of the C chain sequence (Bathgate et al., 2013). Members of the relaxin-type family are all synthesized as a preprohormone, which contains four sequential parts: N-terminal signal peptide, B chain, C chain and C-terminal A chain. The cleavage sites are located at the two ends of the C chain. The bioactive mature relaxin-type peptides are all heterodimers consisting of A and B chains linked via two inter chain disulfide bridges and an intra chain disulfide bridge in the A chain (Steinetz et al., 2009; Bathgate et al., 2013). Moreover, there are characteristic cysteine motifs in the A and B chains, which are CCxxxCxxxxxxxxC or CxxxxxxxxxxxC, respectively (Semmens et al., 2016). The B chain in vertebrate relaxin-like peptides also contains a relaxin-specific receptor-binding motif - RxxxRxxI/V (Bullesbach and Schwabe, 2000; Semmens et al., 2016).

According to phylogenetic and genomic analysis of the predicted relaxin-type neuropeptide precursors, whole genome duplication during early vertebrate evolution gave rise to the diversity of the genes encoding relaxin-type peptides (Yegorov and

Good, 2012; Semmens et al., 2016). It used to be thought that relaxin-3 is the ancestral peptide of the vertebrate relaxin family peptides (Wilkinson et al., 2005). Recently, it was demonstrated that the vertebrate relaxin-type neuropeptide genes are products of an ancestral system that originally consisted of three genes, two of which trace their origins back to the invertebrates (Yegorov and Good, 2012).

2.1.1.3 Physiological roles of relaxins - reproductive and non-reproductive functions

The relaxin-type peptides regulate many physiological processes. Relaxin acts on the cervix, pubic symphysis, vagina, uterus and mammary apparatus, as well as mediating the cardiovascular changes to manage the increased blood volume during pregnancy (Callander and Bathgate, 2010; Klein, 2016). Relaxin softens the cervix (Bathgate et al., 2006), mediates the increased flexibility and elasticity of the interpubic ligament (O'Connor et al., 1966; Steinetz et al., 1983), influences the growth of the vagina (Hall, 1960; Schink and Struck, 1968; Burger and Sherwood, 1995; Zhao et al., 1996; Zhao et al., 2001) and influences uterine contractility (Krantz et al., 1950) and growth (Steinetz et al., 1957) during pregnancy. When it comes to the reproductive physiology of relaxin in males, relaxin is involved in regulation of prostate growth, spermatogenesis, sperm motility and penetration into oocytes (Weiss, 1989; Braun et al., 2015; Elkhawagah et al., 2015). The INSLs are also involved in reproductive processes (Koman et al., 1996), with for example targeted disruption of the *Insl3* gene causing bilateral cryptorchidism (absence of both testes from the scrotum) (Zimmermann et al., 1999). However, relaxin also has non-reproductive physiological functions (Bathgate et al., 2013).

The non-reproductive functions of relaxin include inhibition of inflammation, wound healing, fluid balance and body homeostasis with its ability to reduce matrix synthesis and increase extracellular matrix (ECM) degradation (Samuel et al., 2007; Shabanpoor et al., 2009), regulating the collagenous tissue through its antifibrotic effects (Samuel et al., 2016) and modulating stress responses through interactions with corticotropin releasing factor (Ma et al., 2009; Bathgate et al., 2013). It has been demonstrated that relaxin gene therapy improves diastolic function in pressure-overloaded rats via phospholamban by activating Protein kinase B (Shuai et al., 2016). Relaxins in the nervous system stimulate food intake in male wistar rats (McGowan et al., 2005) and alcohol consumption is increased in relaxin-3 deficient male mice (Shirahase et al., 2016). Moreover, relaxin may contribute to the regulation of the proximal colon motility by the nitric oxide/cGMP/cGMP-dependent protein kinase pathway (Squecco et al., 2015). Recently, it has been reported that relaxin participates in bone remodeling by stimulating the activity of both osteoblast and osteoclasts and facilitates muscle healing by enhancing the recruitment of satellite cells, improving vascular perfusion, inhibiting fibrosis and promoting neo-angiogenesis (Ferlin et al., 2016).

2.1.1.4 G protein-coupled receptors for vertebrate relaxin-type peptides

Four highly conserved family A G protein-coupled receptors (GPCRs), relaxin family peptide receptors 1 - 4 (RXFP1 - 4), mediate the physiological effects of vertebrate relaxin family peptides (Bathgate et al., 2013). RXFP1 (LGR7) and RXFP2 (LGR8), two GPCRs with N-terminal leucine-rich repeats, are the cognate receptors of relaxin-2 and INSL3, respectively. Activation of these receptors leads to generation of second messengers such as cAMP and nitric oxide to activate downstream signaling

pathways. RXFP3 (GPCR135) and RXFP4 (GPCR142) are activated by relaxin-3 and INSL5 to inhibit cAMP production and activate MAP kinases (Bathgate et al., 2013). RXFP1 and RXFP2 both couple to $G\alpha_s$ and to $G\alpha_{OB}$ to exert their effects, but RXFP1 is also able to couple to $G\alpha_{i3}$ to produce a delayed surge in cAMP accumulation. $G\alpha_i$/$G\alpha_O$ proteins are coupled to RXFP3/RXFP4 depending on the cell type the receptor being expressed (Bathgate et al., 2013).

The genes for RXFP1 and RXFP2 are very large, containing 18 exons. A large number of RXFP1 and RXFP2 splice variants have been described (Muda et al., 2005; Scott et al., 2006; Kern et al., 2008) with potential physiological functions as endogenous antagonists (Scott et al., 2005). However, the genes encoding RXFP3 and RXFP4 are intronless and have no splice variants (Bathgate et al., 2013).

2.1.1.5 Expression patterns of relaxin genes in mammals

As mentioned above, relaxin has a variety of roles in reproduction and other physiological processes. Relaxin has been detected not only in reproductive tissues, such as the corpus luteum (Yki-Jarvinen et al., 1983), uterus (Bond et al., 2004), mammary gland, testis and prostate of mammals (Gunnersen et al., 1995; Bathgate et al., 2002), but also in the brain and peripheral tissues such as the heart, kidney, lung, liver and pancreas (Gunnersen et al., 1995) based upon Northern blotting, RT-PCR, southern blotting or immunohistochemistry (Bathgate et al., 2013). Relaxin-3 mRNA is only detected in the brain, especially the nucleus incertus (NI), (Bathgate et al., 2002; Liu et al., 2003; Ma and Gundlach, 2007), but the genes encoding relaxin-1 and 2 are expressed in the ovarian corpus luteum during pregnancy and in the deciduas trophoblast (Hudson et al., 1981; Hudson et al., 1984; Hansell et al., 1991). Moreover,

there is clear level peak during pregnancy of mammals (Bathgate et al., 2006). These expression patterns are consistent with the functions of relaxins.

Turning to the expression of insulin/relaxin-like peptides, INSL3 is highly expressed in the testis Leydig cells of every mammalian species so far examined (Adham et al., 1993; Bathgate et al., 2013; Pitia et al., 2015) and in the ovary as determined by RT-PCR (Tashima et al., 1995; Ivell et al., 1997), Northern blotting (Adham et al., 1993; Burkhardt et al., 1994b; Tashima et al., 1995), *in situ* hybridization (Pusch et al., 1996; Ivell et al., 1997; Balvers et al., 1998; Klonisch et al., 1999; Teerds et al., 1999; Paust et al., 2002) and immunohistochemistry (Balvers et al., 1998; Bamberger et al., 1999; Klonisch et al., 1999; Gnessi et al., 2000; Paust et al., 2002), but in other tissues at much lower levels (Bathgate et al., 2013). The mRNA of INSL4 has been identified in the differentiated syncytiotrophoblast (Laurent et al., 1998), amniotic fluid and maternal serum during normal pregnancy (Mock et al., 1999). The expression of INSL5 has been detected in the rectum, colon, uterine tissue and thymus at high levels (Conklin et al., 1999; Liu et al., 2005) and in the brain and testis (Conklin et al., 1999) at lower levels, by northern blot analysis or RT-PCR. Northern blotting and *in situ* hybridization analysis has shown that INSL6 is highly expressed in human testis (Lok et al., 2000; Lu et al., 2006) and mouse (Kasik et al., 2000) and in other tissues such as kidney, small bowel, heart, brain and thymus but at lower levels (Kasik et al., 2000).

2.1.2 Discovery of relaxin-type neuropeptides in invertebrates

Relaxin and/or insulin/relaxin-like peptides have also been identified in invertebrates. Phylogenetic analysis shows that four putative members (sequence ID 100967, 72897, 74371 and 97394, (Holland et al., 2008)) of the insulin-relaxin

superfamily in the cephalochordate amphioxus belong to the same cluster as vertebrate relaxins but not with the insulin/IGF subfamily (Lecroisey et al., 2015). Amphioxus insulin-like peptide sequences consist of a well-supported group close to both vertebrate insulin and IGFs (Lecroisey et al., 2015). Insulin-like peptides have also been identified in protostomes, including 40 in *Caenorhabditis elegans* (Li C and K, 2008) and 7 in *Drosophila melanogaster* (Brogiolo et al., 2001). However, according to molecular evolution and functional characterization analysis, they are more likely to belong to the insulin/IGF subfamily (Gronke et al., 2010). Relaxin-type neuropeptides have, however, been identified in echinoderms (Mita et al., 2009b; Mita et al., 2015; Haraguchi et al., 2016; Mita and Katayama, 2016; Semmens et al., 2016) and it is these peptides that are the focus of this chapter, building upon the discovery that starfish gonad-stimulating substance is a relaxin-type neuropeptide (Mita et al., 2009b).

2.1.2.1 Starfish gonad-stimulating substance is a relaxin-type neuropeptide

2.1.2.1.1 The discovery of starfish gonad-stimulating substance

The first report of a gonadotropic substance in an invertebrate was the observation of Chaet and McConnaughy (1959) that extracts of radial nerve cords from the starfish *Asterias forbesi* induce shedding of gametes when injected into this species without sex specificity (Chaet and McConnaughy, 1959; Kanatani and Ohguri, 1966). This substance was also found in other starfishes and was named "gamete shedding substance" initially (Chaet and Smith, 1962; Kanatani, 1964). *In vivo* or *in vitro* cross experiments among different starfishes have shown that the substance acts non-species specifically within the same starfish genera (Hartman and Chaet, 1962; Chaet, 1964a; 1966b; a; Kanatani and Shirai, 1967). Some exceptions have been found among different starfish orders, such as the nerve extract of *Asterina* can induce spawning in

Asterias but that of *Asterias* does not work in *Asterina* (Chaet, 1964a; Kanatani, 1973). GSS induces oocyte maturation within the ovary by acting directly on the ovary and diffusing rather slowly within the ovarian tissues (Kanatani, 1964; Kanatani and Shirai, 1969). The active substance was renamed as gonad-stimulating substance (GSS) after further investigation of the GSS mechanism and was characterized biochemically as a peptide hormone (Kanatani and Shirai, 1969; Kanatani and Shirai, 1970).

2.1.2.1.2 The mechanism of starfish gonad-stimulating substance action

With respect to the mechanism of GSS in inducing oocyte maturation and gamete release of the starfish, GSS acts on the follicular cells around the oocyte to stimulate the production of 1-methyladenine (Kanatani, 1983). Then 1-methyladenine induces the synthesis of a third mediator called maturation-promoting factor (MPF), which induces germinal vesicle breakdown and the subsequent processes of oocyte maturation. However, the action of GSS on *Asterina pectinifera* spawning can be antagonized by L-glutamic acid (Ikegami et al., 1967) and asterosaponin A can inhibit 1-methyladenine but not GSS from inducing spawning of isolated ovarian fragment (Ikegami, 1976).

By investigating the concentration of GSS in the coelomic fluid, an annual peak has been observed before spawning (Kanatani and Ohguri, 1966; Kanatani and Shirai, 1969), demonstrating that GSS/RGP acts as hormonal regulator of gamete maturation and release physiologically. The starfish radial nerve cords have been thought to be the source of this hormone to regulate starfish reproduction since it was first reported in 1959 (Chaet and McConnaughy, 1959). But the level of GSS in starfish nerves remains constant throughout the year (Chaet, 1966a; b; Mita, 2013). Is there any substance in the coelom reducing GSS after the breeding season or does the GSS that triggers starfish

spawning come from another tissue? These are questions that will be addressed in experiments reported in this chapter.

2.1.2.1.3 The structural and functional characterization of starfish gonad-stimulating substance

It was proposed that GSS is a polypeptide due to the observation that its activity is destroyed by proteolytic enzymes such as trypsin, chymotrypsin, pepsin and pronase (Kanatani and Noumura, 1962; Chaet, 1964c; Kanatani and Shirai, 1967; Schuetz, 1969). Lots of work has been done to purify this substance (Chaet, 1967; Kanatani and Shirai, 1971) but it was not until 2009 that the molecular identify of GSS was finally determined (Mita et al., 2009b), fifty years after its activity was first reported. Using the Japanese starfish species *Patiria pectinifera* as an experimental system, GSS was purified and identified as a heterodimer comprising two polypeptides - A and B chains. The A and B chains are linked by two disulfide bridges, with the A chain also having a single intramolecular disulfide bridge. Furthermore, the A chain contains a cysteine motif CCxxxCxxxxxxxxC, which is a signature sequence of the relaxin/insulin/IGF superfamily (Mita et al., 2009b). More specifically, phylogenetic sequence analysis revealed that *P. pectinifera* GSS is a member of the relaxin-type peptide subfamily. Therefore, the GSS identified in *P. pectinifera* has been designated as relaxin-like gonad-stimulating peptide (RGP) (Haraguchi et al., 2016). Subsequently, orthologues of *P. pectinifera* RGP (PpeRGP) have been identified in other starfish species, including *Asterias amurensis*, *Asterias rubens* and *Aphelasterias japonica* (Mita et al., 2015; Mita and Katayama, 2016; Semmens et al., 2016). Cross-experiments among different starfish have been performed to test the specificity of RGP identified from *P. pectinifera*, *A. amurensis* and *A. japonica* (Mita et al., 2015; Mita and Katayama, 2016).

AamRGP and AjaRGP can induce oocyte maturation and ovulation in the ovaries of *A. japonica* and *A. amurensis*, respectively. Similar results were obtained in *A. amurensis* and *A. japonica* ovarian fragments after incubation with PpeRGP. However, neither AamRGP nor AjaRGP is active on *P. pectinifera* ovary (Mita et al., 2015; Mita and Katayama, 2016). These results are consistent with the findings of experiments on GSS, as discussed above, that were performed before its molecular identity was determined.

2.1.2.1.4 The expression of starfish relaxin-like gonad-stimulating peptide precursor

It has been found that GSS is present in the ectoneural part of the radial nerve cords, cardiac stomach, tube feet and body wall of starfish (Kanatani and Ohguri, 1966), although it was found to be mainly detected in the neurosecretory granules of the circumoral nerve ring and radial nerve cord based on performic acid-alcian blue, paraldehyde-fuchsin, chromalum-hematoxylin-phloxine and azan staining (Imlay and Chaet, 1967; Atwood and Simon, 1971).

Quantitative PCR revealed expression of RGP in the radial nerve cords, consistent with the original discovery of GSS in this tissue. However, expression was also detected, albeit at much lower levels, in the cardiac stomach and tube feet (Mita et al., 2009a), which suggests that RGP may have non-reproductive functions in starfish. Analysis of RGP expression in *P. pectinifera* at the cellular level, using mRNA *in situ* hybridization techniques, has revealed that it is expressed by a population of cells located in ectoneural epithelium of the radial nerve cords (Mita et al., 2009b). However, a wider analysis of RGP expression in the starfish body using mRNA *in situ* hybridization techniques has, as yet, not been conducted. This is of interest, because it is

not confirmed if the radial nerve cord is the physiological source of RGP that triggers gamete maturation and release in starfish.

2.1.2.2 Identification of two relaxin-type neuropeptide precursor transcripts in the starfish *A. rubens*

Sequencing of the *Asterias rubens* radial nerve transcriptome enabled identification of 40 neuropeptide precursors (Semmens et al., 2016), including two precursors of relaxin-type neuropeptides. The first one was named *A. rubens* relaxin-like gonad-stimulating peptide precursor (AruRGPP), based on its sequence similarity with RGP precursor discovered in *P. pectinifera* (Mita et al., 2009b). AruRGPP is a 109-residue protein (GenBank: KT60172) comprising a 26-residue N-terminal signal peptide followed by a 20-residue polypeptide comprising two cysteine residues (B chain), a 25-residue polypeptide comprising four cysteine residues (A chain) at the C-terminal, and a connecting peptide (C peptide) domain sandwiched between the B and A chain. The second precursor is *A. rubens* relaxin-like peptide precursor 2 (AruRLPP2, GenBank: KT601729), a 119-residue protein with a primary structure similar to AruRGPP. According to the sequences of these two predicted neuropeptides, both the A chains and B chains have the cysteine motifs CCxxxCxxxxxxxxC or CxxxxxxxxxxxC, respectively, which are characteristic of the insulin/insulin-like growth factor (IGF)/relaxin superfamily. So the predicted mature product of AruRGPP and AruRLPP2 are heterodimeric proteins comprising A and B chains, with two inter-chain disulfide bridges and an intra-chain disulfide bridge in the A chain. However, evidence is required to prove the prediction.

2.1.3 Aims and objectives

The aim of the work reported in this chapter was to confirm the sequences of the two *A. rubens* relaxin-type neuropeptide precursors and investigate the expression pattern of these two genes. The sequences of the precursors were determined by cDNA cloning and sequencing and the structures of neuropeptides derived from them were investigated using mass spectrometry. *In situ* hybridization was performed to explore the cellular localization of these two relaxin-type neuropeptide precursors in *A. rubens* and *in vitro* experiments were performed to investigate the actions of AruRGP in *A. rubens*.

2.2 Methods

2.2.1 Animals

Starfish (*A. rubens*) were collected at low tide from the Thanet coast (Kent, UK) or obtained from a fisherman based at Whitstable (Kent, UK). The animals were maintained in a circulating seawater aquarium at ~12^{o}C in the School of Biological and Chemical Sciences at Queen Mary University of London and were fed on mussels (*Mytilus edulis*).

2.2.2 cDNA cloning and sequencing

Two contigs (1122961, 1055767) encoding a 109 residue RGP-type precursor protein (AruRGPP, GenBank: KT601728) and a 119 residue relaxin-like peptide precursor protein (AruRLPP2, GenBank: KT601729), respectively, have been identified via BLAST analysis of *A. rubens* neural transcriptome sequence data using the PpeRGP precursor as a query (Semmens et al., 2016). Here cDNAs encoding AruRGPP and AruRLPP2 have been cloned and sequenced to confirm the contig sequences, which were obtained by assembly of Illumina HiSeq reads, and to obtain templates for probe synthesis.

Total RNA was extracted from radial nerve cords of *A. rubens* using the SV Total RNA Isolation System (Promega) and cDNA was synthesized using the QuantiTect Rev. Transcription Kit (QIAGEN). The cDNAs encoding the entire coding region of the AruRGPP and AruRLPP2 transcripts were amplified by PCR using Phusion high-fidelity PCR master mix (New England Biolabs) with the following oligonucleotide primers: AruRGPP: forward 5'-ATGGCAAACTACCGTCTCAT-3', reverse 5'-GCCACCCATGAAATAGTCAA-3' and AruRLPP2: 5'-

ATGACATCGTGCAGCCAC-3', reverse 5'-TCAGCAAATTCCTGAGTTGGTTA-3', which were synthesized by Sigma-Aldrich.

The PCR products were gel-extracted and purified using a QIAquick gel extraction kit (QIAGEN). Then part of the purified AruRGPP and AruRLPP2 cDNA (7 μL) were cloned into pBluescript SKII (+) vector (Agilent Technologies) separately, which was cut with the EcoRV-HF restriction endonuclease (New England Biolabs) for sequencing.

2.2.3 Analysis of cDNA sequences and genes encoding relaxin-type precursors in starfish

The cDNA sequences of the two *A. rubens* relaxin-type precursors were translated to protein sequences using the ExPASy translate tool (http://web.expasy.org/translate/). SignalP 4.1 (http://www.cbs.dtu.dk/services/SignalP/) was used to predict the signal peptide. Multiple sequence alignment tool T-Coffee (http://www.ebi.ac.uk/Tools/msa/tcoffee/) was used to compare the sequences of the two *A. rubens* relaxin-type neuropeptide precursors with other RGP precursors and A and B chains identified previously in different starfish species (Mita et al., 2009a; Mita et al., 2015; Mita and Katayama, 2016). ClustalW (Thompson et al., 1994) and the neighbor-joining method (Zuckerkandl and Pauling, 1965; Felsenstein, 1985; Saitou and Nei, 1987) in MEGA 7.0.14 (Kumar et al., 2016) were used to investigate the phylogenetic relationships of the starfish relaxin-type precursors with relaxin/insulin/IGF-type precursors from other taxa.

The protein sequences of the AruRGPP and AruRLPP2 were used to identify genes encoding homologous proteins in the *Patiria miniata* genome (http://www.echinobase.org/Echinobase/pm) and the *Acanthaster planci* genome

(http://marinegenomics.oist.jp/cots/viewer/info?project_id=46). Then online gene prediction software FGENESH (http://www.softberry.com/berry.phtml?topic=fgenesh&group=programs&subgroup=gfind) was used to predict the potential open reading frame to find the exon regions, selecting organism-specific gene-finding parameters of *Strongylocentrotus purpuratus*. The related human relaxin/insulin-like neuropeptide precursors were used to search the human genome database (https://www.ncbi.nlm.nih.gov/projects/genome/guide/human/) to identify coding regions and compare the gene structures of the members of this neuropeptide family. Schematic diagrams were prepared using Illustrator for Biological Sequences (IBS, version 1.0.3) software or Photoshop CC (2015.0.0; Adobe Systems, San Jose, CA) running on a MacBook Pro computer (13-inch, with OS X EI Capitan).

2.2.4 Mass spectrometry

Preparation of *A. rubens* radial nerve cord extracts was performed by members of the Elphick research group. Chemical modification and mass spectroscopic analysis of the extracts was performed by Dr Cleidiane G. Zampronio and Dr Alexandra M. Jones at the University of Warwick as described below. More detailed protocols can be found in appendix 9.1 and 9.2.

2.2.4.1 Preparation of *A. rubens* radial nerve cords extracts for mass spectrometry

Extracts of *A. rubens* radial nerve cords were prepared to enable use of mass spectrometry to investigate the presence and structure of AruRGP and AruRLP2 in this tissue. Radial nerve cords were dissected from specimens of *A. rubens* as described previously (Chaet, 1964b) and then transferred into 90% methanol / 9% acetic acid with or without the addition of protease inhibitors (pepstatin A [0.01 mM]; phenylmethylsulfonyl fluoride [PMSF; 0.1mM]). The tissue was sonicated (two 2-min

pulses with 15-sec intervals) and homogenized to lyse cells. The extract was centrifuged (10,000g for 5min at 4^{o}C) and the supernatant transferred to a glass vial. Finally, the solvent was bubbled off using nitrogen gas before being stored at -20^{o}C.

Aliquots of 10 µl of radial nerve extract were diluted using 50 µl of 1mM ammonium bicarbonate (Sigma Aldrich) to neutralize the high concentration of acetic acid used for extraction. Some aliquots were also subject to reduction to break disulfide bridges followed by alkylation of cysteine residues. For reduction, samples were treated with 5 µl of 100mM dithiothreritol (Sigma Aldrich) and heated at 60^{o}C for 15 minutes. Alkylation was performed by adding 5 µl of 200 mM iodoacetamide (Sigma Aldrich) and incubated in the dark at room temperature for 30 minutes. Samples of both reduced/alkylated and nonreduced/nonalkylated material were also digested using 0.5 µg trypsin (Promega) solution and incubated overnight at 37^{o}C, with the digest arrested by addition of 10 µl of 10% formic acid (J.T. Baker, Phillipsburg, NJ).

2.2.4.2 Mass spectrometry procedure

NanoLC-ESI-MS/MS was used to analyze samples of radial nerve extracts, with a 3 µl aliquot of each sample separated by reversed phase chromatography prior to mass spectrometric analysis. Two columns were utilized, an Acclaim PepMap µ-pre-column cartridge (300 µm i.d. x 5mm 5 µm 100 Å) and an Acclaim PepMap RSLC (75 µm x 25cm 2 µm 100 Å) (Thermo Scientific), installed on an Ultimate 3000 RSLCnano system (Dionex, Sunnyvale, CA). Mobile phase buffer A was 0.1% formic acid in water and mobile phase B was 0.1% formic acid in acetonitrile. Samples were loaded onto the µ-pre-column equilibrated in 2% aqueous acetonitrile containing 0.1% trifluoroacetic acid for 8 minutes at 10 µl min^{-1}, after which peptides were eluted onto the analytical column at 300nl min^{-1} by increasing the mobile phase B concentration from 4% B to 25%

over 90 minutes then to 35% B over 10 minutes and 90% B over 5 minutes, followed by a 15-minute re-equilibration at 4% B. Peptides were injected directly from the LC (300nl min^{-1}) via a Triversa Nanomate nanospray source (Advion Biosciences, NY) into a Thermo Orbitrap Fusion (Q-OT-qIT, Thermo Scientific, Pittsburgh, PA) mass spectrometer. Survey scans of peptide precursors from 400 to 1600 m/z were performed at 120K resolution (at 200 m/z) with automatic gain control (AGC) 5 x 10^5. Precursor ions with charge state 2-6 were isolated (isolation at 1.2 Th in the quadrupole) and subjected to HCD fragmentation with normalized collision energy of 35. Tandem mass spectrometry (MS/MS) data were analyzed using the Orbitrap at 30K resolution, AGC was set to 5.4 x 10^4, and the max injection time was 200 ms. Dynamic exclusion duration was set to 60 seconds with a 10ppm tolerance around the selected precursor and its isotopes. Monoisotopic precursor selection was turned on. The instrument was run in top speed mode with 2-second cycles.

2.2.4.3 Mass spectrometry data analysis

Raw data were converted to mascot generic format using MSConvert in ProteoWizard Toolkit (v. 3.0.5759) (Kessner et al., 2008). MS spectra were searched with Mascot engine (Matrix Science, v. 2.4.1) (Nesvizhskii et al., 2003) against a database comprising 40 *A. rubens* neuropeptide precursor proteins (Semmens et al., 2016), all proteins in GenBank from species belonging to the family Asteriidae and the common Repository of Adventitious Proteins Database (http:// www.thegpm.org/cRAP/index.html). Theoretical peptides were generated from a tryptic digestion allowing up to two missed cleavages and variable modifications; carbamidomethyl on cysteine, oxidation on methionine, amidation (by modification of C-terminal glycines), and pyroglutamate (by modification of N-terminal glutamines). A

no-enzyme search was performed for samples not treated with trypsin. Precursor mass tolerance was 10 ppm and product ions were searched at 0.05 Da tolerances. Scaffold (v. Scaffold_4.6.1, Proteome Software) was used to validate MS/MS-based peptide and protein identifications. Peptide identifications were accepted if they could be established at greater than 95.0% probability by the Scaffold Local FDR algorithm. Protein identifications were accepted if they could be established at greater than 95.0% probability and contained at least two identified peptides. Protein probabilities were assigned by the Protein Prophet algorithm (Nesvizhskii et al., 2003). Proteins that contained similar peptides and could not be differentiated based on MS/MS analysis alone were grouped to satisfy the principles of parsimony. Proteins sharing significant peptide evidence were grouped into clusters. The program Stavrox (v. 3.6.0) was used to search for crosslinked spectra (Gotze et al., 2012). Default settings were used except that semitryptic digestion was permitted, disulfide bonds were specified as the crosslinker, and high mass accuracy data were used with precursor mass tolerance of 5ppm and fragment mass tolerance of 15ppm. The full-length AruRGP precursor was used as the reference sequence.

2.2.5 *In vitro* effects of AruRGP and PpeRGP on ovary fragments of *A. rubens*

A. rubens RGP (AruRGP) and *P. pectinifera* RGP (PpeRGP) were synthesized commercially by Peptide Institute Inc. (Osaka, Japan) and their bioactivity was assayed using ovarian fragments from *A. rubens*, as described previously (Shirai, 1986). Modified van't Hoff's artificial seawater (ASW) adjusted to pH 8.2 with 0.02 M borate buffer was prepared (Kanatani and Shirai, 1970) and the ovaries of mature female starfish were excised and cut into small fragments containing only a few lobes using scissors. The ovarian fragments were then incubated in ASW containing synthetic

AruRGP or PpeRGP at a range of concentrations ($5 \times 10^{-8} - 4 \times 10^{-10}$ M) for 1 h. The effective dose for inducing gamete spawning in 50% of ovarian fragments was determined. The data obtained were expressed as means ± SEM for four separate assays using ovaries from different animals and were then analyzed statistically using student's t-tests (Mita et al., 2015).

2.2.6 Localization of relaxin-type neuropeptide precursor transcripts in *A. rubens* using mRNA *in situ* hybridization

2.2.6.1 Preparation of RNA probes

The RNA probes were synthesized by using a PCR method according to protocol that can be found in appendix 9.3.

A pBluescript SKII (+) vector containing the cloned and sequenced AruRGP or AruRLP2 precursor cDNAs were used to synthesize RNA probes. First, a routine PCR was performed using *Taq* DNA polymerase (*Taq* DNA Polymerase with Thermopol Buffer, New England Biolabs) and standard primer M13 (Forward: 5'-GTAAAACGACGGCCAGTG-3', Reverse: 5'-GGAAACAGCTATGACCATG-3', Sigma-Aldrich) to linearize the plasmid and amplify the insert. The PCR product, which included the AruRGP or AruRLP2 precursor cDNA sequence and T3 and T7 RNA polymerase sites, was purified using a QIAquick gel extraction kit (QIAGEN).

RNA probes were synthesized from the PCR product using a digoxygenin (DIG)-labeled nucleotide triphosphate mix (Roche) supplemented with dithiothreitol (Promega), a placental RNase inhibitor (Promega) and RNA polymerases (New England Biolabs), according to the manufacturer's instructions. T3 or T7 RNA polymerase (New England Biolabs) was used for synthesis of the antisense or sense

probes, respectively. Reaction products were digested with RNase free DNase (New England Biolabs) to remove template DNA and then stored at -20^{o}C in 25% formamide made up in 2X saline-sodium citrate (SSC) buffer.

2.2.6.2 Tissue fixation

Specimens of *A. rubens* (diameter 4-6 cm) were fixed in 4% paraformaldehyde (PFA) in phosphate-buffered saline (PBS, pH 7.4) overnight at 4°C. Different protocols (appendix 9.4) were used to prepare paraffin-embedded sections or frozen sections of fixed tissue.

To prepare specimens for embedding in paraffin wax, fixed starfish were cut with scissors to separate the five arms from the central disk region. Tissues were washed in autoclaved PBS for 10 min and then transferred to Morse's solution (10 % sodium citrate; 20% formic acid in autoclaved water) for decalcification (typically 3 h for arms and 8 h for central disk). Then tissues were washed in distilled water for 10 min and dehydrated through a graded series of ethanol (50%, 70%, 90%, 3 x 100%; 30 min for each step). After clearing in xylene (1 x 5 min and 1 x 8 min) (VWR Chemicals), the tissue was incubated in molten paraffin wax (3 x 1 h) in an oven at ~58^{o}C. The tissue was embedded in wax using L-shaped brass molds and stored at room temperature for sectioning.

To enable visualization of the pigmented eye spot located at the tips of the arms, frozen sections of arm tips were also prepared because the pigment is lost with the wax embedding method. After fixation, arm tips were washed in PBS (3 x 5 min) and then cryoprotected by incubation in sucrose solutions of ascending concentration (10%, 20%, 30% sucrose for 3 h each step, at room temperature). The arm tips were embedded in

RA Lamb OCT embedding cryoembedding Matrix (Fischer Scientific) and immediately frozen on dry ice.

2.2.6.3 Tissue sectioning

The arms and central disks from at least three starfish were embedded in wax and sectioned (12 μm) using a Leica RM2145 microtome and then the sections were placed on poly-L-lysine coated slides (Polysine®; VWR) covered with dH_2O. After about 10 minutes, the excess dH2O was removed and the slides were left to completely dry for further usage. The arm tips placed into frozen embedding matrix were cut into 12 μm thick serial sections by using Leica CM3050 S cryomicrotome. The sections were placed on poly-L-lysine coated slides (Polysine®; VWR) and stored at -20 ^{o}C until used for mRNA *in situ* hybridization.

2.2.6.4 Probe hybridization and immunodetection

To increase adherence of sections, slides with paraffin wax embedded sections were placed in the oven at 65 ^{o}C for 45 min followed by 15 min at room temperature to cool down. Slides were then incubated in xylene (3 x 7 min) (VWR Chemicals) to remove the wax and rehydrated through a descending ethanol series (2 x 7 min 100%, 1 x 7 min 90%, 1 x 7 min 70%, 1 x 7 min 50%, 1x 7 min 30%). The slides were then washed in PBS (2 x 7 min) and post-fixed in 4% PFA/PBS for 20 min at room temperature. Following washes in PBS/0.1% Tween-20 (National Diagnostics) (3 x 5 min), sections were incubated at 37 ^{o}C for 12 min in Proteinase K (QIAGEN) solution at a concentration of 10 μg/ml in a buffer containing 50 mM Tris-HCl (pH 7.5) and 6.25 mM EDTA. Sections were post-fixed in 4% PFA/PBS for 5 min at room temperature and washed in PBS/0.1% Tween-20 (National Diagnostics) (3 x 5 min). Sections were then acetylated for 10 min in 1.325% triethanolamine (pH 7-8) (VWR Chemicals), 0.25%

acetic anhydride (VWR Chemicals) and 0.175% acetic acid (VWR Chemicals) made up in distilled water, with continuous stirring. After washes in PBS/0.1% Tween-20 (2 x 5 min) (National Diagnostics) and 5X SSC (5 min) at room temperature, slides were pre-hybridized in hybridization buffer (50% formamide (Amresco, Inc.); 5X SSC; 500 µg/ml yeast total RNA (Sigma-Aldrich); 50 µg/ml heparin (Sigma-Aldrich); 0.1% Tween-20 (National Diagnostics) in distilled water) in a humid chamber for 2 hours. Hybridization was performed overnight in a humid chamber at 65^{o}C by incubation of slides in hybridization buffer containing 800 ng/ml of denatured DIG-labeled mRNA antisense or sense probes (100 µl per slide) with a coverslip made of Parafilm (Bemis Company, Inc.).

The following day the slides were incubated in 5X SSC with slight shaking until the parafilm coverslip had floated off. Then slides were washed in 0.2X SSC (2 x 40 min at 65^{o}C followed by 10 min at room temperature) followed by buffer B1 (10 mM Tris-HCl, pH 7.5; 150 mM NaCl in autoclaved water) for 10 min at room temperature. After blocking slides with 5% goat serum (Sigma-Aldrich)/B1 buffer in a humid chamber for 2 hours at room temperature, slides were incubated with alkaline phosphatase (AP)-conjugated anti-DIG antibody (Roche) at 1:3000 dilution in 2.5% goat serum (Sigma-Aldrich)/B1 buffer in a humid chamber overnight at 4^{o}C.

On the third day, slides were washed in B1 buffer (3 x 5 min at room temperature) followed by buffer B3 (100 mM Tris-HCl, pH 9.5; 100 mM NaCl; 50 mM $MgCl_2$ in distilled water) for 10 min at room temperature. Alkaline phosphatase substrate was prepared in buffer B3 by adding 4.5 µl/ml of nitro-blue tetrazolium chloride (NBT) (Amresco, Inc.) stock solution (75 mg/ml) in 70 % dimethylformamide (Avantor formerly Mallinkrodt Baker) and 3.5 µl/ml of 5-bromo-4-chloro-3'-

indolyphosphate p-toluidine (BCIP) (Panreac AppliChem) stock solution (50 mg/ml in 70% dimethylformamide) and applied to slides (500 µl per slide). Slides were then incubated in a humid chamber and checked regularly. Once strong staining was observed, the reaction was terminated by washing slides in distilled water (3 x 5 min). Slides were then dried on a hotplate and then incubated in 100% ethanol (2 x 10 sec) followed by clearing in HistoClear® (National Diagnostics) for 2 x 7 min. Finally, slides were mounted with HistoMount™ (National Diagnostics) and cover-slipped.

The method used for mRNA *in situ* hybridization on sections of frozen tissue was the same as described above but with the following modifications. The initial oven-drying, dewaxing and hydration steps were not necessary, so these steps were omitted and instead slides were dried at room temperature prior to washing in PBS (2 x 7 min). Following staining of sections, slides were mounted with an aqueous mounting medium (Hydromount; Natural Diagnostics) and cover-slipped. Mounted slides were left at room temperature to dry for 1-2 hours and then stored kept at 4 ^{o}C.

2.2.7 Immunohistochemistry using monoclonal antibody 1E11

To facilitate interpretation of the expression pattern of AruRGP transcripts in starfish arm tips revealed using mRNA *in situ* hybridization methods, adjacent frozen sections were processed for immunohistochemical analysis using monoclonal antibody 1E11, which was generously provided by Dr. Robert D. Burke (University of Victoria, Canada; RRID AB_2617214). 1E11 is a neuron-specific antibody to synaptotagmin B and is a marker of neural structures in echinoderms, including starfish (Burke et al., 2006; Saha et al., 2006). Importantly, the specificity of 1E11 for synaptotagmin B has been demonstrated by Western blot analysis of radial nerve extracts from the sea urchin Strongylocentrotus purpuratus and comparison of immunostaining patterns observed

with 1E11 and with antibodies to *S. purpuratus* synaptotagmin B. Further evidence of the specificity of 1E11 has been obtained by comparison of the distribution of 1E11 immunoreactivity with the distribution of synaptotagmin B mRNA in sea urchin revealed using mRNA *in situ* hybridization methods (Burke et al., 2006).

For immunohistochemistry with monoclonal antibody 1E11, starfish arm tips were lightly fixed (up to 30 minutes in 4% PFA/PBS; pH 7.4) because immunostaining with the 1E11 antibody is fixation-sensitive (R.D. Burke, pers. commun.). Frozen sections of starfish arm tips mounted on slides were washed in PBS and then incubated for 20 minutes in PBS containing 1% hydrogen peroxide to quench endogenous peroxidases. Following washing with PBST, slides were blocked with 5% goat serum/PBST for 2 hours at room temperature. The slides were then incubated overnight at 4^{o}C with the 1E11 antibody, diluted 1:3 with 5% goat serum/PBST. After washing with PBST, slides were then incubated for 3 hours at room temperature with goat-antimouse horseradish peroxidase conjugated secondary antibodies immunoglobulins (Jackson ImmunoResearch, West Grove, PA) diluted 1:500 in PBST containing 2% goat serum. After washing in PBST, staining buffer (0.05% diaminobenzidine, 0.05% nickel chloride, 0.015% hydrogen peroxide in PBS) was applied to each slide until staining was observed. Slides were washed sequentially in PBS and autoclaved water and then coverslips were mounted using Hydromount (Natural Diagnostics). Detailed protocol can be found in appendix 9.6. Photographs of immunostained sections and adjacent sections processed for AruRGP mRNA *in situ* hybridization were obtained as described below.

2.2.8 Documentation and data analysis

Photographs of sections were captured with a QIClick™ CCD Camera (01-QICLICK-R-F-CLR-12; QImaging) linked to a DMRA2 light microscope (Leica), using Volocity® v.6.3.1 image analysis software (Perkin-Elmer) running on an iMac computer (27-inch with OS X Yosemite, version 10.10). Images were compiled into montages and labeled using Photoshop CC (2015.0.0; Adobe Systems, San Jose, CA), including use of cropping and contrast adjustment tools, running on a MacBook Pro computer (13-inch, with OS X EI Capitan).

2.3 Results

2.3.1 Cloning and sequencing of two *A. rubens* relaxin-type neuropeptide precursors

Two *A. rubens* relaxin-type neuropeptide precursors have been cloned and sequenced, one of which is named as *A. rubens* relaxin-like gonad-stimulating peptide precursor (AruRGPP, Figure 2.2A), a 560 base cDNA encoding a 109 amino acid protein including a 26 amino acid signal peptide followed by the B (20 amino acids), C (38 amino acids) and A chain (25 amino acids). Two putative dibasic proteolytic sites (KR) are located at either end of the C chain, and one more is contained inside the C chain. The other one is called relaxin-like peptide precursor 2 (AruRLPP2, Figure 2.2B), a 360 base cDNA encoding a 119 amino acid neuropeptide precursor with a 30-residue N-terminal signal peptide. AruRLPP2 has a similar structure to AruRGPP, with a B-chain (26 amino acids) following the signal peptide, A chain (26 amino acids) located at the C-terminal and C chain (35 amino acids) sandwiched between the B and A-chains. Two cleavage sites (KR) are predicted between the A/B chains and C chain. Alignment of the AruRGPP, AruRLPP2 with RGP precursors from *A. amurensis* (AamRGPP, GenBank accession number LC040882), *A. japonica* (AjaRGPP, GenBank accession number LC104980), and *P. pectinifera* (PpeRGPP, GenBank accession number AB496611) shows that amino acid sequence identity is mainly conserved in the A and B chains (Figure 2.2C). More specifically, more amino acid residues are shared by these five precursors in the A chain (10) than in B chain (5), with sequence identity of 40% and 25%, respectively.

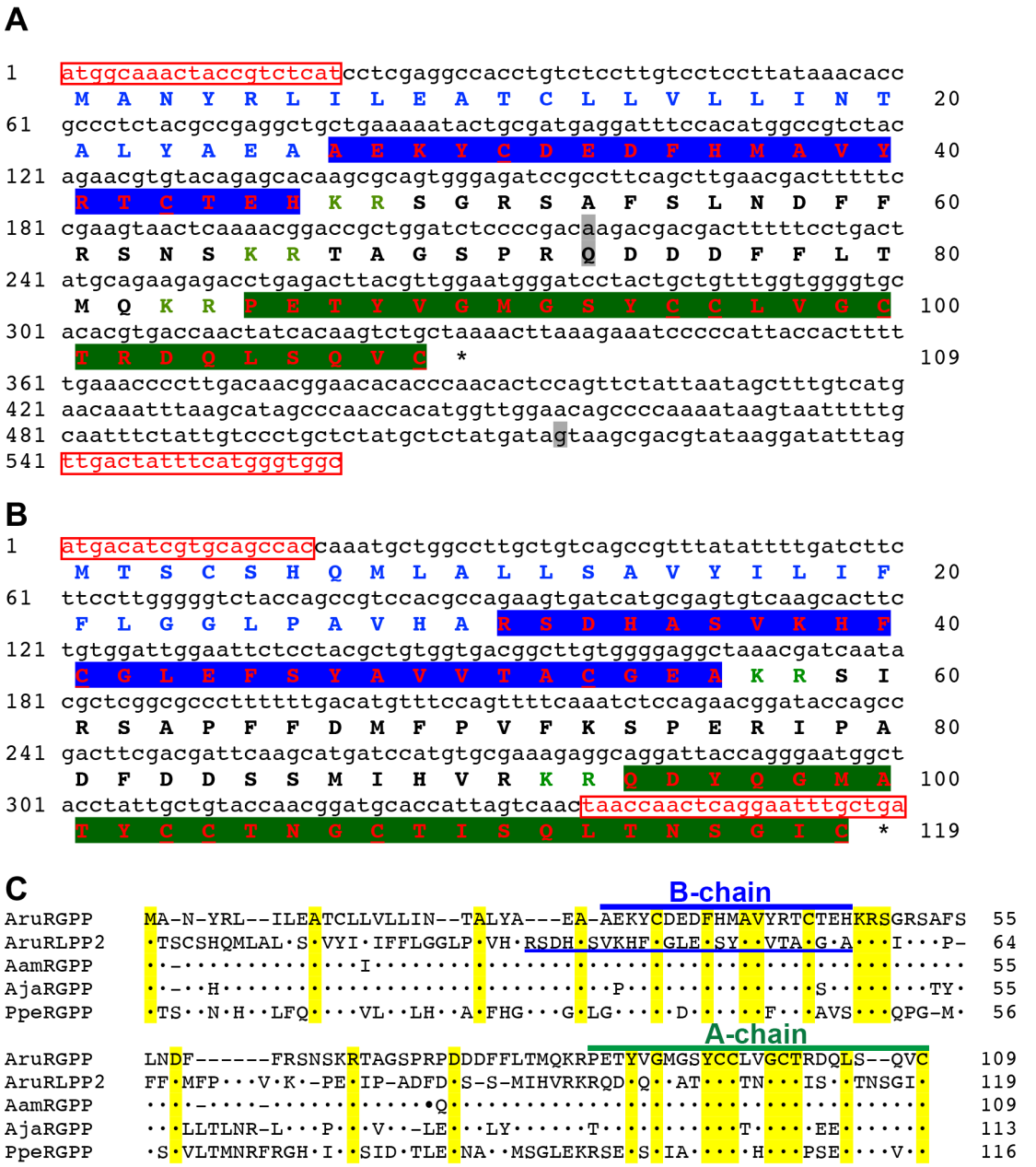

Figure 2.2 *A. rubens* relaxin-like gonad-stimulating peptide precursor (AruRGPP), relaxin-like peptide precursor 2 (AruRLPP2) and comparison with RGP precursors from other starfish species.

A: The AruRGPP cDNA sequence (lowercase, 560 bases) encoding the AruRGP precursor protein (uppercase, 109 amino acid residues) is shown. AruRGP (with cysteine [C] residues underlined) are shown in red, with the A and B chains highlighted in green and blue, respectively. **B:** The AruRLPP2 cDNA sequence (lowercase, 360 bases) encoding the AruRLP2 precursor protein (uppercase, 119 amino acid residues) is shown. AruRLP2 (with cysteine [C] residues underlined) are shown in red, with the A and B chains highlighted in green and blue, respectively. The predicted signal peptide is shown in blue and predicted dibasic cleavage sites are shown in green. Nucleotide sequences that were used as primers for cDNA cloning are shown in red within red boxes and the asterisk shows the position of the stop codon. Nucleotides and amino acids that differ from the previously reported AruRGPP cDNA and protein sequence that was assembled from transcriptome sequence data (GenBank accession number

KT601728; Semmens et al., 2016) are highlighted in gray. **C:** Alignment of the AruRGPP, AruRLPP2 with RGP precursors from *A. amurensis* (AamRGPP, GenBank accession number LC040882), *A. japonica* (AjaRGPP, GenBank accession number LC104980), and *P. pectinifera* (PpeRGPP, GenBank accession number AB496611) using T-Coffee. Regions of the precursors corresponding to the A and B chains are labeled green and blue, respectively. The B chain amino acid residues of AruRLPP2 are underlined. Amino acid residues that are identical in all five precursors are highlighted in yellow.

Alignment the A and B chains of AruRLP2 and RGP from *A. rubens*, *A. amurensis*, *A. japonica* and *P. pectinifera* was performed (Figure 2.3). It was found that the mature RGPs sequences comprising the A and B chains in *A. rubens* and *A. amurensis* (AamRGP) (Mita et al., 2015) are exactly the same (100% identity). AruRGP shares less similarity with *A. japonica* relaxin-like gonad-stimulating peptide (AjaRGP) (Mita and Katayama, 2016) and *P. pectinifera* relaxin-like gonad-stimulating peptide (PpeRGP) (Mita et al., 2009b), 84% and 90% identity for A and B chain of AjaRGP and 58% and 73% identity for A and B chains of PpeRGP. The similarity between AruRGP and AruRLP2 is even lower than that among the RGPs, 50% and 27% for A and B chains, respectively. Compared with AruRGP, the evolutionary relationship between AruRLP2 and other RGPs is more distant. Because the identity between AruRGP and AamRGP is 100%, AruRLP2 shares 50% and 27% identity for A and B chains of AamRGP. But AruRLP2 is more similar to AjaRGP and PpeRGP, 52% and 35% identity for AjaRGP A and B chains and 54% and 32% identity for PpeRGP A and B chains.

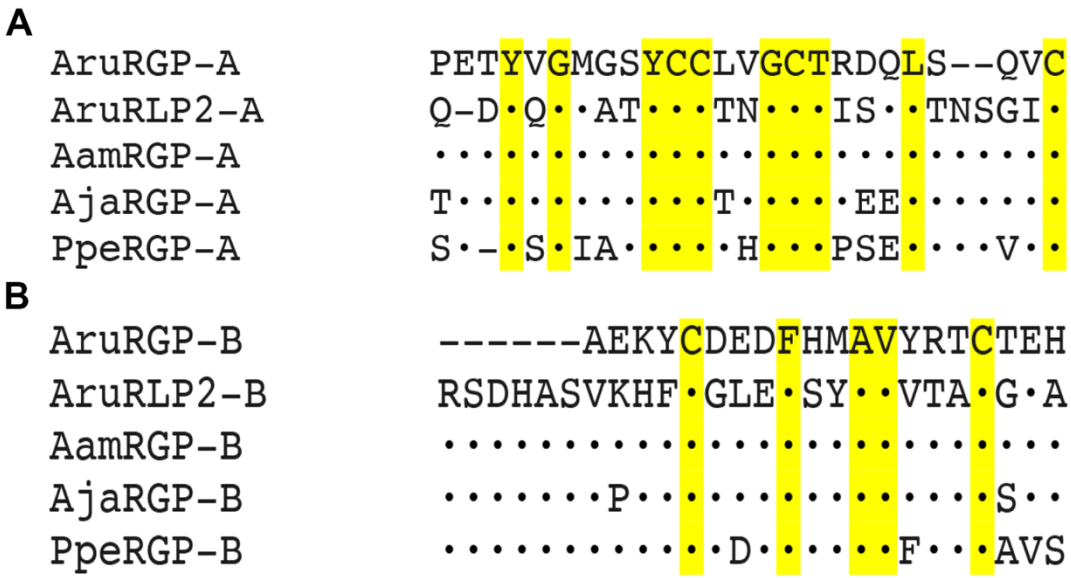

Figure 2.3 Alignment the A and B chains of AruRLP2 and RGP from *A. rubens*, *A. amurensis*, *A. japonica* and *P. pectinifera*.
A: Alignment the A chains of AruRLP2 and RGP from *A. rubens*, *A. amurensis*, *A. japonica* and *P. pectinifera*. Ten amino acide residues (YxGxxxYCCxxGCTxxxLxxxxxC) are conserved among these five sequences, including the CCxxxCxxxxxxxxxxC motif. **B:** Alignment the B chains of AruRLP2 and RGP from *A. rubens*, *A. amurensis*, *A. japonica* and *P. pectinifera*. Amino acid residues that are identical in all five chains are highlighted in yellow. Five amino acide residues (CxxxFxxAVxxxC) are conserved among these five sequences, including the CxxxxxxxxxxC motif.

2.3.2 Phylogenetic and gene structural analysis indicate that AruRGP and AruRLP2 are both relaxin-type neuropeptides

Phylogenetic analysis of the relaxin-type neuropeptide precursors has been performed including several insulins, IGFs, and protostome insulin-like peptide precursors (Figure 2.4). As expected, the phylogenetic tree is divided into two clusters, one containing the relaxin-type neuropeptide precursors and the rest forming another branch. According to the evolutionary tree including AruRLPP2, the RGPPs and RLPP2s from different starfish species and other members of relaxin/insulin/IGF neuropeptide family, AruRLPP2 and the starfish RGPs RLP2s are closer to the relaxin-type neuropeptide precursors. Although RLPP2s belong to same clade as the RGPs, the RGPs are more closely related to each other. AruRLPP2 is located in the same branch

as PmiRLPP2 and AplRLPP2, which is clearly different from the branch made up of the starfish RGPPs. Moreover, within these two branches, the evolutionary relationship of the starfish RGPPs and RLPP2s is consistent with the different orders/families they belong to, *A. rubens* belonging to Order Forcipulatida while *P. miniata* (Family: Asterinidae) and *A. planci* (Family: Acanthasteridae) belonging to the same Order Valvatida but different families.

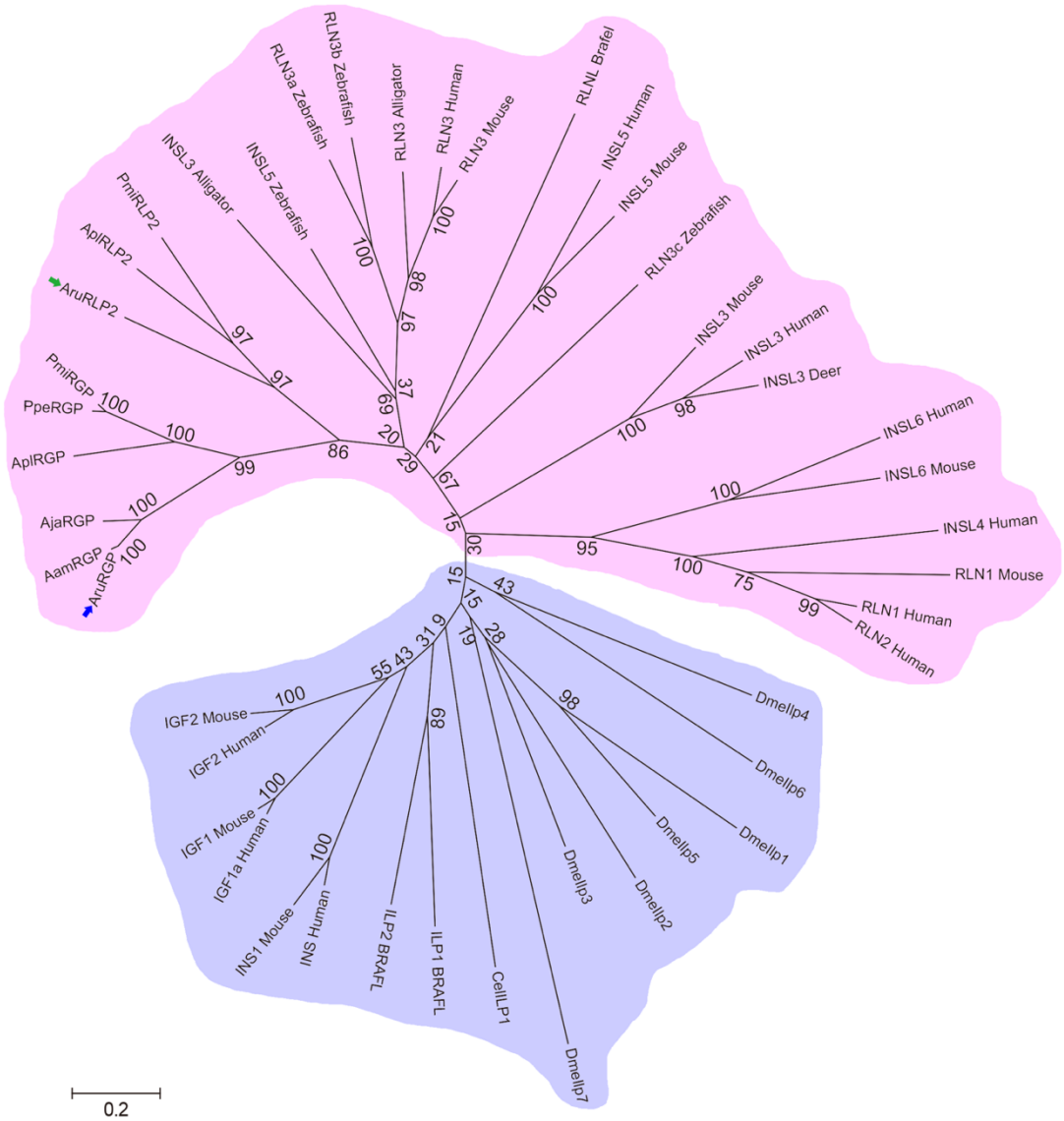

Figure 2.4 Neighbour joining tree showing the relationships of starfish relaxin-type peptide precursors with precursors of other members of the relaxin/insulin/insulin-like growth factor (IGF) peptide family.
The *A. rubens* RGP (AruRGP) precursor (blue arrow) and other starfish RGP precursors form a distinct clade within the relaxin/insulin-like precursor family, which is highlighted in pink to distinguish it from the insulin/IGF precursor family that is

highlighted in purple. A second *A. rubens* relaxin-type precursor (AruRLP2; green arrow) is a paralog of the AruRGP precursor that is also positioned within the relaxin/insulin-like clade of precursors. The starfish RGPs and RLPs form different branches. The full names and accession numbers of the 45 protein sequences included in the tree are as follows: AruRGP, relaxin-like gonad-stimulating peptide (ALJ99970.1, *Asterias rubens*); AruRLP2, relaxin-like peptide precursor 2 (ALJ99971.1, *Asterias rubens*); AamRGP, relaxin-like gonad-stimulating peptide precursor (BAR40315.1, *Asterias amurensis*); AjaRGP, relaxin-like gonad-stimulating peptide precursor (BAU20369.1, *Aphelasterias japonica*); PpeRGP, relaxin-like gonad-stimulating peptide precursor (BAI44654.1, *Patiria pectinifera*); AplRGP, relaxin-like gonad-stimulating peptide precursor (gbr_scaffold8, *Acanthaster planci*); AplRLP2, relaxin-like peptide precursor 2 (gbr_scaffold3, *Acanthaster planci*); PmiRGP, relaxin-like gonad-stimulating peptide precursor (LC057656.1, *Patiria miniata*); PmiRLP2, relaxin-like peptide precursor 2 (this study, *Patiria miniata*); RLN1 Human, relaxin 1 precursor (NP_008842.1, *Homo sapiens*); RLN2 Human, relaxin 2 precursor (NP_604390.1, *Homo sapiens*); RLN3 Human, relaxin 3 precursor (NP_543140.1, *Homo sapiens*); RLN1 Mouse, relaxin 1 precursor (NP_035402.2, *Mus musculus*); RLN3 Mouse, relaxin 3 precursor (NP_775276.1, *Mus musculus*); RLN3 Alligator, relaxin 3 precursor (XP_006023546.1, *Alligator sinensis*); INSL3 Alligator, insulin-like 3 (XP_006017481.1, *Alligator sinensis*); RLN3a Zebrafish, relaxin 3a precursor (NP_001032892.1, *Danio rerio*); RLN3b Zebrafish, relaxin 3b precursor (NP_001108535.1, *Danio rerio*); RLN3c Zebrafish, relaxin 3c precursor (NP_001108525.2, *Danio rerio*); INS Human, insulin precursor (NP_000198.1, *Homo sapiens*); INSL3 Human, insulin-like peptide 3 precursor, (NP_005534.2, *Homo sapiens*); INSL4 Human, insulin-like peptide 4 precursor (NP_002186.1, *Homo sapiens*); INSL5 Human, insulin-like peptide 5 precursor (NP_005469.2, *Homo sapiens*); INSL6 Human, insulin-like peptide 6 precursor (NP_009110.2, *Homo sapiens*); INSL3 Mouse, insulin-like 3 precursor (NP_038592.3, *Mus musculus*); INSL5 Mouse, insulin-like peptide precursor (NP_035961.1, *Mus musculus*); INSL6 Mouse, insulin-like peptide precursor (NP_038782.1, *Mus musculus*); INSL5 Zebrafish, insulin-like 5 precursor (NP_001122028.1, *Danio rerio*); INSL3 Deer, relaxin-like peptide (AAR25542.1, *Capreolus capreolus*); IGF1a Human, insulin-like growth factor 1 precursor (NP_000609.1, *Homo sapiens*); IGF2 Human, insulin-like growth factor 2 precursor (NP_000603.1, *Homo sapiens*); IGF1 Mouse, insulin-like growth factor 1 precursor (NP_001104745.1, *Mus musculus*); IGF2 Mouse, insulin-like growth factor 2 precursor (NP_034644.2, *Mus musculus*); INS1 Mouse, insulin-1 precursor (NP_032412.3, *Mus musculus*); RLNL BRAFL, relaxin-like peptide (EEA41967.1, *Branchiostoma floridae*); ILPl BRAFL, insulin-like peptide 1 precursor ((Mita et al., 2009b), *Branchiostoma floridae*); ILP2 BRAFL, insulin-like peptide 2 precursor ((Mita et al., 2009b), *Branchiostoma floridae*); DmeIlp1, insulin-like peptide 1 precursor (NM_140102.2, *Drosophila melanogaster*); DmeIlp2, insulin-like peptide 2 precursor (NM_079288.3, *Drosophila melanogaster*); DmeIlp3, insulin-like peptide 3 precursor (NM_140103.3, *Drosophila melanogaster*); DmeIlp4, insulin-like peptide 4 precursor (NM_140104.3, *Drosophila melanogaster*); DmeIlp5, insulin-like peptide 5 precursor (NM_206315.2, *Drosophila melanogaster*); DmeIlp6, insulin-like peptide 6 precursor (NM_001201609.1, *Drosophila melanogaster*); DmeIlp7, insulin-like peptide 2 precursor (NM_130714.2, *Drosophila melanogaster*); CelILP1, insulin-like peptide 1 precursor (AF070472.1, *Caenorhabditis elegans*). Bootstrap values for selected nodes are shown.

Homologues of AruRGPP and AruRLPP2, named PmiRGPP (AKZP01031377.1) (Supplementary figure 2.1A), AplRGPP (gbr_scaffold8) (Supplementary figure 2.1B) and PmiRLPP2 (AKZP01053386.1) (Supplementary figure 2.1C), AplRLPP2 (gbr_scaffold3) (Supplementary figure 2.1D), have been identified by analysis of the *Patiria miniata* and *Acanthaster planci* genome sequences, respectively. As shown in Figure 2.5, the relaxin/insulin-like neuropeptide precursors including PmiRGPP, PmiRLPP2, AplRGPP and AplRLPP2 are encoded by two exons, one for the signal peptide, B chain and part of C chain and the other for the rest of the C chain and A chain, while the insulin-like growth factor precursors comprise four exons. The IGF first exon is mainly responsible for the signal peptide. The B chain is encoded by both the second and the third exons and the third exon also includes the A chain region. There are also differences in the relaxin/insulin-like neuropeptide precursors. Human RLN1 and RLN2 have the longest C chains in the precursors selected, and the human INSL5 and RLN3 have the medium sized C chains. These four precursors form two groups, which is consistent with phylogenetic analysis (Figure 2.4).

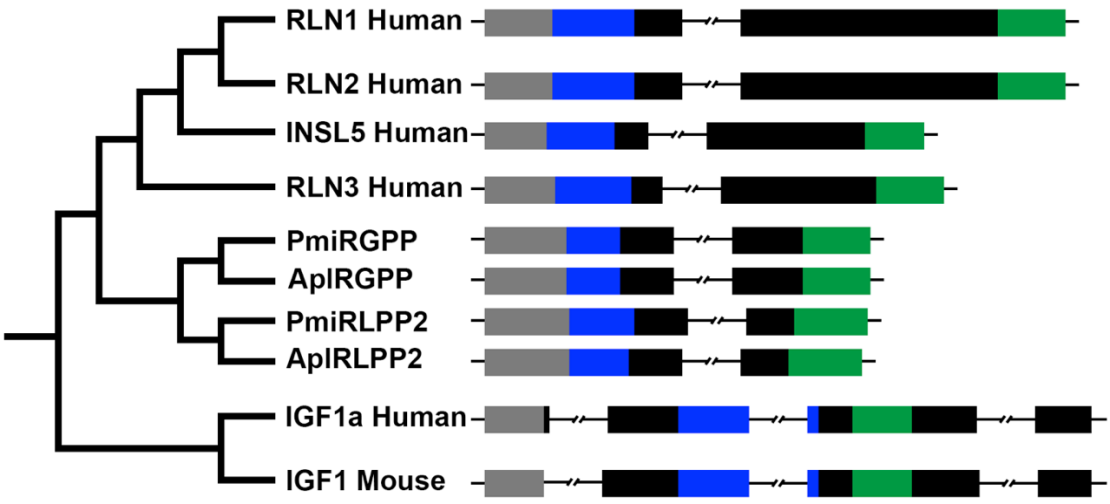

Figure 2.5 A simplified phylogenetic tree of the relaxin/insulin/insulin-like growth factor (IGF) peptide family showing the gene structure of starfish relaxin-like gonad-stimulating peptide precursors and relaxin-like peptide precursor 2 with precursors of other members of this peptide family.

The exons are shown as rectangles with the region encoding the signal peptide in gray, B chain in blue, C chain in black and A chain in green. The introns are shown by uncontinuous black lines. The full names and accession numbers of these 10 protein sequences included in the tree are as follows: PmiRGPP, relaxin-like gonad-stimulating peptide precursor (AKZP01031377.1, *Patiria miniata*); PmiRLPP2, relaxin-like peptide precursor 2 (AKZP01053386.1, *Patiria miniata*); AplRGPP, relaxin-like gonad-stimulating peptide precursor (gbr_scaffold8, *Acanthaster planci*); AplRLPP2, relaxin-like peptide precursor 2 (gbr_scaffold3, *Acanthaster planci*); RLN1 Human, relaxin 1 precursor (NP_008842.1, *Homo sapiens*); RLN2 Human, relaxin 2 precursor (NP_604390.1, *Homo sapiens*); RLN3 Human, relaxin 3 precursor (NP_543140.1, *Homo sapiens*); INSL5 Human, insulin-like peptide 5 precursor (NP_005469.2, *Homo sapiens*); IGF1a Human, insulin-like growth factor 1 precursor (NP_000609.1, *Homo sapiens*); IGF1 Mouse, insulin-like growth factor 1 precursor (NP_001104745.1, *Mus musculus*).

2.3.3 Mass spectrometric detection of AruRGP and AruRLP2 in *A. rubens* radial nerve extracts

To determine if the AruRGP and AruRLP2 precursors (Figure 2.2) are processed to form mature peptides in a manner consistent with other relaxin-type peptides (Figure 2.1B) (Schwabe and McDonald, 1977b; Sherwood, 2004), *A. rubens* radial nerve extracts with and without reduction/alkylation and with and without trypsin digestion were analyzed. The AruRLP2 A and B chains were not detected by mass spectrometry in the radial nerve cord extract sample, which may reflect the expression pattern of AruRLPP2 (2.3.6). Mass spectrometric data were, however, obtained for AruRGP.

In samples subjected to reduction and alkylation, the A chain and B chain of AruRGP were identified by LC-MS/MS, while in the absence of reduction these peptides were not detected, indicating that the A and B chains are linked by disulfide bridges. The A chain (PETYVGMGSYCCLVGCTRDQLSQVC) was observed as 3+ ions (980.75 m/z; Figure 2.6B) and the B chain (AEKYCDEDFHMAVYRTCTEH) was observed as 3+ ions (860.02 m/z; Figure 2.6C) and 4+ ions, with and without oxidized methionine. Although these long and highly charged peptides had significant Mascot scores (Figure 2.6B, C), they fragmented poorly. Therefore, to obtain further

confirmation of the sequences of A chain and B chain peptides, radial nerve extract samples incubated with trypsin were analyzed, which cleaves after lysine and arginine residues to yield peptides that could be completely sequenced using MS/MS. Trypsin was used with or without prior reduction of the peptides and therefore in principle masses and spectra for both disulfide bridge crosslinked and unlinked peptides could be detected under the relevant conditions. In samples subjected to reduction followed by trypsin treatment, the expected fragments of the A chain (PETYVGMG-SYCCLVGCTR [2+ 1055.44; Figure 2.6D]) and B chain (YCDEDFHMAVYR [2+ 541.22; Figure 2.6E]) were detected and sequenced, respectively.

Treatment of non-reduced samples of radial nerve extracts with trypsin would be expected, based on the predicted structure of AruRGP (Figure 2.6A), to produce two dimeric peptides linked by single disulfide bridges. The larger of these predicted peptides comprising the N-terminal region of the A chain (PETYVGMGSYCCLVGCTR) linked to the central region of the B chain (YCDEDFHMAVYR) were unable to be detected. However, the smaller dimeric peptide comprising the C-terminal regions of the A chain (DQLSQVC) and B chain (TCTEH) in two charge states (690.28, 2+ and 460.52 3+) (Figure 2.7) have been detected.

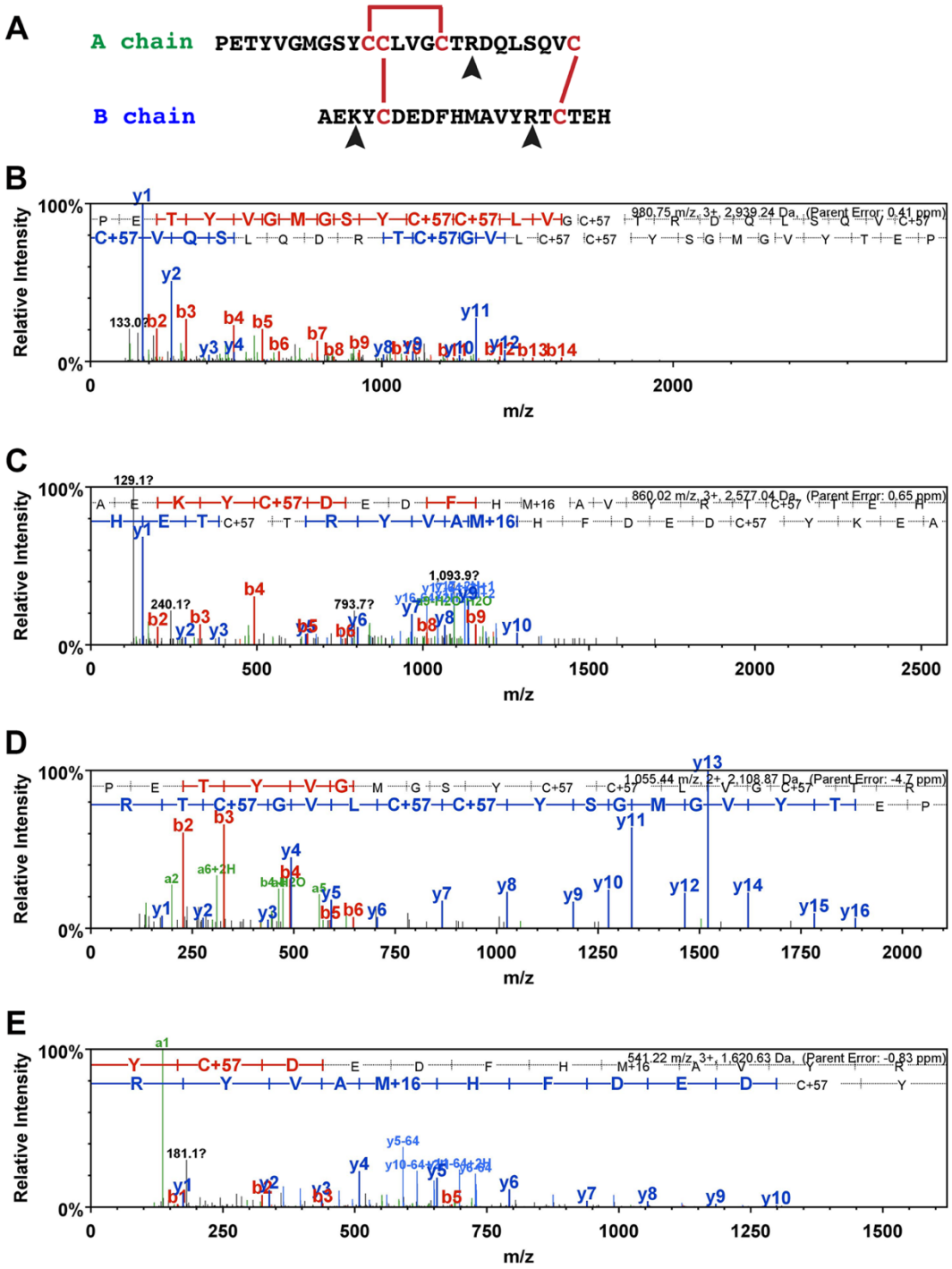

Figure 2.6 Mass spectrometric identification of AruRGP A chain and B chain in extracts of *A. rubens* radial nerve cords.
A: Predicted dimeric structure of AruRGP, showing the sequences of the A chain and B chain. The positions of disulfide bridges are shown with red lines and tryptic cleavage sites are marked with arrowheads. **B, C:** MS/MS data for the A chain and B chain, respectively, from reduced and alkylated samples of radial nerve extract without tryptic digestion. The b series of peptide fragment ions are shown in red, the y series in blue and additional identified peptide fragment ions in green. The amino acid sequence identified in the mass spectrum is highlighted at the top of the figures. C+57 represents cysteine modified by carbamidomethylation and M+16 represents oxidized methionine. The observed m/z of the precursor ion for the A chain

(PETYVGMGSYCCLVGCTRDQLSQVC; B) is 980.75 with a charge state 3+ and an error of 0.41 ppm between the experimentally determined and predicted values (Mascot score = 57). The observed m/z of the precursor ion for the B chain (AEKYCDEDFHMAVYRTCTEH; C) is 860.02 with a charge state of 3+ and an error of 0.65 ppm between the experimentally determined and predicted values (Mascot score = 31). **D, E:** MS/MS data for the complete sequences of fragments of the A chain and B chain, respectively, derived from reduced and alkylated samples of radial nerve extract subjected to tryptic digestion, with annotations in the same format as in B and C. The observed m/z of the precursor ion for the A chain fragment (PETYVGMGSYCCLVGCTR; D) is 1055.44 with a charge state of 2+ and an error of -4.7 ppm between the experimentally determined and predicted values (Mascot score = 98). The observed m/z of the precursor ion for the B chain fragment (YCDEDFHMAVYR; E) is 541.22 with a charge state of 3+ and an error of -0.83 ppm between the experimentally determined value and predicted value (Mascot score = 45).

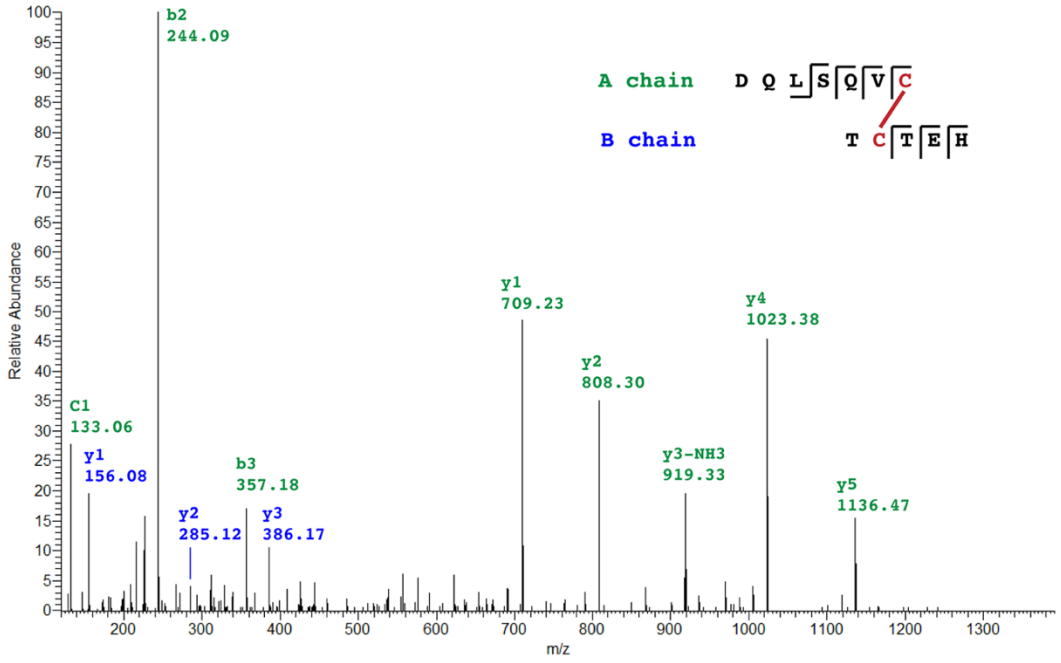

Figure 2.7 Mass spectrometric identification of a dimeric fragment of AruRGP in an extract of *A. rubens* radial nerve cords.
The mass spectrum of a disulfide bridge linked dimeric peptide comprising DQLSQVC from the AruRGP A chain and TCTEH from the AruRGP B chain is shown. This dimeric peptide was detected in samples of radial nerve extract that were subjected to tryptic digestion without reduction. Peptide fragments from the A chain are shown in green and peptide fragments from the B chain are shown in blue. The observed m/z of the precursor ion is 690.28 with a charge state 2+ and an error of -0.73 ppm between the experimentally determined value and predicted value (Stavrox score = 145).

2.3.4 AruRGP is more potent than PpeRGP in causing spawning of ovarian fragments from *A. rubens*

AruRGP and PpeRGP were synthesized to test their effects on *A. rubens* ovarian fragments (Figure 2.8A). AruRGP induced oocyte maturation and ovulation in ovarian fragments from *A. rubens* within 30 minutes (Figure 2.8B), which is consistent with effects of RGPs in other starfish species. PpeRGP cause dose-dependent induction of *A. rubens* ovarian fragment spawning (Figure 2.8C), but the concentration required was much higher than AruRGP. The median effective concentration (EC_{50}) to induce spawning for AruRGP was 1.33 ± 0.09 nM, while it was 14 ± 1 nM for PpeRGP, over tenfold higher. Control tests in which ASW was added to the ovarian fragments did not cause spawning.

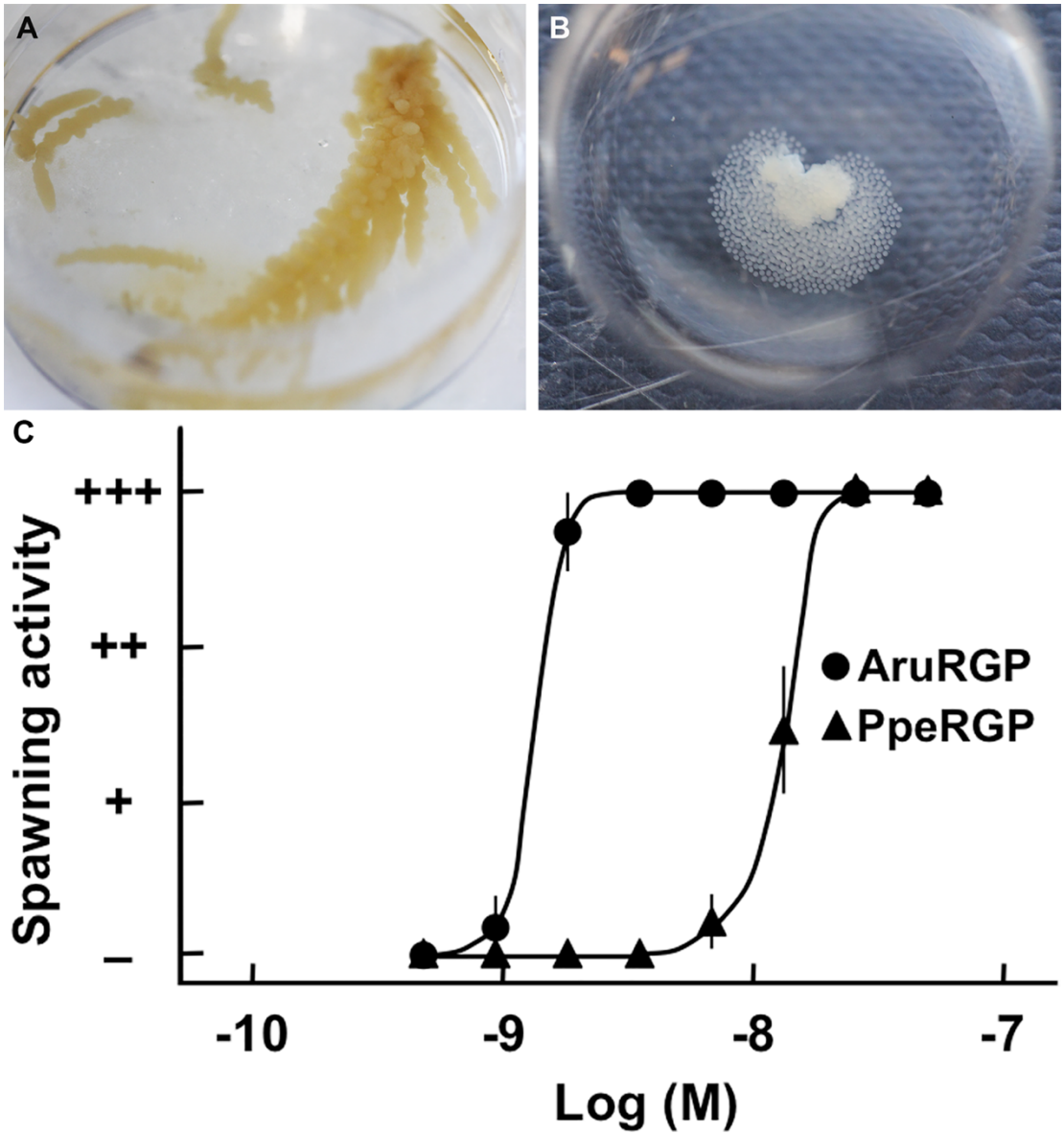

Figure 2.8 Comparison of the *in vitro* bioactivity of AruRGP and PpeRGP as inducers of spawning in *A. rubens*.
A: Isolated ovary from *A. rubens*. **B:** AruRGP-induced spawning of an ovary fragment from *A. rubens*. **C:** Graph showing the dose-dependent effects of AruRGP (●) and PpeRGP (▲) in causing spawning of ovarian fragments. +++ denotes spawning occurred and most of oocytes were matured, ++ denotes about 50% oocytes were matured, + denotes a few oocytes were matured, and - denotes no spawning occurred. Means ± SEM for five separate assays using ovarian tissue from different animals are shown. The median effective concentration (EC_{50}) of AruRGP required to induce spawning (1.33±0.09nM) is approximately 10-fold lower than for PpeRGP (14 ± 1nM).

2.3.5 AruRGPP is expressed by cells in the radial nerve cords, circumoral nerve ring and tube feet in *A. rubens*

According to the *in situ* hybridisation results, limited expression of AruRGP precursor mRNA was detected in the radial nerve cord (Figure 2.9A-D), circumoral nerve ring (Figure 2.9E, F) and tube feet (Figure 2.10). Sense probes were used for control experiments to confirm the specificity of the staining with anti-sense probes (Figure 2.9A inset). Longitudinal and transverse sections were analysed to detect the expression of AruRGP precursor mRNA in the radial nerve cord (Figure 2.9A-D). The transverse sections show two or three stained cells are present on both sides of the "V" shaped radial nerve in the ectoneural region (Figure 2.9A, B). When it comes to the longitudinal sections, dispersed stained cells are mainly present in the epithelium of the ectoneural region along the length of the radial nerve cord, separated by gaps of 20 - 80 μm (Figure 2.9C, D). No staining was detected in the hyponeural region in the transverse or longitudinal sections (Figure 2.9A-D). AruRGPP was also expressed in the circumoral nerve ring (Figure 2.9E, F). Stained cells were only detected in the ectoneural layer of the circumoral nerve ring (Figure 2.9E, F), which is similar to the result in radial nerve cord (Figure 2.9A-D). Stained cells were also observed in the lateral region of the tube feet (Figure 2.10C) proximal to radial nerve cord and circumoral nerve ring and in the subepithelial plexus along the shaft of the tube feet (Figure 2.10A, B) and near the tube foot sucker (Figure 2.10D, E).

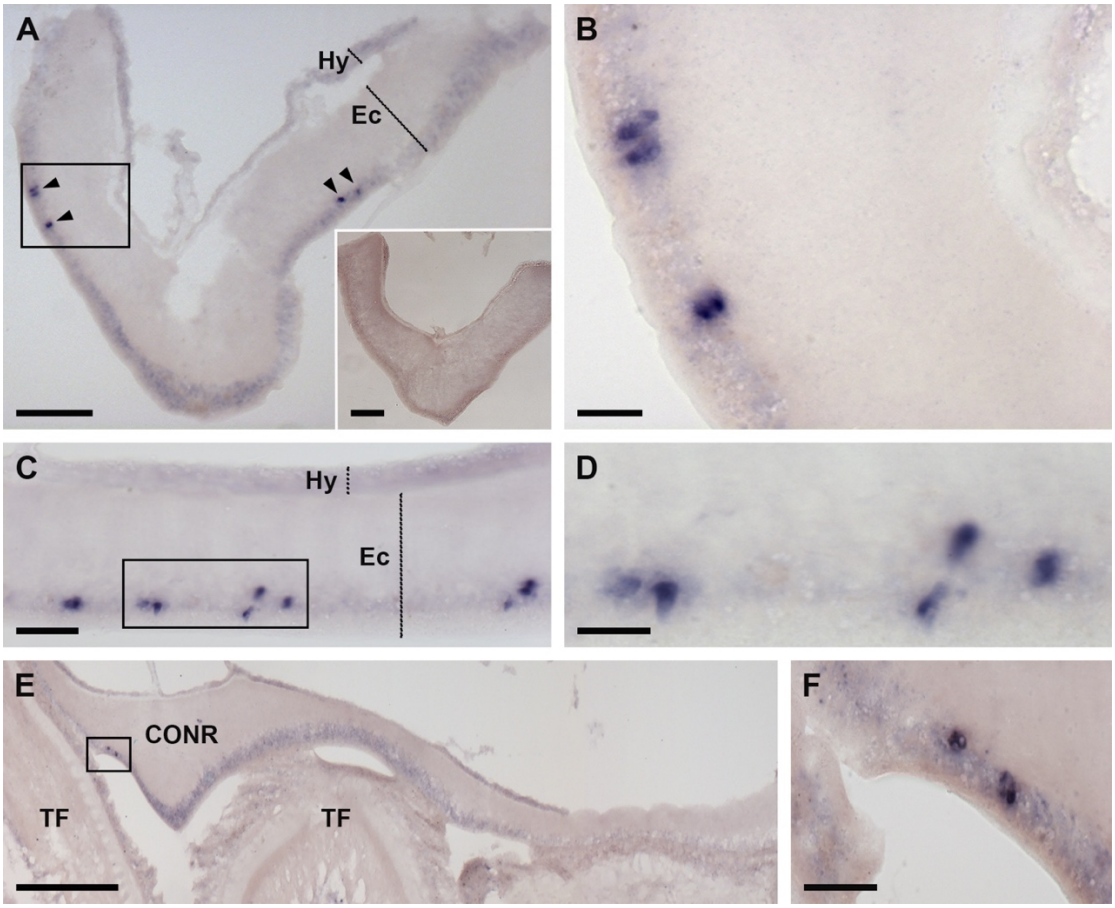

Figure 2.9 Localization of AruRGP precursor mRNA in the radial nerve cord and circumoral nerve ring of *A. rubens* using *in situ* hybridization.
A, B: Transverse sections of radial nerve cord incubated with antisense probes (main panels of A and B) showing a bilaterally symmetrical group of 2-3 stained cells (arrowheads) in the epithelium of the ectoneural region of the nerve cord. Panel B shows a high-magnification view of the rectangular region highlighted in panel A. The inset of panel A shows the absence of staining in a transverse section of radial nerve cord incubated with sense probes, demonstrating the specificity of staining observed with antisense probes. **C, D:** Longitudinal parasagittal sections of the radial nerve cords incubated with antisense probes showing groups of cells interspersed along the length of the nerve cord in the ectoneural epithelium. Panel D shows a high-magnification view of the rectangular region highlighted in panel C. **E, F:** Transverse section of the disk region in *A. rubens* incubated with antisense probes, showing the circumoral nerve ring and tube feet. Stained cells can be seen in the ectoneural epithelium of the nerve cord, highlighted by the rectangle in E and shown at higher magnification in F. CONR, circumoral nerve ring; Ec, ectoneural region of radial nerve cord; Hy, hyponeural region of radial nerve cord; TF, tube foot. Scale bars: 50 μm in A and A inset; 10 μm in B, D; 25 μm in C; 200 μm in E; 20 μm in F. Refer to Figure 1.7 (page 38) and 1.8 (page 39) for details of starfish anatomy.

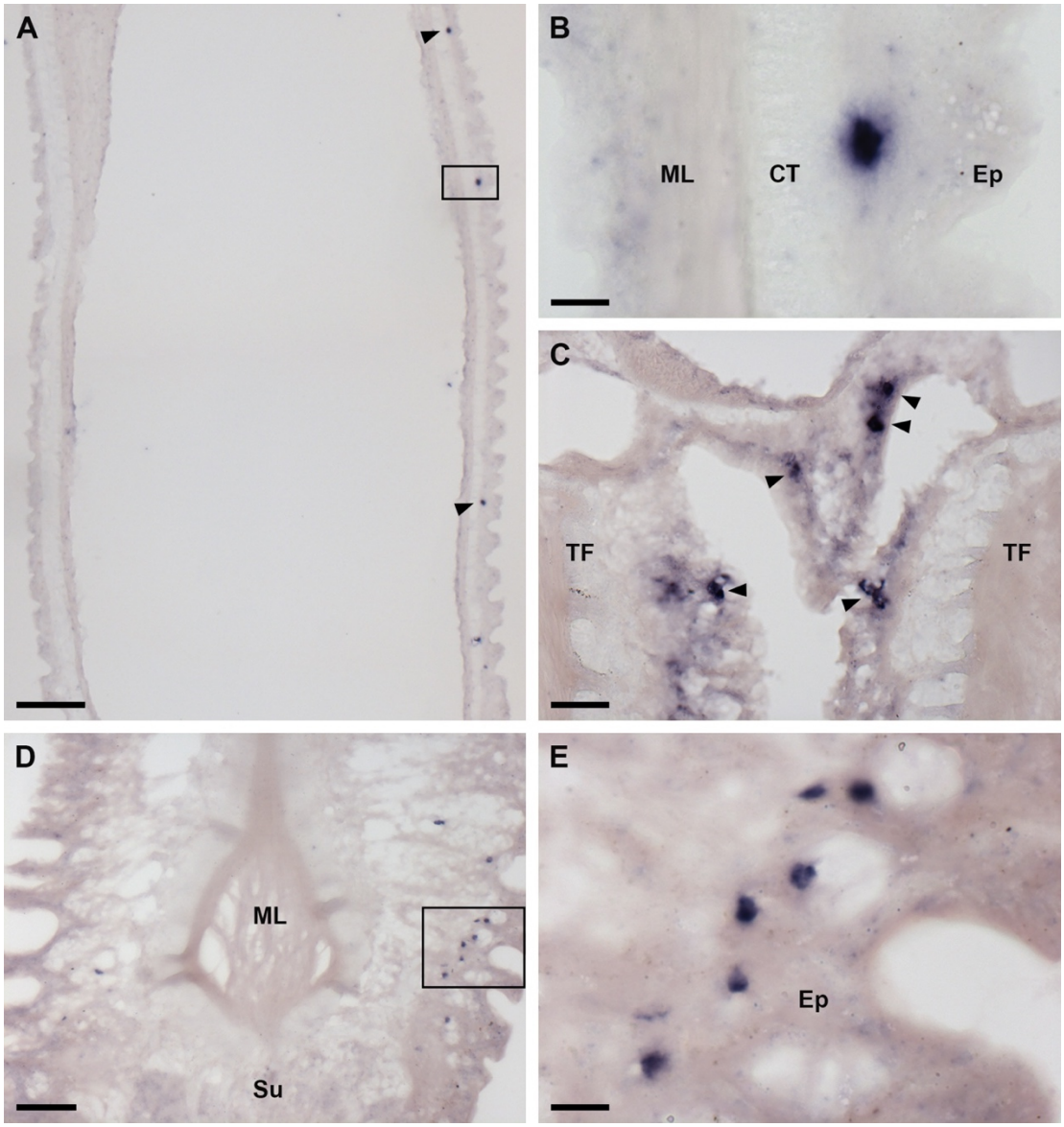

Figure 2.10 Localization of AruRGP precursor mRNA in tube feet of *A. rubens* using *in situ* hybridization.
A: Longitudinal section of a tube foot showing three stained cells (arrowheads and rectangle) in the subepithelial layer of the stem. **B:** The region highlighted with a rectangle in A is shown here at higher magnification, with a stained cell located between the external epithelium and collagenous tissue layer. **C:** Stained cells (arrowheads) located in the subepithelial layer near to the base of adjacent tube feet. **D:** A group of stained cells (see rectangle) in the tube foot subepithelial layer just above the sucker. **E:** The region highlighted with a rectangle in D is shown here at higher magnification. CT, collagenous tissue layer; Ep, epithelium; ML, muscle layer; Su, sucker TF: tube foot. Scale bars: 100 µm in A; 10 µm in B; 25 µm in C; 50 µm in D; 10 µm in E. Refer to Figure 1.7 (page 38) and 1.8 (page 39) for details of starfish anatomy.

2.3.6 Both AruRGPP and AruRLPP2 transcripts are expressed by cells in the arm tip epithelium in *A. rubens*

AruRGPP and AruRLPP2 transcripts share a similar expression pattern in the arm tips of *A. rubens*. These two genes are both highly expressed by neuron-like cells in the starfish arm tips epithelium that surround the terminal tentacle and optic cushion (Figure 2.11-14).

2.3.6.1 The AruRGPP transcript is highly expressed by neurons in the arm tip epithelium of *A. rubens*

The most striking expression of AruRGP transcripts was revealed in the tip regions of the arms (Figure 2.11). To facilitate interpretation of the staining shown in Figure 2.11, a labeled photograph of the arm tip region of a live specimen of *A. rubens* is shown in Figure 2.11A. The most prominent feature of the arm tip is the pigmented optic cushion, which is located at the base of a tube foot-like organ specialized for sensory functions that is known as the terminal tentacle (Figure 2.11A, B). Consistent with expression of AruRGP in tube feet (Figure 2.10), cells expressing AruRGP transcripts were also revealed in the terminal tentacle (Figure 2.11C, D). However, more exten- sive expression of AruRGP is present in the body wall epithelium that lines the cavity containing the terminal tentacle and optic cushion. Here AruRGP-expressing cells are located in the epithelium forming the "ceiling" (Figure 2.11B) and "walls" (Figure 2.11C) of the cavity, extending right up to distal tip of the arm (Figure 2.11E). The staining observed in these cells is not observed in sections of arm tips incubated with sense probes, demonstrating the specificity of the labeling (Figure 2.11E, inset). Observation of clusters of AruRGP-expressing cells in the arm tip body wall epithelium at high magnification revealed a meshwork of stained processes, suggesting that these cells are neurons (Figure 2.11F).

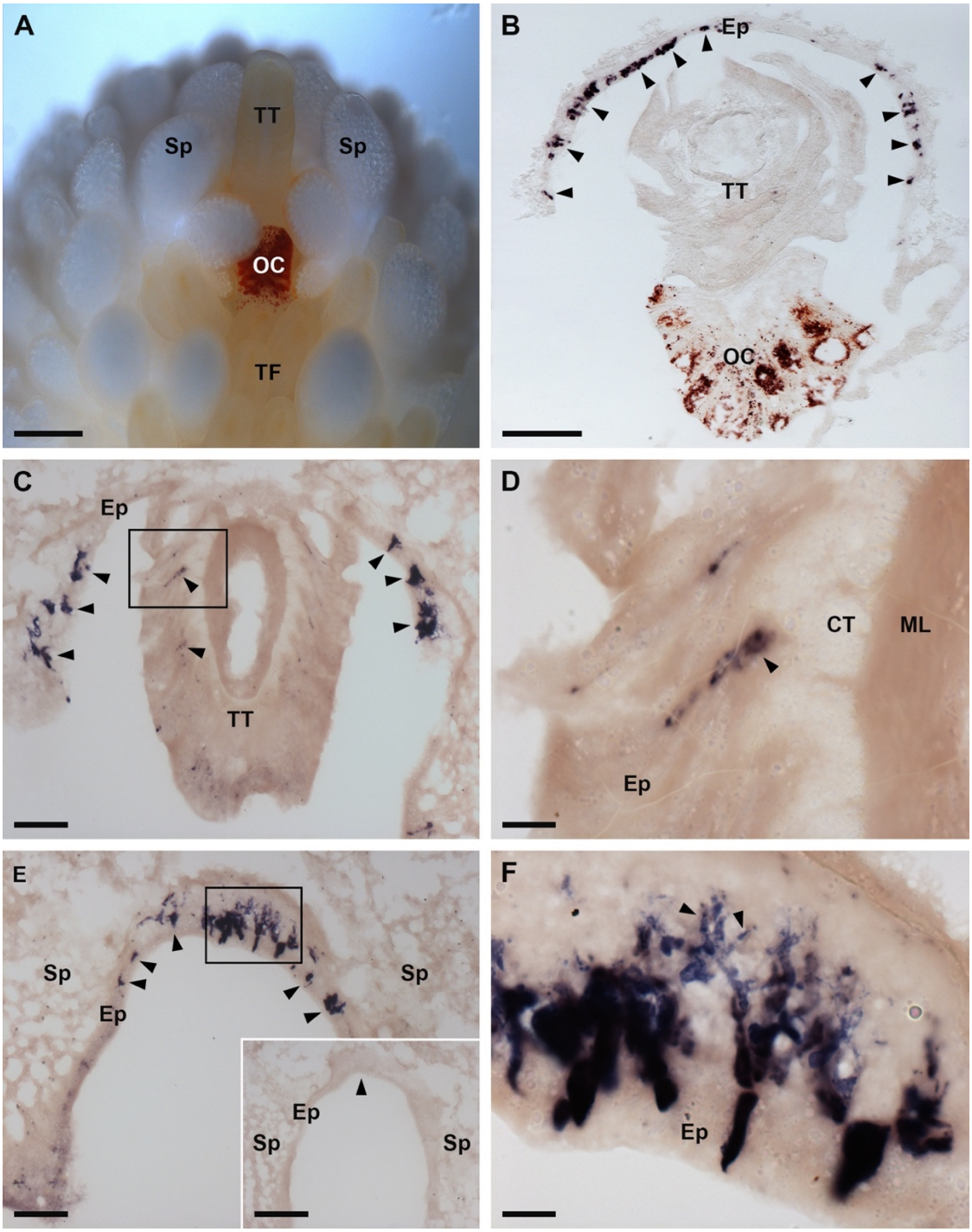

Figure 2.11 Localization of AruRGP precursor mRNA in the arm tips of *A. rubens* using *in situ* hybridization.

A: Photograph of a living specimen of *A. rubens* showing the arm tip region viewed from the underside (oral) of the animal, taken using a Leica DFC420 C camera linked to a Leica S8 APO microscope. The most prominent feature is the pigmented optic cushion, which is located at the base of the terminal tentacle. The terminal tentacle and optic cushion are bounded on each side by spines and rows of tube feet can be seen adjacent to the optic cushion. **B:** Section of the arm tip showing the pigmented optic cushion and terminal tentacle. Stained cells expressing AruRGP precursor transcripts (arrowheads) can be seen in the body wall epithelium lining a cavity that surrounds the terminal tentacle and optic cushion. **C:** Section of an arm tip showing the terminal tentacle cut obliquely. Stained cells can be seen in the terminal tentacle (rectangle and

arrowheads) and in the body wall epithelium at the base of the spines that surround the terminal tentacle (arrowheads). **D:** Detail of the region highlighted with a rectangle in panel C, showing stained cells (arrowhead) in the subepithelial layer of the terminal tentacle. **E:** Section through the distal region of the arm tip beyond the terminal tentacle, showing stained cells (arrowheads and rectangle) in the body wall epithelium at the base of two adjacent spines; the region highlighted with a rectangle is shown in panel F. The inset shows absence of staining (arrowhead) in a section of the arm tip adjacent to the section shown in the main panel and which was incubated with sense probes instead of the antisense probes used in the main panel E. **F:** Detail of the region highlighted with a rectangle in panel E, showing stained cells with processes (arrowheads) at high magnification. CT, collagenous tissue layer of terminal tentacle; Ep, epithelium of body wall; ML, muscle layer of terminal tentacle; OC, optic cushion; Sp, spine; TF, tube foot; TT, terminal tentacle. Scale bars: 400 μm in A; 100 μm in B, E inset; 50 μm in C, E; 10 μm in D, F. Refer to Figure 1.7 (page 38) and 1.8 (page 39) for details of starfish anatomy.

To more specifically investigate if the AruRGP-expressing cells in the arm tip body wall epithelium are neurons, both transverse and longitudinal sections of arm tips were analyzed at high magnification. This revealed example of solitary cells or pairs of cells that clearly have stained processes emanating basally from an intraepithelial cell body (Fig. 2.12A, B). Furthermore, double-labeling experiments using the neural-specific antibody 1E11 revealed a layer of immunostained neural processes immediately beneath the layer of AruRGP-expressing cell bodies in arm tip epithelium (Figure 2.12C-F). Therefore, collectively these observations indicate that AruRGP-expressing cells in the arm tip epithelium are neurons.

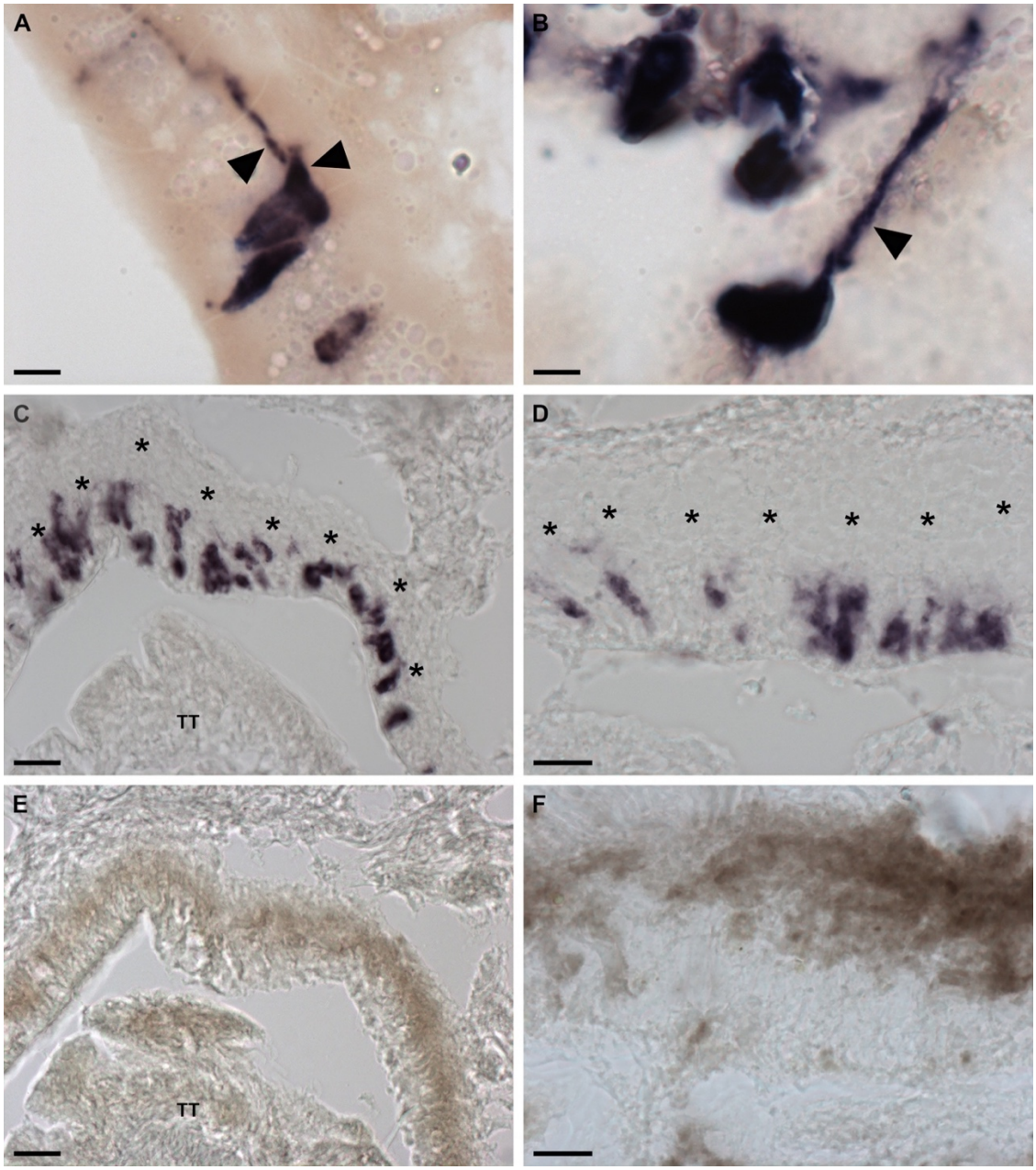

Figure 2.12 Neuron-like characteristics of cells expressing AruRGP in the arm tips of *A. rubens*.

A: Transverse section of *A. rubens* arm tip showing two cells in the body wall epithelium that express the AruRGP precursor, as revealed by mRNA *in situ* hybridization, and that have stained axon-like processes (arrowheads). **B:** Longitudinal section of *A. rubens* arm tip showing a cell in the body wall epithelium that expresses the AruRGP precursor, as revealed by mRNA *in situ* hybridization, and that has a stained axon-like process (arrowhead). **C, D:** Transverse sections of *A. rubens* arm tip showing cells expressing AruRGP precursor transcripts, as revealed by mRNA *in situ* hybridization, in the body wall epithelium lining the cavity that contains the terminal tentacle (TT). **E, F:** Transverse sections of *A. rubens* arm tip adjacent to the sections shown in panels C and D, respectively, showing that the unstained region in panels C and D underlying the AruRGP expressing cells (see asterisks in panels C and D) is immunoreactive with monoclonal antibodies (1E11) to the axonal protein synaptotagmin B. This provides supporting evidence that the AruRGP expressing cells

in the arm tip epithelium are neurons. Scale bars: 5 μm in A, B; 20 μm in C, E; 10 μm in D, F. Refer to Figure 1.7 (page 38) and 1.8 (page 39) for details of starfish anatomy.

2.3.6.2 AruRLPP2 transcript is only detected in the arm tips of *A. rubens*

In situ hybridization was also used to investigate the expression of AruRLPP2 transcripts in *A. rubens*. Although the cDNA of AruRLPP2 was cloned from the radial nerve cord, no signal was detected in the radial nerve cord and circumoral nerve ring. Expression of this precursor was only detected in the arm tips of *A. rubens* (Figure 2.13, 14). AruRLPP2 transcript is expressed not only by the epithelial cells (Figure 2.13, 2.14A, B, D, E) surrounding the terminal tentacle and optic cushion but also by cells in the terminal tentacle (Figure 2.14A, C). Because the neural processes of the epithelial and terminal tentacle cells are all stained by the neural-specific antibody 1E11 (Figure 2.12E, F), the AruRLPP2-expressing cells are likely to be neurons.

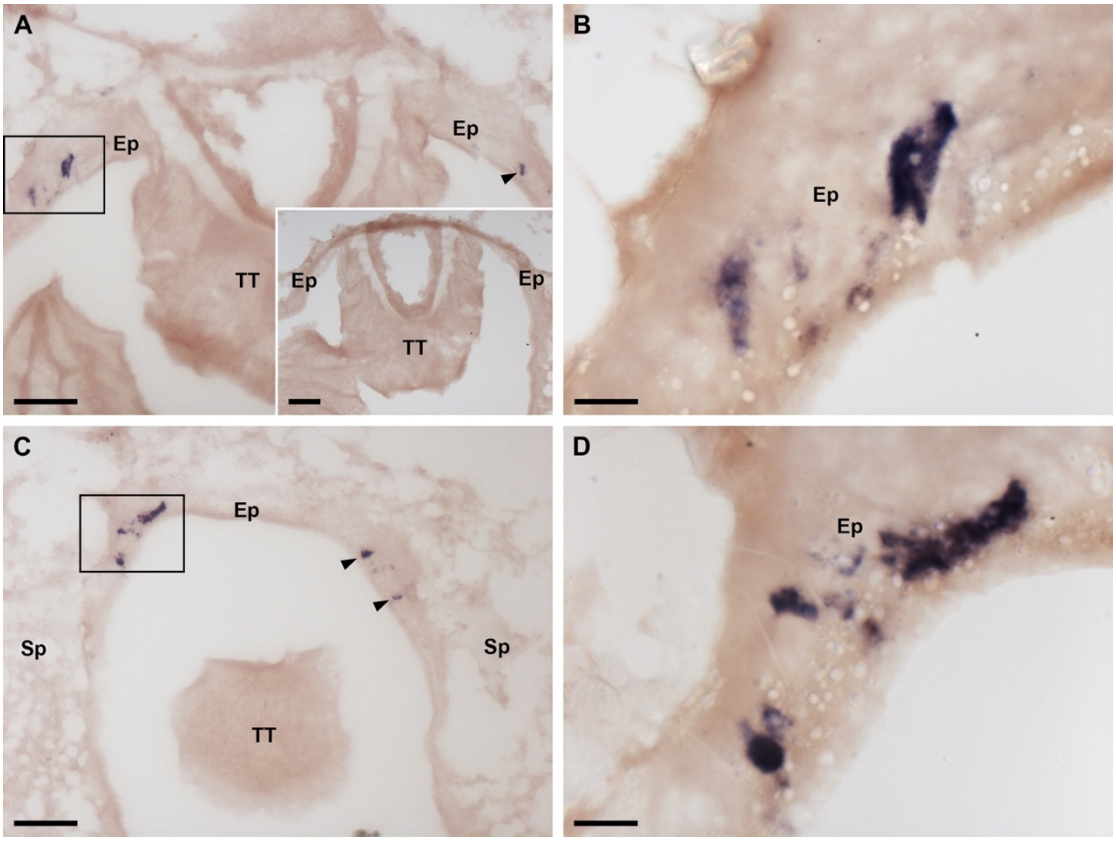

Figure 2.13 Localization of AruRLP2 precursor mRNA in the arm tips of *A. rubens* using *in situ* hybridization with paraffin sections.

A: Section of an arm tip showing the terminal tentacle. Stained cells can be seen in the body wall epithelium at the base of the spines that surround the terminal tentacle (rectangle and arrowhead). The inset shows absence of staining in a section of the arm tip adjacent to the section shown in the main panel and which was incubated with sense probes instead of the antisense probes used in the main panel A. **B:** Detail of the region highlighted with a rectangle in panel A, showing stained cells in the subepithelial layer of the body wall. **C:** Section through the distal region of the arm tip beyond the terminal tentacle, showing stained cells (arrowheads and rectangle) in the body wall epithelium at the base of two adjacent spines; the region highlighted with a rectangle is shown in panel D. **D:** Detail of the region highlighted with a rectangle in panel C, showing stained cells in the subepithelial layer of the body wall at high magnification. Ep, epithelium of body wall; Sp, spine; TF, tube foot; TT, terminal tentacle. Scale bars: 50 µm in A, A inset and C; 10 µm in B, D. Refer to Figure 1.7 (page 38) and 1.8 (page 39) for details of starfish anatomy.

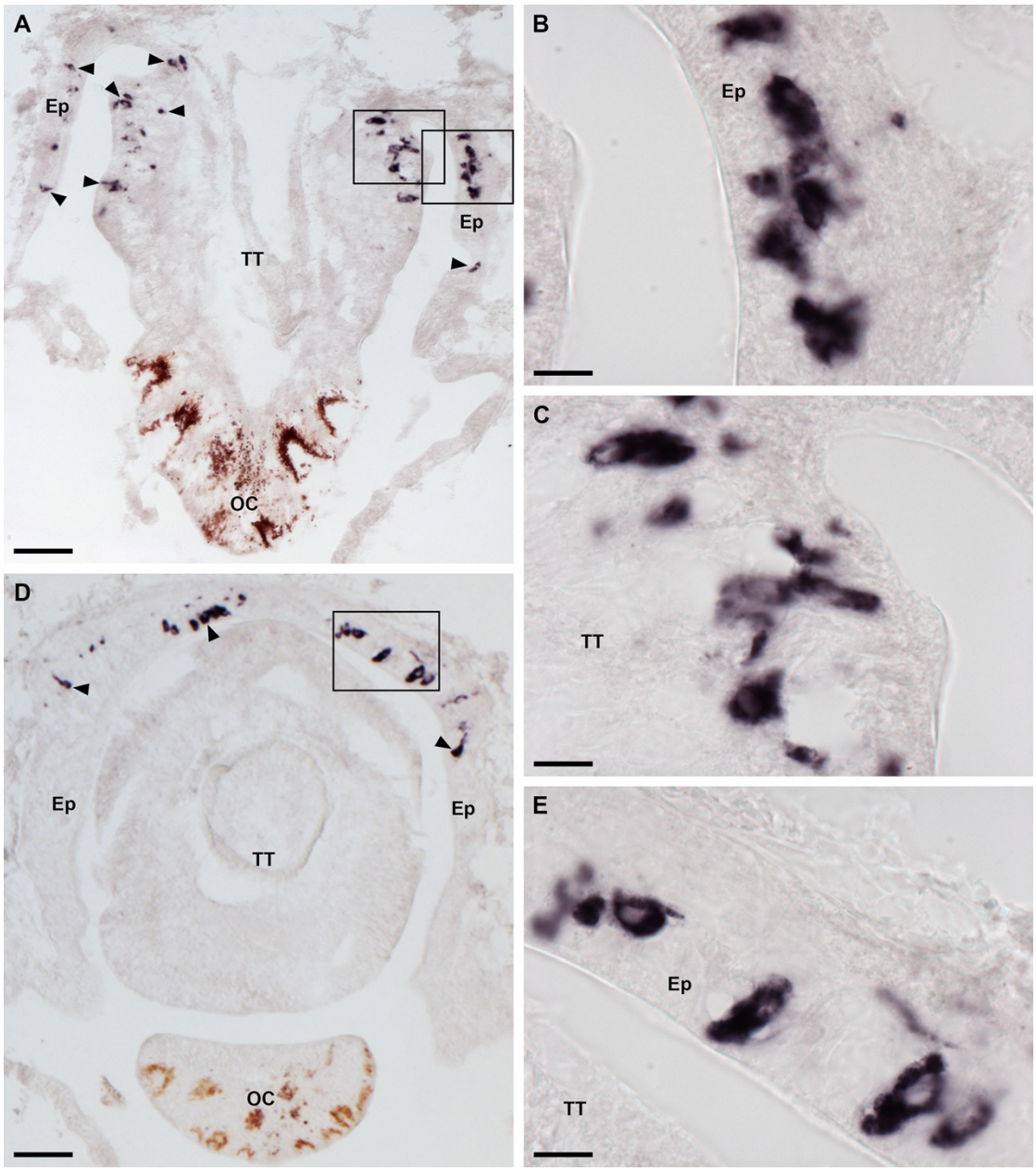

Figure 2.14 Localization of AruRLP2 precursor mRNA in the arm tips of *A. rubens* using *in situ* hybridization with frozen sections.
A: Section of the arm tip showing the pigmented optic cushion and terminal tentacle. Stained cells expressing AruRLP2 precursor transcripts (rectangle and arrowheads) can be seen in the terminal tentacle and body wall epithelium lining a cavity that surrounds the terminal tentacle and optic cushion. **B:** Detail of the region highlighted with a rectangle in panel A, showing stained cells in the body wall epithelium at high magnification. **C:** Detail of the region highlighted with a rectangle in panel A, showing stained cells in the terminal tentacle at high magnification. **D:** Section of the arm tip showing the pigmented optic cushion and terminal tentacle. Stained cells expressing AruRLP2 precursor transcripts (rectangle and arrowheads) can be seen in the body wall epithelium lining a cavity that surrounds the terminal tentacle and optic cushion. **E:** Detail of the region highlighted with a rectangle in panel D, showing stained cells in the body wall epithelium at high magnification. Ep, epithelium of body wall; OC, optic cushion; TT, terminal tentacle. Scale bars: 50 μm in A, D; 10 μm in B, C, E. Refer to Figure 1.7 (page 38) and 1.8 (page 39) for details of starfish anatomy.

2.4 Discussion

The dimeric structure of PpeRGP has been described before by Mita et al in 2009 (Mita et al., 2009b) via inferring the intrachain and interchain disulfide bridges from vertebrate relaxins (Schwabe and McDonald, 1977b; Sherwood, 2004). The fact that monomeric PpeRGP A/B chain or a mixture of these two chains lack gonadotropic bioactivity but synthetic PpeRGP with the predicted dimeric structure has the same effect as RGP purified from radial nerve extract confirmed the correct prediction of the disulfide bonds (Mita et al., 2009b). Here mass spectrometry was used to confirm the presence and sequences of both the A chain and B chain of AruRGP in *A. rubens* radial nerve extracts (Figure 2.6B-E). Furthermore, the presence of one of the two disulfide bridges that link the A chain and B chain was demonstrated (Figure 2.7).

Informed by these findings and the conserved structure of relaxin-type peptides (Schwabe and McDonald, 1977b; Sherwood, 2004), dimeric AruRGP was synthesized with the structure shown in Figure 2.6A. The bioactivity of this synthetic AruRGP as a potent stimulator of spawning from *A. rubens* ovarian fragments was demonstrated here. Furthermore, as was found in a previous study on *A. amurensis* (Mita et al., 2015), AruRGP is 10-fold more potent than PpeRGP, consistent with the differences in the sequences of AruRGP and PpeRGP. Moreover, similar results were found with other cross-experiments using ovarian fragments of *A. amurensis, A. japonica* and *P. pectinifera* to test the specificity of AamRGP, AjaRGP and PpeRGP (Mita et al., 2015; Mita and Katayama, 2016). *P. pectinifera* is a member of the Order Valvatida, while *A. rubens* belongs to the Order Forcipulatida. So starfish RGPs tend to exhibit species specificity, which presumably reflects co-evolution of RGPs and their corresponding receptors (Mirabeau and Joly, 2013).

The AruRLP2 was not detected in radial nerve extracts using mass spectrometry, which may be due to the low expression of this neuropeptide in the radial nerve cords. As the AruRLPP2 expression was only found in arms tips of *A. rubens* by *in situ* hybridization, it would be of interest to test arm tip extracts, especially the area including the terminal tentacle and optic cushion, to check for the presence and sequence of AruRLP2.

The main novel objective of this study was to comprehensively analyze the expression of AruRGP and AruRLPP2 in *A. rubens* using mRNA *in situ* hybridization. Consistent with the original discovery of GSS/RGP in extracts of radial nerve cords (Chaet and McConnaughy, 1959), cells expressing AruRGP transcripts were revealed in the epithelium of the ectoneural region of the radial nerve cords. Along the length of the V-shaped radial nerve cord, two or three stained cells were found in bilaterally symmetrical groups. This is similar to findings in *P. pectinifera*, where four or five bilaterally symmetrical stained cells were observed in the radial nerve cords (Mita et al., 2009b). However, the exact location of the RGP-expressing cells in the radial nerve cord is different in *P. pectinifera* and *A. rubens*. The mRNA of PpeRGPP was detected in the epithelium of ectoneural region, near the bottom of V-shaped radial nerve cord, while AruRGPP expression was observed more laterally on both sides of the radial nerve cord (Figure 2.9A, B). It is not clear whether this difference in location RGP-expressing cells in the radial nerve cord reflect any differences in the functions of RGP in the two species. The circumoral nerve ring, connecting the radial nerve cords in the central disk region of starfish, shows similar AruRGPP expression pattern as in the radial nerve cord.

Previous studies have revealed that GSS/RGP expression/activity is also detected in the cardiac stomach and tube feet of *P. pectinifera*, albeit at much lower levels than in the radial nerve cords (Mita et al., 2009a). In this study, serial sections covering the whole animal were used for mRNA *in situ* hybridization, but no AruRGPP expression was found in the cardiac stomach. This may be because the expression is too low to be detected with the methods or there many be interspecies differences in the RGPP expression patterns. However, cells expressing AruRGPP were found in the sub-epithelium plexus at the base of the stems and along the stem until near the tube foot sucker.

The original discovery of GSS/RGP of starfish (Chaet and McConnaughy, 1959; Mita et al., 2009b) established a hypothesis that the radial nerve cords is the physiological source of GSS/RGP triggerring gamete maturation and release (Chaet, 1966a; Kanatani, 1979; Mita, 2013). Moreover, GSS was thought to be synthesized by supporting cells before the identification of GSS as RGP (Kanatani, 1979). The supporting cells are radial glia-like cells located in the nerve cord extoneural epithelial layer with processes (fibers) extending across the ectoneural neuropile. There was an assumption that GSS are transported along the supporting cell fibers and released as hormones from the inner surface of the radial nerve in the form of secretory granules (Unger, 1962). But histochemical analysis of the radial nerve cords is inconsistent with this hypothesis because supporting cell fibers do not reach as far as the inner surface but terminate as the collagenous tissue boundary between the ectoneural and hyponeural regions of the radial nerve cords (Mashanov et al., 2016). Furthermore, supporting cells are present throughout entire ectoneural region of the radial nerve cords (Mashanov et al., 2016), but only limited numbers of cells express RGPP in *P. pectinifera* (Mita et al., 2009b) and in *A. rubens* (this study). Although there is possibility that certain

supporting cells express RGP, it is more likely that neurons in the radial nerve cords express RGPP. But as with supporting cells, the processes of neuronal cell bodies located in the ectoneural epithelium are confined to neuropile of the ectoneural region (Moore and Thorndyke, 1993; Mashanov et al., 2016), and therefore it is hard to explain how RGP is transported to act as a hormone. The RGPP expression in the tube feet and radial nerve cords may be unrelated to reproduction, with roles in regulation of tube foot activity seeming more likely. Moreover, the concentration of GSS/RGP in the coelomic fluid has a clear annual peak before the spawning (Kanatani and Ohguri, 1966; Kanatani and Shirai, 1969) demonstrating that GSS/RGP acts as hormonal regulator of gamete maturation and release physiologically, while the expression of GSS/RGP in the radial nerve cords remains constant throughout the year (Chaet and Smith, 1962; Chaet, 1966a; Mita, 2013). What then is the source of GSS/RGP as a gonadotropic hormone in starfish if it is not the radial nerve cords?

The most interesting discovery of this study is the detection of RGP expression in *A. rubens* arm tips, which contain two important sensory organs. The terminal tentacle is structurally similar to the locomotory tube feet but with non-locomotory sensory functions (Hennebert et al., 2013). The pigmented optic cushion containing photoreceptive cells at the base of the terminal tentacle works as a simple eye enabling visual orientation (Penn and Alexander, 1980; Garm and Nilsson, 2014). The AruRGP precursor was found highly expressed in the epithelium surrounding the terminal tentacle and optic cushion. This discovery makes the arm tips good candidates as the physiological source of RGP that triggers spawning in response to environmental cues. Furthermore, high magnification images show that RGP expressing cells and processes in the arm tips are neuron-like. However, the sites where RGP may be released from these cells is unknown and to address this issue antibodies against AruRGP should be

produced. An antiserum against PpeRGP has been produced, but it is so specific that AamRGP, an identical RGP to AruRGP, cannot be detected (Katayama and Mita, 2016; Yamamoto et al., 2016). However, the strategy used to develop antibodies to PpeRGP could be applied to AruRGP in the future.

A variety of environmental factors are thought to be important in triggering spawning in starfish (Mercier and Hamel, 2013), including increasing day length (Pearse et al., 1986; Byrne et al., 1997), changes in water temperature (Pearse and Walker, 1986), and the release of gametes by conspecifics (Hamel and Mercier, 1995). The RGP-expressing cells in the arm tips are ideally positioned to detect and integrate such environmental cues, located as they are in the arm tip body wall epithelium and in close proximity to the sensory terminal tentacle and optic cushion. Identification of these cells provides a basis for experimental studies in which their role as putative sources of RGP as a gonadotropic hormone in starfish could be investigated.

In this study, the expression of AruRLPP2 mRNA has also been described (Figure 2.13, 14) and it is similar to that of the AruRGP precursor. Nothing is yet known about RLP2 function. Here, the identification of RLP2-like neuropeptide precursors in *P. miniata* and *A. planci* genome provides evidence that RLP2 is a second relaxin-type neuropeptide not only in *A. rubens* but also in other starfish and potentially in other echinoderms. The discovery and localization of the expression of AruRLP2 in *A. rubens* provides a basis for investigating the physiological roles of a second relaxin-like peptide in starfish.

3 Identification, localization and functional characterization of neuropeptides derived from pedal peptide-like neuropeptide precursor 1 in the starfish *Asterias rubens*

3.1 Introduction

3.1.1 Discovery of pedal peptides in *Aplysia californica* and other mollusks

The isolation and structural identification of neuropeptides was first accomplished through use of bioassays to monitor chromatographic purification of pharmacologically active components in neural extracts (O'Shea and Schaffer, 1985). For example, using this approach the cardioactive neuropeptide FMRFamide was discovered in bivalve mollusks (Price and Greenberg, 1977). A different approach to neuropeptide discovery was adopted by Lloyd and Connolly (1989) - they sought to identify neuropeptides in the mollusk *Aplysia californica* that are synthesized preferentially in particular ganglia. A neuropeptide that is synthesized by cell bodies in the pedal ganglia was purified and sequenced (PLDSVYGTHGMSGFA) and then appropriately named “pedal peptide” (Lloyd and Connolly, 1989).

Immunohistochemical localization of pedal peptide in *Aplysia* revealed that it is synthesized by a population of neurons located mostly in the pedal ganglia with processes projecting peripherally and predominantly innervating the foot (Pearson and Lloyd, 1989; Hall and Lloyd, 1990). Consistent with this pattern of expression, pedal peptide causes an increase in the amplitude and relaxation rate of nerve-evoked contractions of *Aplysia* foot muscle (Hall and Lloyd, 1990). Furthermore, pedal peptide-expressing neurons fire in phase with each pedal wave during locomotor activity and stop firing during defensive contractions of the foot (Hall and Lloyd, 1990). Thus, pedal

peptide-releasing neurons appear to modulate foot muscle contractility during locomotion. However, pedal peptide is not only involved in control of foot activity because pedal peptide-expressing neurons also innervate other organs (e.g. the hermaphroditic duct) (Hall and Lloyd, 1990). Furthermore, sequencing of the *Aplysia* neural transcriptome revealed that pedal peptide is just one of a large family of related neuropeptides in this species, which are derived from four precursor proteins (Moroz et al., 2006).

Multiple pedal peptide-type neuropeptides and precursor proteins have also been identified in other mollusks, including the limpet *Lottia gigantea* (Veenstra, 2010) and the nudibranch *Tritonia diomedia* (Lloyd et al., 1996). Investigation of the pharmacological effects of pedal peptides in *Tritonia* revealed that they cause an increase in the ciliary beat frequency of cells in the pedal epithelium, again providing evidence of a physiological role in regulation of locomotor activity (Willows et al., 1997). Furthermore, immunohistochemical analysis of pedal peptide expression in *Tritonia* indicated roles in a variety of other behavioral activities, including orientation, swimming and feeding (Gaston, 1998; Beck et al., 2000). Accordingly, a pedal peptide was found to cause an increase in the ciliary beat frequency of cells in the salivary duct of *Tritonia*, indicative of a physiological role in regulation of salivary transport associated with feeding (Gaston, 1998).

3.1.2 Discovery of orcokinins in crustaceans and other arthropods

Molluscan pedal peptide-type neuropeptides belong to a family of related neuropeptides that also occur in other phyla, including arthropod orcokinins (Rowe and Elphick, 2012; Jekely, 2013). Orcokinin was first identified in the crayfish *Orconectes limosus* as a neuropeptide (NFDEIDRSGFGFN) that is a potent stimulator of the hind-

gut, enhancing the frequency and amplitude of spontaneous contractions (Stangier et al., 1992). Molecular characterization of orcokinins in the crayfish *Procambarus clarkia* revealed that orcokinin and other orcokinin-like peptides are derived from two closely related precursor proteins - preproorcokinin-A and -B (Yasuda-Kamatani and Yasuda, 2000). Furthermore, orcokinin-type neuropeptides have also been identified in other arthropods, including insects. This has revealed that multiple orcokinin isoforms occur in each species (Pascual et al., 2004) and, as in crustaceans, alternatively-spliced transcripts encoding preproorcokinin-A and -B have been identified in *Drosophila melanogaster* and other insects (Liu et al., 2006; Sterkel et al., 2012; Veenstra and Ida, 2014).

Immunohistochemical investigation of the expression of orcokinins in the crayfish *Orconectes limosus* revealed immunostained cell bodies in the sixth abdominal ganglion with axonal processes that innervate hind-gut muscles, consistent with the myoexcitatory effects of orcokinins on the hind-gut (Dircksen et al., 2000). Orcokinin-expressing neurons have also been mapped in the stomatogastric nervous system of three crustacean species and accordingly orcokinins alter the rhythmic motor output of the stomatogastric nervous system (Li et al., 2002; Skiebe et al., 2002). Thus, orcokinins act as neuromodulators in the central nervous system and the peripheral neuromuscular system of crustaceans.

Immunohistochemical localization of orcokinins in insects has revealed widespread patterns of expression in the brain (Hofer et al., 2005). More specifically, the presence of orcokinin-expressing neurons in a region of the optic lobes known as the accessory medulla was noted because this region of the insect brain houses the master circadian clock that controls circadian locomotor activity. Accordingly, injection of an

orcokinin into the accessory medulla of cockroaches causes a phase-dependent shift in circadian locomotor activity (Hofer and Homberg, 2006). More recent studies on orcokinin function, employing use of RNA interference-based gene knockdown methods, indicate that orcokinins are regulators of "awakening" behavior in the beetle *Tribolium castaneum* (Jiang et al., 2015) and regulators of ecdysis in the kissing bug *Rhodnius prolixus* (Wulff et al., 2017).

3.1.3 Discovery of PP/OK-type neuropeptides in other phyla, including echinoderms

Genome/transcriptome sequencing has enabled the discovery of pedal peptide/orcokinin (PP/OK)-type neuropeptides in other phyla, aside from mollusks and arthropods. Thus, two precursors of multiple pedal peptide-like neuropeptides were identified in the annelid *Capitella teleta* (Veenstra, 2011) and a precursor of orcokinin-like peptides was identified in the tardigrade *Milnesium tardigradum* (Christie et al., 2011). Furthermore, discovery of two genes encoding PP/OK-type precursors in an echinoderm species, the sea urchin *Strongylocentrotus purpuratus*, provided new insights on the evolution of this neuropeptide family (Rowe and Elphick, 2012). These were the first genes encoding PP/OK-type neuropeptides to be discovered in a deuterostome, which was an important finding because it revealed that the evolutionary history of PP/OK-type neuropeptides can be traced back to the common ancestor of protostomes and deuterostomes. Thus far, genes encoding PP/OK-type neuropeptides have not been identified in other deuterostomian invertebrates (i.e. hemichordates, cephalochordates, urochordates) or vertebrates. Therefore, it is possible that within the deuterostomian branch of the animal kingdom PP/OK-type neuropeptides have been retained only in the echinoderm lineage. Interestingly, it was the discovery of PP/OK-

type neuropeptides in *S. purpuratus* that first enabled recognition that molluscan pedal peptides and arthropodan orcokinins are members of the same bilaterian neuropeptide family (Rowe and Elphick, 2012). Hitherto, research on pedal peptides in mollusks and orcokinins in arthropods had been pursued independently without reported recognition that these neuropeptides are related. Furthermore, identification of the PP/OK-type neuropeptide precursors in *S. purpuratus* also facilitated identification of two neuropeptide precursors (NLP14 (GI:392926792), NLP15 (GI:7498042)) in the nematode *Caenorhabditis elegans* (*C. elegans* Sequencing Consortium, 1998) as precursors of PP/OK-type neuropeptides. Thus, neuropeptides from lophotrochozoan protostomes (mollusks, annelids), ecdysozoan protostomes (arthropods, nematodes) and deuterostomes (echinoderms) were unified for the first time as members of a bilaterian family of PP/OK-type peptides (Rowe and Elphick, 2012). Subsequently, the relationship between pedal peptides and orcokinins was demonstrated independently using similarity-based clustering methods (Jekely, 2013).

The discovery of two PP/OK-type neuropeptide precursors (SpPPLNP1 and SpPPLNP2) in an echinoderm, the sea urchin *S. purpuratus*, has provided a basis for investigation of the physiological roles of PP/OK-type neuropeptides in the deuterostomian branch of the animal kingdom. The structures of PP/OK-type neuropeptides derived from SpPPLNP1 and SpPPLNP2 have been determined by mass spectroscopic analysis of extracts of *S. purpuratus* (Menschaert et al., 2010; Rowe and Elphick, 2012). Furthermore, one of the peptides derived from SpPPLNP1 (SpPPLN1c) has been tested for myoactivity on sea urchin tube foot and esophagus preparations, but no effects were observed (Rowe and Elphick, 2012).

A major advance in our knowledge of PP/OK-type neuropeptide function in echinoderms was accomplished recently with the discovery that a myorelaxant purified from the starfish species *Patiria pectinifera* is a member of the PP/OK-type neuropeptide family (Kim et al., 2016). Using the apical muscle of *P. pectinifera* as a bioassay for myoactive peptides, a peptide that causes relaxation of the apical muscle was purified and sequenced (FGKGGAYDPLSAGFTD) and named starfish myorelaxant peptide (SMP). Cloning and sequencing of a cDNA encoding the *P. pectinifera* SMP precursor revealed that it comprises 12 copies of SMP and 3 related peptides (7 copies in total). Furthermore, analysis of the sequence of SMP and the SMP precursor revealed that SMP is a PP/OK-type neuropeptide (Kim et al., 2016). Investigation of the expression of the SMP precursor in *P. pectinifera* using quantitative PCR revealed that it is widely expressed in this starfish species, with the highest levels of expression in the radial nerve cords and lower levels of expression in the apical muscle, tube feet, coelomic lining, cardiac stomach, pyloric stomach and pyloric caeca (Kim et al., 2016). Consistent with this widespread pattern of expression it was found that SMP, in addition to causing relaxation of the apical muscle, also causes relaxation of cardiac stomach and tube foot preparations from *P. pectinifera*. Further insights into the physiological roles of SMP could be obtained by investigating its anatomical pattern of expression in starfish.

In this chapter, the cloning and sequencing of a cDNA encoding the SMP precursor in the common European starfish *Asterias rubens* is reported. This precursor is also referred to as *A. rubens* pedal peptide-like neuropeptide precursor 1 (or ArPPLNP1) because a partial sequence of a second pedal peptide-type precursor has also been identified in *A. rubens* (Semmens et al., 2016). This second precursor was originally named ArPPLNP (Semmens et al., 2016) but henceforth it is referred to as

ArPPLNP2 to distinguish it from the SMP-type precursor ArPPLNP1. A detailed functional characterization of ArPPLNP2 and peptides derived from this precursor is reported in the following chapter (chapter 4).

3.1.4 Aims and objectives

The main aim of the experimental work reported in this chapter was to use mRNA *in situ* hybridization and immunohistochemistry (employing use of novel antibodies) to investigate the expression patterns of ArPPLNP1 and neuropeptides derived from this precursor in *A. rubens*. This is the first study to examine the expression of PP/OK-type neuropeptides at the cellular level in a deuterostome. Informed by the anatomical data obtained, the *in vitro* pharmacological actions of one of the neuropeptides derived from ArPPLNP1 (ArSMP or ArPPLN1b) were also examined. Collectively, the findings reported in this chapter provide new insights into the physiological roles of PP/OK-type neuropeptides in starfish.

3.2 Methods

3.2.1 Animals

Starfish (*A. rubens*) with a diameter > 4 cm were collected at low tide from the Thanet coast (Kent, UK) or were obtained from a fisherman based at Whitstable (Kent, UK). These animals were maintained in a circulating seawater aquarium at ~12 ^{o}C in the School of Biological and Chemical Sciences at Queen Mary University of London and were fed on mussels (*Mytilus edulis*). Smaller juvenile specimens of *A. rubens* (diameter 0.5 - 1.5 cm) were collected at the University of Gothenberg Sven Lovén Centre for Marine Infrastructure (Kristineberg, Sweden) and were fixed in Bouin's solution.

3.2.2 cDNA cloning and sequence analysis

To enable cloning and sequencing of a cDNA encoding an *A. rubens* SMP/PPLNP1-type precursor, *A. rubens* radial nerve cord transcriptome data (Semmens et al., 2016) was analysed using BLAST, with the *P. pectinifera* SMP precursor as a query sequence. A 444 bp *A. rubens* contig (1025452) comprising a partial sequence corresponding to the 3' region of the *P. pectinifera* SMP precursor cDNA was identified. Then ovarian transcriptome sequence data obtained from multiple echinoderm species ((Reich et al., 2015); http://www.echinobase.org/Echinobase/Blasts) was analysed and non-overlapping contigs encoding the 5' region (GAUS01027726.1) and the 3' region (GAUS01027727.1) of a SMP-type precursor transcript was identified from the starfish species *Asterias forbesi.* Combining these partial sequence data from *A. rubens* and *A. forbesi*, primers (forward: 5'-ATGCGGCTCATCATGCAC-3'; reverse: 5'-TACACACCAAGCAGTGACA-3') were designed to enable PCR amplification of the full-length PP/OK/SMP-type precursor coding sequence from *A. rubens*, as described

below. A part of this precursor (477 bases) was cloned and sequenced to provide a template for production of probes used for mRNA *in situ* hybridization (see below). The method employed was the same above but using the following pair of oligo primers: 5'-GCTTCACAGACAAGCGTTT-3' (forward); 5'-TACACACCAAGCAGTGACA-3' (reverse).

The methods used for total RNA extraction, cDNA cloning and analysis were similar to the those reported in chapter 2, with slight modifications. Zero Blunt TOPO PCR cloning kit (Invitrogen, Carlsbad, CA, USA) was used to ligate the PCR product into the pCR-Blunt II with TOPO vector for cloning of a cDNA encoding the complete ArPPLNP1 sequence, while pBluescript II SK (+/–) was used for cloning of a cDNA encoding a partial sequence of ArPPLNP1.

3.2.3 Mass spectrometry

Mass spectrometry was used to determine the structures of neuropeptides derived from ArPPLNP1 by analysis of *A. rubens* radial nerve cords extracted in 90% methanol / 9% acetic acid and then reduced and alkylated, as described in chapter 2. Therefore, here only a short overview of the methods is reported. The pH of the radial nerve cord extract was adjusted using ammonium bicarbonate and the extract was reduced with dithiothreitol (DTT) and then alkylated using iodoacetamide but not treated with trypsin or any other proteolytic enzyme. Samples of the extract were analysed by nanoLC-ESI-MS/MS using an Orbitrap Fusion (ThermoScientific) and data analysis was performed as described in chapter 2, except that more recent versions of Mascot (Matrix Science, London, UK; version 2.5.0) and Scaffold (version Scaffold_4.5.3, Proteome Software Inc., Portland, OR) were used to annotate spectra. Mascot was searched with a fragment ion mass tolerance of 0.050 Da and a parent ion

tolerance of 10.0 PPM. Conversion of Gln to pyro-Glu at the N-terminus, amidation of the C-terminus, oxidation of methionine residues and carbamidomethyl of cysteine residues were specified in Mascot as variable modifications.

3.2.4 Localization of ArPPLNP1 using mRNA *in situ* hybridization

A cDNA encoding a partial ORF (477 bases) was cloned in pBluescript SKII (+) vector and used as a template for production of digoxygenin (DIG)-labeled RNA probes. The methods employed for i) production of anti-sense and sense DIG-labeled RNA probes, ii) preparation of sections of fixed specimens of *A. rubens* and iii) visualization of ArPPLNP1 transcripts in sections of *A. rubens* were the same as those reported in chapter 2.

3.2.5 Localization of ArPPLN1b using immunohistochemistry

3.2.5.1 Production of antibodies to ArPPLN1b

As ArPPLN1b (ArSMP) is the most abundant of the peptides derived from ArPPLNP1 (four out of nine peptide copies) it was selected as an antigen for generation of antibodies to be used for immunhistochemical localization of ArPPLN1-type peptides in *A. rubens*. A peptide comprising the C-terminal twelve amino acid residues of ArPPLN1b with the addition of an N-terminal lysine residue (KGAFDPLSAGFTD) was designed as an antigen (ag) peptide (ArPPLN1b-ag) and synthesized by Peptide Protein Research Ltd. (Hampshire, UK). ArPPLN1b-ag was conjugated to porcine thyroglobulin (Sigma-Aldrich) as a carrier protein, using 5% glutaraldehyde in phosphate buffer (PB, 0.1 M, pH 7.2) as a coupling reagent. Following dialysis in distilled water to remove glutaraldehyde and any uncoupled peptide, the conjugate solution was divided into aliquots containing approximately 50 nmol conjugated antigen

peptide per tube and then frozen. A rabbit was used for antibody production with immunization and serum collection performed by Charles River Labs (Margate, UK) according to the following protocol. On day 0 pre-immune serum was collected and the first immunization (~100 nmol of conjugated ArPPLN1b-ag in Freund's complete adjuvant) was administered. Booster immunizations (~50 nmol of conjugated ArPPLN1b-ag in Freund's incomplete adjuvant) were administered on days 28, 42 and 56). Antiserum samples were collected on days 37 and 51 and a final bleed was collected on day 70.

3.2.5.2 Characterisation of antisera to ArPPLN1b using ELISA

To assess production of antibodies during the immunization protocol and following collection of a terminal bleed, antisera were tested for antibodies to ArPPLN1b-ag using Enzyme-Linked ImmunoSorbent Assays (ELISA) in two formats. Firstly, an assay where a fixed amount of ArPPLN1b-ag peptide (100 µl of 1 µM) was added to each well and then incubated with varying dilutions of pre-immune serum or antiserum (10^{-3} - 10^{-8} diluted in 5% goat serum/PBS; n =2). Secondly, an assay where varying amounts of ArPPLN1b-ag peptide (100 µl; 10^{-6} - 10^{-11} M; n = 2) was added to each well and then incubated with pre-immune serum or antiserum at a fixed dilution of 10^{-4}. For both assay formats the ArPPLN1b-ag peptide was dissolved in carbonate/bicarbonate buffer (25 mM anhydrous sodium carbonate, 25 mM sodium bicarbonate, pH 9.8) and added to wells of a polystyrene microtiter plate (Microlon®; Greiner Bio-One International), which was then covered with Parafilm M® (Starlab) and incubated overnight at 4°C. The following day the liquid contents of the plate were disposed of, the wells were rinsed with 200 µl PBS (3 x 10 min) and the plate was drained on blotting paper. Then 200 µl of a blocking solution containing 5% goat

antiserum/PBS was added to each well and left at room temperature for 2 h. The blocking buffer was discarded and each well was washed with PBS containing 0.1% Tween20 (PBST; 200 µl, 3 x 10 min) and then the plate was drained, as above. Antiserum diluted in 5% goat antiserum (Sigma-Aldrich)/PBS was added to each well and incubated overnight at 4 ^{o}C. The antiserum was discarded and each well was washed with PBST (200 µl; 3 x 10 min) and then the plate was drained. Alkaline phosphatase-conjugated goat anti-rabbit IgG secondary antibodies (Vector Laboratories; diluted 1:3000 in 5% normal goat serum/PBST) were added to each well and incubated for 3 h at room temperature. After washing the plate with PBST (4 x 10 min), 100 µl *p*-Nitrophenylphosphate Alkaline Phosphatase Substrate (pNPP, Vector Laboratories) prepared in carbonate/bicarbonate buffer was added to each well and after a 20 min incubation at room temperature the absorbance at 415 nm was measured using FLUOstar Omega (BMG LABTECH - The Microplate Reader Company). Mean absorbance values were calculated and plotted using Prism 6.0c.

3.2.5.3 Localization of ArPPLN1b in *A. rubens* using immunohistochemistry

For immunohistochemistry, small specimens of *A. rubens* (< 6 cm diameter) were fixed in Bouin's solution (75ml saturated picric acid in seawater, 25ml 37% formaldehyde, 5ml acetic acid) at 4 ^{o}C for 2 days. Fixed starfish were decalcified in 2% ascorbic acid/0.15 M sodium chloride (~ 1 week at 4^{o}C with regular changes of the solution), embedded in paraffin wax, sectioned (8-12 µm) using a Leica RM2145 microtome and mounted on chrome alum-gelatin coated glass slides.

Xylene was used to remove wax from sections (3 x 10 min at room temperature) and then slides were incubated in 100% ethanol (2 x 10 min). The slides were incubated in 1% hydrogen peroxide in methanol for 30 minutes to quench endogenous peroxidase

and then rehydrated through a graded series of ethanol (90%, 70%, 50%; 10 minutes for each) into distilled water. Subsequent steps were the same as those described previously in chapter 2 for immunohistochemistry with 1E11 monoclonal antibodies, with the exception of the primary antibodies (rabbit ArPPLN1b antiserum diluted to 10^{-5} in 5% goat serum/PBST) and secondary antibodies (goat anti-rabbit horseradish peroxidase conjugated immunoglobulins [Jackson ImmunoResearch via Stratech Scientific, Newmarket, Suffolk, UK] diluted 1:500 or 1:1000 in 2% goat serum/PBST) used. Immunostaining was visualised using diaminobenzidine (DAB, VWR Chemicals) and when intense immunostaining was observed, the DAB was washed off with distilled water (10 min). Following dehydration through an ethanol series (50%, 70%, 90%, 2 x 100%; 10 min each), slides were cleared in xylene (2 x 10 min) and mounted with coverslips using DPX Mountant (VWR Chemicals).

To assess the specificity of immunostaining, control experiments were performed where slides were incubated with antiserum pre-absorbed with the antigen peptide. Antiserum pre-absorption was performed by incubating the antiserum diluted to 10^{-4} in PBS with ArPPLN1b-ag (200 μM) for 1-2 h on a rocking shaker at room temperature. Then the pre-absorbed antiserum was diluted ten fold to 10^{-5} in 5% goat antiserum/PBST and tested on starfish sections, as described above.

To facilitate interpretation of immunostaining in some regions of the starfish body, sections adjacent to immunostained sections were stained using Masson's trichrome staining, which differentiates collagenous (blue) from non-collagenous (red) tissue. The method employed for trichrome staining of starfish sections has been described recently (Blowes et al., 2017). The protocol for Masson's trichrome staining can be found in appendix 9.7.

Photographs of immunostained and trichrome stained sections were obtained and assembled into montages, as described in chapter 2. A QIClick CCD Camera (QImaging) linked to a DMRA2 light microscope (Leica) and Volocity v.6.3.1 image analysis software (Perkin-Elmer, Boston, MA) running on an iMac computer (27-inch with OS X Yosemite, v. 10.10) were used to capture the photographs. Images were compiled into montages and labeled using Photoshop CC (2015.0.0; Adobe Systems, San Jose, CA), including use of cropping and contrast adjustment tools, on a MacBook Pro computer (13-inch, with OS X EI Capitan).

3.2.6 *In vitro* and *in vivo* bioassay and pharmacology

3.2.6.1 *In vitro* pharmacology

ArPPLN1b or ArSMP (FGGKGAFDPLSAGFTD) was selected for *in vitro* pharmacological tests because it is the most abundant (4 copies) of the five neuropeptides derived from ArPPLNP1(Figure 3.2). The structure of this peptide having been confirmed by mass spectrometry (Figure 3.3c), it was synthesized commercially by Peptide Protein Research Ltd. (Hampshire, UK). ArPPLN1b was tested on apical muscle, tube foot and cardiac stomach preparations from *A. rubens,* with the SALMFamide neuropeptide S2 (SGPYSFNSGLTF-NH_2) tested as a control peptide that causes relaxation of all three of these preparations (Elphick et al., 1995; Melarange and Elphick, 2003; Kim et al., 2016).

Apical muscles were dissected from the aboral body wall of starfish arms and cut into segments approximately 1 cm in length (Melarange and Elphick, 2003) and cotton ligatures were tied at each end (Figure 3.1a). Tube foot preparations were obtained by dissecting from starfish arms a small square-shaped piece of ambulacral body wall containing a single intact tube foot stem and its associated ampulla. Cotton

ligatures were tied around the body wall and the tube foot sucker, as illustrated previously (Melarange and Elphick, 2003) and Figure 3.1b. Cardiac stomach preparations were dissected as described and illustrated previously (Elphick et al., 1995) and then cotton ligatures were tied around the esophagus and around the aboral region of the cardiac stomach (Figure 3.1c).

Ligatures at one end of the preparation (body wall segment and esophagus for tube foot and cardiac stomach preparations, respectively) were attached to a fixed metal hook in a 20 ml glass organ bath containing artificial seawater at ~11^{o}C. The other ligature was tied to a High Grade Isotonic Transducer (ADinstruments MLT0015) connected to PowerLab data acquisition hardware (ADinstruments PowerLab 2/26). Output from Powerlab was recorded using LabChart (v8.0.7) software installed on a laptop computer (Lenovo E540, Windows 7 Professional).

The resting tension applied to preparations was adjusted to 0.25 g followed by an equilibration period in ASW of ~ 20 min. Then preparations were induced to contract by application of 10 μM acetylcholine (ACh; for apical muscle and tube foot preparations) or ASW containing 30 mM added KCl (cardiac stomach preparations). Once a stable baseline contracted state was reached, synthetic ArPPLN1b or S2 was added to sequentially achieve organ bath concentrations between 10^{-10} M and 10^{-5} M. Cumulative dose-response curves were constructed by expressing relaxation as a percentage reversal of the contraction induced by ACh or KCl. Each peptide concentration was tested on at least five preparations.

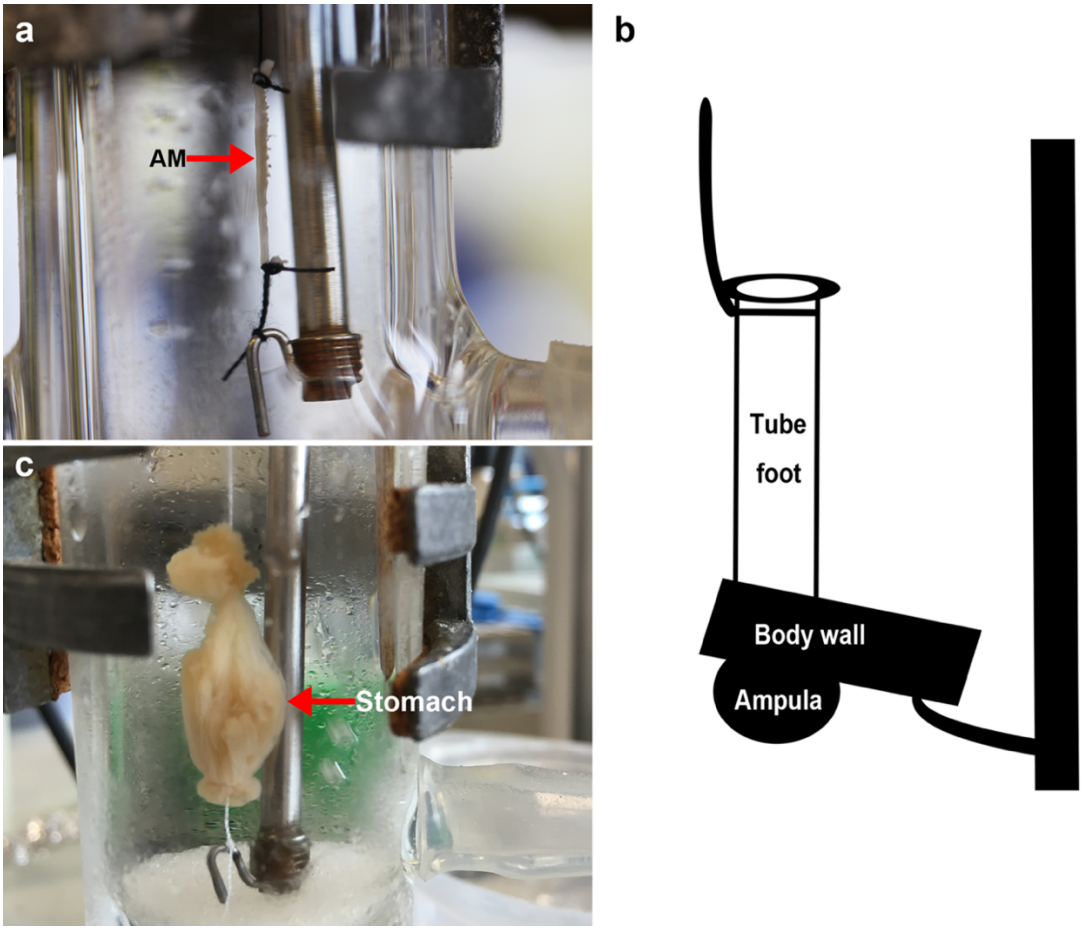

Figure 3.1 Diagram and images showing the *in vitro* preparation of apical muscle (a), tube foot (b) and stomach (c), respectively.
The apical muscle and stomach are highlighted with a red arrow in (a) and (c), respectively.

3.2.6.2 *In vivo* pharmacology

Previous studies have revealed that an ArPPLN1b-like peptide (SMP) causes dose-dependent relaxation of *in vitro* preparations of the cardiac stomach from *P. pectinifera* (Kim et al., 2016). The SALMFamide neuropeptide S2 also causes dose-dependent cardiac stomach relaxation in *A. rubens* (Elphick et al., 1995; Melarange et al., 1999) and in *P. pectinifera* (Kim et al., 2016). Furthermore, consistent with the *in vitro* actions of S2, *in vivo* injection of S2 into *A. rubens* triggers eversion of the cardiac stomach (Melarange et al., 1999). Therefore, here experiments were performed to investigate if injection of ArPPLN1b also triggers cardiac stomach eversion in *A. rubens*, employing the same method as reported previously for tests with S2 (Melarange et al.,

1999). Specimens of *A. rubens* (6 - 12 cm in diameter) were starved for three days and then each starfish was moved one at a time to glass testing tank. Ten starfish were injected with 100 µl of 1 mM ArPPLN1b at two or three sites in the aboral body wall of the arms proximal to the junctions with the central disk region and then were observed. As a positive control experiment ten other starfish were injected with 100 µl of 1 mM S2.

3.3 Results

3.3.1 Cloning and sequencing of a cDNA encoding ArPPLNP1

A cDNA encoding ArPPLNP1 was cloned and sequenced (GenBank accession number KT870153) as shown in Figure 3.2. The ArPPLNP1 transcript is a 948-base cDNA comprising an opening reading frame of 675 bases followed by a 273-base 3' untranslated region (Figure 3.2). ArPPLNP1 is a 224 amino acid protein comprising a predicted 20-residue signal peptide and five putative SMP-like peptides (nine copies in total), which were referred to as ArPPLN1a (16 residues; 1 copy), ArPPLN1b (16 residues; 4 copies), ArPPLN1c (17 residues; 2 copies), ArPPLN1d (18 residues; 1 copy) and ArPPLN1e (13 residues; 1 copy) (Figure 3.2, 3.3a). The C-terminal nonapeptide (DPLSAGFTD) of three of these peptides (ArPPLN1a-c) is identical to the corresponding region of *P. pectinifera* SMP (Kim et al., 2016).

```
  1 atgcggctcatcatgcactctgtggtgctgctactggccgtgatcggtcttagcatggca
    M  R  L  I  M  H  S  V  V  L  L  L  A  V  I  G  L  S  M  A    20
 61 ttaccagctagcaaggattctgaggacaaggagaagctaacagaaaaggaaaaagaagaa
    L  P  A  S  K  D  S  E  D  K  E  K  L  T  E  K  E  K  E  E    40
121 atcttcgaagagtttggtgaagaagatgatggcaaaagagggtttggaatgggtgcatac
    I  F  E  E  F  G  E  E  D  D  G  K  R  G  F  G  M  G  A  Y    60
181 gacccctctcagctggcttcacagacaagcgtttcggcgggaaaggggccttcgaccct
    D  P  L  S  A  G  F  T  D  K  R  F  G  G  K  G  A  F  D  P    80
241 ctctcagctggcttcacagacaagcgttttggcggaaaggggccttcgaccctctctca
    L  S  A  G  F  T  D  K  R  F  G  G  K  G  A  F  D  P  L  S   100
301 gctggcttcacagacaagcgtttcggtggcagtagaggagccttcgaccctctctcagct
    A  G  F  T  D  K  R  F  G  G  S  R  G  A  F  D  P  L  S  A   120
361 ggcttcacagacaagcgttttggcggaaaaggagccttcgaccctctctcagctggcttc
    G  F  T  D  K  R  F  G  G  K  G  A  F  D  P  L  S  A  G  F   140
421 acagacaagcgtttcggcggcagtagaggagccttcgaccctctctcagctggcttcaca
    T  D  K  R  F  G  G  S  R  G  A  F  D  P  L  S  A  G  F  T   160
481 gacaagcgtttcggcgggaaggggccttcgacccgctctcagctggcttcacagacaag
    D  K  R  F  G  G  K  G  A  F  D  P  L  S  A  G  F  T  D  K   180
541 cgaagctttgtacacggcgatttcgaccctcttagcaccggctttgtcgacggtgataag
    R  S  F  V  H  G  D  F  D  P  L  S  T  G  F  V  D  G  D  K   200
601 agagcagggtttatgaacggagttttcatccacttgttgcaaagcgggttccagaaaag
    R  A  G  F  M  N  G  V  F  H  P  L  V  A  K  R  V  P  E  K   220
661 aaggacagacgataggatggcacgcgtaggtcaatcttacctacatgaaaacatggtcga
    K  D  R  R  *                                               224
721 actttatactgaacttttagctaaacagactggatactttcagagcgtgggtcttttgca
781 aaggtcaaaagtcttagggtcaaatgatgctatctgccaattccttgggcacgcattgtt
841 gttgtttttaattggggaagaagtaaactttactataagcctccattattccttgacgtt
901 gaaaaccccaccaaaaaacaagtcttcttttgtcactgcttggtgtgta
```

Figure 3.2 *A. rubens* pedal peptide-like neuropeptide precursor 1 (ArPPLNP1). The nucleotide sequence (lowercase, 948 bases) encoding ArPPLNP1 (uppercase, 224 amino acid residues) including a 3' untranslated region is shown above. The predicted signal peptide is shown in blue, 8 putative peptides are shown in red and putative

dibasic cleavage sites are shown in green. The nucleotide sequence used for primer design is highlighted in red within red boxes. Nucleotide sequences that were used as primers for cDNA cloning are shown in red and the asterisk shows the position of the stop codon.

3.3.2 Mass spectrometric detection of ArPPLNP1-derived peptides in *A. rubens* radial nerve extracts

All five of the PP/OK-type peptides predicted to be derived from ArPPLNP1 were detected in extracts of *A. rubens* radial nerve cords using LC-MS/MS. Four peptides (ArPPLN1a-d) gave a good series of b fragment ions, as expected for peptides that do not contain a basic C-terminal amino acid. The fifth peptide (ArPPLN1e) gave nearly complete coverage of b and y ions. The following peptides were observed and selected for MS/MS (Figure 3.3b-f): ArPPLN1a (GFGMGAYDPLSAGFTD, 811.35 m/z, 2+ ion); ArPPLN1b (FGGKGAFDPLSAGFTD, 793.88 m/z, 2+ ion); ArPPLN1c (FGGSRGAFDPLSAGFTD, 851.40 m/z, 2+ ion), ArPPLN1d (SFVHGDFDPLSTGFVDGD, 956.42 m/z, 2+ ion) and ArPPLN1e (AGFMNGVFHPLVA, 680.35 m/z, 2+ ion).

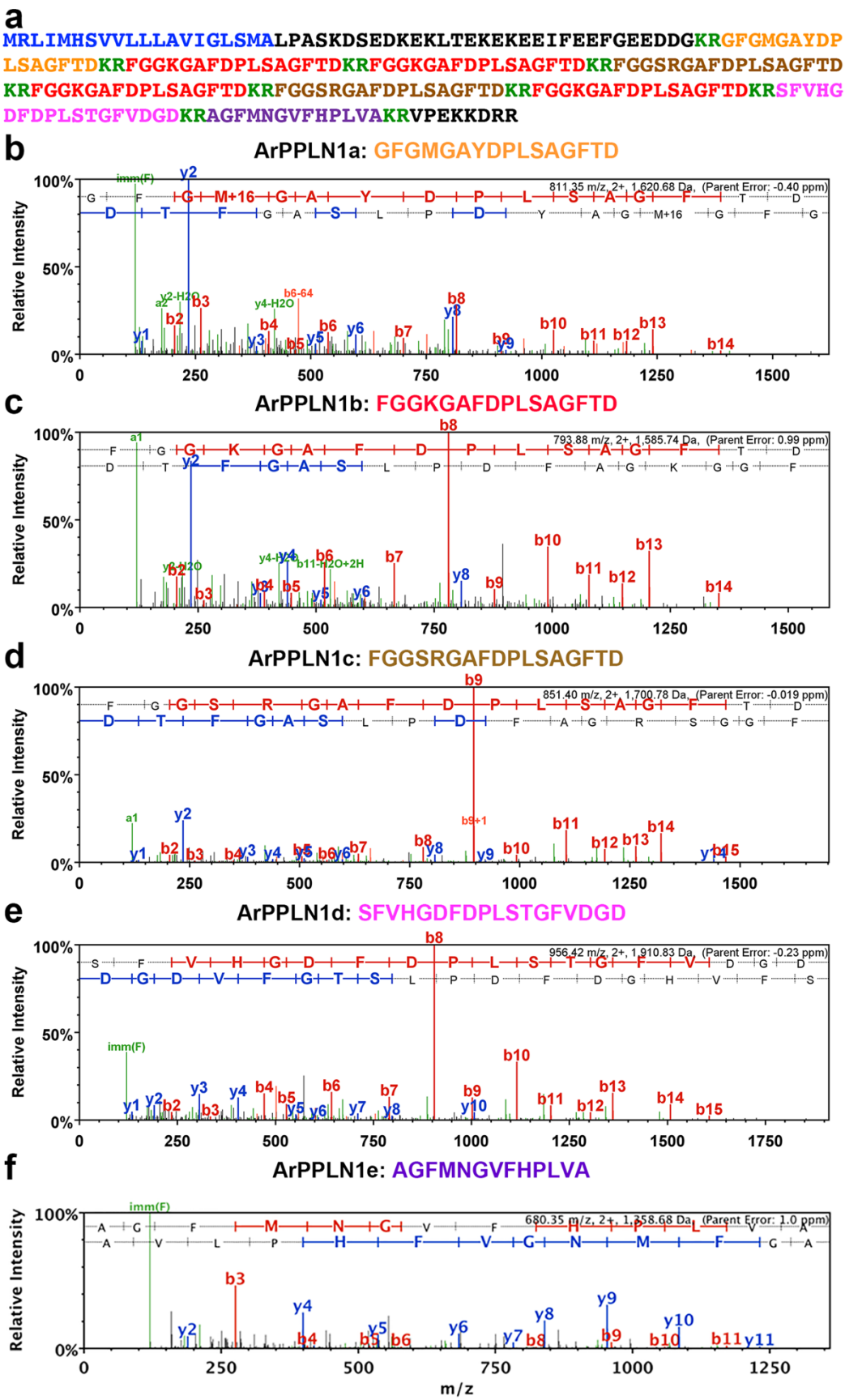

Figure 3.3 Mass spectrometric identification of peptides derived from the ArPPLNP1 in an extract of *A. rubens* radial nerve cords.

(a) Amino acid sequence of ArPPLNP1 with the predicted signal peptide shown in blue, predicted cleavage sites shown in green and peptides derived from the precursor shown in orange (ArPPLN1a), red (ArPPLN1b), brown (ArPPLN1c), pink (ArPPLN1d) and purple (ArPPLN1e). (b-f) annotated MS/MS spectra for ArPPLN1a-e, respectively. The b series of peptide fragment ions are shown in red, the y series in blue and additional identified peptide fragment ions in green. The amino acid sequence identified in the mass spectrum is highlighted at the top of each figure and M + 16 represents oxidized methionine. (b) MS/MS spectrum for the ArPPLN1a (GFGMGAYDPLSAGFTD) observed at 811.35 *m/z*, 2+ ion, with precursor mass error -0.40 ppm (Mascot score 84). (c) MS/MS spectrum for ArPPLN1b (FGGKGAFDPLSAGFTD) observed at 793.88 *m/z*, 2+ ion, with precursor mass error 0.99 ppm (Mascot score 61). (d) MS/MS spectrum for ArPPLN1c (FGGSRGAFDPLSAGFTD) observed at 851.40 *m/z*, 2+ ion, with precursor mass error -0.019 ppm (Mascot score 60). (e) MS/MS spectrum for ArPPLN1d (SFVHGDFDPLSTGFVDGD) observed at 956.42 *m/z*, 2+ ion, with precursor mass error -0.23 ppm (Mascot score 69). (f) MS/MS spectrum for ArPPLN1e (AGFMNGVFHPLVA) observed at 680.35 *m/z*, 2+ ion, with precursor mass error 1.0 ppm (Mascot score 42).

3.3.3 Localization of ArPPLNP1 transcripts in *A. rubens* using mRNA *in situ* hybridization

Analysis of the distribution of ArPPLNP1 transcripts in *A. rubens* using mRNA *in situ* hybridization revealed a widespread pattern of expression, including stained cells in the radial nerve cords and circumoral nerve ring that form the main tracts of the nervous system (Figure 3.4), the tube feet (Figure 3.5), the terminal tentacle (Figure 3.6), the digestive system (Figure 3.7, 3.8) and the ceolomic epithelial lining of the body wall (Figure 3.9).

In longitudinal sections of the radial nerve cord, stained cells can be seen in the hyponeural region (Figure 3.4a, b) and along the length of the ectoneural region in the sub-cuticular epithelium (Figure 3.4a, c). The specificity of the staining observed with anti-sense probes (Figure 3.4a) was demonstrated by control experiments where no staining was observed with sense probes (Figure 3.4a inset). Transverse sections of the radial nerve cords revealed that the stained cells in the ectoneural region are concentrated in the lateral regions of the radial nerve cords (Figure 3.4d) and this

population of cells extends into the epithelium of adjacent tube feet (Figure 3.4e). In contrast, stained cells are only sparsely distributed in the ectoneural epithelium at the apex of the V-shaped nerve cord (Figure 3.4d). By way of comparison, a dense population of stained cells is present throughout much of the hyponeural region of the radial nerve cord (Figure 3.4a, b, f). The pattern of expression in the circumoral nerve ring is consistent with that seen in the radial nerve cords. Thus, cells are present in both the hyponeural and ectoneural regions; however, in the ectoneural epithelium stained cells are concentrated in the region adjacent to the perioral tube feet and are sparser in the region adjacent to the peristomial membrane (Figure 3.4g, h).

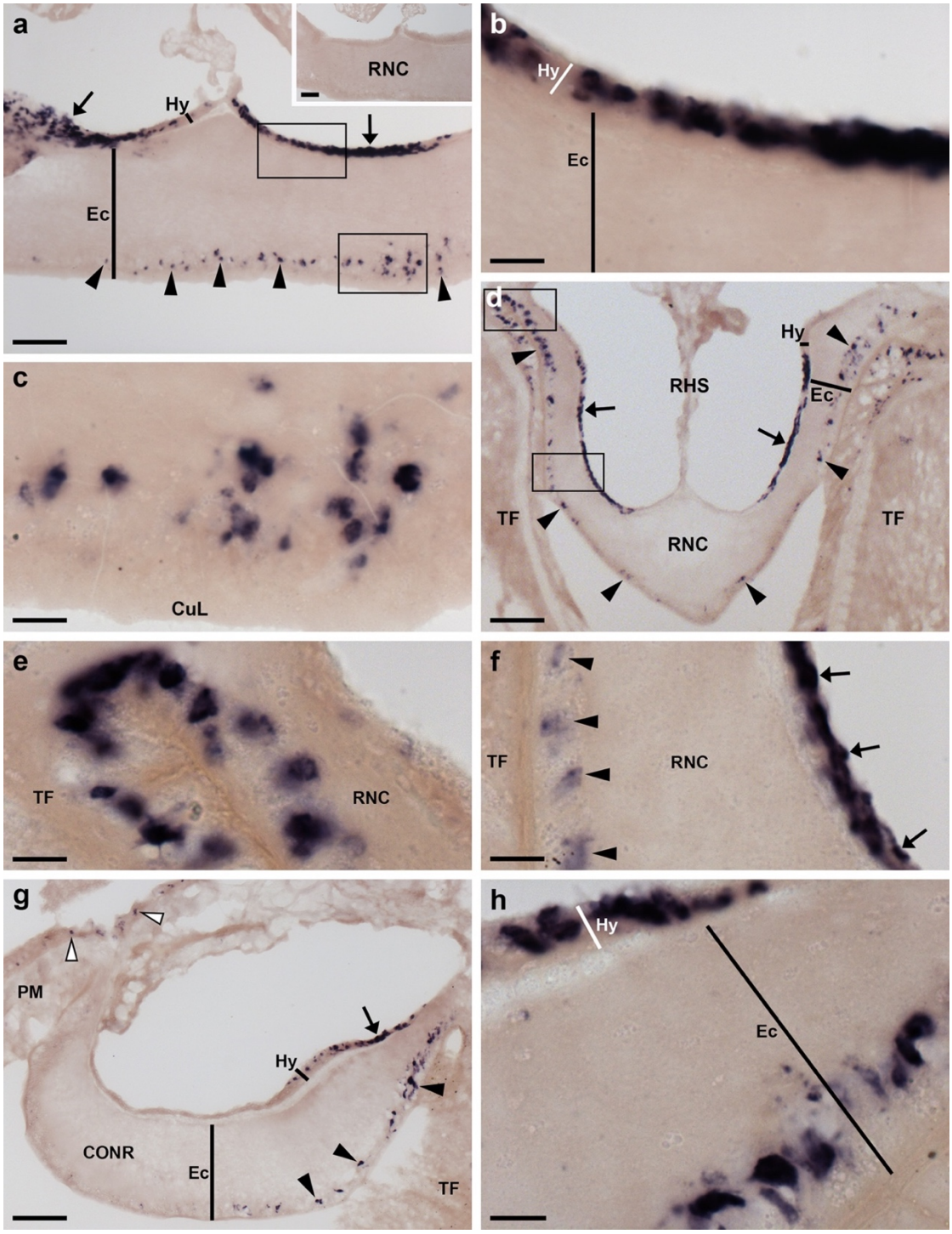

Figure 3.4 Localization of ArPPLNP1 mRNA in the radial nerve cord and circumoral nerve ring of *A. rubens* using *in situ* hybridization.
(a) Longitudinal parasagittal section of the radial nerve cords incubated with antisense probes showing stained cells in the ectoneural (arrowheads) and hyponeural (arrows) regions. Higher magnification images of the boxed regions are shown in (b) and (c). The inset of panel (a) shows the absence of staining in a longitudinal parasagittal section of radial nerve cord incubated with sense probes, demonstrating the specificity of staining observed with antisense probes. (b) High magnification image showing stained cells in the hyponeural region of the radial nerve cord. (c) High magnification image showing stained cells in the ectoneural region of the radial nerve cord. (d) Transverse section of radial nerve cord showing stained cells in the ectoneural

(arrowheads) and hyponeural (arrows) regions. Higher magnification images of the boxed regions are shown in (e) and (f). (e) High magnification image showing stained cells at the junction between the ectoneural region of the radial nerve cord and an adjacent tube foot. (f) High magnification image showing stained cells in the ectoneural (arrowheads) and hyponeural (arrows) regions of the nerve cord. (g) Transverse section of the circumoral nerve ring showing stained cells in the ectoneural (arrowheads) and hyponeural (arrow) regions. Stained cells can also be seen in the coelomic epithelial lining of the peristomial membrane (white arrowheads). (h) High magnification image of circumoral nerve ring showing stained cells in the ectoneural and hyponeural regions. CONR, circumoral nerve ring; CuL, cuticular layer; Ec, ectoneural region; Hy, hyponeural region; PM, peristomial membrane; RHS, radial hemal strand; RNC, radial nerve cord; TF, tube foot. Scale bars: 50 μm in (a), (a) inset, (d), (g); 10 μm in (b), (c), (e), (f), (h). Refer to Figure 1.7 (page 38) and 1.8 (page 39) for details of starfish anatomy.

In the tube feet, which enable locomotor activity in starfish, stained cells are present in a basiepithelial position at the junction between the tube feet and the radial nerve cord or circumoral nerve ring (Figure 3.5a), along the length of the tube foot stem (Figure 3.5a, b) and at the junction between adjacent tube feet (Figure 3.5c). Stained cells are also present in the tube foot sucker, in close proximity to the basal nerve ring (Figure 3.5d, e).

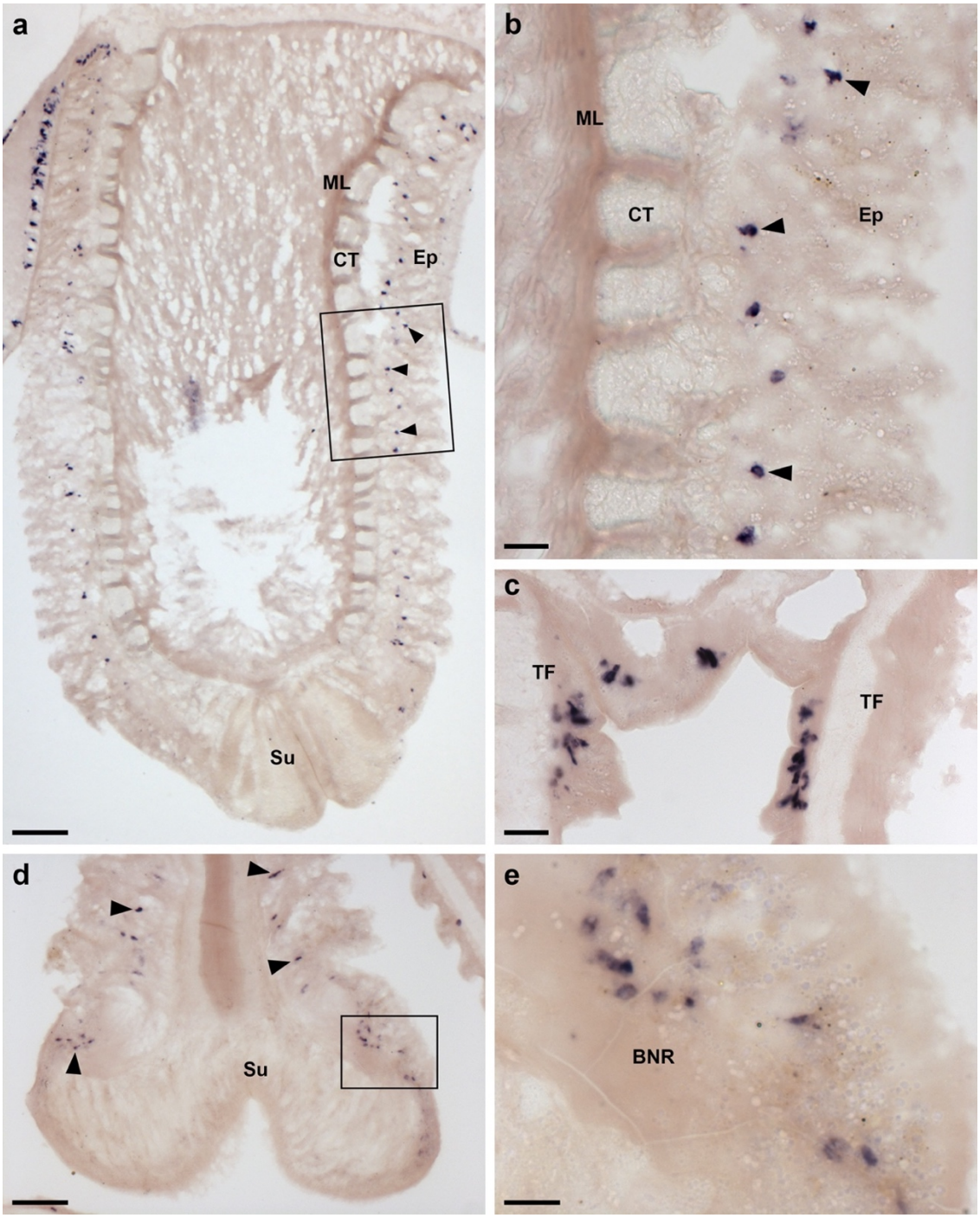

Figure 3.5 Localization of ArPPLNP1 mRNA in tube feet of *A. rubens* using *in situ* hybridization.
(a, b) Longitudinal section of a tube foot showing stained cells (arrowheads) in the sub-epithelial layer of the tube foot stem. The boxed region in panel (a) is shown at higher magnification in (b). (c) Stained cells located in the sub-epithelial layer at the junction between adjacent tube feet. (d) Stained cells (arrowheads) in the sub-epithelial layer just above the tube foot sucker. The boxed region is shown at higher magnification in (e). (e) Stained cells located near to the tube foot basal nerve ring. BNR, basal nerve ring; CT, collagenous tissue; Ep, epithelium; ML, muscle layer; Su, sucker; TF: tube foot. Scale bars: 100 μm in (a); 20 μm in (b), (c); 50 μm in (d); 10 μm in (e). Refer to Figure 1.7 (page 38) and 1.8 (page 39) for details of starfish anatomy.

The terminal tentacle is a non-locomotory but tube foot-like sensory organ located at the tip of each starfish arm and, consistent with the expression of ArPPLNP1 in tube feet, stained cells are also present in the terminal tentacle (Figure 3.6). Stained cells are present in the wall of the terminal tentacle (Figure 3.6) and in lateral lappets (Figure 3.6c, d), flaps of epithelial tissue that hang down from the body wall on both sides of the terminal tentacle. Stained cells are also present in the body wall epithelium that forms the roof and wall of the cavity containing the terminal tentacle (Figure 3.6a). However, no stained cells were observed in the pigmented photosensory optic cushion, which is located at the base of the terminal tentacle (Figure 3.6c).

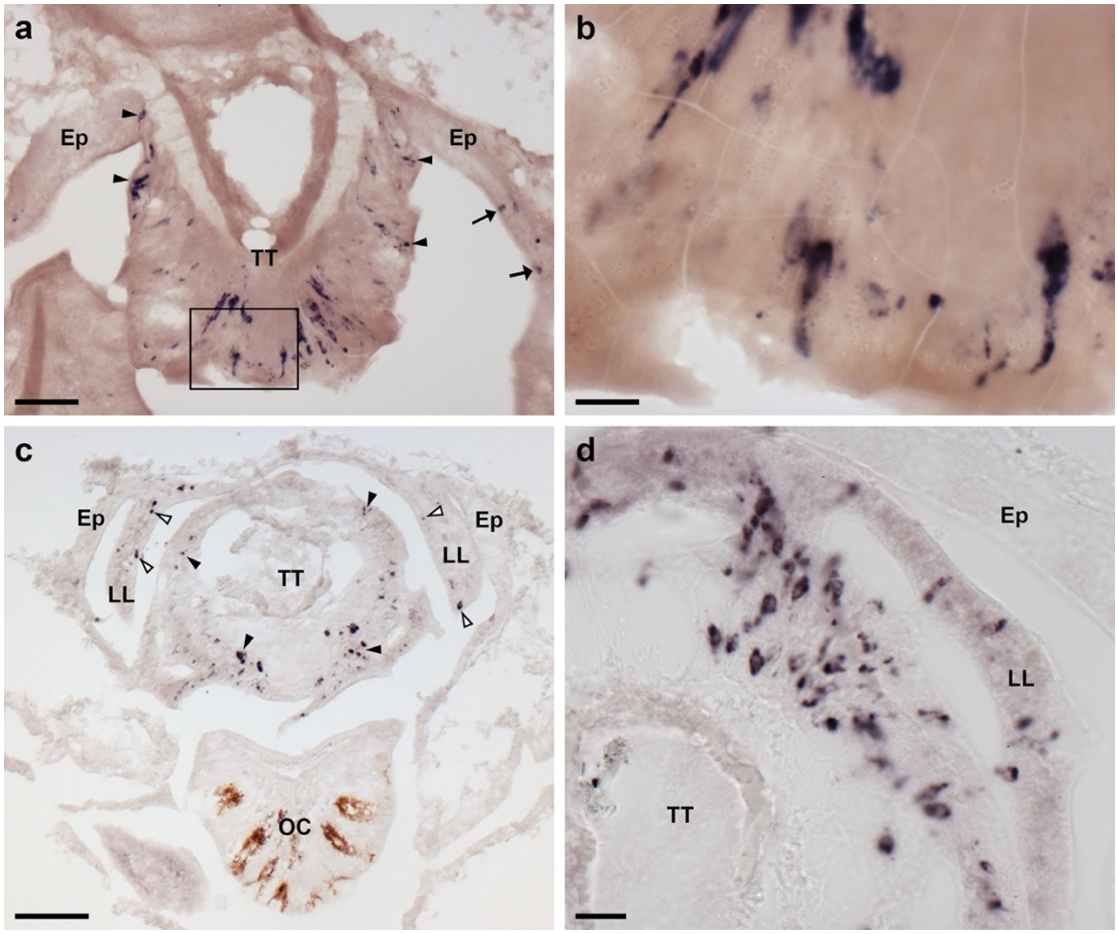

Figure 3.6 Localization of ArPPLNP1 mRNA in the arm tip region of *A. rubens* using *in situ* hybridization.
(a, b) Transverse section of a paraffin wax embedded arm tip showing the terminal tentacle cut obliquely. Stained cells can be seen in the external epithelial layer of the terminal tentacle (arrowheads) and in the body wall epithelium (arrows) that surrounds the terminal tentacle. The boxed region in (a) is shown at higher magnification in panel

(b). (c) Transverse cryostat section of an arm tip showing the pigmented optic cushion and terminal tentacle. Stained cells can be seen in the terminal tentacle external epithelium (black arrowheads) and in the lateral lappets (white arrowheads). (d) A high-magnification image of an arm tip showing stained cells in the terminal tentacle and lateral lappet. Ep, epithelium; LL, lateral lappet; OC, optic cushion; TT, terminal tentacle. Scale bars: 50 μm in (a), (c); 10 μm in (b); 20 μm in (d). Refer to Figure 1.7 (page 38) and 1.8 (page 39) for details of starfish anatomy.

In the digestive system, ArPPLNP1 mRNA expression was detected in the peristomial membrane (Figure 3.7a), esophagus (Figure 3.7b), cardiac stomach (Figure 3.7c, d), pyloric stomach (Figure 3.7e, f), pyloric ducts (Figure 3.8a, b) and pyloric caeca (Figure 3.8c, d). In the peristomial membrane and esophagus, stained cells are present in the coelomic epithelium and in the external epithelium (Figure 3.7a, b). In the cardiac stomach, ArPPLNP1 is widely expressed. Stained cells are present in the mucosa of the floor (Figure 3.7c), pouches and roof (Figure 3.7c, d) of the cardiac stomach. The floor of the pyloric stomach has a similar pattern of expression as the roof of the cardiac stomach (Figure 3.7e, f).

The pyloric ducts, which link the pyloric stomach with the paired pyloric caeca in each arm contain stained cells, which are concentrated in the mucosal epithelium on the oral side of the ducts (Figure 3.8a, b). Similarly, stained cells are concentrated in the mucosal epithelium on the oral side of the central canal of the pyloric caeca (Figure 3.8c, d), which is directly connected to the pyloric ducts (Anderson, 1953).

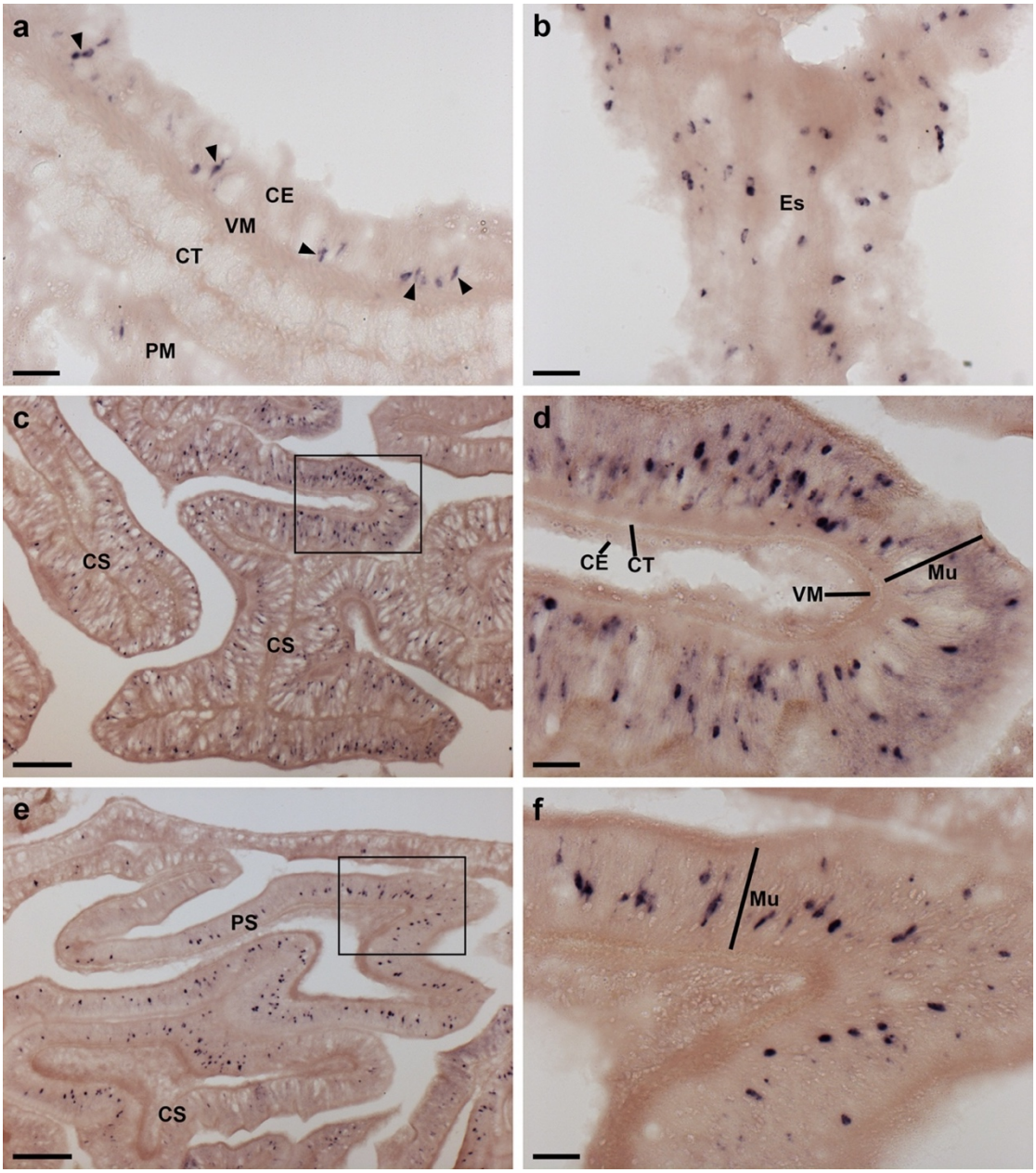

Figure 3.7 Localization of ArPPLNP1 mRNA in the digestive system of *A. rubens* using *in situ* hybridization.
(a) Transverse section of the peristomial membrane showing stained cells (arrowheads) in the coelomic epithelium. (b) Longitudinal section of the esophagus showing stained cells in the coelomic epithelium. (c, d) Transverse section of central disk showing stained cells in the cardiac stomach. The boxed region in (c) is shown at higher magnification in panel (d), where stained cells can be seen in mucosal layer. (e, f) Transverse section of central disk showing stained cells in the cardiac stomach and pyloric stomach. The boxed region of the pyloric stomach in (e) is shown at higher magnification in panel (f), where stained cells can be seen in mucosal layer. CE, coelomic epithelium; CS, cardiac stomach; CT, collagenous tissue; Es, esophagus; Mu, mucosa; PM, peristomial membrane; PS, pyloric stomach; VM, visceral muscle. Scale bars: 20 μm in (a), (b), (d), (f); 100 μm in (c), (e). Refer to Figure 1.7 (page 38) and 1.8 (page 39) for details of starfish anatomy.

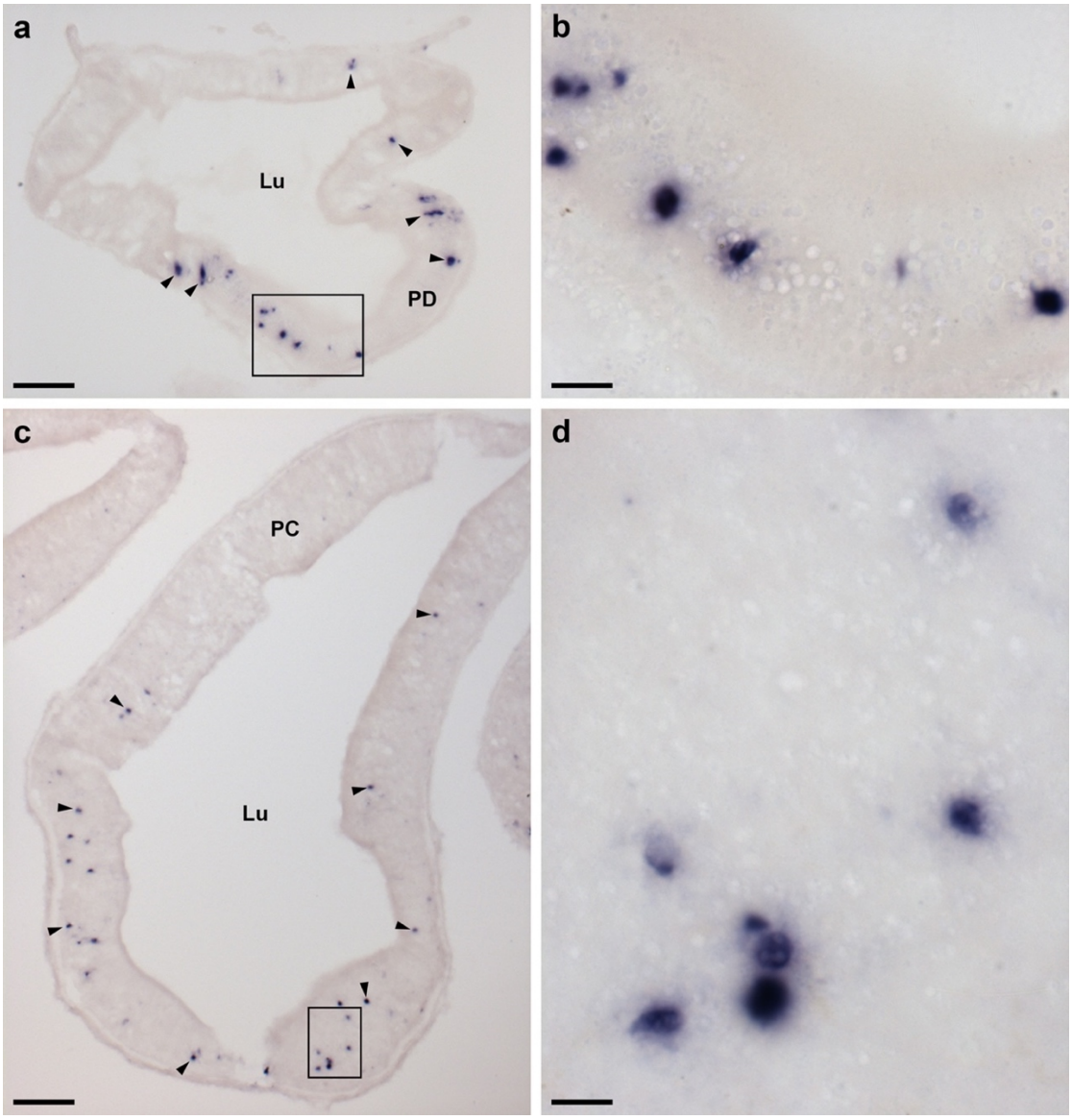

Figure 3.8 Localization of ArPPLNP1 mRNA in the pyloric duct and pyloric caeca of *A. rubens* using *in situ* hybridization.
(a, b) Transverse section of a pyloric duct showing stained cells (arrowheads) that are concentrated in the oral (lower) domain of the duct. The boxed region in (a) is shown at higher magnification in panel (b), where stained cells can be seen in the mucosal layer. (c, d) Transverse section of a pyloric caecum showing stained cells (arrowheads) that are concentrated in the oral (lower) domain of a pyloric caecum diverticulum. The boxed region in (c) is shown at higher magnification in panel (d), where stained cells can be seen in the mucosal layer. Lu, lumen; PC, pyloric caeca; PD, pyloric duct. Scale bars: 50 μm in (a); 10 μm in (b), (d); 100 μm in (c). Refer to Figure 1.7 (page 38) and 1.8 (page 39) for details of starfish anatomy.

ArPPLNP1-expressing cells are present within the aboral coelomic epithelium. Stained cells can be seen associated with the longitudinally orientated apical muscle, which is shown here in both transverse (Figure 3.9a, b) and longitudinal (Figure 3.9c, d) sections of the starfish arm. Stained cells can also be seen in the coelomic epithelium

located at the base of the finger-like papulae, which project through the body wall to the external aboral surface of the arms (Figure 3.9e, f).

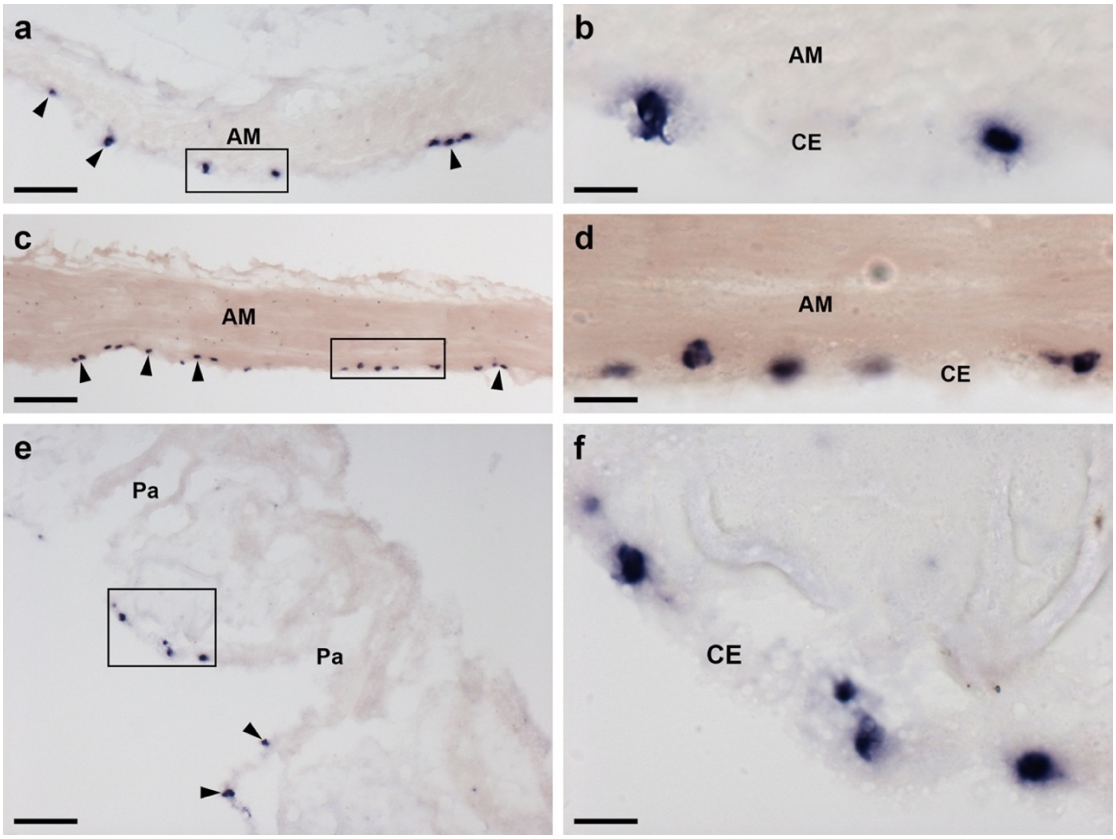

Figure 3.9 Localization of ArPPLNP1 mRNA in the apical muscle and coelomic lining of the body wall in *A. rubens* using *in situ* hybridization.
(a, b) Transverse section of apical muscle showing stained cells (arrowheads) in the coelomic epithelium. The boxed region in (a) is shown at higher magnification in panel (b). (c, d) Longitudinal section of apical muscle showing stained cells (arrowheads) in the coelomic epithelium. The boxed region in (c) is shown at higher magnification in panel (d). (e, f) Transverse section of an arm showing stained cells (arrowheads) in the coelomic epithelium at the base of a papula. The boxed region in (e) is shown at higher magnification in panel (f). AM, apical muscle; CE, coelomic epithelium; Pa, papulae. Scale bars: 50 μm in (a), (c), (e); 10 μm in (b), (d), (f). Refer to Figure 1.7 (page 38) and 1.8 (page 39) for details of starfish anatomy.

3.3.4 Localization of neuropeptides derived from ArPPLNP1 using immunohistochemistry

3.3.4.1 Characterisation of a rabbit antiserum to ArPPLN1b using ELISA

To assess the presence and titre of antibodies to the ArPPLN1-ag peptide in rabbit sera, antiserum and pre-immune serum were incubated at a range of dilutions (10^{-}

^{3} - 10^{-8}) with a fixed amount of the antigen peptide added to each well of the microtitre plate (10^{-10} moles). As expected, no ArPPLN1-ag immunoreactivity was detected with pre-immune serum but ArPPLN1-ag immunoreactivity was detected with antiserum at dilutions ranging from 10^{-3} to 10^{-5} (Figure 3.10a). To assess the sensitivity of the antiserum for detection of the ArPPLN1-ag peptide, the antiserum (diluted to10^{-4}) was incubated with different amounts of peptide ranging from 10^{-10} to 10^{-15} moles. At this antiserum dilution, the peptide was detected in the range from 10^{-10} moles to 10^{-12} moles (Figure 3.10b). Collectively, these data indicate that the antiserum contains a high titre of antibodies to the ArPPLN1-ag peptide.

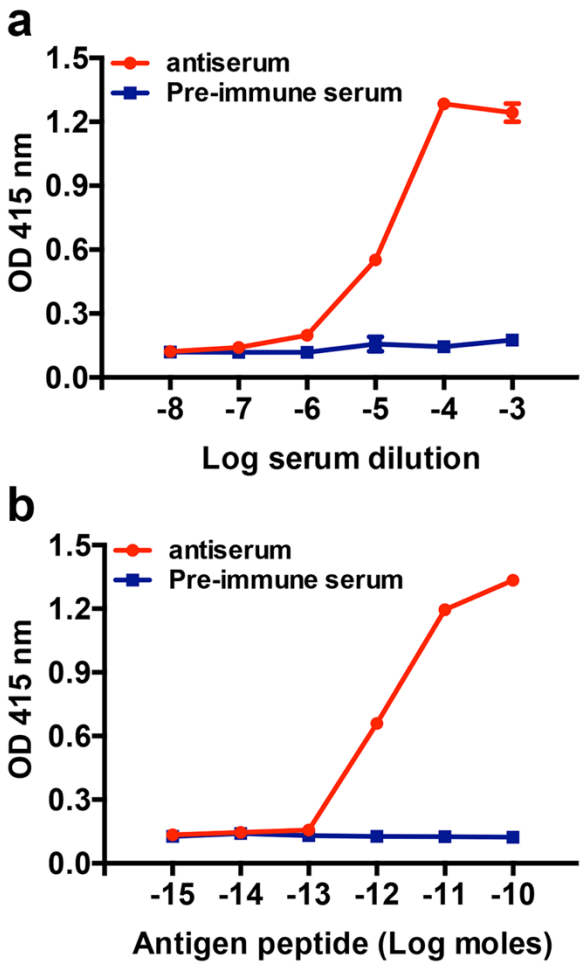

Figure 3.10 Characterization of rabbit antiserum to ArPPLN1b using an enzyme-linked immunosorbent assay (ELISA).
(a) Incubation of antiserum (red) and pre-immune serum (blue) at dilutions between 10^{-3} and 10^{-8} with 0.1 nmol of antigen peptide (ArPPLN1-ag) per well reveals no immunoreaction with pre-immune serum, whereas with the antiserum the antigen is

detected at well above the background optical density (OD) with dilutions from 10^{-3} to 10^{-5}. (b) Incubation of antiserum (red) and pre-immune serum (blue) at 10^{-4} dilution with between 10^{-15} and 10^{-10} moles of antigen peptide (ArPPLN1-ag) per well reveals no immunoreaction with pre-immune serum, whereas with the antiserum the antigen is detected at well above the background OD with 10^{-12} to 10^{-10} moles per well. All data points are mean values from two separate experiments performed in duplicate.

3.3.4.2 Immunohistochemical localization of neuropeptides derived from ArPPLNP1 in *A. rubens*

Antiserum to the C-terminal region of ArPPLN1b (KGAFDPLSAGFTD; see above) was used to investigate the distribution of this peptide in *A. rubens* using immunohistochemistry. It should be noted, however, that two of the other peptides derived from ArPPLNP1 (ArPPLN1a and ArPPLN1c) have the same C-terminal DPLSAGFTD sequence as ArPPLN1b and so it is likely that these are also immunoreactive with the antiserum. Having demonstrated using ELISA that the antiserum contains a high titre of antibodies to the antigen peptide (Figure 3.10), the antiserum was used for immunohistochemistry at a dilution of 10^{-5}.

3.3.4.2.1 Radial nerve cords, circumoral nerve ring, marginal nerve cords and lateral motor nerves

An extensive and intense pattern of ArPPLN1b-immunoreactivity (ir) was revealed in radial nerve cord of *A. rubens* (Figure 3.11a). The specificity of this immunostaining was confirmed in control experiments testing antiserum that had been pre-absorbed with the antigen peptide. Thus, in tests with pre-absorbed antiserum no immunostaining was observed in the radial nerve cords (Figure 3.11a inset) or in other parts of the starfish body (data not shown).

ArPPLN1b-ir was revealed in bipolar cell bodies located in the epithelium of the ectoneural region of the radial nerve cord and in a dense meshwork of fibers in the

underlying neuropile (Figure 3.11a, b). Interestingly, the intensity of immunostaining in the ectoneural neuropile is not homogeneous; for example, in the region that forms the tip of the V-shaped nerve cord there is zone of neuropile with a lower density of stained fibers that is bounded above (aboral) and below (oral) by zones with a higher density of stained fibers (Figure 3.11a, c). ArPPLN1b-ir was also revealed in monopolar cell bodies in the hyponeural region of the radial nerve cord and the axonal processes of these neurons (Figure 3.11a, d), which can be seen projecting to the base of the adjacent tube foot stem and to the transverse infra-ambulacral muscle (Figure 3.11e). Immunostained processes in the neuropile of the ectoneural region of the radial nerve cord are continuous with the basiepithelial nerve plexus of the adjacent tube foot (Figure 3.11f).

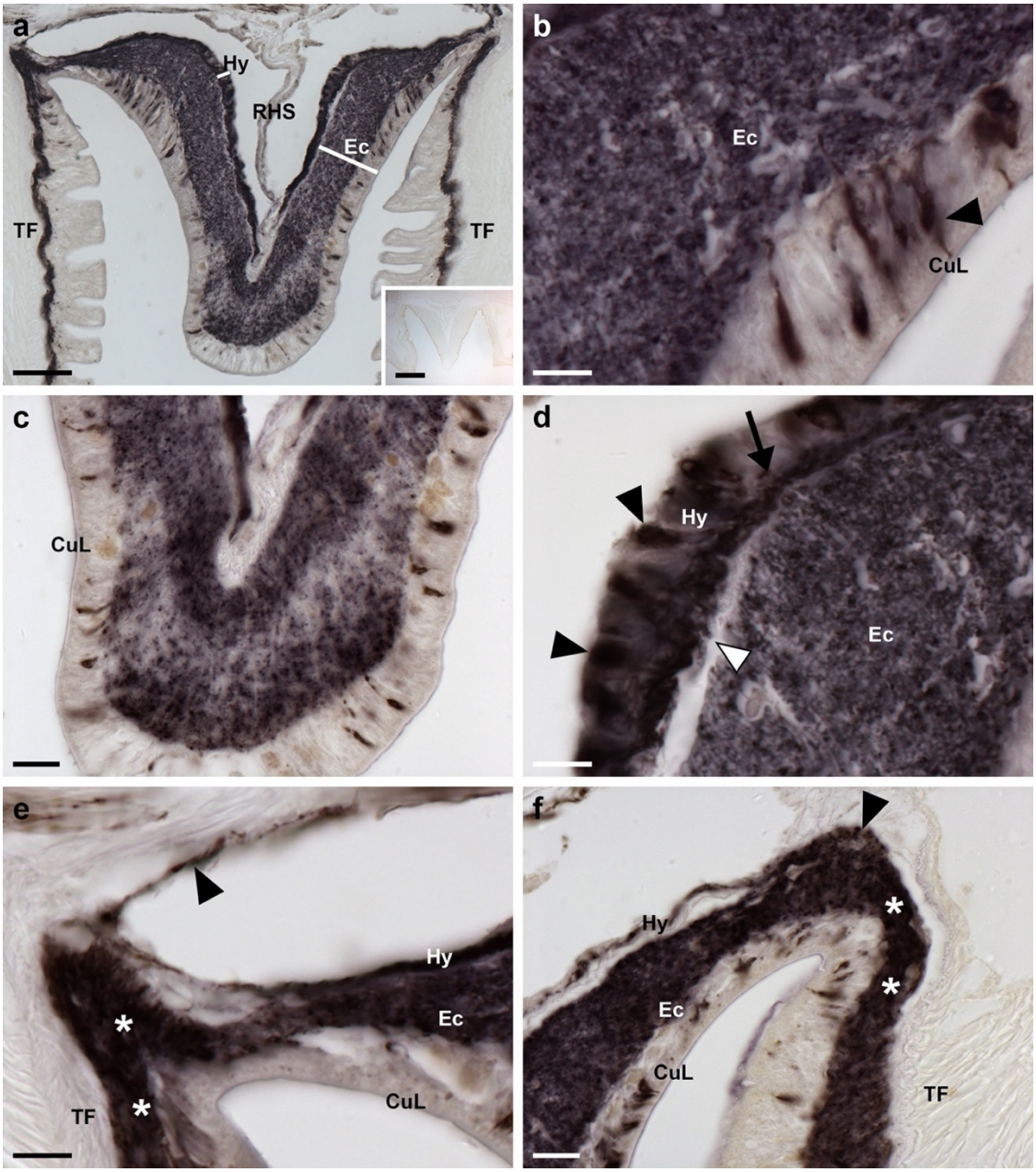

Figure 3.11 Localization of ArPPLN1b-immunoreactivity (ArPPLN1b-ir) in the radial nerve cord of *A. rubens*.

(a) Tranvserse section of a radial nerve cord showing ArPPLN1b-ir in both the ectoneural and hyponeural regions. The inset of (a) shows absence of immunostaining in a radial nerve cord section incubated with ArPPLN1b antiserum pre-absorbed with the antigen peptide (ArPPLN1b-ag), demonstrating the specificity of immunostaining observed with the ArPPLN1b antiserum. (b) High magnification image of the ectoneural region of the radial nerve cord showing immunostained bipolar shaped cells in the sub-cuticular epithelium (arrowheads) and densely packed immunostained processes in the underlying neuropile region. (c) High magnification image of the ectoneural region at the tip of the V-shaped radial nerve cord showing layer-specific variation in the density of immunostained processes. (d) High magnification image showing immunostained monopolar shaped cells (arrowheads) and their stained processes (arrow) in hyponeural region of the radial nerve cord. The unstained collagenous tissue layer (white arrowhead) that separates the hyponeural region from the densely stained ectoneural neuropile can also be seen here. (e, f) High magnification

images showing immunostaining at the junction between the radial nerve cord and an adjacent tube foot. The continuity of immunostaining in the ectoneural region of the radial nerve and in the basiepithelial nerve plexus of the tube foot (asterisks) can be seen here. In (e) the stained process(es) (arrowhead) of a hyponeural neuron(s) can be seen projecting over the roof of the perihemal canal in close association with the transverse infra-ambulacral muscle. In (f) the stained processes (arrowhead) of hyponeural neurons can be seen projecting to the base of the adjacent tube foot. CuL, cuticle layer; Ec, ectoneural region; Hy, hyponeural region; RHS, radial hemal strand; TF, tube foot. Scale bars: 50 μm in (a); 200 μm in (a) inset; 10 μm in (b), (d), (e); 20 μm in (c), (f). Refer to Figure 1.7 (page 38) and 1.8 (page 39) for details of starfish anatomy.

The pattern of immunostaining in the circumoral nerve ring (Figure 3.12a, b) is consistent with that in the radial nerve cords, with bipolar cell bodies in the ectoneural epithelium projecting into the densely stained underlying neuropile and with the processes of stained monopolar cells in the hyponeural region projecting into underlying nerve tract that is separated from the ectoneural neuropile by a thin layer of unstained collagenous tissue (Figure 3.12b, c). As in the radial nerve cord, there was regional variability in the density of immunostained fibers in the ectoneural neuropile. Thus, in the region of the circumoral nerve ring proximal to the peristomial membrane there is a layer of neuropile with a lower density of immunostained fibers that are bounded on either side by layers of neuropile with a higher density of immunostained fibers (Figure 3.12c). This pattern of staining seen in the circumoral nerve ring is anatomically equivalent to the "banded" pattern of staining seen in the tip region of the radial nerve cord (see above). Stained fibers in the ectoneural neuropile are continuous with the basiepithelial plexus of the adjacent peristomial membrane (Figure 3.12a).

Located lateral to the outer row of tube feet on each side of the arm is the marginal nerve, which is a thickening of the basiepithelial nerve plexus (Smith, 1937; 1950). Cells exhibiting ArPPLN1b-ir are present in the epithelial layer of the marginal nerve and ArPPLN1b-ir is present in the underlying neuropile (Figure 3.12d). Closely associated with the marginal nerve are the lateral motor nerves, which contain the axons

of hyponeural motor neurons that innervate the body wall musculature and the coelomic lining of the aboral body wall (Smith, 1950). ArPPLN1b-ir is present in the lateral motor nerve and stained processes emerging from a lateral motor nerve can be seen innervating the muscle that links the ambulacral and adambulacral ossicles (Figure 3.12d).

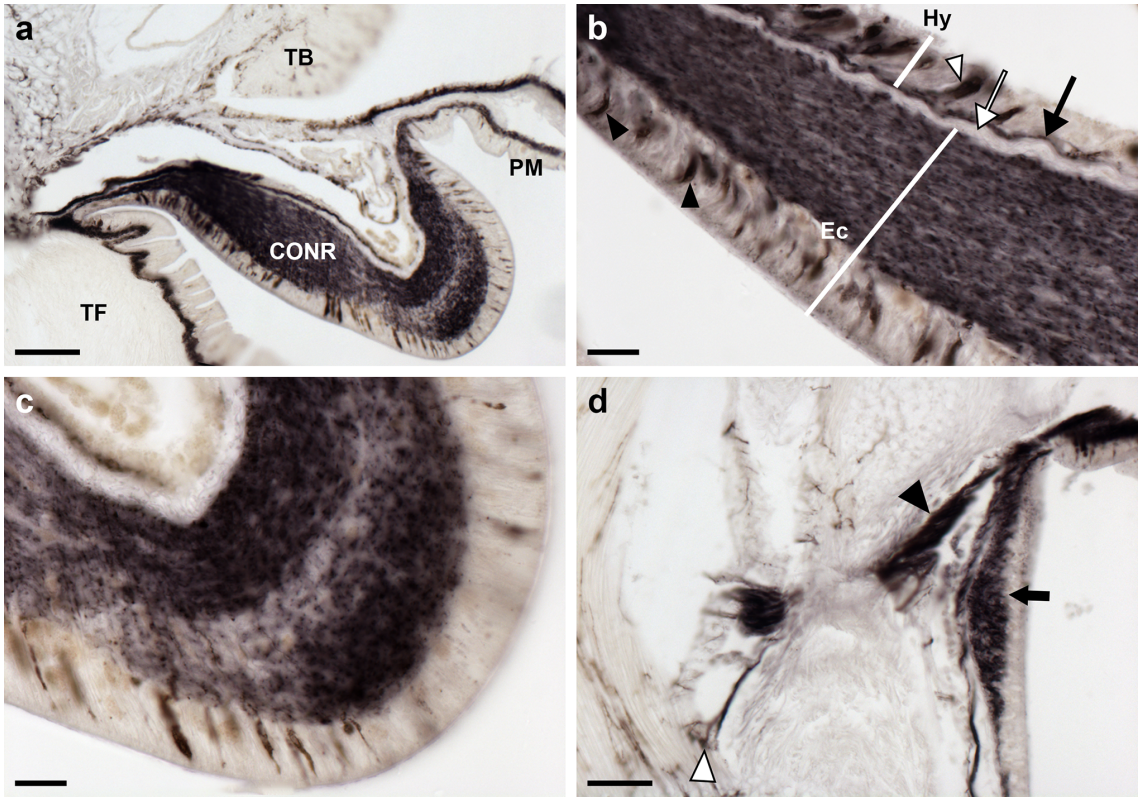

Figure 3.12 Localization of ArPPLN1b-immunoreactivity in the circumoral nerve ring and marginal nerve of *A. rubens*.
(a) ArPPLN1b-ir in a transverse section of the circumoral nerve ring; here immunostained processes can also be seen in the peristomial membrane, an adjacent oral tube foot and in a Tiedemann's body. (b) A high-magnification image of circumoral nerve ring showing immunostained bipolar shaped cells in the sub-cuticular epithelium (arrowheads) of the ectoneural region and densely packed immunostained processes in the underlying neuropile. In the hyponeural region immunostained monopolar shaped cells (white arrowhead) can be seen with their stained processes (arrow) adjacent to the unstained collagenous tissue layer (white arrow). (c) High magnification image of the ectoneural region of the circumoral nerve ring showing layer-specific variation in the density of immunostained processes. (d) Immunostaining in a sub-epithelial thickening of the basiepithelial plexus known as the marginal nerve (arrow), which is located at the junction between the outer row of tube feet and the adjacent body wall. Internal to the marginal nerve, separated by a thin layer of collagenous tissue, can be seen stained axonal processes that coalesce to form the lateral motor nerve (arrowhead). Individual stained axonal processes derived from the lateral motor nerve can be seen here innervating an adjacent inter-ossicular muscle (white

arrowhead). CONR, circumoral nerve ring; Ec, ectoneural region; Hy, hyponeural region; PM, peristomial membrane; TB, Tiedemann's body; TF, tube foot. Scale bars: 100 µm in (a); 20 µm in (b), (c); 50 µm in (d). Refer to Figure 1.7 (page 38) and 1.8 (page 39) for details of starfish anatomy.

3.3.4.2.2 Hemal system and Tiedemann's bodies

Anatomically associated with the radial nerve cords and circumoral nerve ring are the radial hemal strands and the oral hemal ring, respectively, which constitute, at least in part, the circulatory system of starfish (Ferguson, 1984). ArPPLN1b-ir is present in fibers located in the walls of the radial hemal strands and the oral hemal ring (Figure 3.13a, b). Forming a completely separate system of fluid-filled canals in starfish are the radial water canals and ring canal, components of the water vascular system that are in continuity with the fluid-filled lumen of the tube feet and ampullae (Smith, 1950). Closely associated with the ring canal are five pairs of organs known as Tiedemann's bodies, which also contain fibers that exhibit ArPPLN1b-ir (Figure 3.13c, d).

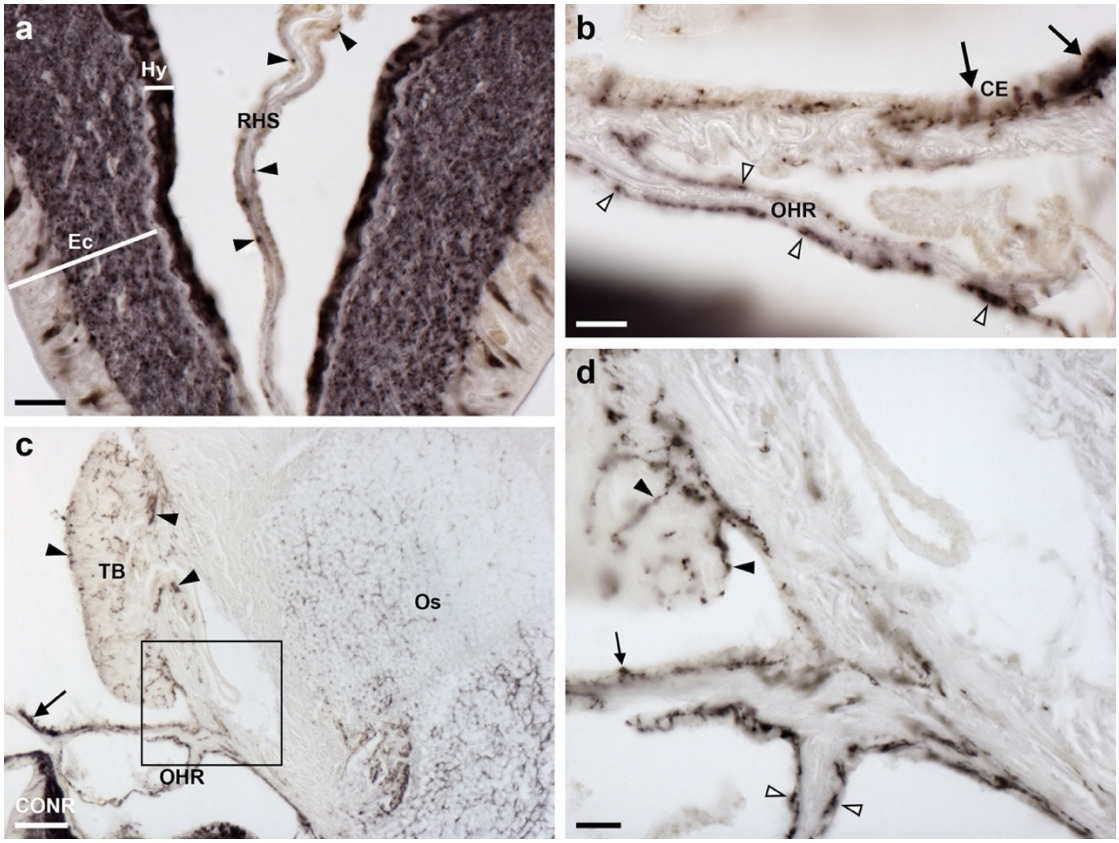

Figure 3.13 Localization ArPPLN1b immunoreactivity in the hemal system and Tiedemann's bodies of *A. rubens*.
(a) Immunostained processes (arrowheads) are present in the radial hemal strand, which is anatomically connected with the intensely stained radial nerve cord. (b) Immunostained processes (white arrowheads) are present in the oral hemal ring, which is anatomically connected to the circumoral nerve ring (out of focus at bottom left). Immunostained processes can also be seen here in the coelomic epithelium (arrows). (c, d) Immunostained processes can be seen here in one of the ten Tiedemann's bodies, which are located aboral to the circumoral nerve ring in the central disk. Immunostained processes can also be seen on the right side of the image, where they are associated with inter-ossicular muscles of the body wall (see figure 3.19). The boxed region in (c) is shown at higher magnification in panel (d), where immunostained processes can be seen in the Tiedemann's body (black arrowheads), the coelomic epithelium (arrow) and the oral hemal ring (white arrowheads). CE, coelomic epithelium; CONR, circumoral nerve ring; Ec, ectoneural region; Hy, hyponeural region; OHR, oral hemal ring; Os, ossicle; RHS, radial hemal strand; TB, Tiedemann's body. Scale bars: 20 μm in (a), (b), (d); 100 μm in (c). Refer to Figure 1.7 (page 38) and 1.8 (page 39) for details of starfish anatomy.

3.3.4.2.3 Tube feet and terminal tentacle

Strong immunostaining is present throughout the basiepithelial nerve plexus of the tube foot stem (Figure 3.14a, b) and in the basal nerve ring located in the tube foot sucker (Figure 3.14c, d). Immunostained processes can be seen extending from the basiepithelial nerve plexus into each fold of the contracted tube foot stem (Figure 3.14b). Likewise, immunostained processes extend from the basal nerve ring into the sucker (Figure 3.14c). Immunostained processes are also present beneath the coelomic epithelium of the tube foot ampulla (Figure 3.14e, f).

In the terminal tentacle, immunostained bipolar-shaped cells are present in the epithelial wall of this organ and in the underlying basiepithelial nerve plexus. Stained cells and underlying processes are also present in the optic cushion, the lateral lappets of the terminal tentacle and in the body wall epithelium that surrounds the cavity containing the terminal tentacle (Figure 3.15a-d).

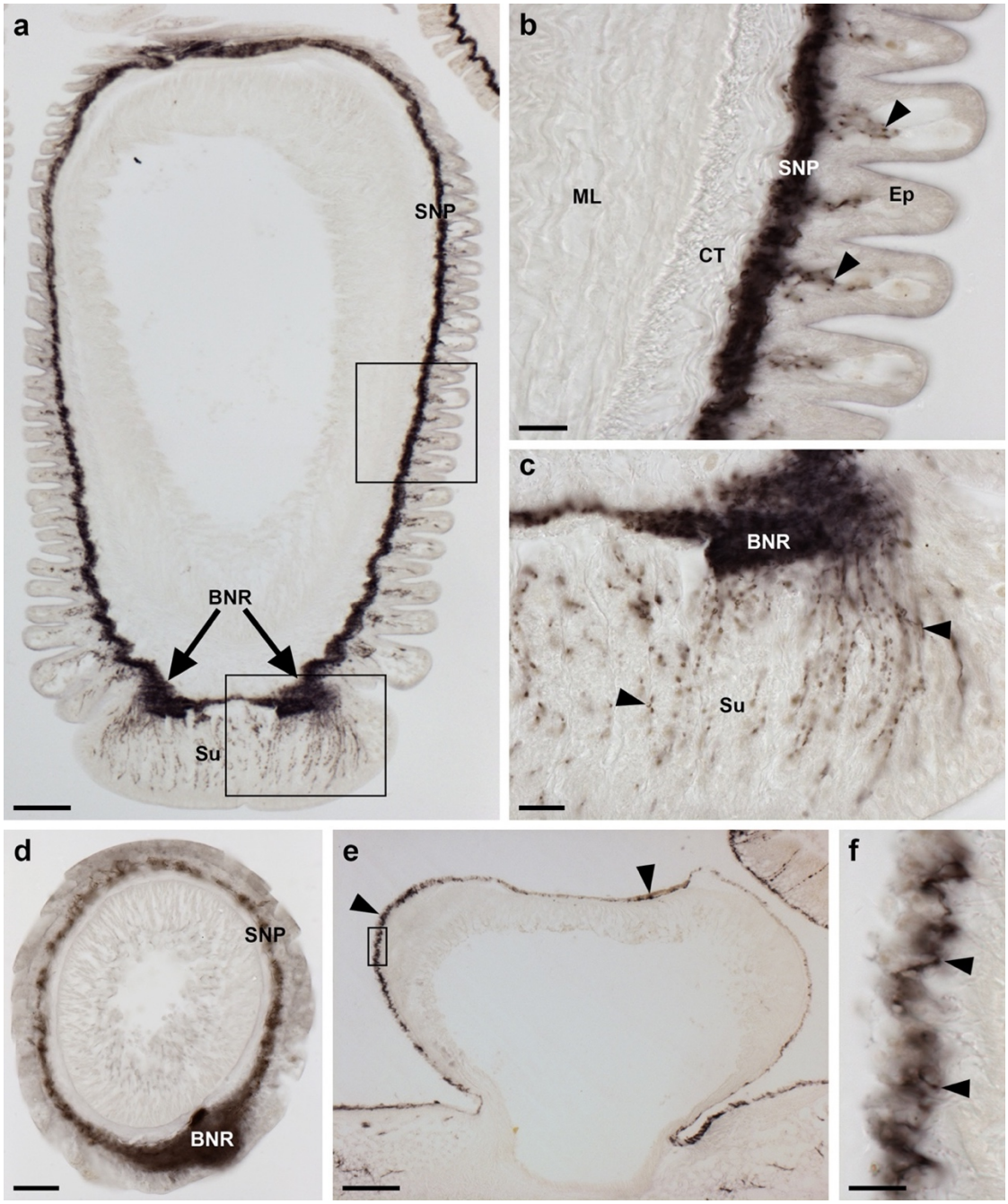

Figure 3.14 Localization of ArPPLN1b immunoreactivity in tube feet and ampullae of *A. rubens*.

(a) Longitudinal section of a tube foot showing immunostaining in the sub-epithelial nerve plexus, basal nerve ring and sucker. The boxed regions are shown at higher magnification in panels (b) and (c). (b) High magnification image showing immunostaining in the sub-epithelial nerve plexus and in processes projecting into epithelial folds of the contracted tube foot (arrowheads). (c) High magnification image showing immunostaining in the basal nerve ring and in processes projecting into the tube foot sucker (arrowheads). (d) Immunostaining in a transverse section of a tube foot showing immunostaining in the sub-epithelial nerve plexus and basal nerve ring. (e, f) Immunostaining in the sub-epithelial nerve plexus of an ampulla (arrowheads). The boxed region in panel (e) is shown at higher magnification in panel (f). BNR, basal nerve ring; CT, collagenous tissue; Ep, epithelium; ML, muscle layer; SNP, sub-epithelial nerve plexus; Su, sucker. Scale bars: 100 μm in (a), (e); 20 μm in (b), (c), (d);

10 µm in (f). Refer to Figure 1.7 (page 38) and 1.8 (page 39) for details of starfish anatomy.

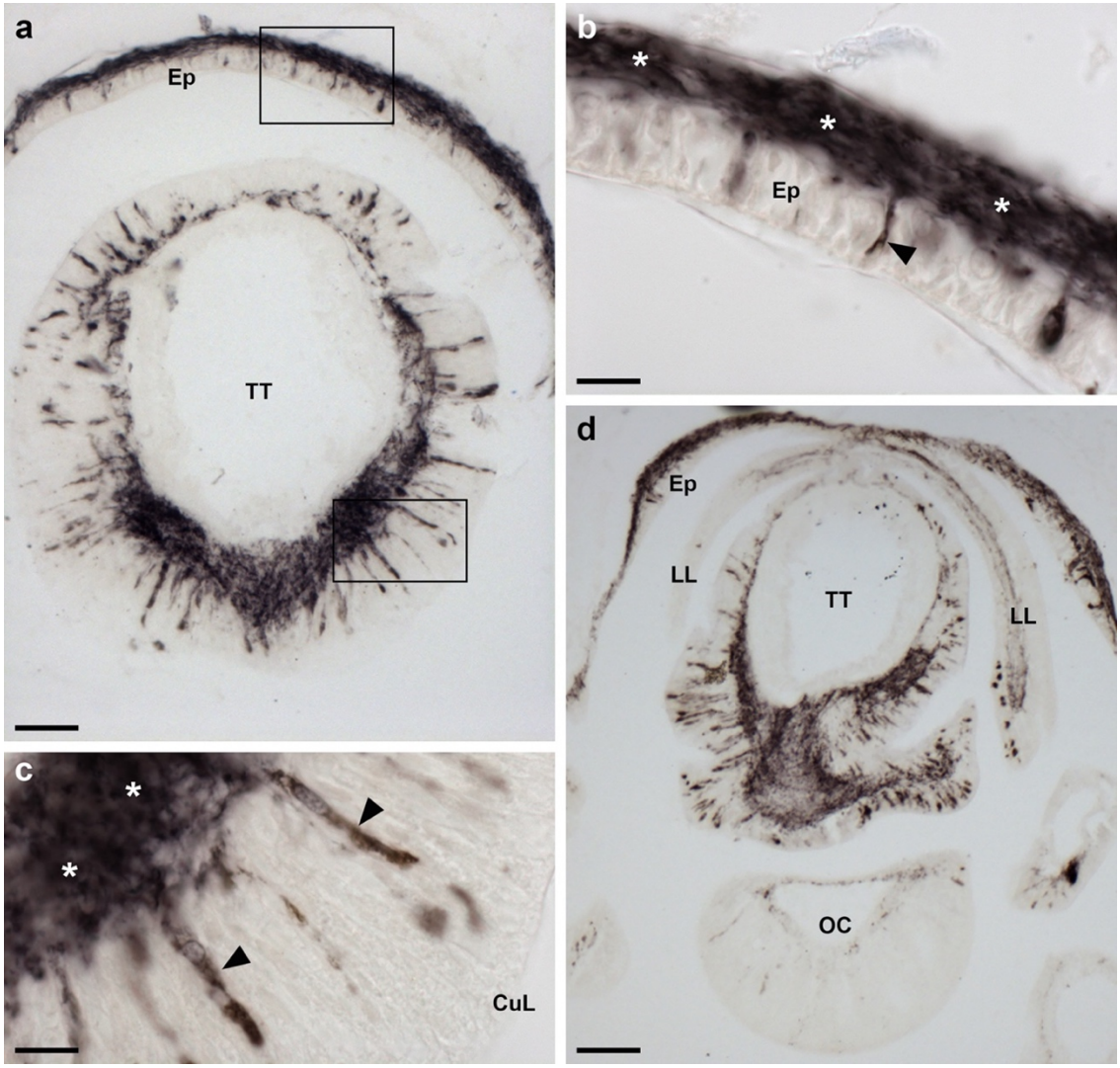

Figure 3.15 Localization of ArPPLN1b immunoreactivity in the terminal tentacle and associated structures in the arm tip of *A. rubens*.
(a) Immunostaining in a transverse section of a terminal tentacle and in the surrounding body wall epithelium. The boxed regions are shown at higher magnification in panel (b) and (c). (b) A high magnification image of arm tip body wall epithelium showing immunostained bipolar shaped cells (arrowhead) and in a dense meshwork of fibers in the underlying basiepithelial plexus (asterisks). (c) High magnification image of the terminal tentacle showing immunostained bipolar shaped cells in the epithelium (arrowheads) and in a dense meshwork of fibers in the underlying basiepithelial plexus (asterisks). (d) Immunostaining in a transverse section at the base of the terminal tentacle. Immunostained cells and processes can be seen here in the body wall epithelium, the terminal tentacle and associated lateral lappets and the optic cushion. CuL, cuticle layer; Ep, epithelium; LL, lateral lappet; OC, optic cushion; TT, terminal tentacle. Scale bars: 50 µm in (a); 10 µm in (b), (c); 100 µm in (d). Refer to Figure 1.7 (page 38) and 1.8 (page 39) for details of starfish anatomy.

3.3.4.2.4 Digestive system

Immunostained cells are present in the coelomic epithelium of the peristomial membrane and esophagus and in the underlying nerve plexus (Figure 3.16). The basiepithelial nerve plexus underlying the external epithelial layer of the peristomial membrane and esophagus also contains immunostained processes. Thus, the peristomial membrane and esophagus have two distinct layers of immunostained processes.

Immunostaining is present throughout the cardiac stomach (Figure 3.17a), including the floor of the cardiac stomach, the highly-folded pouches of the cardiac stomach and the roof of the cardiac stomach. This immunostaining is localized in bipolar shaped cells present in the mucosal layer of the cardiac stomach and in their underlying processes which project into the intensely stained basiepithelial nerve plexus (Figure 3.17a, b). A similar pattern of immunostaining is present in the pyloric stomach (Figure 3.17a, c) and in the pyloric ducts (Figure 3.17d, e) that connect the pyloric stomach with the paired digestive glands (pyloric caeca) located in each arm (Figure 3.17d, f). Immunostained mucosal cells and processes in the underlying basiepithelial nerve plexus are also present in the pyloric caeca (Figure 3.17d, f).

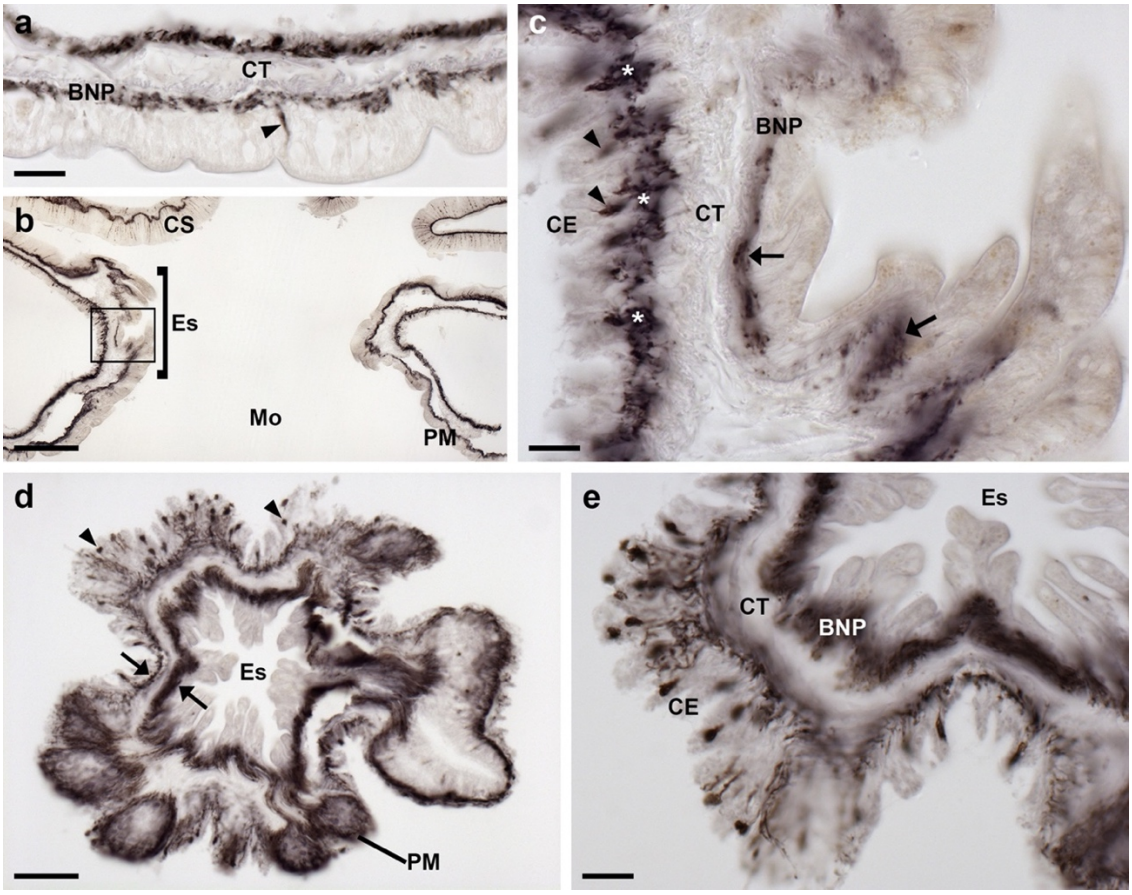

Figure 3.16 Localization of ArPPLN1b immunoreactivity in the peristomial membrane and esophagus of *A. rubens*.
(a) An immunostained bipolar shaped cell can be seen here in the external epithelial layer of the peristomial membrane (arrowhead) and in processes located in the underlying basiepithelial nerve plexus. Immunostaining is also present in cells and processes located beneath the coelomic epithelium, which is separated from the basiepithelial nerve plexus by a layer of collagenous tissue. (b) Transverse section of the central disk showing immunostaining in the peristomial membrane, the esophagus and the cardiac stomach. The boxed region is shown at higher magnification in panel (c). (c) High magnification image of a longitudinal section of the esophagus (in a transverse section of the central disk) showing immunostained cells (arrowheads) and processes (asterisks) beneath the coelomic epithelium and stained processes (arrows) in the basiepithelial nerve plexus beneath the epithelial layer that forms the external lining of the esophagus. (d) Horizontal section of the central disk at the level of the junction between the esophagus and the peristomial membrane showing immunostained cells (arrowheads) and processes (arrows). (e) High magnification transverse section of the esophagus (in a horizontal section of the central disk) showing immunostained cells and processes beneath the folded coelomic epithelium and dense immunostaining in the basiepithelial plexus beneath the epithelial lining of the eosophagus lumen. BNP, basiepithelial nerve plexus; CE, coelomic epithelium; CS, cardiac stomach; CT, collagenous tissue; Es, esophagus; Mo, mouth; PM, peristomial membrane. Scale bars: 20 μm in (a), (c), (e); 100 μm in (b); 50 μm in (d). Refer to Figure 1.7 (page 38) and 1.8 (page 39) for details of starfish anatomy.

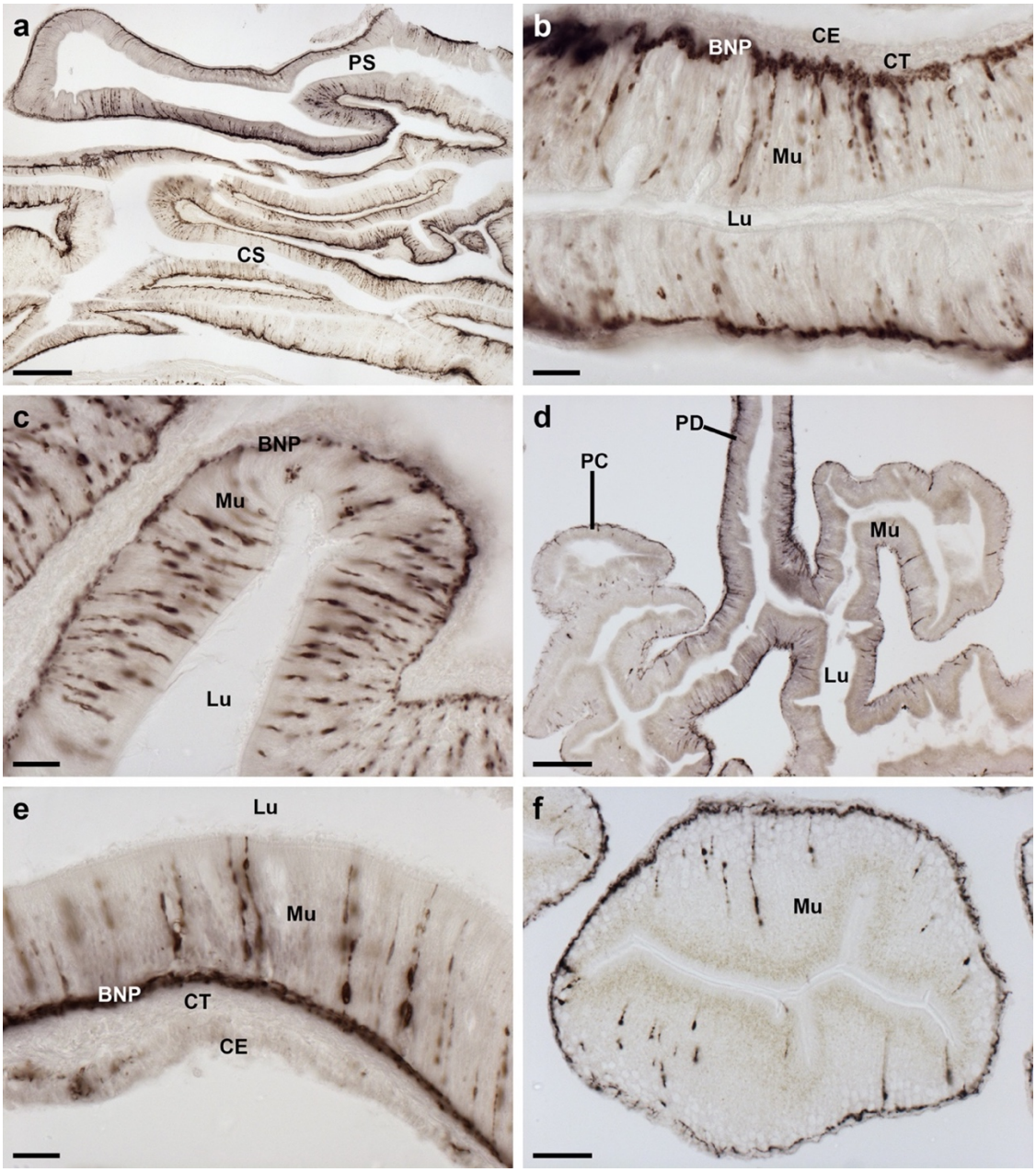

Figure 3.17 Localization of ArPPLN1b immunoreactivity in the cardiac stomach, pyloric stomach, pyloric duct and pyloric caeca of *A. rubens*.
(a) Transverse section of the central disk region showing immunostaining in the cardiac stomach and pyloric stomach. (b) High magnification image of the cardiac stomach showing immunostaining in bipolar-shaped cells in the mucosa and in the underlying basiepithelial nerve plexus. (c) High magnification image of the pyloric stomach showing immunostaining in bipolar-shaped cells in the mucosa and in the underlying basiepithelial nerve plexus. (d) Horizontal section of the arm of a juvenile starfish showing immunostaing in the pyloric duct and pyloric caeca. (e) High magnification image of a transverse section of pyloric duct showing immunostaining in bipolar shaped mucosal cells and in the underlying basiepithelial nerve plexus. (f) High magnification image of a transverse section through a lobe of a pyloric caecum showing immunostaining in bipolar shaped mucosal cells and in the underlying basiepithelial nerve plexus (arrowheads). BNP, basiepithelial nerve plexus; CE, coelomic epithelium; CS, cardiac stomach; CT, collagenous tissue; Lu, lumen; Mu, mucosa; PC, pyloric caeca; PD, pyloric duct; PS, pyloric stomach. Scale bars: 200 µm in (a); 20 µm in (b),

(c), (d); 100 μm in (e); 50 μm in (f). Refer to Figure 1.7 (page 38) and 1.8 (page 39) for details of starfish anatomy.

3.3.4.2.5 Coelomic epithelium, apical muscle, papulae and spines

Immunostained cells are present in the coelomic epithelium that forms the aboral lining of the coelom in each arm (Figure 3.18a, b). The processes of these cells form a sub-epithelial plexus that is closely associated with an underlying thin layer of longitudinally orientated muscle (Figure 3.18c). Separated from the longitudinal muscle by a layer of collagenous tissue, immunostained processes are also present in close association with a layer of circularly orientated muscle. Thus, the coelomic lining is characterized by two separate layers of immunostained fibers. The apical muscle is a thickening of the longitudinal muscle layer of the coelomic lining, which runs in sagittal position along the length of the arm into the central disk region. Immunostained cells are present in the coelomic epithelial lining of the apical muscle and the cross-sectional profiles of immunostained processes can be seen within the apical muscle. As in other regions of the aboral coelomic lining, stained processes are also present in the thin circular muscle layer underneath the apical muscle. The pattern of immunostaining observed in the coelomic epithelium also extends into the lining of the papulae (Figure 3.18a, d), thin-walled finger-like structures that project externally through the body wall. Furthermore, immunostained processes are present in the sub-epithelial plexus of the outer epithelium of the body wall (Figure 3.18a, e).

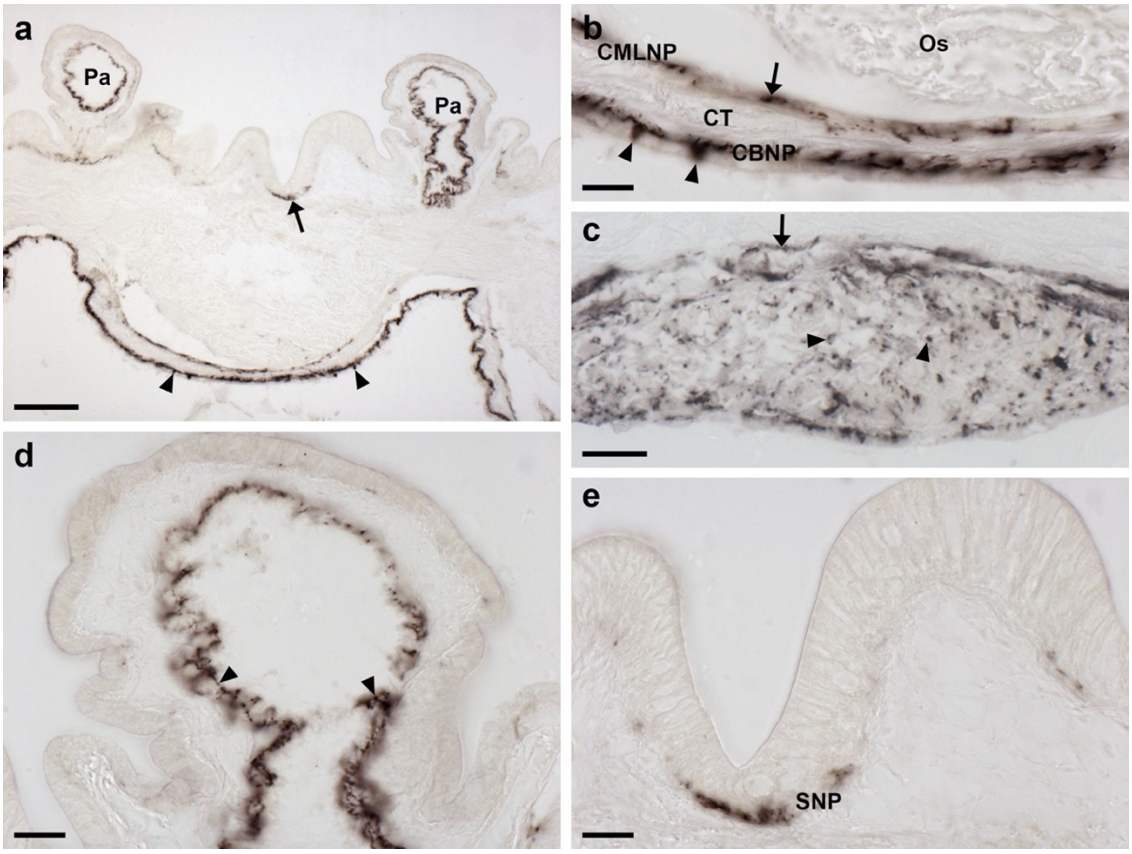

Figure 3.18 Localization of ArPPLN1b immunoreactivity in the body wall, apical muscle and body wall appendages of *A. rubens*.
(a) Transverse section of aboral body wall showing immunostaining in the coelomic lining of the body wall (arrowheads), the coelomic lining of papulae and in the sub-epithelial plexus (arrow) of the external body wall epithelium. (b) High magnification image of the coelomic lining of the body wall showing stained cells in the coelomic epithelium (arrowheads) and in the underlying basiepithelial plexus. Immunostaining is also present in a nerve plexus (arrow) that is closely associated with a layer of circularly orientated muscle. (c) Immunostained axon profiles (arrowheads) in a transverse section of the apical muscle. Longitudinally orientated immunostained processes (arrow) can also be seen associated with a layer of circularly orientated muscle. (d) High magnification view of a longitudinal section of a papula showing immunostaining in the coelomic lining (arrowheads). (e) High magnification of the body wall external epithelium showing immunostaining in the sub-epithelial nerve plexus. CBNP, coelomic basiepithelial nerve plexus; CMLNP, circular muscle layer nerve plexus; CT, collagenous tissue; CuL, cuticle layer; Os, ossicle; Pa, papulae; SNP, sub-epithelial nerve plexus; Sp, spine. Scale bars: 100 μm in (a); 20 μm in (b), (d), (e); 50 μm in (c). Refer to Figure 1.7 (page 38) and 1.8 (page 39) for details of starfish anatomy.

3.3.4.2.6 Interossicular muscles

Immunostained nerve processes can be seen ramifying amongst the muscle fibers of inter-ossicular muscles throughout the body wall (Figure 3.19a-e, g). Comparison of the immunostained sections with adjacent sections stained using

Masson's trichrome method confirmed that the immunostaining fibers are clearly associated with muscles linking adjacent skeletal osscicles and do not appear to be present in the adjacent interossicular collagenous ligaments (Figure 3.19f, g). Furthermore, the immunostained processes extend along the length of muscle fibers into the ossicles (Figure 3.19e, g).

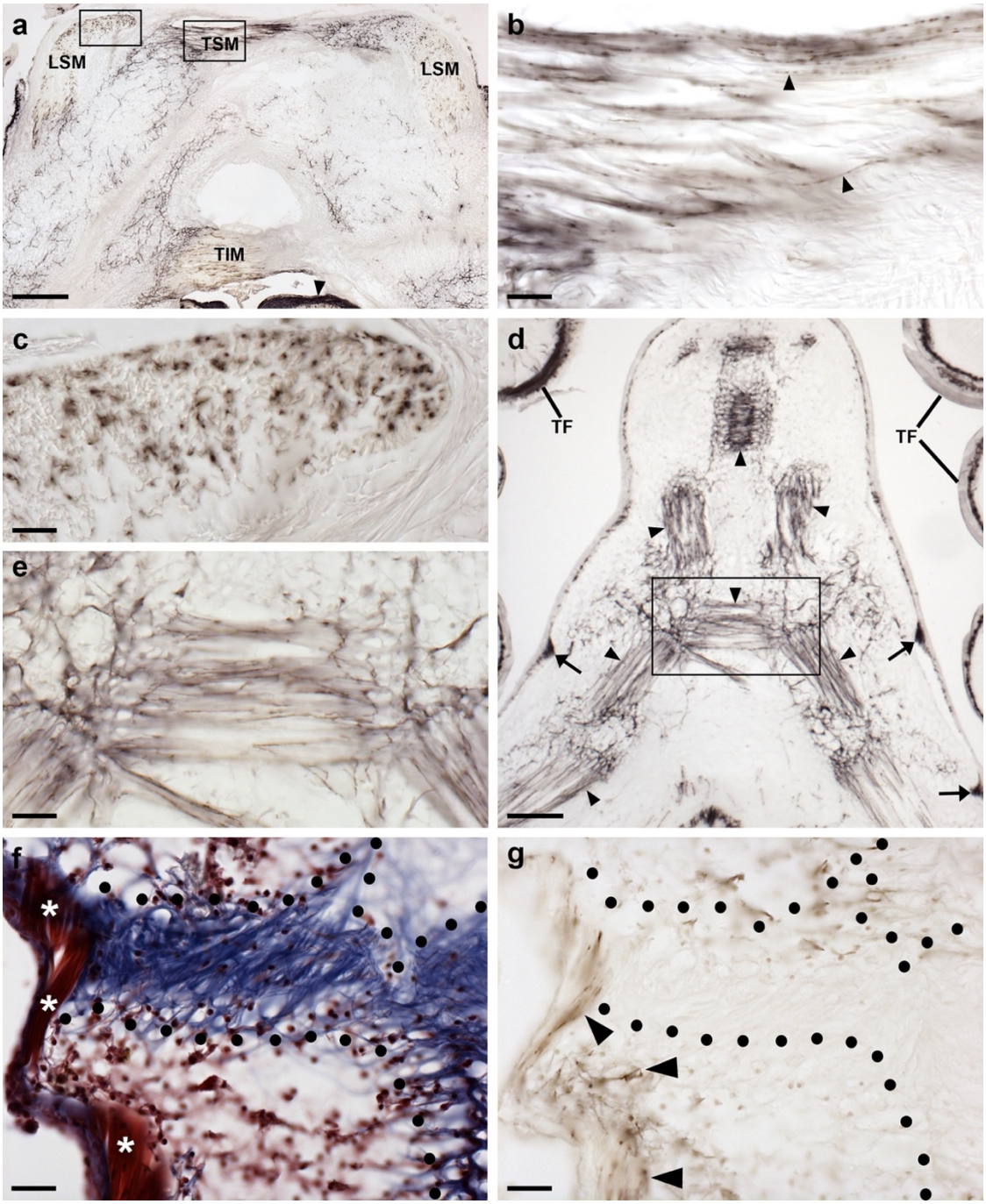

Figure 3.19 Localization of ArPPLN1b immunoreactivity in the innervation of inter-ossicular muscles in *A. rubens*.

(a) Transverse section of the ambulacrum showing immunostaining associated with muscles linking the ambulacral ossicles, which include the TSM, TIM and LSM. The intensely stained radial nerve cord (arrowhead) can also be seen in this image. The boxed regions are shown at higher magnification in panels (b) and (c). (b) A high magnification image showing immunostained nerve fibers (arrowheads) in a longitudinal section through the TSM. (c) A high magnification image showing the immunostained profiles of nerve fibers in a transverse section through the LSM. (d, e) Immunostaining in the body wall at the junction between two arms in a juvenile starfish. Immunostained fibers can be seen associated with muscles that link adambulacral ossicles (arrowheads). Stained fibers are also evident in thickenings of the sub-epithelial nerve plexus of the body wall (arrows) and in the tube feet. (e) High magnification image of the boxed region in (d). (f) Trichrome stained section of the body wall showing an interossicular muscle (white asterisks) and collagenous tissue (area bounded by black dots) linking adjacent ossicles. (g) Immunostained section adjacent to the section shown in panel (f). By comparing the immunstaining with the trichrome staining it can be seen that the immunostained fibers are associated with the inter-ossicular muscle but not with the collagenous tissue (area bounded by black dots). LSM, longitudinal supra-ambulacral muscle; TF, tube foot; TIM, transverse infra-ambulacral muscle; TSM, transverse supra-ambulacral muscle. Scale bars: 200 μm in (a); 20 μm in (b), (c), (e), (f), (g); 100 μm in (d). Refer to Figure 1.7 (page 38) and 1.8 (page 39) for details of starfish anatomy.

3.3.5 Bioactivity of ArPPLN1b in *A. rubens*

3.3.5.1 ArPPLN1b causes dose-dependent relaxation of *in vitro* preparations of apical muscle, tube feet and cardiac stomach from *A. rubens*

ArPPLN1b (FGGKGAFDPLSAGFTD) caused dose-dependent relaxation of apical muscle when tested at *in vitro* concentrations ranging from 10^{-8} to 10^{-6} M and was more effective than S2 (SGPYSFNSGLTF-NH_2) as a relaxant of this preparation (Figure 3.20b). Thus, the relative relaxing effect of ArPPLN1b at 10^{-6} M was 16.29± 2.09% (n = 13), whereas the relative relaxing effect of S2 at 10^{-6} M was only 7.53± 1.70% (n = 11), which is only marginally higher than the relative relaxing effect ArPPLN1b at 10^{-7} M (4.90±0.70%; n = 11).

ArPPLN1b caused dose-dependent relaxation of tube feet when tested at *in vitro* concentrations ranging from 10^{-8} to 10^{-5} M and was more effective than S2 as a relaxant of this preparation (Figure 3.20d). Thus, the relative relaxing effect of ArPPLN1b at 10^{-}

^{5} M was 22.17±1.59% (n = 6), whereas the relative relaxing effect of S2 at 10^{-5} M was only 11.67±1.75% (n = 7), which is the same as the relative relaxing effect ArPPLN1b at 10^{-6} M (11.64±1.24%; n = 6).

ArPPLN1b caused dose-dependent relaxation of cardiac stomach when tested at *in vitro* concentrations ranging from 10^{-10} to 10^{-6} M but was much less effective than S2 as a relaxant of this preparation (Figure 3.20f). Thus, the relative relaxing effect of ArPPLN1b at 10^{-6} M was only 10.43±1.60% (n = 11), whereas the relative relaxing effect of S2 at 10^{-6} M was 48.03±8.17% (n = 5).

Control tests in which 20 µl of the vehicle (water) were added to the organ bath did not cause relaxation or contraction of any of the three preparations used here.

3.3.5.2 ArPPLN1b does not induce cardiac stomach eversion in *A. rubens*

Cardiac stomach eversion was observed within 5 min after injection of S2 (SGPYSFNSGLTF-NH_2) in seven out of ten starfish. By comparison, stomach eversion was not observed in any of the ten starfish injected with ArPPLN1b, even after a 15-min period of observation.

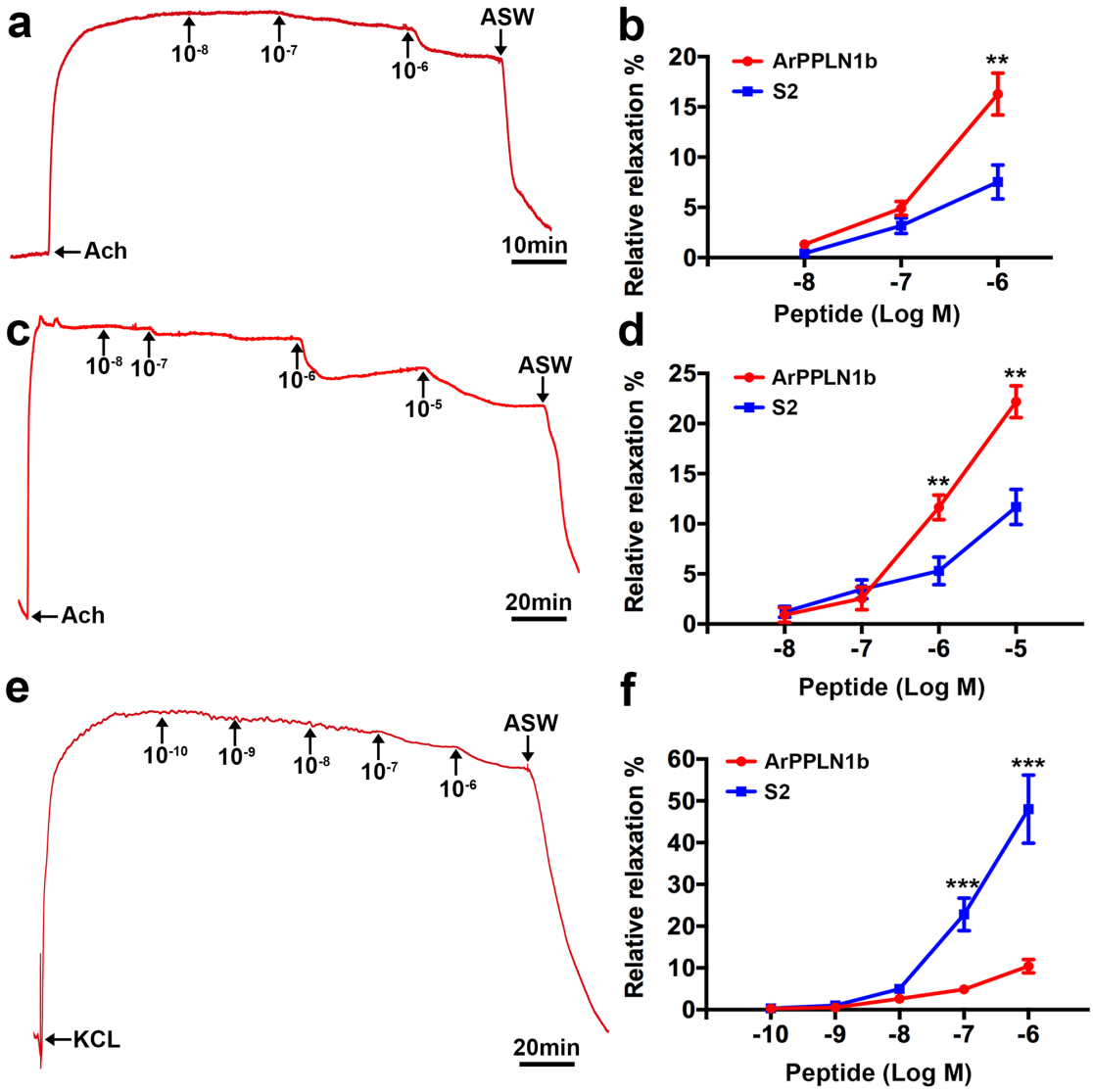

Figure 3.20 Graphs comparing the concentration-dependent relaxing effects of ArPPLN1b (FGGKGAFDPLSAGFTD) and the SALMFamide neuropeptide S2 (SGPYSFNSGLTF-NH_2) on *in vitro* apical muscle, tube foot and cardiac stomach preparations from *A. rubens*.
(a) Representative recording showing the dose-dependent relaxing effect of ArPPLN1b (10^{-8} - 10^{-6} M) on an apical muscle preparation pre-contracted with artificial seawater containing 10^{-6} M added Ach (leftward arrow). (b) Apical muscle, where ArPPLN1b is more effective as a relaxant than S2 when tested at 10^{-6} M ($p = 0.004$; t-test). (c) Representative recording showing the dose-dependent relaxing effect of ArPPLN1b (10^{-8} - 10^{-5} M) on a tube foot preparation pre-contracted with artificial seawater containing 10^{-6} M added Ach (leftward arrow). (d) Tube foot, where where ArPPLN1b is more effective as a relaxant than S2 when tested at 10^{-6} M ($p = 0.007$; t-test) and 10^{-5} M ($p = 0.001$; t-test). (e) Representative recording showing the dose-dependent relaxing effect of ArPPLN1b (10^{-10} - 10^{-6} M) on a cardiac stomach preparation pre-contracted with artificial seawater containing 10 mM added KCL (leftward arrow). (f) Cardiac stomach, where ArPPLN1b is less effective as a relaxant than S2 when tested at 10^{-7} M ($p = 0.0002$; t-test) and 10^{-6} M ($p = 0.00002$; t-test). Following each test with ArPPLN1b, the preparation was washed with artificial seawater (downward arrow). Each point represents the mean ± SEM from at least four separate experiments, with the effect

calculated as the percentage reversal of contraction induced by application of 10 μM acetylcholine (apical muscle and tube foot) or 30 mM KCl (stomach). Ach, acetyl choline; ASW, artificial seawater.

3.4 Discussion

The anatomical distribution and pharmacological actions of PP/OK-type neuropeptides have been characterized in protostomian invertebrates, including mollusks and arthropods (Pearson and Lloyd, 1989; Hall and Lloyd, 1990; Lloyd et al., 1996; De Lange et al., 1997; Beck et al., 2000; Dircksen et al., 2000; Jiang et al., 2015; Wulff et al., 2017). Here the first detailed anatomical analysis of PP/OK-type neuropeptide expression in a deuterostomian invertebrate, the starfish *A. rubens* is reported. Use of both mRNA *in situ* hybridization and immunohistochemistry revealed a widespread pattern of expression of ArPPLNP1 and neuropeptides derived from this precursor, including cells and/or fibers in the radial nerve cords and circumoral nerve ring, tube feet, terminal tentacle, digestive system, coelomic lining, papulae and inter-ossicular muscles. Consistent with previous studies on the starfish *P. pectinifera* (Kim et al., 2016) *in vitro* pharmacological tests revealed that the most abundant of the neuropeptides derived from ArPPLNP1 (ArPPLN1b or ArSMP) causes relaxation of apical muscle, tube foot and cardiac stomach preparations from *A. rubens*. Importantly, these findings indicate that PP/OK-type neuropeptides may act as inhibitory neuromuscular transmitters in starfish. This is interesting because, as discussed in more detail below, it provides new insights into the mechanisms of neuromuscular signaling in echinoderms and the evolution of PP/OK-type neuropeptide function in the animal kingdom. However, it would be simplistic to conclude that the sole function of PP/OK-type neuropeptides derived from the ArPPLNP1 precursor is to act as inhibitory neuromuscular transmitters because the patterns of ArPPLN1b-ir in *A. rubens* indicate signaling roles that extend beyond neuromuscular systems, as also discussed in more detail below.

3.4.1 Physiological interpretation of the anatomy and pharmacological actions of ArPPLNP1-derived neuropeptides in *A. rubens*

3.4.1.1 Radial nerve cords, circumoral nerve ring, tube feet and terminal tentacle

Localization of ArPPLNP1 expression in the radial nerve cords and circumoral nerve ring is consistent with the detection of ArPPLNP1 transcripts in the radial nerve cords of *A. rubens* and *P. pectinifera* using PCR (Kim et al., 2016). More specifically, the visualization of ArPPLNP1 transcripts in cells of both the ectoneural and hyponeural regions of the radial nerve cords and circumoral nerve ring can be interpreted from a physiological perspective. Our knowledge of the functional architecture of the nervous system of starfish and other echinoderms is clearly rather limited by comparison with other invertebrate species that are used as model systems in neurobiology (e.g. *Drosophila*, *C. elegans*, *Aplysia*). Nevertheless, anatomical and electrophysiological studies indicate that the hyponeural region has a purely motor function, whereas the ectoneural region comprises a mixed population of sensory neurons, interneurons and motor neurons (Smith, 1937; 1950; Cobb, 1970; Mashanov et al., 2016). The primary function of the radial nerve cords and circumoral nerve ring is to co-ordinate the activity of tube feet to enable whole-animal locomotor activity (Smith, 1950). Therefore, the expression of ArPPLNP1 and neuropeptides derived from it in ectoneural cell bodies and their processes is indicative of roles in mediating intercellular signaling associated with neural control of tube foot-mediated locomotor activity in starfish. The neuropile of the ectoneural region of the radial nerve cords and circumoral nerve ring is continuous with the basi-epithelial nerve plexus of the tube feet. Therefore, ectoneural neurons in the radial nerve cord and circumoral nerve ring can, in principle, directly control tube foot activity. However, cells expressing ArPPLNP1 are also

located along the length of the tube foot stem in *A. rubens* in close association with the basi-epithelial nerve plexus, which is strongly immunoreactive with antibodies to ArPPLN1b. Accordingly, it has been shown that synthetic ArPPLN1b causes relaxation of *A. rubens* tube foot preparations *in vitro* here. Thus, combining anatomical and pharmacological findings, neuropeptides derived from ArPPLNP1 may act physiologically to cause relaxation of the longitudinally orientated muscle layer in tube feet. This action could be functionally relevant for tube foot extension associated with the cyclical patterns of tube foot activity during starfish locomotor activity (Smith, 1950; Hennebert et al., 2013). Interestingly, ArPPLNP1 is also expressed by cells closely associated with the basal nerve ring in the tube foot sucker, which attaches to and detaches from the substratum during locomotor activity (Smith, 1950; Hennebert et al., 2013), and one possibility is that ArPPLNP1-derived peptides involved in regulation of the secretion of adhesive proteins (Hennebert et al., 2012).

The expression of ArPPLNP1 by cells in the hyponeural region of the radial nerve cords and circumoral nerve ring is consistent with the notion that neuropeptides derived from this precursor act as neuromuscular transmitters in starfish (Smith, 1950; Cobb, 1970; Mashanov et al., 2016). Thus, hyponeural neurons directly innervate the muscle layer of the ampullae, bulb-shaped and fluid-filled contractile organs that control the entry or withdrawal of fluid from the lumen of the tube feet during locomotor activity (Smith, 1950; Hennebert et al., 2013). In accordance with hyponeural expression of ArPPLNP1, ArPPLN1b-ir nerve fibres are present in the ampulla (Figure 3.14). If ArPPLNP1-derived neuropeptides cause relaxation of muscle in the ampulla, then this action could be physiologically relevant in enabling accommodation of fluid in the ampulla during tube foot retraction. Furthermore, the axons of hyponeural neurons project to the lateral motor nerves (Smith, 1950), which also exhibit strong ArPPLN1b-

ir. This is the first study to demonstrate the presence of a neuropeptide in the lateral motor nerves, which is important because the presence of immunostained fibers in the lateral motor nerves is consistent with notion that ArPPLN1-type neuropeptides act as neuromuscular transmitters that control the activity of body wall interossicular muscles, as discussed in more detail below.

The terminal tentacle is a specialized tube foot-like sensory organ located at the tips of each arm in starfish, which can be extended and retracted (Hennebert et al., 2013). Consistent with the expression of ArPPLNP1 by cells along the length of tube foot stems, this precursor and neuropeptides derived from it are also expressed by cells in the wall of the terminal tentacle. Accordingly, by analogy with tube feet, neuropeptides derived from ArPPLNP1 could act as muscle relaxants to enable extension of the terminal tentacle. Interestingly, ArPPLNP1 expressing cells and ArPPLN1b-ir cells and fibres are also present in flaps of tissue known as lateral lappets (Smith, 1937), which are located on both sides of the terminal tentacle. To the best of our knowledge, the functions of these structures has not been investigated. One possibility is that the lateral lappets have a chemosensory function, providing an expanded surface area for detection of environmental chemical cues from, for example, conspecifics or prey. It is noteworthy that ArPPLN1b-ir is also present in the optic cushion, a photo sensory organ located at the base of each terminal tentacle, and further studies are required to investigate the functional significance this.

3.4.1.2 Digestive system

ArPPLNP1 transcripts and ArPPLN1b-ir are present in many regions of the digestive system, including the peristomial membrane that surrounds the oral opening, the esophagus, cardiac stomach, pyloric stomach and the pyloric caeca. *In vitro*

pharmacological tests with ArPPLN1b revealed that this peptide causes relaxation of cardiac stomach preparations. However, ArPPLN1b was less effective as a relaxant of the cardiac stomach than the *A. rubens* neuropeptide SALMFamide-2 (S2). This contrasts with a previous study on the starfish *P. pectinifera*, where *P. pectinifera* SMP (a homolog of ArPPLN1b) was found to be equally as effective as *A. rubens* S2 in causing *in vitro* relaxation of the cardiac stomach (Kim et al., 2016). A likely explanation for this is that S2 is not a naturally occurring neuropeptide in this species, based on analysis of genome/transcriptome sequence data from the closely related species *P. miniata* (Elphick et al., 2015). In *P. miniata* there is an S2-like peptide but its sequence is different to that of S2 from *A. rubens* and therefore S2 may be less effective as a cardiac stomach relaxant in *P. pectinifer*a than the naturally occurring S2-like peptide in this species.

S2 belongs to a family of neuropeptides known as SALMFamides, which were the first echinoderm neuropeptides to be sequenced (Elphick et al., 2015). Immunocytochemical analysis of the expression of S2 in *A. rubens* reveals that, like ArPPLNP1-derived neuropeptides, it is widely expressed, including the cardiac stomach and other regions of the digestive system (Newman et al., 1995a). Injection of *A. rubens* with S2 can induce cardiac stomach eversion, indicating a physiological role in the regulation of the extraoral feeding behaviour of starfish (Melarange et al., 1999). Here it has been compared that the effects of injecting equimolar amounts of S2 and ArPPLN1b in *A. rubens* and found that S2 induced stomach eversion in seven out ten animals but stomach eversion was not observed in any of the animals injected with ArPPLN1b. These findings are consistent with *in vitro* pharmacological experiments, where ArPPLN1b was found to be less effective as a cardiac stomach relaxant than S2. Collectively, these observations lead us to conclude that the physiological roles of

ArPPLNP1-derived neuropeptides in the digestive system *A. rubens* may not be limited to acting as muscle relaxants. If this is the case, then what other roles might ArPPLNP1-derived neuropeptides have in the digestive system of *A. rubens*?

Previous studies have revealed that molluscan pedal peptides stimulate ciliary activity on the surface of the foot in *Aplysia* and in the salivary ducts of *Tritonia* (Willows et al., 1997; Gaston, 1998). It is noteworthy, therefore, that cells expressing ArPPLNP1 and associated ArPPLN1b-ir are located in regions of the digestive system in *A. rubens* that enable ciliary-mediated movement of food material. For example, the pyloric ducts transfer food material from the pyloric stomach to the pyloric caeca. Experimental observation of ciliary-generated currents has revealed that cells on the oral side of the pyloric duct generate centrifuge currents that move material from the pyloric stomach to pyloric caeca, whereas cells on the aboral side of the pyloric duct generate centripete currents that move material from the pyloric caeca to the pyloric stomach (Irving, 1924; Jangoux, 1982). Interestingly, ArPPLNP1-expressing cells (Figure 3.8a) and ArPPLN1b-ir are more abundant on the oral side of the pyloric duct in *A. rubens*. Furthermore, ciliary-mediated movement of food material occurs throughout the starfish digestive system (Anderson, 1953; 1954) and a potential role for ArPPLNP1-derived neuropeptides would be in regulation of ciliary-mediated movement of food material through the digestive system of *A. rubens*.

3.4.1.3 Coelomic lining, apical muscle, papulae and body wall sub-epithelial plexus

The most prominent components of the nervous system in starfish are the ectoneural and hyponeural systems that form the radial nerve cords and circumoral nerve ring, as highlighted above. However, in crinoid echinoderms (e.g. feather stars) there is a third component to the nervous system that is more prominent than the

ectoneural and hyponeural systems - this is the entoneural or aboral system (Smith, 1937). In starfish, the entoneural system is also present but is relatively inconspicuous when compared to that in crinoids. It comprises neurons located within the coelomic lining of the aboral body wall in close association with an underlying layer of longitudinally orientated muscle and another population of neurons associated with a deeper layer of circularly orientated muscle. A prominent feature associated with the aboral nervous system in starfish is the apical muscle, a thickening of the longitudinally orientated muscle layer that is located along the midline of each arm. Furthermore, from a functional perspective, contraction of the apical muscle facilitates flexion of the arms during behaviors that require changes in arm posture (e.g. feeding and righting behavior) (Smith, 1950).

It was the use of the apical muscle as a bioassay system for myoactive neuropeptides that enabled the purification of starfish myorelaxant peptide (SMP) from *P. pectinifera* (Kim et al., 2016). ArPPLN1b is a homolog of SMP from *P. pectinifera* and accordingly here ArPPLN1b was found to cause relaxation of *in vitro* preparations of the apical muscle from *A. rubens* (Figure 3.20b).

Previous studies have reported that the SALMFamide neuropeptide S2 also causes relaxation of the apical muscle in *A. rubens*, although only at relatively high concentrations (Melarange and Elphick, 2003). Consistent with previously reported findings from *P. pectinifera*, here it is shown that ArPPLN1b is more potent/effective than the SALMFamide neuropeptide S2 in causing relaxation of the apical muscle. This contrasts with converse findings from cardiac stomach preparations, where S2 is more potent/effective than ArPPLN1b (see above and Figure 3.20f).

Consistent with the *in vitro* pharmacological effects of ArPPLN1b on apical muscle preparations, cells expressing ArPPLNP1 transcripts are located in the coelomic epithelium overlying the apical muscle (Figure 3.9a-d) and the immunostained axonal processes of these cells can be seen in transverse sections of the apical muscle (Figure 3.18c). Expression of ArPPLNP1 also extends beyond the apical muscle to cells in the coelomic epithelium located throughout the lining of the aboral body wall and accordingly ArPPLNP1-ir is present in throughout the longitudinally orientated muscle layer of the coelomic lining aborally. Immunostained processes are also present in the underlying circularly orientated muscle layer of the coelomic lining (Figure 3.18a, b), which may be derived from the lateral motor nerves (Smith, 1950).

The coelomic lining of the aboral body wall extends into papulae, thin-walled and retractable dermal appendages that penetrate through the body wall to enable gas exchange between the external seawater and the coelomic fluid (Cobb, 1978). ArPPLN1b-ir is present in fibres located within the coelomic lining of the papulae and these fibres are continuous with the innervation of the longitudinally and circularly orientated muscle layers of the coelomic lining of the aboral body wall (Figure 3.18a, d). Given that ArPPLN1b (ArSMP) acts as relaxant of the apical muscle, it seems likely that ArPPLNP1-derived neuropeptides also cause relaxation of muscle associated with the dermal papulae. Therefore, PP/OK-type neuropeptides may participate in neural mechanisms controlling the protraction of papulae from the aboral body surface of starfish.

ArPPLN1b-ir is also present within the sub-epithelial nerve plexus below the external epithelium of the body wall and associated with appendages, such as spines and pedicellariae. These two types of appendages are mainly involved in passive and active

defense in starfish (Dubois and Ameye, 2001) and ArPPLNP1-drived peptides may be involved in regulation of the activity of these appendages.

3.4.1.4 Interossicular muscles

One of the most striking features of ArPPLN1b-ir in *A. rubens* is the presence of immunoreactive nerve fibres associated with interossicular muscles. The starfish endoskeleton comprises calcite ossicles that are interlinked by both collagenous ligaments and interossicular muscles (Blowes et al., 2017) and changes in body posture are mediated by changes in the contractile state of the muscles that connect adjacent ossicles. Importantly, this is the first study to report the presence of neuropeptide-expressing nerve fibres in the inter-ossicular muscles of starfish. Consistent with the presence of ArPPLN1b-ir in nerve processes in the inter-ossicular muscles, ArPPLN1b-ir is also present in the lateral motor nerves (see above).

As ArPPLN1b (ArSMP) causes relaxation of muscle associated with the apical muscle, tube feet and cardiac stomach, it seems likely that ArPPLNP1-derived neuropeptides also act to cause relaxation of the inter-ossicular muscles. Experimental studies specifically designed to investigate the effect of ArPPLNP1-derived neuropeptides on inter-ossicular muscles are now required to address this hypothesis.

4 Identification, localization and functional characterization of neuropeptides derived from pedal peptide-like neuropeptide precursor 2 in the starfish *Asterias rubens*

4.1 Introduction

In chapter 3, a detailed analysis of the anatomy of ArPPLNP1 expression in *A. rubens* using mRNA *in situ* hybridization and immunohistochemistry was reported. Consistent with qPCR data from *P. pectinifera* (Kim et al., 2016), a widespread pattern of expression of ArPPLNP1 and the neuropeptides derived from this precursor was revealed in *A. rubens*. Thus, cells expressing ArPPLNP1 transcripts were detected, for example, in the radial nerve cords, circumoral nerve ring, esophagus, cardiac stomach, pyloric stomach, pyloric caeca, tube feet and body wall. Immunohistochemical analysis using antibodies to one of the neuropeptides derived from ArPPLNP1 (ArPPLN1b) revealed a pattern of immunostained cells consistent with data obtained using mRNA *in situ* hybridization. Furthermore, immunohistochemistry revealed extensive networks of immunostained processes in the radial nerve cords, circumoral nerve ring, digestive system, tube feet, coelomic lining, apical muscle and body wall. One of the most striking features of the immunostaining was the presence of labeled processes in close association with interossicular muscles that link the calcite ossicles of the endoskeleton. Consistent with this pattern of expression, intense immunostaining was also observed in the lateral motor nerves, components of the starfish nervous system that were first described based on analysis of histochemical staining (Smith, 1937). Investigation of the *in vitro* pharmacological effects of ArPPLN1b (ArSMP) revealed that it causes dose-dependent relaxation of three preparations from *A. rubens* - apical muscle, tube feet and cardiac stomach, consistent with previous findings from *P. pectinifera* (Kim et

al., 2016). Thus, collectively the data obtained from experimental studies on SMP/PPLN1-type neuropeptides in *P. pectinifera* and *A. rubens* indicate that a physiological role of these peptides is to act as inhibitory neuromuscular transmitters in starfish.

A partial sequence of a second *A. rubens* PP/OK-type precursor, now referred to as ArPPLNP2, has been reported, which comprises a 31-residue N-terminal signal peptide and seven putative neuropeptides bounded by dibasic cleavage sites ((Semmens et al., 2016; GenBank: KT601720). A putative peptide (SAFSGSRGLTNLASGFN) derived from this partial ArPPLNP2 shares sequence similarity with other PP/OK-type peptide representatives in lophotrochozoans (e.g. *Capitella, Lottia*) and orcokinin-type peptides in arthropods (e.g. *Drosophila*).

4.1.1 Aims and objectives

Nothing is known about the expression pattern or actions of neuropeptides derived from the second PP/OK-type neuropeptide precursor in *A. rubens* - ArPPLNP2. Therefore, the objective of the experimental work reported in this chapter was to address this issue. Firstly, a cDNA encoding the full length amino acid sequence of ArPPLNP2 was cloned and sequenced. Secondly, mass spectrometry was used to determine the structures of neuropeptides derived from ArPPLN2 by analyzing *A. rubens* radial nerve cord extracts. Thirdly, mRNA *in situ* hybridization was used to map the expression of ArPPLNP2 transcripts in *A. rubens*. Fourthly, an antiserum to one of the peptides derived from ArPPLNP2 (ArPPLN2h) was generated and characterized using an enzyme-linked immunosorbent assay (ELISA). Fifthly, immunohistochemistry was used to map the expression of ArPPLN2h in *A. rubens*. Lastly, *in vitro* pharmacology was used to investigate the effects of ArPPLN2h on the three

preparations from *A. rubens* – apical muscle, tube foot and cardiac stomach. The findings of this study provide new insights into the physiology of PP/OK-type neuropeptide signaling in the phylum Echinodermata.

4.2 Methods

4.2.1 Animals

Starfish (*A. rubens*) with a diameter > 4 cm were collected at low tide from the Thanet coast (Kent, UK) or were obtained from a fisherman based at Whitstable (Kent, UK). These animals were maintained in a circulating seawater aquarium at ~12 ^{o}C in the School of Biological and Chemical Sciences at Queen Mary University of London and were fed on mussels (*Mytilus edulis*). Smaller juvenile specimens of *A. rubens* (diameter 0.5 - 1.5 cm) were collected at the University of Gothenberg Sven Lovén Centre for Marine Infrastructure (Kristenberg, Sweden) and fixed in Bouin's solution.

4.2.2 cDNA cloning and sequence analysis

Analysis of *A. rubens* radial nerve cord transcriptome sequence data has enabled identification of a contig encoding the partial sequence (325 residues) of pedal peptide-like neuropeptide precursor 2 (ArPPLNP2), which comprises a 31-residue N-terminal signal peptide and seven putative neuropeptides bounded by dibasic cleavage sites (Semmens et al., 2016; GenBank Accession number KT601720). To facilitate cloning and sequencing of the complete open reading frame of ArPPLNP2, ovarian transcriptome sequence data obtained from other starfish species was analysed [(Reich et al., 2015); http://www.echinobase.org/Echinobase/Blasts] and a contig (GAUS01023767.1) comprising the 3' region of PPLNP2 was identified in *Asterias forbesi*. Combining the partial PPLNP2 transcript sequences from *A. rubens* and *A. forbesi*, forward and reverse primers (5'-GAGACATCGAGGGTGGTTTTG-3', 5'-GGCCCGGCCTAAGAATCAT-3') were designed to enable PCR amplification of a full-length ArPPLNP2 cDNA from *A. rubens*.

The methods used for RNA extraction, cloning and sequencing were as described previously in chapter 2, but with minor modifications. Zero Blunt TOPO PCR cloning kit (Invitrogen, Carlsbad, CA, USA) was used to ligate the PCR product into the pCR-Blunt II with TOPO vector for sequencing of a ArPPLNP2 cDNA comprising the entire ORF. T-easy vector (Promega) was employed for cloning a cDNA comprising a partial ORF of ArPPLNP2, using the following primers: 5'-CTATTCTGTCTGGCTCTT-3' (forward) and 5'- GACAGCTTCTTCTCTCTTA-3' (reverse).

4.2.3 Mass spectrometry

The structures of neuropeptides derived from ArPPLNP2 were determined by MS/MS analysis of *A. rubens* radial nerve cords extracted in 90% methanol/9% acetic acid, as described previously in chapter 2. The pH of the extracts was adjusted using ammonium bicarbonate and then the extracts were reduced with dithiothreitol (DTT) and alkylated using iodoacetamide, but the extracts were not treated with trypsin or any other proteolytic enzyme. Samples of the extract were analysed using nanoLC-ESI-MS/MS using an Orbitrap Fusion (ThermoScientific) and data analysis was performed as described in chapter 2, except that more recent versions of Mascot (Matrix Science, London, UK; version 2.5.0) and Scaffold (version Scaffold_4.5.3, Proteome Software Inc., Portland, OR) were used to annotate the spectra presented in the results section. Mascot was searched with a fragment ion mass tolerance of 0.050 Da and a parent ion tolerance of 10.0 PPM. Conversion of Gln- to pyro-Glu at the N-terminus, amidation of the C-terminus, oxidation of methionine and carbamidomethyl of cysteine were specified in Mascot as variable modifications.

4.2.4 Localization of ArPPLNP2 using mRNA *in situ* hybridization

A cDNA comprising a partial ORF of ArPPLNP2 was used as a template for synthesis of probes for mRNA *in situ* hybridization. The methods employed for i) production of anti-sense and sense DIG-labeled RNA probes, ii) preparation of sections of fixed specimens (diameter 4 - 6 cm) of *A. rubens* and iii) visualization of ArPPLNP2 transcripts in sections of *A. rubens* were the same as reported in chapter 2.

4.2.5 Localization of ArPPLNP2-derived neuropeptides using immunohistochemistry

4.2.5.1 Production and characterization of rabbit antisera to ArPPLNP2-derived neuropeptides

The peptide ArPPLN2h (GRTSLSGSSGLTHLSSGFH) was selected as representative target antigen for production of rabbit antibodies to ArPPLN2-derived neuropeptides. A peptide comprising the C-terminal octapeptide of ArPPLN2h but with the addition of N-terminal lysine and tyrosine residues (KYTHLSSGFH) was designed as an antigen (ag) peptide (ArPPLN2h-ag) and synthesized by Peptide Protein Research Ltd. (Hampshire, UK). The inclusion of a lysine residue was to enable glutaraldehyde-mediated coupling to a carrier protein (thyroglobulin) and the inclusion of a tyrosine was to enable production of a 125-iodine-labelled peptide so that the antibodies could be used for radioimmunoassay, if required. Rabbit immunization with the ArPPLN2h-ag - thyroglobulin conjugate and serum collection was performed by Charles River Labs (Margate, UK), as described previously for ArPPLN1b (chapter 3).

To assess production of antibodies during the immunization protocol and following collection of a terminal bleed, antisera were tested for antibodies to ArPPLN2h-ag using Enzyme-Linked ImmunoSorbent Assays (ELISA), employing the same methods as described previously for ArPPLN1b (chapter 3).

4.2.5.2 Tissue fixation, sectioning and immunostaining

The methods employed for i) preparation of sections of fixed specimens (diameter 4 - 6 cm) of *A. rubens*, ii) visualization of ArPPLN2h expression in sections of *A. rubens* using immunohistochemistry (including pre-absorption tests) and iii) photography of immunostained sections and preparation of montages were the same as those reported for ArPPLN1b in chapter 3.

4.2.6 *In vitro* and *in vivo* bioassay and pharmacology

Consistent with the selection of ArPPLN2h (GRTSLSGSSGLTHLSSGFH) as a representative neuropeptide for generation of antibodies (see above), ArPPLN2h was also selected as a representative ArPPLNP2-derived peptide for *in vitro* and *in vivo* pharmacological experiments. ArPPLN2h was synthesized by Peptide Protein Research Ltd. (Hampshire, UK) and was tested on *in vitro* preparations of the cardiac stomach, apical muscle and tube foot from *A. rubens,* using the same methods reported previously for ArPPLNP1b (chapter 3). The SALMFamide neuropeptide S2 (SGPYSFNSGLTF-NH_2), which is a known relaxant of the cardiac stomach, apical muscle and tube feet in *A. rubens* (Melarange et al., 1999; Melarange and Elphick, 2003), was tested in parallel with ArPPLN2h both as a positive control and to enable comparative analysis of potency/efficacy. A previous study demonstrated that S2 causes eversion of the cardiac stomach in *A. rubens* when injected *in vivo* (Melarange et al., 1999). Therefore, here the effect of *in vivo* injection of ArPPLN2h in *A. rubens* was investigated by intracoelomic injection of starfish (n = 10) with 100 µl of 1 mM ArPPLN2h.

4.3 Results

4.3.1 Cloning and sequencing of a cDNA encoding ArPPLNP2

A cDNA encoding ArPPLNP2 was cloned and sequenced (GenBank accession number KT601720), as illustrated in Figure 4.1. The ArPPLNP2 transcript is a 1761-base cDNA comprising an opening reading frame of 1692-bases and a 69-base 5' untranslated region (Figure 4.1). The ArPPLNP2 ORF encodes a 563 amino acid residue protein comprising a 31-residue signal peptide and 13 copies of predicted PP/OK-type peptides, which are named ArPPLN2a-k according to their position in the precursor protein. Thus, there are three copies of ArPPLN2h (GRTSLSGSSGLTHLSSGFH) and one copy of each of the following: GRTNMYGSSQLSRLSSGFN (ArPPLN2a), GRSSFAGSSRLTNLGSGFT (ArPPLN2b), GRSSFTGSSRLTNLASGFN (ArPPLN2c), GRSAFSGSRGLTNLASGFN (ArPPLN2d), GRSSFAGVSGLTHLGSGFN (ArPPLN2e), GRSAFSGSKGLTNLASGFN (ArPPLN2f), GRTSLSGSGGLTNLSSGFH (ArPPLN2g), GRSSFSGSNGLTNLGSGFH (ArPPLN2i) GRTSLSGSSGLTHLGSGFH (ArPPLN2j), GRSHFTGSSRLTNLNSGFN (ArPPLN2k) (Figure 4.1, 4.2a). As illustrated in Figure 4.2a, all the peptides have the conserved motifs GRT/S and LTH/NLxSGFH/N located N-terminally and C-terminally, respectively. Furthermore, comparison of ArPPLN2h, as a representative peptide, with other PP/OK-type peptides revealed sequence conservation at several positions, but most notably three hydrophobic residues: Leu^{5} located in the N-terminal region and Leu^{14} and Phe^{18} located in the C-terminal region.

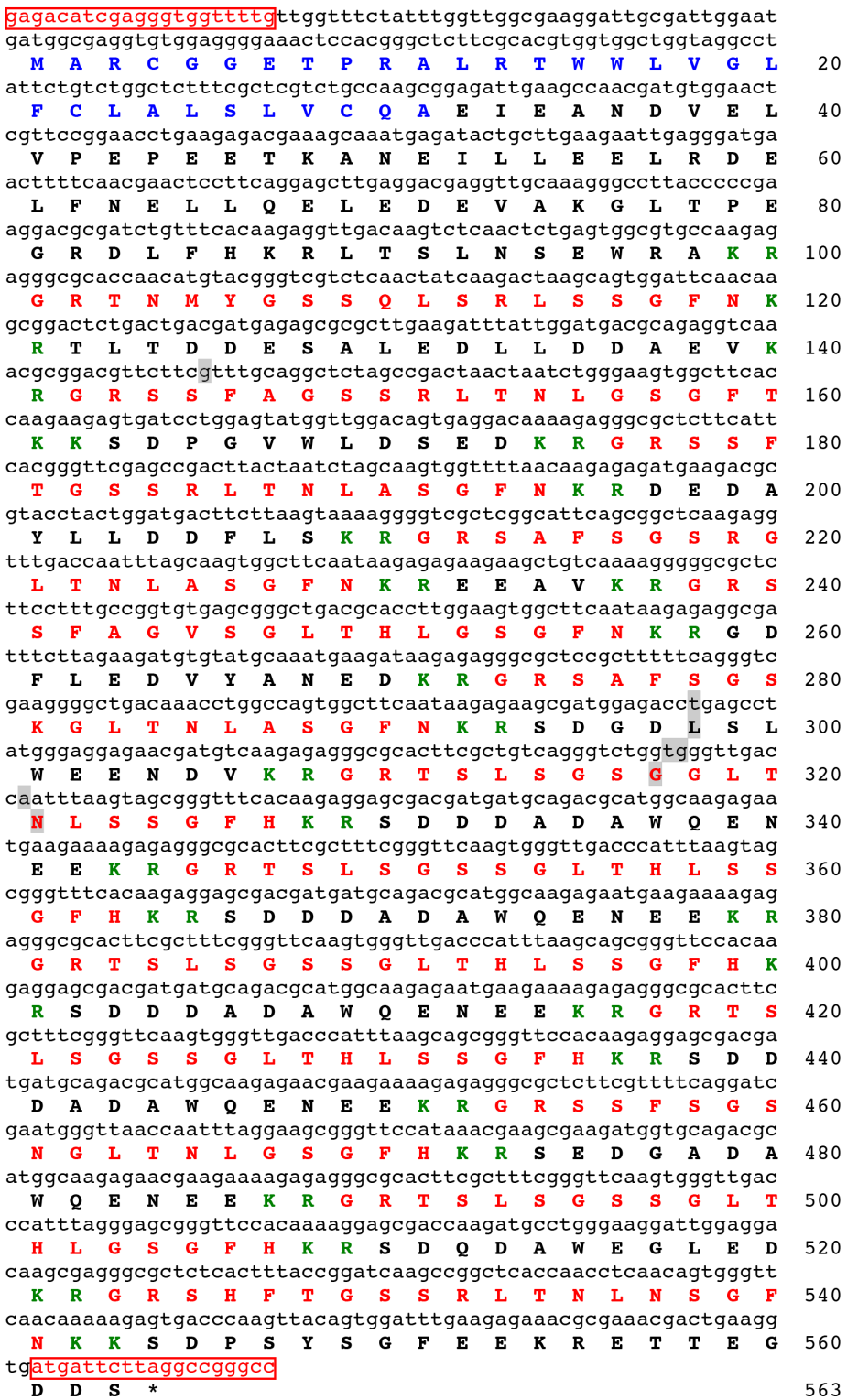

Figure 4.1 *A. rubens* pedal peptide-like neuropeptide precursor 2 (ArPPLNP2). The nucleotide sequence (lowercase, 1761 bases) of a cloned cDNA encoding ArPPLNP2 (uppercase, 563 amino acid residues) is shown. The predicted signal peptide is shown in blue, thirteen putative neuropeptides derived from the precursor protein are shown in red and putative dibasic cleavage sites are shown in green. The asterisk shows the position of the stop codon. The nucleotide sequences used for primer design are highlighted in red within red boxes. Nucleotides and amino acids that differ from the previously reported partial contig assembled from transcriptome sequence data

(Semmens et al., 2016) are highlighted in grey. The ArPPLNP2 cDNA sequence has been deposited under GenBank accession number KT601720.

a

```
ArPP2h          GRTSLSGSSGLTHLSSGFH
ArPP2a          ···NMY···Q·SR·····N
ArPP2b          ··S·FA···R··N·G···T
ArPP2c          ··S·FT···R··N·A···N
ArPP2d          ··SAF···R···N·A···N
ArPP2e          ··S·FA·V·····G···N
ArPP2f          ··SAF···K···N·A···N
ArPP2g          ·········G···N·····
ArPP2i          ··S·F···N···N·G····
ArPP2j          ·············G····
ArPP2k          ··SHFT···R··N·N···N
```

b

Phylum	Species	Peptide name	Sequence
Echinodermata	*A. rubens*	ArPPLN2h	GRTSLSGSSG-LTHLSSGFH
Echinodermata	*A. rubens*	ArPPLN1b	FGGK-GAFDPLSAGFTD
Echinodermata	*P. pectinifera*	PpeSMPa	FGKG-GAYDPLSAGFTD
Echinodermata	*S. purpuratus*	SpPPLN1d	GFNS--GAMEPLGSGFI
Echinodermata	*S. purpuratus*	SpPPLN2h	-FG---GANEPMRSGFF
Echinodermata	*A. japonicus*	AjPPLN2a	FGN-SN-MDPLVHSLIGG
Mollusca	*A. californica*	PP1-peptide	PLDSVYG-THGM-SGFA
Mollusca	*A. californica*	PP3-peptide	RLDSIAG-SSGF-SNFG
Annelida	*P. dumerilii*	FDSIG-peptide	SFDSI-GHSSNF-AGLD
Nematoda	*C. elegans*	NLP14-peptide	ALDGLDG--AGF--GFD
Nematoda	*C. elegans*	NLP15-peptide	AFDSLAG--SGFDNGFN
Arthropoda	*O. limosus*	Orcokinin	NFDEIDR--SGF--GFN

Figure 4.2 Alignment of predicted neuropeptides derived from ArPPLNP2 (a) and alignment of ArPPLN2h as a representative ArPPLNP2-derived peptide with PP/OK-type peptides in other species (b).
(a) Three copies of ArPPLN2h occur in ArPPLNP2, whereas all the other peptides occur singly (see Figure 4.1). Therefore, the alignment compares the sequences of the single-copy peptides with the sequence of ArPPLN2h. All of the predicted peptides derived from ArPPLNP2 comprise nineteen residues. Residues that are identical to the corresponding residue in ArPPLN2h are shown with a black dot. Eight of the residues in ArPPLN2h are conserved in the ten other peptides (highlighted in yellow). (b) Manual alignment of ArPPLN2h with ArPPLN1b and with PP/OK-type peptides from other species. Hydrophobic residues (Phe, Leu or Met) are conserved at three positions (highlighted in yellow), one located in the N-terminal region and two located in the C-terminal region. Other residues that are conserved between peptides from at least one deuterostome (echinoderm) species and at least one protostome species are highlighted in grey. Citations and/or accession numbers for the peptide sequences included here are as follows: ArPPLN2h (this paper; KT601720); ArPPLN1b (Kim et al., 2016; Chapter 3; KT870153); PpeSMPa (Kim et al. 2016; KT870152); SpPPLN1d (Rowe and Elphick, 2012; XP_785647); SpPPLN2h (Rowe and Elphick, 2012; XP_003727926); AjPPLN2a (Rowe et al., 2014; Isotig 17873); PP1-peptide (Lloyd and Connolly, 1989; Moroz et al., 2006; NP_001191585); PP3-peptide (Moroz et al., 2006; NP_001191625); NLP14-peptide (NP_001257067); NLP15-peptide (T20275); orcokinin (Stangier et al., 1992; P37086).

4.3.2 Mass spectrometric detection of ArPPLNP2-drived neuropeptides in *A. rubens* radial nerve cords extract

Ten of the eleven predicted peptides derived from ArPPLNP2 (Figure 4.3, 4.4) were detected by MS/MS in an acidified methanol extract of radial nerve cord that was subject to reduction and alkylation but without additional protease (trypsin) treatment. ArPPLN2a (GRTNMYGSSQLSRLSSGFN, 688.00 m/z, 3+ ions, Figure 4.3b), ArPPLN2b (GRSSFAGSSRLTNLGSGFT, 634.65 m/z, 3+ ion, Figure 4.3c), ArPPLN2d (GRSAFSGSRGLTNLASGFN, 633.65 m/z, 3+ ion, Figure 4.3d), ArPPLN2e (GRSSFAGVSGLTHLGSGFN, 617.64 m/z, 3+ ions, Figure 4.3e), ArPPLN2f (GRSAFSGSKGLTNLASGFN, 624.32 m/z, 3+ ions, Figure 4.3f), ArPPLN2g-partial (GRTSLSGSGGLT, observed at 546.78 m/z, 2+ ion, Figure 4.4a), ArPPLN2h (GRTSLSGSSGLTHLSSGFH, 629.98 m/z, 3+ ions, Figure 4.4b), ArPPLN2i (GRSSFSGSNGLTNLGSGFH, 627.97 m/z, 3+ ions, Figure 4.4c), ArPPLN2j (GRTSLSGSSGLTHLGSGFH, 619.98 m/z, 3+ ions, Figure 4.4d), ArPPLN2k (GRSHFTGSSRLTNLNSGFN, observed at 513.76 m/z, 4+ ion, Figure 4.4e) were detected in the radial nerve extract. ArPPLN2a, e, f, h, i, j were detected with high quality MS/MS data, whereas ArPPLN2b, d, g, k were detected with low quality MS/MS data.

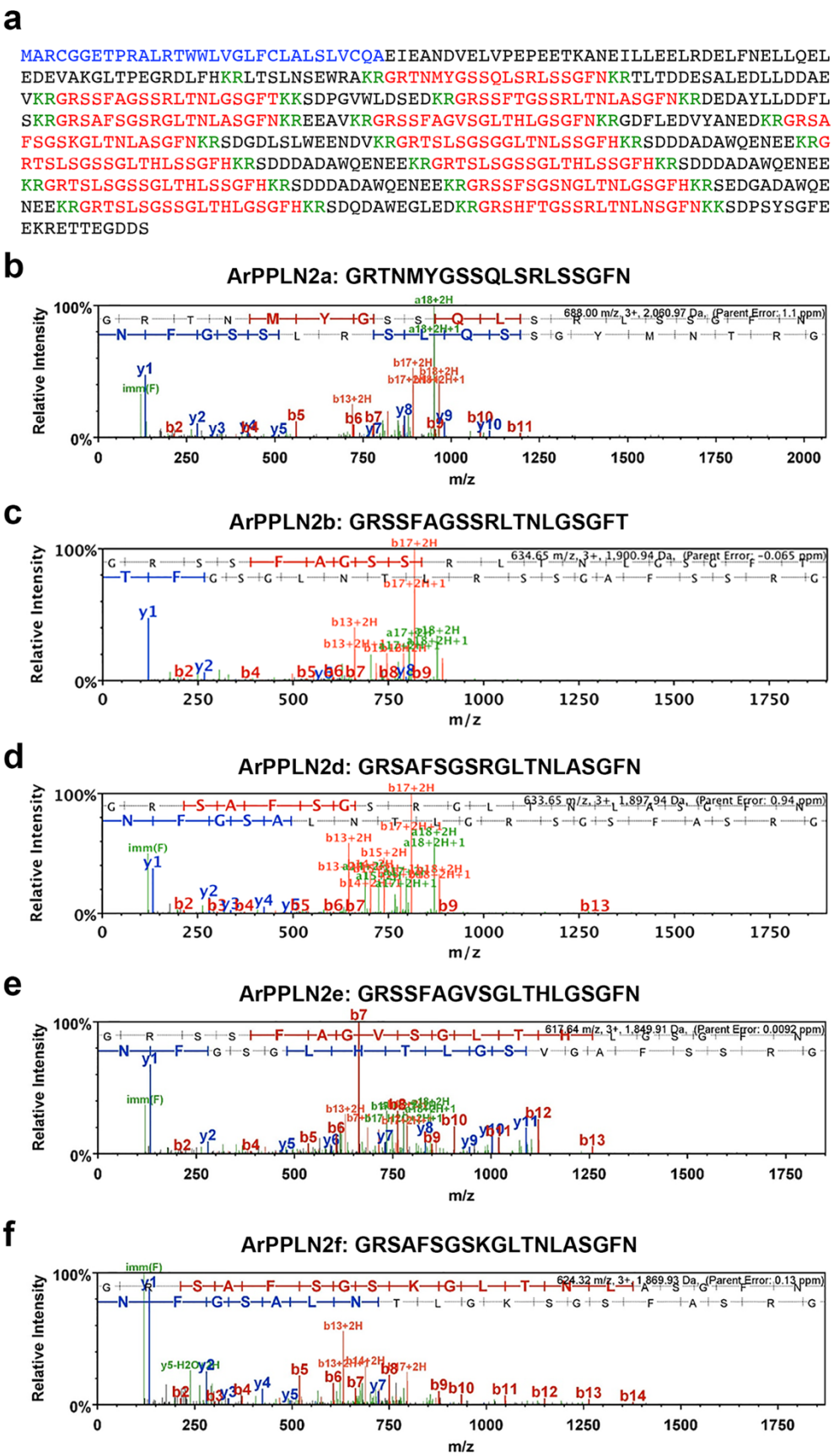

Figure 4.3 Mass spectrometric identification of ArPPLN2 peptides in an extract of *A. rubens* radial nerve cords.
(a) Sequence of ArPPLNP2 with the predicted signal peptide marked in blue, predicted

cleavage sites marked in green, and peptides ArPPLN2 a to k marked in red. (b - f) annotated MS/MS spectra for ArPPLN2a, b, d, e, f, respectively. The b series of peptide fragment ions are shown in red, the y series in blue and additional identified peptide fragment ions in green. The amino acid sequence identified in the mass spectrum is highlighted at the top of the figures. (b) MS/MS spectrum for the ArPPLN2a peptide, GRTNMYGSSQLSRLSSGFN, observed at 688.00 m/z, 3+ ion, with precursor mass error 1.1 ppm (Mascot score 31.30). (c) MS/MS spectrum for the ArPPLN2b peptide, GRSSFAGSSRLTNLGSGFT, observed at 634.65 m/z, 3+ ion, with precursor mass error -0.065 ppm (Mascot score 24.54). (d) MS/MS spectrum for the ArPPLN2d peptide, GRSAFSGSRGLTNLASGFN, observed at 633.65 m/z, 3+ ion, with precursor mass error 0.94 ppm (Mascot score 31.76). (e) MS/MS spectrum for the ArPPLN2e peptide, GRSSFAGVSGLTHLGSGFN, observed at 617.64 m/z, 3+ ion, with precursor mass error 0.0092 ppm (Mascot score 38.01). (f) MS/MS spectrum for the ArPPLN2f peptide, GRSAFSGSKGLTNLASGFN, observed at 624.32 m/z, 3+ ion, with precursor mass error 0.13 ppm (Mascot score 64.86).

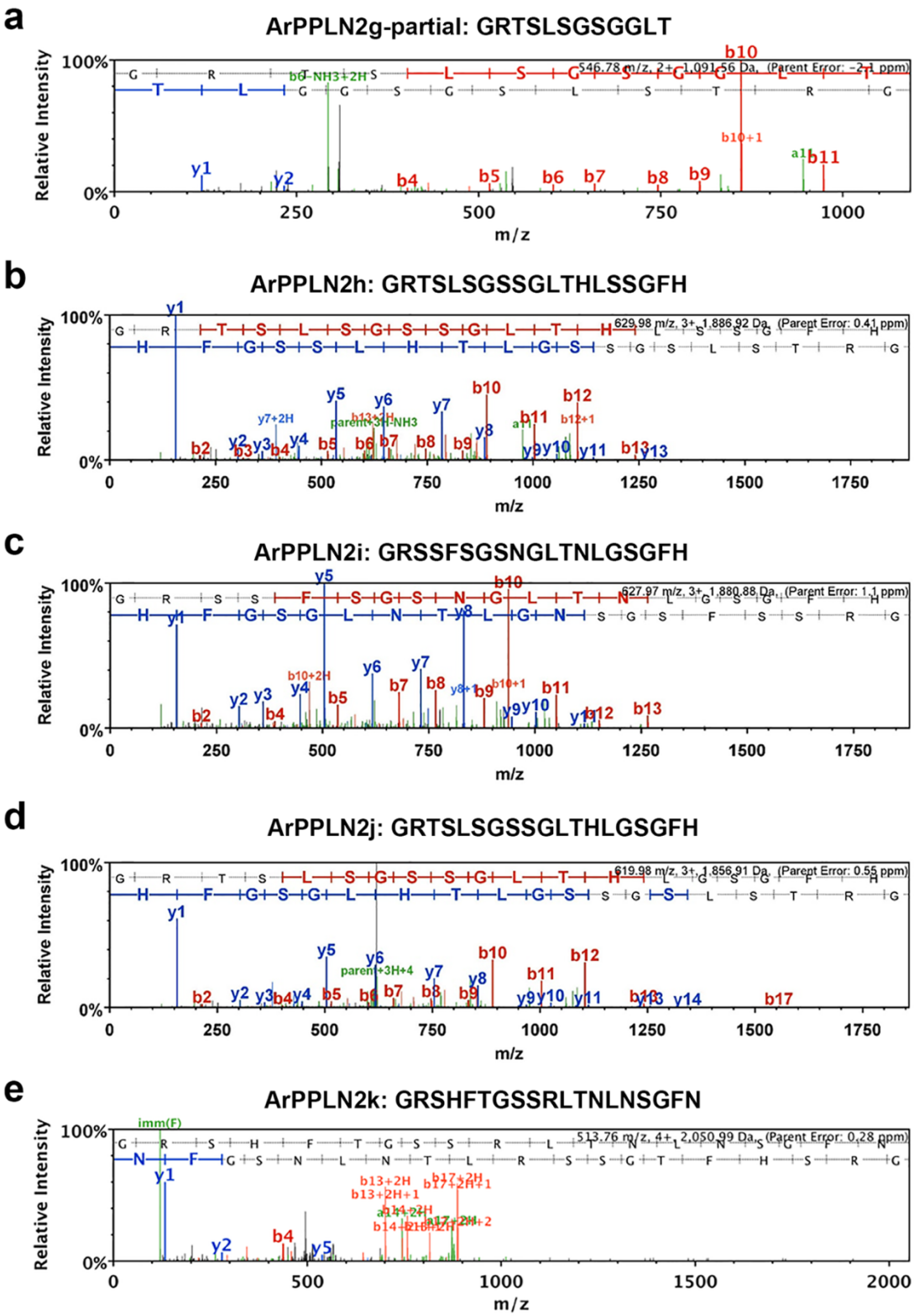

Figure 4.4 Mass spectrometric identification of ArPPLN2 peptides in an extract of *A. rubens* radial nerve cords.

(a - e) annotated MS/MS spectra for ArPPLN2g-partial, h, i, j, k, respectively. The b series of peptide fragment ions are shown in red, the y series in blue and additional identified peptide fragment ions in green. The amino acid sequence identified in the mass spectrum is highlighted at the top of the figures. (a) MS/MS spectrum for the ArPPLN2g-partial peptide, GRTSLSGSGGLT, observed at 546.78 m/z, 2+ ion, with

precursor mass error -2.1 ppm (Mascot score 31.77). (b) MS/MS spectrum for the ArPPLN2h peptide, GRTSLSGSSGLTHLSSGFH, observed at 629.98 m/z, 3+ ion, with precursor mass error 0.41 ppm (Mascot score 67.8). (c) MS/MS spectrum for the ArPPLN2i peptide, GRSSFSGSNGLTNLGSGFH, observed at 627.97 m/z, 3+ ion, with precursor mass error 1.1 ppm (Mascot score 65.62). (d) MS/MS spectrum for the ArPPLN2j peptide, GRTSLSGSSGLTHLGSGFH, observed at 619.98 m/z, 3+ ion, with precursor mass error 0.55 ppm (Mascot score 67.47). (e) MS/MS spectrum for the ArPPLN2k peptide, GRSHFTGSSRLTNLNSGFN, observed at 513.76 m/z, 4+ ion, with precursor mass error 0.28 ppm (Mascot score 11.74).

4.3.3 Localization of ArPPLNP2 transcripts in *A. rubens* using mRNA *in situ* hybridization

Analysis of the distribution of ArPPLNP2 transcripts in *A. rubens* revealed a widespread pattern of expression, including stained cells in the radial nerve cords and circumoral nerve ring (Figure 4.5, 4.6), tube feet (Figure 4.7), terminal tentacle (Figure 4.8) and digestive system (Figure 4.9, 4.10).

In longitudinal sections of the radial nerve cords, stained cells can be seen as clusters in the hyponeural region (Figure 4.5a, b), whilst in the ectoneural region stained cells were observed quite sparsely along the length of the epithelial layer (Figure 4.5a, c). The specificity of the staining observed with anti-sense probes (Figure 4.5a) was demonstrated by control experiments where no staining was observed with sense probes (Figure 4.5a inset). Transverse sections of the radial nerve also revealed the clustered arrangement of hyponeural cell bodies expressing ArPPLNP2, with more stained cells present in some sections (Figure 4.5d, e) than others (Figure 4.5f). Transverse sections of radial nerve cords also revealed that stained cells in the ectoneural epithelium are more concentrated in the lateral regions of the radial nerve cords (Figure 4.5d, f), and extend into the epithelium of adjacent tube feet (Figure 4.5f, g).

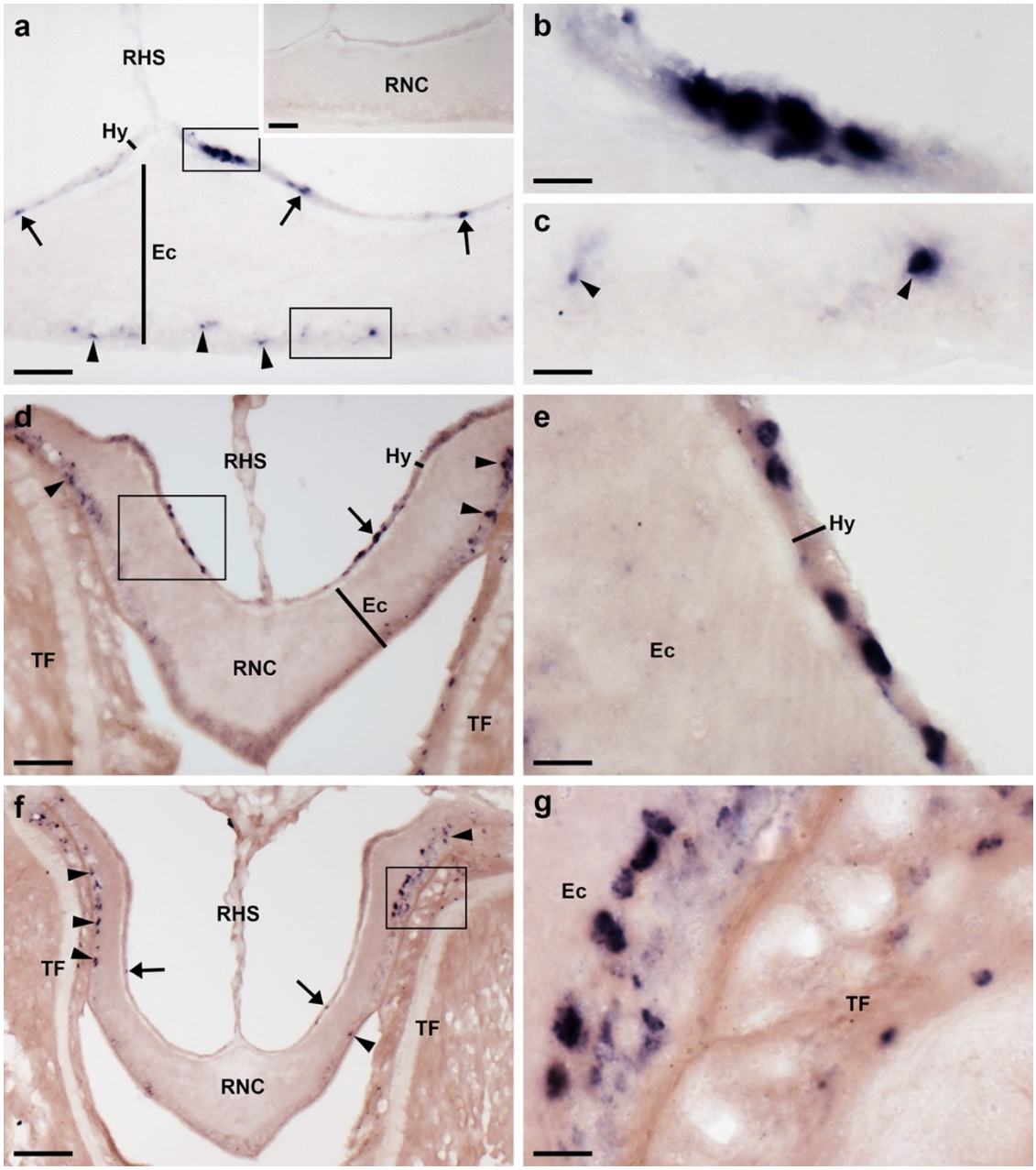

Figure 4.5 Localization of ArPPLNP2 mRNA in the radial nerve cord of *A. rubens* using *in situ* hybridization.

(a) Longitudinal parasagittal section of the radial nerve cords incubated with antisense probes showing groups of cells interspersed along the length of the nerve cord in the hyponeural (rectangle and arrows) and ectoneural regions (rectangle and arrowheads). Higher magnification images of the boxed regions are shown in (b) and (c). The inset of panel (a) shows the absence of staining in a longitudinal parasagittal section of radial nerve cord incubated with sense probes, demonstrating the specificity of staining observed with antisense probes. (b) High magnification image showing stained cells in the hyponeural region of the radial nerve cord. (c) High magnification image showing stained cells in the ectoneural region of the radial nerve cord. (d) Transverse section of radial nerve cord incubated with antisense probes showing groups of cells in the hyponeural (rectangle and arrow) and ectoneural regions (arrowheads). (e) High magnification view of hyponeural region highlighted by rectangle in panel (d). (f) Transverse section of radial nerve cord incubated with antisense probes showing groups of cells in the ectoneural regions (rectangle and arrowheads). (g) High magnification

view of ectoneural region highlighted by rectangle in panel (f). Ec, ectoneural region of radial nerve cord; Hy, hyponeural region of radial nerve cord; RHS, radial hemal strand; RNC, radial nerve cord; TF, tube foot. Scale bars: 50 µm in (a), (a) inset, (d), (f); 10 µm in (b), (c), (e), (g). Refer to Figure 1.7 (page 38) and 1.8 (page 39) for details of starfish anatomy.

Transverse sections of the circumoral nerve ring revealed that stained cells are largely concentrated in the outer and inner regions of the ectoneural epithelium, proximal to peri-oral tube feet and the peristomial membrane, respectively (Figure 4.6a, b, c). Stained cells are also present in the hyponeural region of the circumoral nerve ring (Figure 4.6c), but because this tissue is sometimes damaged or lost during tissue processing the stained hyponeural cells are not always seen (Figure 4.6a).

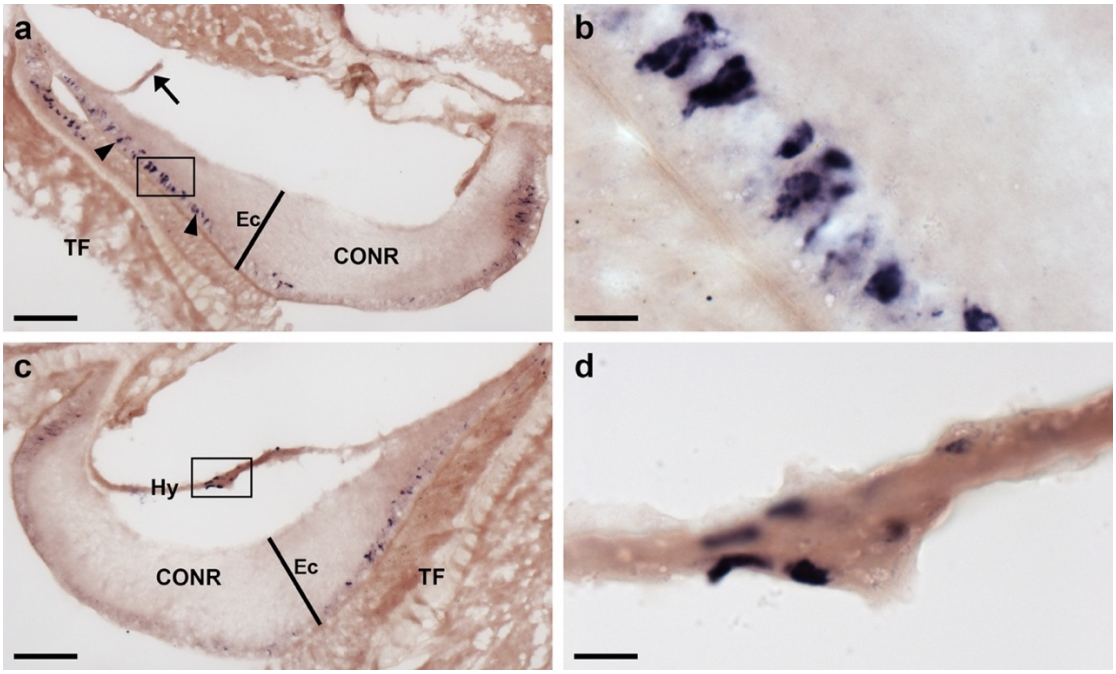

Figure 4.6 Localization of ArPPLNP2 mRNA in the circumoral nerve ring of *A. rubens* using *in situ* hybridization.
(a) Transverse section of circumoral nerve ring showing stained cells in the epithelium of ectoneural region (arrowheads). A higher magnification image of the boxed region is shown in (b). Note that in this section no hyponeural staining is evident because the hyponeural tissue is damaged (arrow). (b) High magnification image of stained cells in the epithelial layer of the ectoneural region of the circumoral nerve ring. (c) Transverse section of circumoral nerve ring incubated with antisense probes showing stained cells in the ectoneural region and in the hyponeural region, which has become detached from the larger during tissue processing (arrowheads). A higher magnification image of the boxed region is shown in (d). (d) High magnification image of stained cells in a detached hyponeural region of the cirumoral nerve ring. CONR, circumoral nerve ring; Ec, ectoneural region of radial nerve cord; Hy, hyponeural region of radial nerve cord;

Os, ossicle; TF, tube foot. Scale bars: 50 μm in (a), (c); 10 μm in (b), (d). Refer to Figure 1.7 (page 38) and 1.8 (page 39) for details of starfish anatomy.

In tube feet, stained cells were observed in a sub-epithelial position at the base of tube feet proximal to radial nerve cord (Figure 4.5g, 4.7a, 4.7b) or circumoral nerve ring (Figure 4.6a, c) or between adjacent tube feet (Figure 4.7a). Stained cells are also in the tube foot sucker, closely associated with the basal nerve ring (Figure 4.7d). In the tube foot-like terminal tentacles stained cells were observed in or below the external epithelial layer of the terminal tentacles (Figure 4.8a, c, d, f) and in the body wall epithelium that surrounds the terminal tentacle (Figure 4.8a, b, d, e). Stained cells were also observed in the photoreceptor cell layer of the optic cushion, which is located at the base of each terminal tentacle.

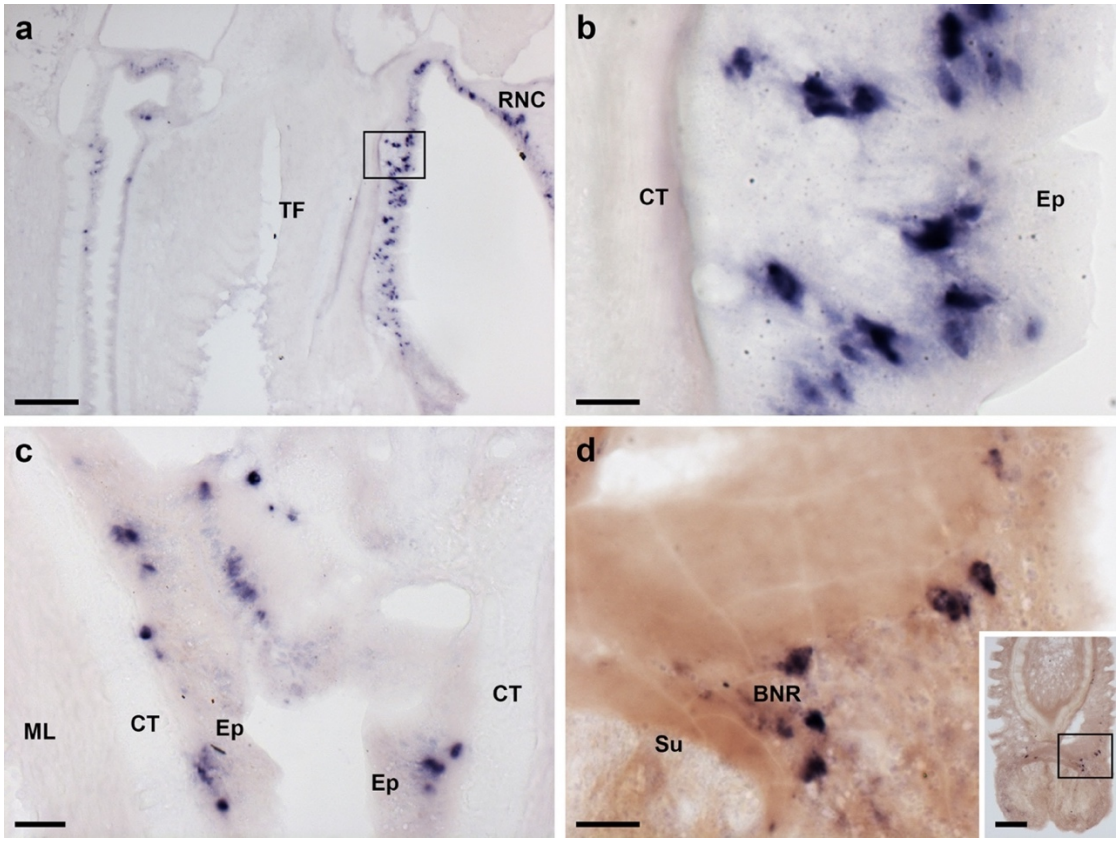

Figure 4.7 Localization of ArPPLNP2 mRNA in tube feet of *A. rubens* using *in situ* hybridization.
(a, b) Longitudinal section of a tube foot showing stained cells (rectangle) in the sub-epithelial layer of the tube foot stem near to the junction with the adjacent radial nerve cord. The boxed region in panel (a) is shown at higher magnification in (b). (c) Stained cells located in the sub-epithelial layer at the junction between adjacent tube feet. (d)

Stained cells located near to the tube foot basal nerve ring. The inset of shows the location of the stained cells (rectangle) in a lower magnification image that shows the part of the tube foot stem and the sucker. BNR, basal nerve ring; CT, collagenous tissue tissue; Ep, epithelium; ML, muscle layer; RNC, radial nerve cord; Su, sucker; TF, tube foot. Scale bars: 100 µm in (a), (d) inset; 10 µm in (b), (d); 20 µm in (c). Refer to Figure 1.7 (page 38) and 1.8 (page 39) for details of starfish anatomy.

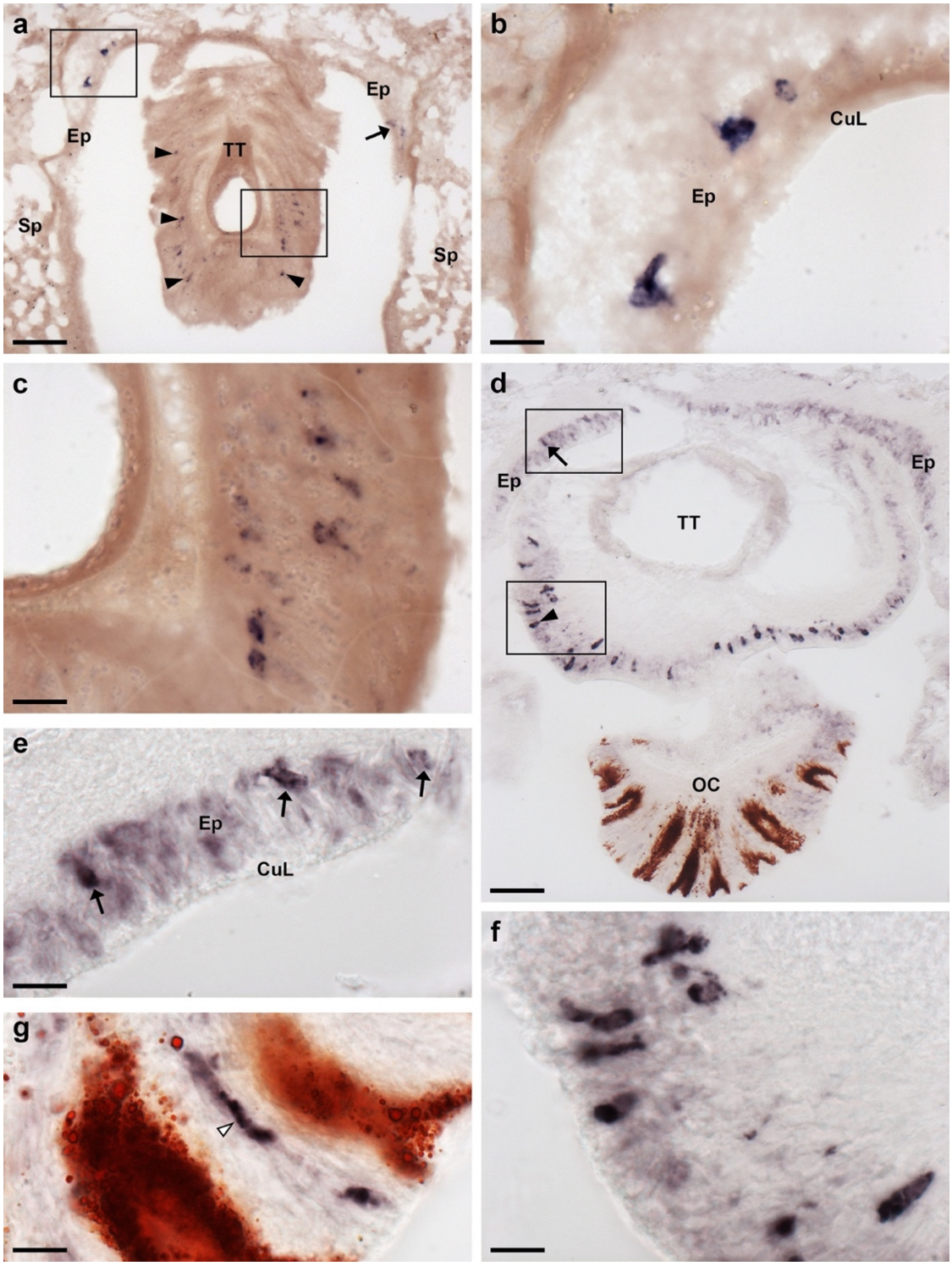

Figure 4.8 Localization of ArPPLNP2 mRNA in the arm tip region of *A. rubens* using *in situ* hybridization.

(a) Transverse section of a paraffin wax embedded arm tip showing the terminal tentacle cut obliquely. Stained cells can be seen in the external epithelial layer of the terminal tentacle (arrowheads) and in the body wall epithelium (arrow) that surrounds the terminal tentacle. The boxed regions are shown at higher magnification in panels (b) and (c). (d) Transverse cryostat section of an arm tip showing the pigmented optic cushion and terminal tentacle. Stained cells can be seen in the terminal tentacle external epithelium (rectangle with arrowhead) and in the body wall epithelium (rectangle with arrow). The boxed areas in (d) are shown at higher magnification in (e) and (f). (g) High magnification image of in the photoreceptor cell layer of an optic cushion showing a stained cell (white arrowhead) between pigmented cells. CuL, cuticle layer; Ep, epithelium; OC, optic cushion; Sp, spine; TT, terminal tentacle. Scale bars: 50 μm in (a), (d); 10 μm in (b), (c), (e), (f), (g). Refer to Figure 1.7 (page 38) and 1.8 (page 39) for details of starfish anatomy.

In the digestive system, ArPPLNP2 mRNA expression was detected in cardiac stomach (Figure 4.9a), pyloric stomach (Figure 4.9b), pyloric duct (Figure 4.9c, d), pyloric caeca (Figure 4.9e, f). In all of these regions of the digestive system the stained cells appear to be largely located in the the coelomic epithelium (Figure 4.9a-d), which is closely associated with an underlying visceral muscle layer. In the pyloric ducts and in diverticula of the pyloric caeca the stained cells are concentrated on the oral (lowermost) side (Figure 4.9e, f).

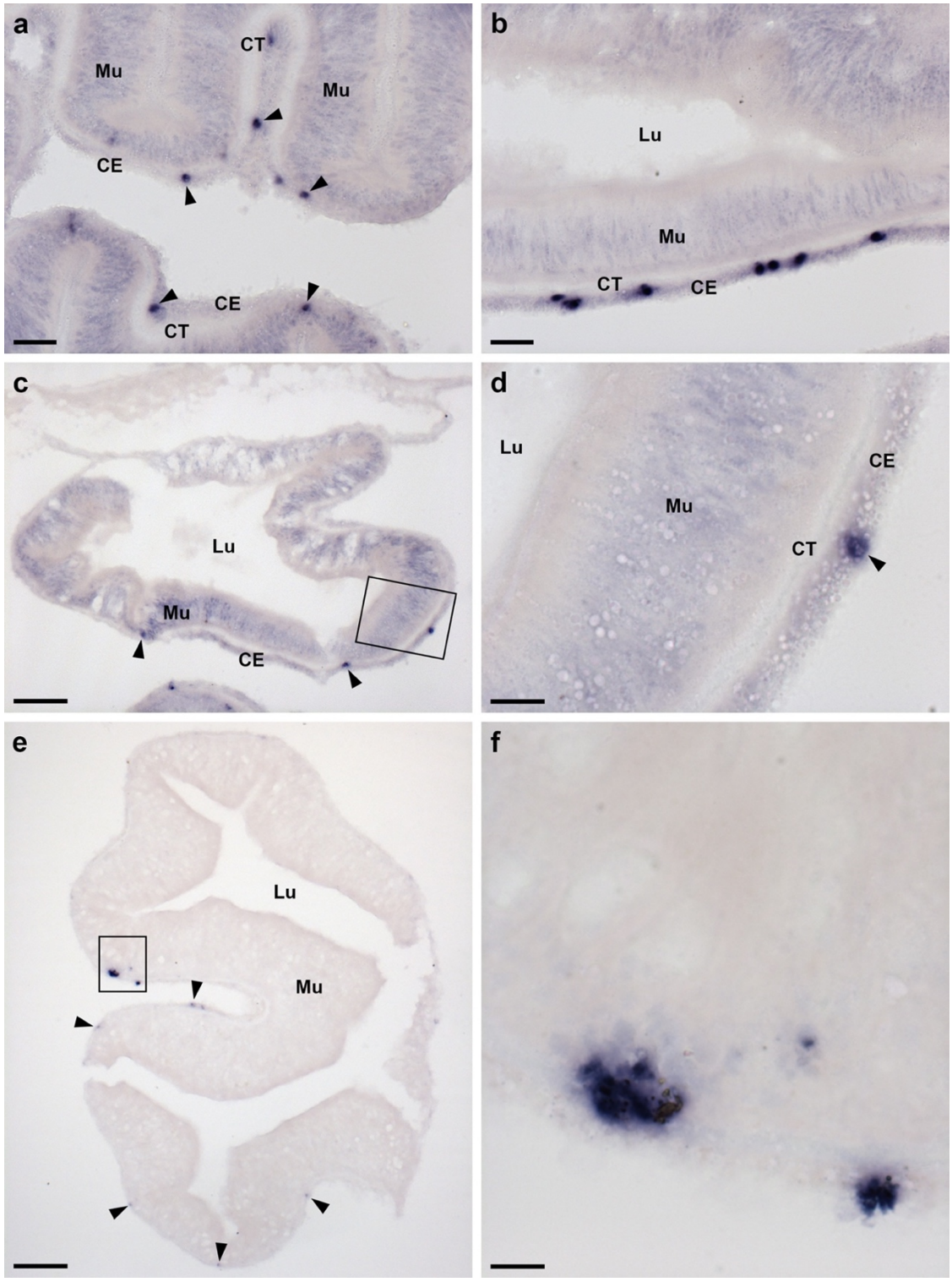

Figure 4.9 Localization of ArPPLNP2 mRNA in the digestive system of *A. rubens* using *in situ* hybridization.

(a) Section of a cardiac stomach showing stained cells (arrowheads) in the coelomic epithelium. (b) Section of pyloric stomach showing stained cells in the coelomic epithelium. (c, d) Transverse section of a pyloric duct showing stained cells (rectangle and arrowheads) in the coelomic epithelium. The boxed region in (c) is shown at higher magnification in panel (d). (e, f) Transverse section of a pyloric caecum diverticulum showing stained cells (rectangle and arrowheads) in the coelomic epithelium layer. The boxed region in (e) is shown at higher magnification in panel (f). CE, coelomic

epithelium; CT, collagenous tissue; Lu, lumen; Mu, mucosa. Scale bars: 20 µm in (a), (b); 50 µm in (c); 10 µm in (d), (f); 100 µm in (e). Refer to Figure 1.7 (page 38) and 1.8 (page 39) for details of starfish anatomy.

The cardiac stomach is attached to the ambulacrum in each of the five arms of *A. rubens* by extrinsic retractor strands. The paired extrinsic retractor strands coalesce to form a nodule that connects the extrinsic retractor strands with the intrinsic retractor strands located within the wall of the cardiac stomach (Anderson, 1954). Large numbers of ArPPLNP2-expressing cells were observed in the coelomic lining of the nodule and in mesenteries that link the extrinsic retractor strands with ambulacral ossicles (Figure 4.10a, b, c).

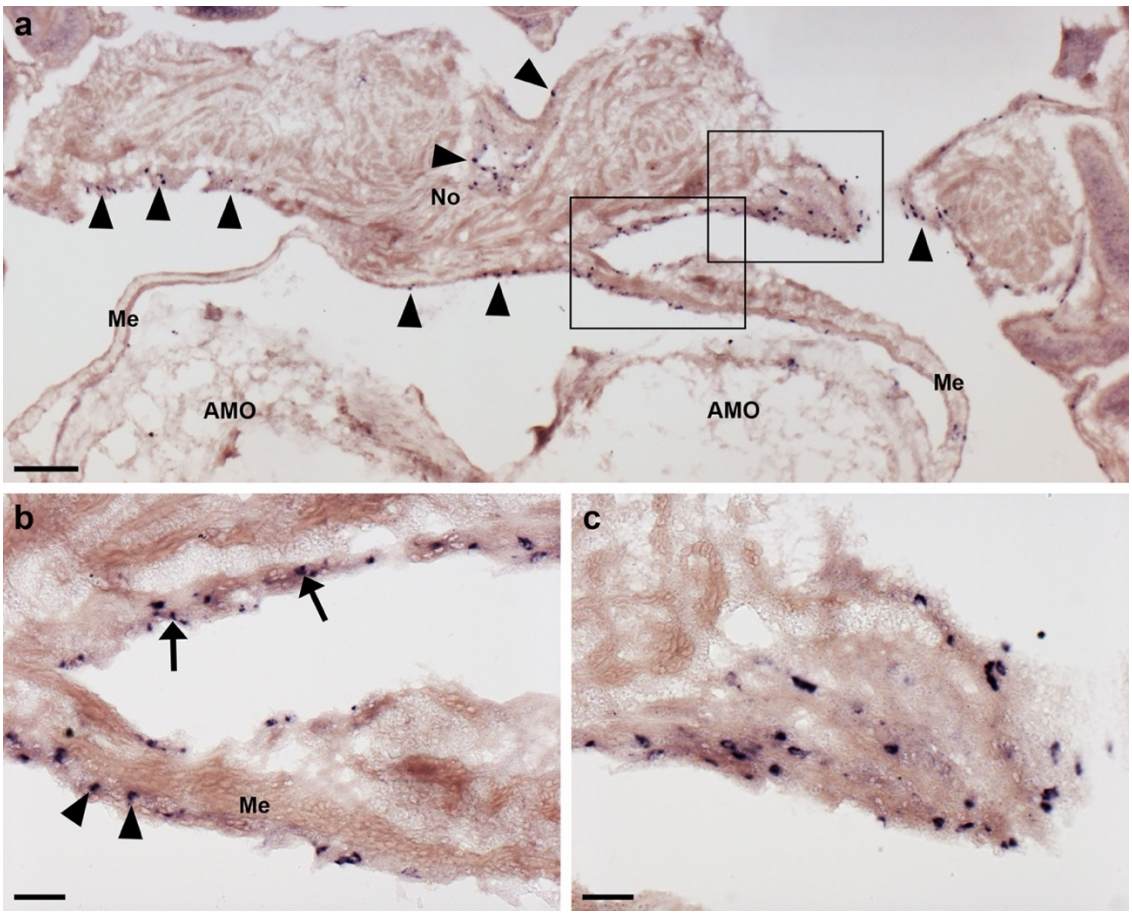

Figure 4.10 Localization of ArPPLNP2 mRNA in cardiac stomach extrinsic retractor strand nodule of *A. rubens* using *in situ* hybridization.
(a) Transverse section of an arm showing stained cells (rectangles and arrowheads) in the coelomic epithelium of a cardiac stomach extrinsic retractor strand nodule and in mesenteries that attach the extrinsic retractor strands to the ambulacral ossicles. The boxed regions in (a) are shown at higher magnification in (b) and (c). In (b) stained cells can be seen in the coelomic epithelium of a mesentery (arrowheads) and in the coelomic

epithelium of a nodule. AMO, ambulacral ossicle; Me, mesentery; No, nodule. Scale bars: 100 μm in (a); 20 μm in (b), (c). Refer to Figure 1.7 (page 38) and 1.8 (page 39) for details of starfish anatomy.

4.3.4 Localization of ArPPLN2h using immunohistochemistry

4.3.4.1 Characterisation of a rabbit antiserum to ArPPLN2h using ELISA

To assess the presence and titre of antibodies to the ArPPLN2h-ag peptide in rabbit sera, antiserum and pre-immune serum were incubated at a range of dilutions (10^{-3} - 10^{-8}) with a fixed amount of the antigen peptide added to each well of the microtitre plate (10^{-10} moles). As expected, no ArPPLN2h-ag immunoreactivity was detected with pre-immune serum but ArPPLN2h-ag immunoreactivity was detected with antiserum at dilutions ranging from 10^{-3} to 10^{-6}. Furthermore, to assess the specificity of the antiserum it was also tested in the same way with a peptide (ArPPLN1b) derived from ArPPLNP1 and, importantly, no immunoreactivity was observed (Figure 4.11a).

To assess the sensitivity of the antiserum for detection of the ArPPLN2h-ag peptide, the antiserum (diluted to10^{-4}) was incubated with different amounts of peptide ranging from 10^{-10} to 10^{-15} moles. At this antiserum dilution, the ArPPLN2h-ag peptide was detected in the range from 10^{-10} to 10^{-12} moles, whereas the pre-immune serum exhibited no reactivity with ArPPLN2h and the antiserum exhibited no reactivity with ArPPLN1b antigen peptide (Figure 4.11b). Collectively, these data indicate that the antiserum contains a high titre of specific antibodies to the ArPPLN2h-ag peptide.

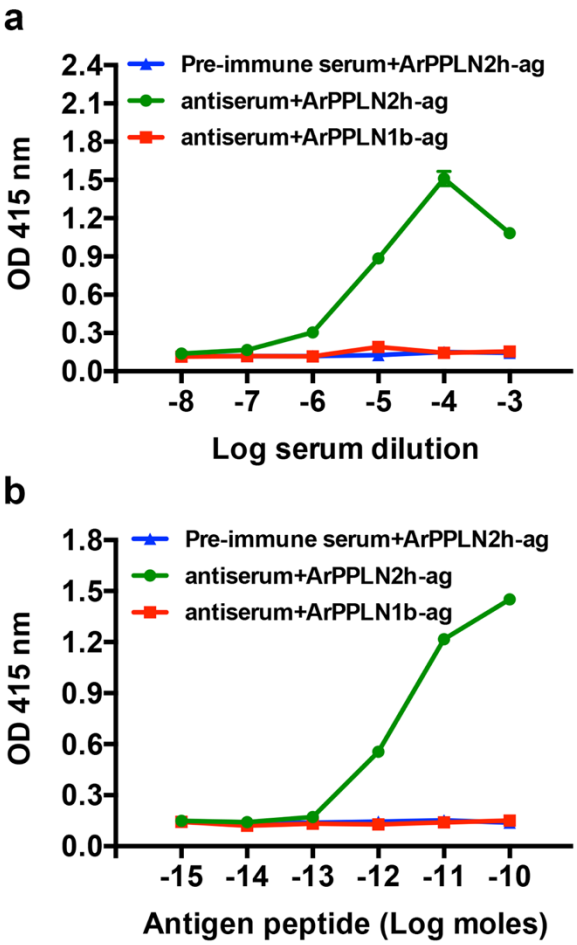

Figure 4.11 Characterization of rabbit antiserum to ArPPLN2h using an enzyme-linked immunosorbent assay (ELISA).
(a) Incubation of antiserum at dilutions between 10^{-3} and 10^{-8} with 0.1 nmol of the antigen peptide ArPPLN2-ag (green) reveals antigen detection at well above the background optical density (OD) with dilutions from 10^{-3} to 10^{-5}, whereas no immunoreaction is observed with pre-immune serum (blue). When the ArPPLLN2h-antiserum was tested with a ArPPLN1-ag peptide (also 0.1 nmol per well) there was no immunoreaction (red), demonstrating that ArPPLLN2h-antiserum does not cross-react with ArPPLN1-type peptides. (b) Incubation of antiserum (green) and pre-immune serum (blue) at 10^{-4} dilution with between 10^{-15} and 10^{-10} moles of the ArPPLN2-ag peptide per well reveals no immunoreaction with pre-immune serum, whereas with the antiserum the antigen is detected at well above the background OD with 10^{-12} to 10^{-10} moles per well. When the antiserum is tested in the same way with a ArPPLN1-ag peptide there is no immunoreaction, again demonstrating the specificity of the antiserum for ArPPLN-type neuropeptides. All data points are mean values from two separate experiments performed in duplicate.

4.3.4.2 Immunohistochemical localization of neuropeptides derived from ArPPLNP2 in *A. rubens*

Antiserum to the C-terminal region of ArPPLN2h (KYTHLSSGFH) was used for immunohistochemical analysis of ArPPLN2-type neuropeptide expression in *A.*

rubens. It is noteworthy, however, that the ArPPLN2h antigen peptide used for antibody production shares a high level of sequence similarity with other peptides derived from ArPPLNP2, in particular ArPPLN2g, ArPPLN2i and ArPPLN2j (Figure 4.2a). Therefore, it is likely that when the antiserum is used for immunohistochemistry it labels not only ArPPLN2h, as demonstrated by ELISA (Figure 4.11), but also other peptides derived from ArPPLNP2.

4.3.4.2.1 Radial nerve cords, circumoral nerve ring, marginal nerve cords and lateral motor nerves

The ArPPLN2h antiserum revealed extensive immunostaining in the radial nerve cords, in both the ectoneural and hyponeural regions (Figure 4.12a). Importantly, the specificity of this immunostaining was demonstrated in pre-absorption experiments, where pre-incubation of the antiserum with the ArPPLN2h antigen peptide resulted in a complete loss of immunostaining in the radial nerve cords (Figure 4.12a inset). Immunostained bipolar shaped cells were observed throughout the ectoneural epithelium of the radial nerve cords, with the cells having a process projecting toward the cuticular surface and another process projecting into the underlying densely stained neuropile (Figure 4.12b). In the hyponeural region monopolar shaped cells were observed with a single process projecting into an underlying fiber plexus. (Figure 4.12c). Nerve processes derived from the hyponeural region of the radial nerve cords could also be seen to project around the wall of the peri-hemal coelom to innervate the transverse infra-ambulacral muscle (Figure 4.12d), whilst immunostained fibers in the ectoneural region are continuous with the basiepithelial nerve plexus of adjacent tube feet (Figure 4.12d).

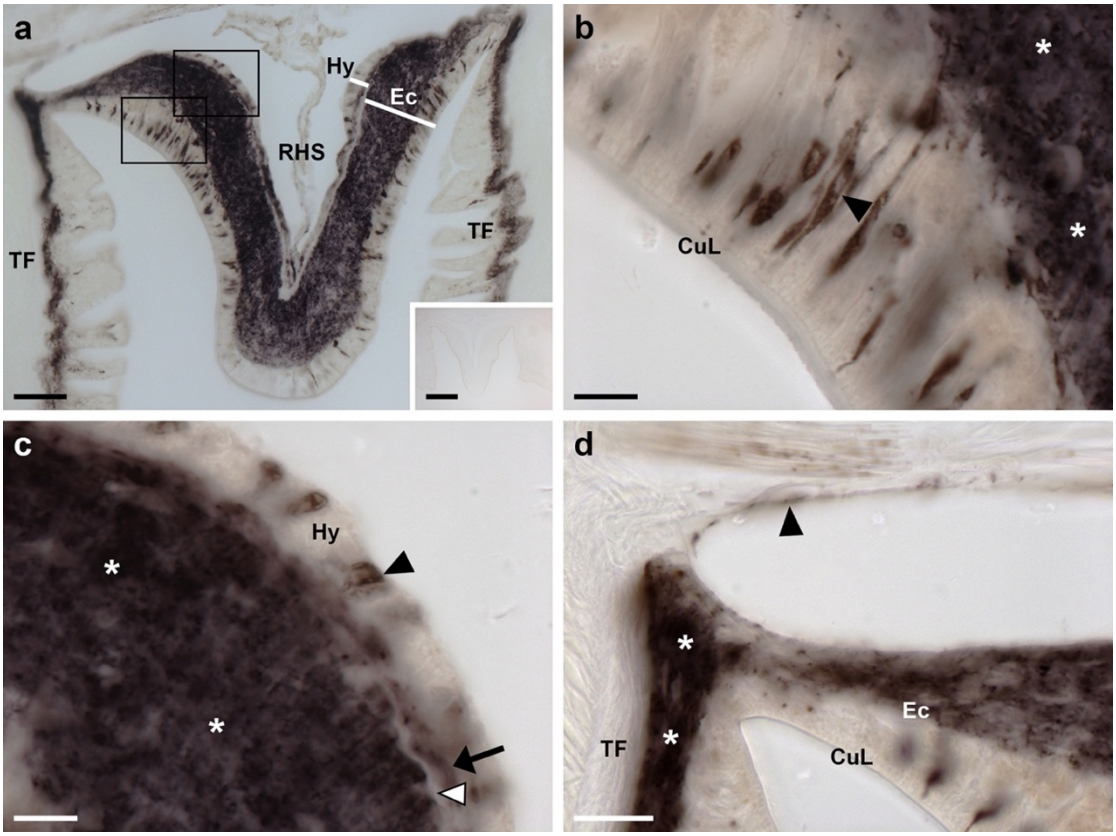

Figure 4.12 Localization of ArPPLN2h-immunoreactivity (ArPPLN2h-ir) in the radial nerve cord of *A. rubens*.
(a) Transverse section of a radial nerve cord showing ArPPLN2h-ir in both the ectoneural and hyponeural regions. The inset of (a) shows absence of immunostaining in a radial nerve cord section incubated with ArPPLN1b antiserum pre-absorbed with the antigen peptide (ArPPLN2h-ag), demonstrating the specificity of immunostaining observed with the ArPPLN2 antiserum. (b) High magnification image of the ectoneural region of the radial nerve cord showing immunostained bipolar shaped cells in the sub-cuticular epithelium (arrowheads) and densely packed immunostained processes (asterisks) in the underlying neuropile region. (c) High magnification image showing immunostained monopolar shaped cells (arrowhead) and their stained processes (arrow) in hyponeural region of the radial nerve cord. Densely packed immunostained processes (asterisks) in the ectoneural region. The unstained collagenous tissue layer (white arrowhead) that separates the hyponeural region from the densely stained ectoneural neuropile can also be seen here. (d) High magnification images showing immunostaining at the junction between the radial nerve cord and an adjacent tube foot. The continuity of immunostaining in the ectoneural region of the radial nerve and in the basiepithelial nerve plexus of the tube foot (asterisks) can be seen here. The stained process(es) (arrowhead) of a hyponeural neuron(s) can be seen projecting over the roof of the perihemal canal in close association with the transverse infra-ambulacral muscle. CuL, cuticle layer; Ec, ectoneural region; Hy, hyponeural region; RHS, radial hemal strand; TF, tube foot. Scale bars: 50 μm in (a); 200 μm in (a) inset; 10 μm in (b), (c); 20 μm in (d). Refer to Figure 1.7 (page 38) and 1.8 (page 39) for details of starfish anatomy.

The pattern of immunostaining in the circumoral nerve ring (Figure 4.13a) was consistent with that in the radial nerve cords, with bipolar shaped immunostained cells

located throughout the ectoneural epithelium (Figure 4.13a, b), intense immunostaining in the ectoneural neuropile (Figure 4.13 a, b, c) and monopolar shaped immunostained cells in the hyponeural region projecting into an underlying nerve plexus (Figure 4.13a, c). Lateral to the outer rows of tube feet in each arm are thickenings of the sub-epidermal nerve plexus known as the marginal nerves, which have immunostained cells in an external epithelium and immunostained processes in an underlying neuropile (Figure 4.13d). Internal to the marginal nerve immunostaining was observed in the lateral motor nerve (Figure 4.13d).

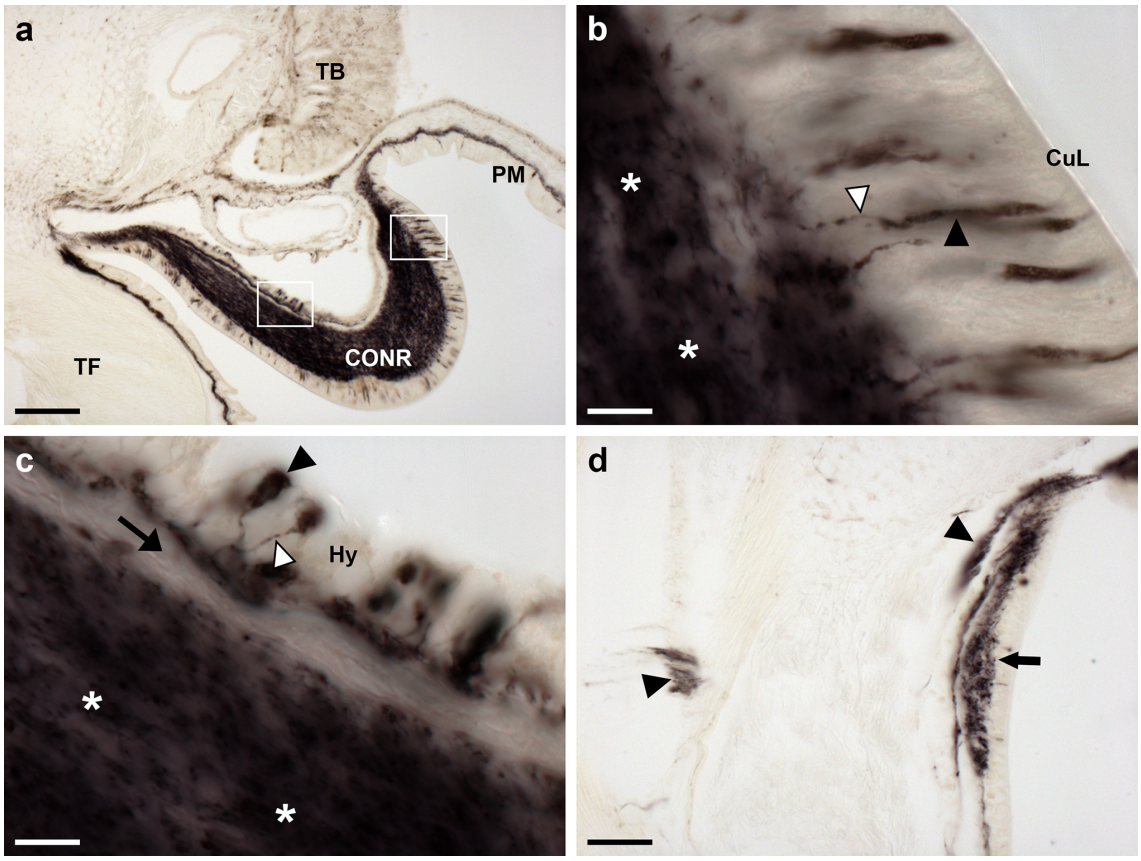

Figure 4.13 Localization of ArPPLN2h-immunoreactivity in the circumoral nerve ring and marginal nerve of *A. rubens*.
(a) Immunostaining in a transverse section of the circumoral nerve ring; here immunostained processes can also be seen here in the peristomial membrane, an adjacent oral tube foot and in a Tiedemann's body. High magnification images of the boxed regions can be seen in (b) and (c). (b) A high-magnification image of a circumoral nerve ring showing immunostained bipolar-shaped cells (arrowhead) in the sub-cuticular epithelium of the ectoneural region and intense staining (asterisks) in the underlying neuropile. Stained processes projecting from bipolar cells into the neuropile can also be seen here (white arrowhead). (c) A high-magnification image of a

circumoral nerve ring showing immunostained monopolar shaped cells (black arrowheads) in the hyponeural region with stained processes (white arrowhead) projecting into a fiber layer that is adjacent to the unstained collagenous tissue layer (arrow). The intensely stained ectoneural neuropile is labeled here with an asterisk. (d) Immunostaining in a sub-epithelial thickening of the basi-epithelial nerve plexus known as the marginal nerve (arrow), which is located at the junction between the outer row of tube feet and the adjacent body wall. Internal to the marginal nerve, separated by a thin layer of collagenous tissue, can be seen stained axonal processes in the lateral motor nerve (arrowheads). CONR, circumoral nerve ring; CuL, cuticle layer; Ec, ectoneural region; Hy, hyponeural region; PM, peristomial membrane; TB, Tiedemann's body; TF, tube foot. Scale bars: 100 μm in (a); 10 μm in (b), (c); 50 μm in (d). Refer to Figure 1.7 (page 38) and 1.8 (page 39) for details of starfish anatomy.

4.3.4.2.2 Hemal system and Tiedemann's bodies

Closely associated with the radial nerve cords and the circumoral nerve ring, is the hemal system comprising the radial hemal strand and the oral hemal ring. Immunostained processes were observed in both the radial hemal strand (Figure 4.14a) and the oral hemal ring (Fig 4.14b). Immunostaining was also observed in Tiedemann's bodies (Figure 4.14c, d), which are linked to the ring canal of the water vascular system in starfish.

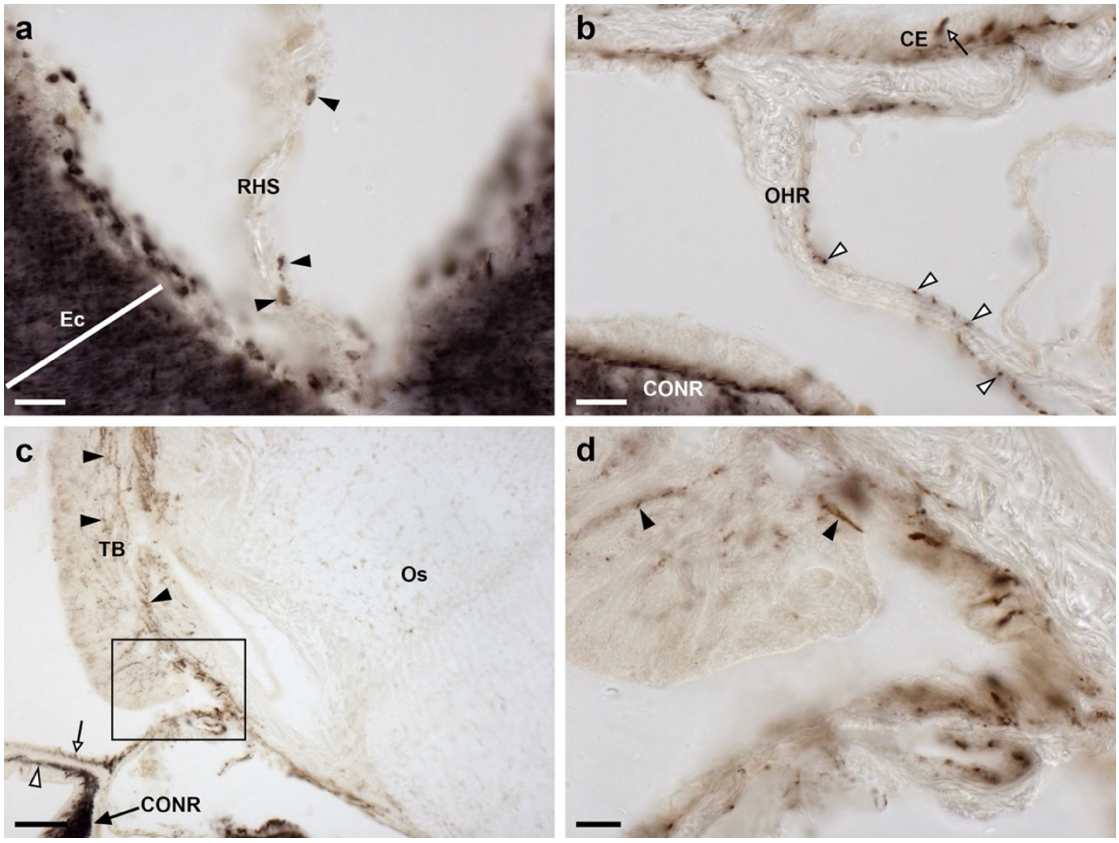

Figure 4.14 Localization of ArPPLN2h immunoreactivity in the hemal system and Tiedemann's bodies of *A. rubens*.
(a) Immunostaining (arrowheads) in the radial hemal strand, which is anatomically connected to the hyponeural region of the adjacent radial nerve cord. (b) Immunostained processes (white arrowheads) in the oral hemal ring, which is anatomically connected to the circumoral nerve ring (at bottom right). Immunostaining can also be seen here in the coelomic epithelium (white arrow). (c, d) Immunostained processs can be seen here in one of the ten Tiedemann's bodies (black arrowheads), which are located aboral to the circumoral nerve ring in the central disk, the coelomic epithelium (white arrow) and the peristomial membrane (white arrowhead). The boxed region in (c) is shown at higher magnification in panel (d). CE, coelomic epithelium; CONR, circumoral nerve ring; Ec, ectoneural region; Hy, hyponeural region; OHR, oral hemal ring; Os, ossicle; RHS, radial hemal strand; TB, Tiedemann's body; TF, tube foot. Scale bars: 20 μm in (a), (b), (d); 100 μm in (c). Refer to Figure 1.7 (page 38) and 1.8 (page 39) for details of starfish anatomy.

4.3.4.2.3 Tube feet and terminal tentacle

Immunostaining is present throughout the basiepithelial nerve plexus of tube feet stems (Figure 4.15a, b) and in the basal nerve ring located in the tube foot sucker (Figure 4.15a, c, d). Immunostained processes can be seen extending from the basiepithelial nerve plexus into epidermal folds of the tube foot stem when it is in a contracted state (Figure 4.15b). Immunostained processes also extend from the basal

nerve ring into the tube foot sucker (Figure 4.15c). Immunostained processes are also present beneath the coelomic epithelium of the tube foot ampulla (Figure 4.15e, f).

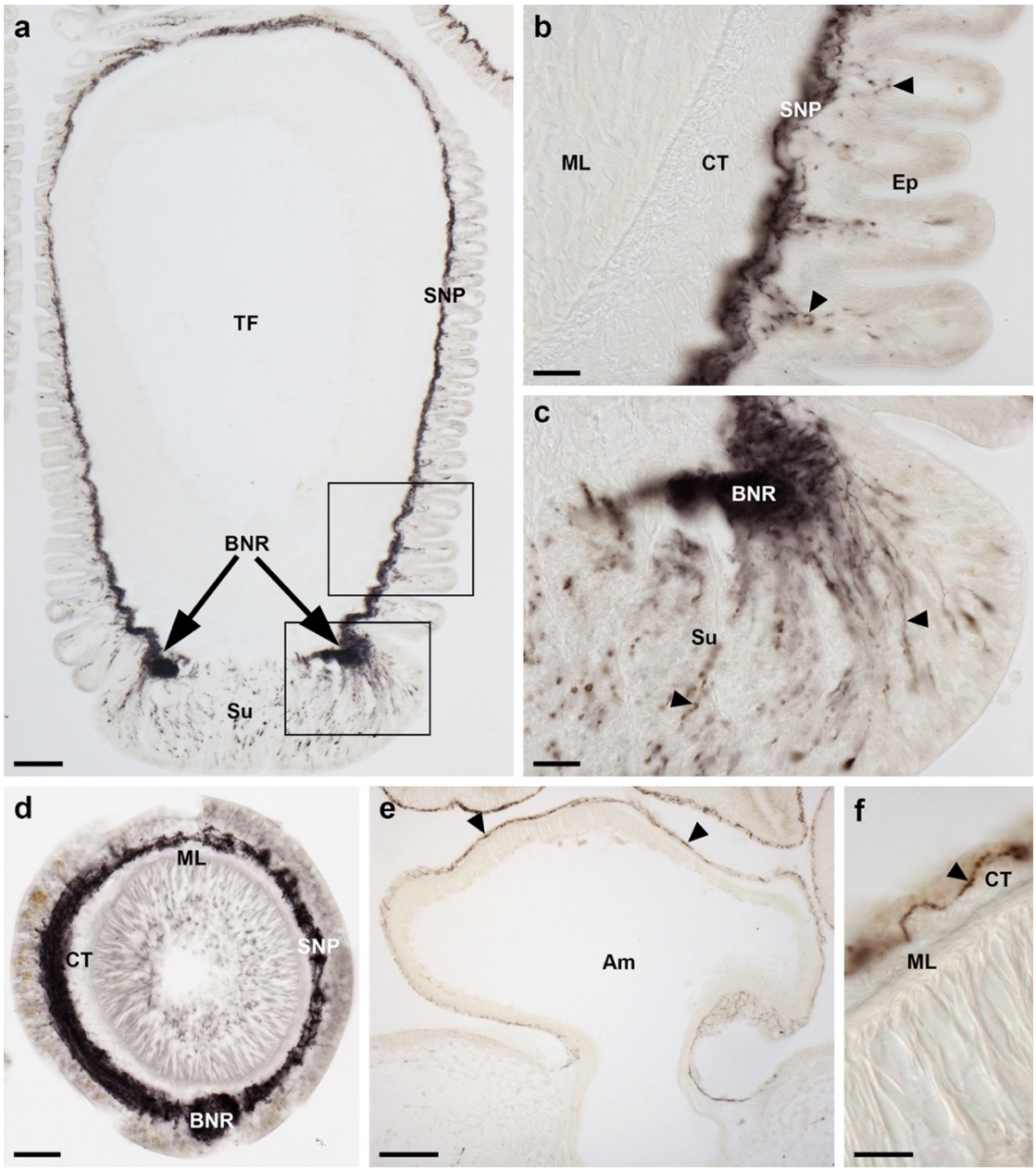

Figure 4.15 Localization of ArPPLN2h immunoreactivity in tube feet and ampullae of *A. rubens*.
(a) Longitudinal section of a tube foot showing immunostaining in the sub-epithelial nerve plexus, basal nerve ring and sucker. The boxed regions are shown at higher magnification in panels (b) and (c). (b) High magnification image showing immunostaining in the sub-epithelial nerve plexus and in processes projecting into epithelial folds of the contracted tube foot (arrowheads). (c) High magnification image showing immunostaining in the basal nerve ring and in processes projecting into the tube foot sucker (arrowheads). (d) Transverse section of a tube foot showing immunostaining in the sub-epithelial nerve plexus and basal nerve ring. (e, f) Immunostaining in the sub-epithelial nerve plexus of an ampulla (arrowheads). (f). High

magnification image showing immunostained processes (arrowhead) in the coelomic lining of an ampulla. Am, ampulla; BNR, basal nerve ring; CT, collagenous tissue; Ep, epithelium; ML, muscle layer; SNP, sub-epithelial nerve plexus; Su, sucker. Scale bars: 100 μm in (a), (e); 20 μm in (b), (c), (d); 10 μm in (f). Refer to Figure 1.7 (page 38) and 1.8 (page 39) for details of starfish anatomy.

Stained cells and processes are present in the body wall epithelium and its underlying basiepithelial nerve plexus surrounding the terminal tentacle (Figure 4.16a, b). In the terminal tentacle, immunostained bipolar shaped cells are present in the external epithelial layer and in the underlying nerve plexus (Figure 4.16a, c). Immunostaining is also present in the lateral lappets of the terminal tentacle (Figure 4.16d) and in the optic cushion, which is located at the base of the terminal tentacle (Figure 4.16d).

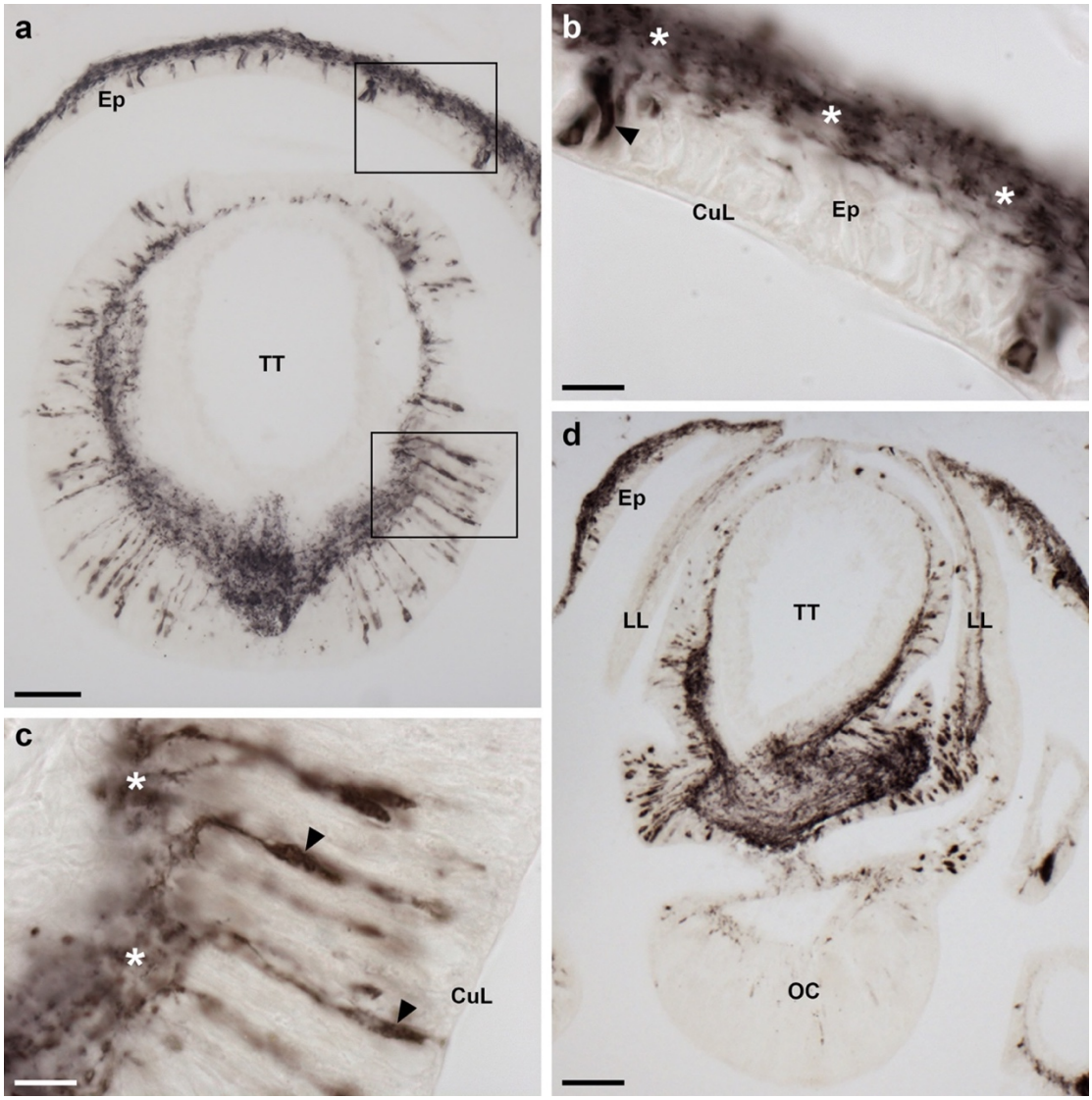

Figure 4.16 Localization of ArPPLN2h immunoreactivity in the terminal tentacle and associated structures in the arm tip of *A. rubens*.
(a) Immunostaining in a transverse section of a terminal tentacle and in the surrounding body wall epithelium. The boxed regions are shown at higher magnification in panel (b) and (c). (b) A high magnification image of arm tip epithelium showing immunostained bipolar shaped cells in the epithelium (arrowhead) and in a dense meshwork of fibers in the underlying basiepithelial plexus (asterisks). (c) High magnification image of the terminal tentacle showing immunostained bipolar shaped cells in the epithelium (arrowheads) with stained processes projecting into a dense meshwork of fibers in the underlying basiepithelial plexus (asterisks). (d) Immunostaining in a transverse section at the base of the terminal tentacle. Immunostained cells and processes can be seen here in the body wall epithelium, the terminal tentacle and associated lateral lappets and the optic cushion. CuL, cuticle layer; Ep, epithelium; LL, lateral lappet; TT, terminal tentacle; OC, optic cushion. Scale bars: 50 μm in (a); 10 μm in (b), (c); 100 μm in (d). Refer to Figure 1.7 (page 38) and 1.8 (page 39) for details of starfish anatomy.

4.3.4.2.4 Digestive system

The external epithelial layer of the peristomial membrane that surrounds the mouth contains immunostained cells and immunostained processes are present in the underlying basiepithelial nerve plexus (Figure 4.17a, b). A similar pattern of immunostaining is observed in the short esophagus that is located between the peristomial membrane and the cardiac stomach (Figure 4.17b, c, d).

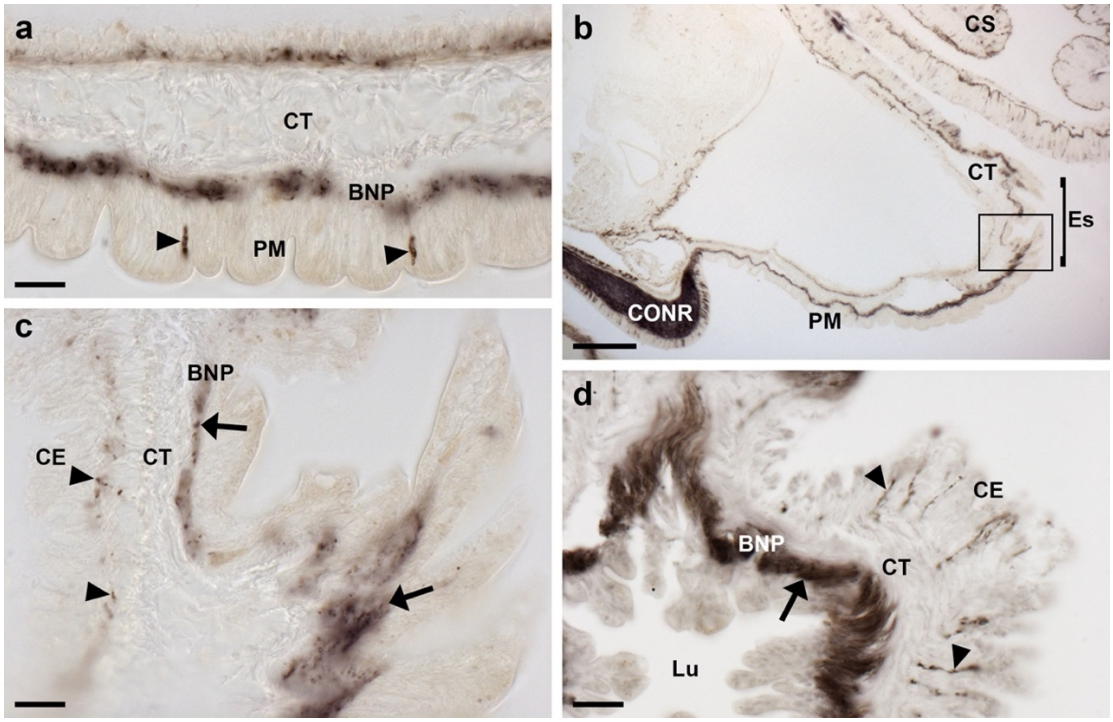

Figure 4.17 Localization of ArPPLN2h immunoreactivity in the peristomial membrane and esophagus of *A. rubens*.
(a) Immunostained bipolar shaped cells can be seen here in the external epithelial layer of the peristomial membrane (arrowheads) and in processes located in the underlying basiepithelial nerve plexus. Immunostaining is also present in the coelomic epithelium, which is separated from the basiepithelial nerve plexus by a layer of collagenous tissue. (b) Transverse section of the central disk showing immunostaining in the peristomial membrane, the esophagus and the cardiac stomach. The intensely stained circumoral nerve ring can also be seen here. The boxed region is shown at higher magnification in panel (c). (c) High magnification image of a longitudinal section of the esophagus showing immunostained processes beneath the coelomic epithelium (arrowheads) in the basiepithelial nerve plexus beneath the epithelial layer that lines the lumen of the esophagus. (d) High magnification transverse section of the esophagus showing immunostained cells and processes in the coelomic lining (arrowheads) and dense immunostaining in the basiepithelial plexus beneath the lumenal epithelial lining of the esophagus. BNP, basiepithelial nerve plexus; CE, coelomic epithelium; CONR, circumoral nerve ring; CS, cardiac stomach; CT, collagenous tissue; Es, esophagus; Lu,

lumen; PM, peristome membrane. Scale bars: 20 μm in (a), (c), (e); 200 μm in (b); 50 μm in (d). Refer to Figure 1.7 (page 38) and 1.8 (page 39) for details of starfish anatomy.

A widespread pattern of immunostaining was observed in the cardiac stomach (Figure 4.18a) and in the extrinsic extractor strands that link the cardiac stomach to the ambulacrum in each of the five arms. The paired extrinsic retractor strands coalesce to form a nodule that is located close to a site of insertion on the wall of the cardiac stomach and a dense meshwork of immunolabelled fibers can be seen in the nodule (Figure 4.18b). Immunostained bipolar shaped cells are present in the mucosa of the cardiac stomach and in the underlying basiepithelial nerve plexus (Figure 4.18c). Immunostained processes are also present in the visceral nerve plexus located beneath the coelomic epithelium of the cardiac stomach. A similar pattern of immunostaining to that seen in the cardiac stomach is also observed in the pyloric stomach (Figure 4.18d). The pyloric duct and pyloric caeca also exhibit immunostaining (Figure 4.18e), with stained processes in the visceral nerve plexus and immunolabelled bipolar shaped cells in the mucosal layer giving rise to immunoreactive fiber networks in the basiepithelial nerve plexus (Figure 4.18e, f).

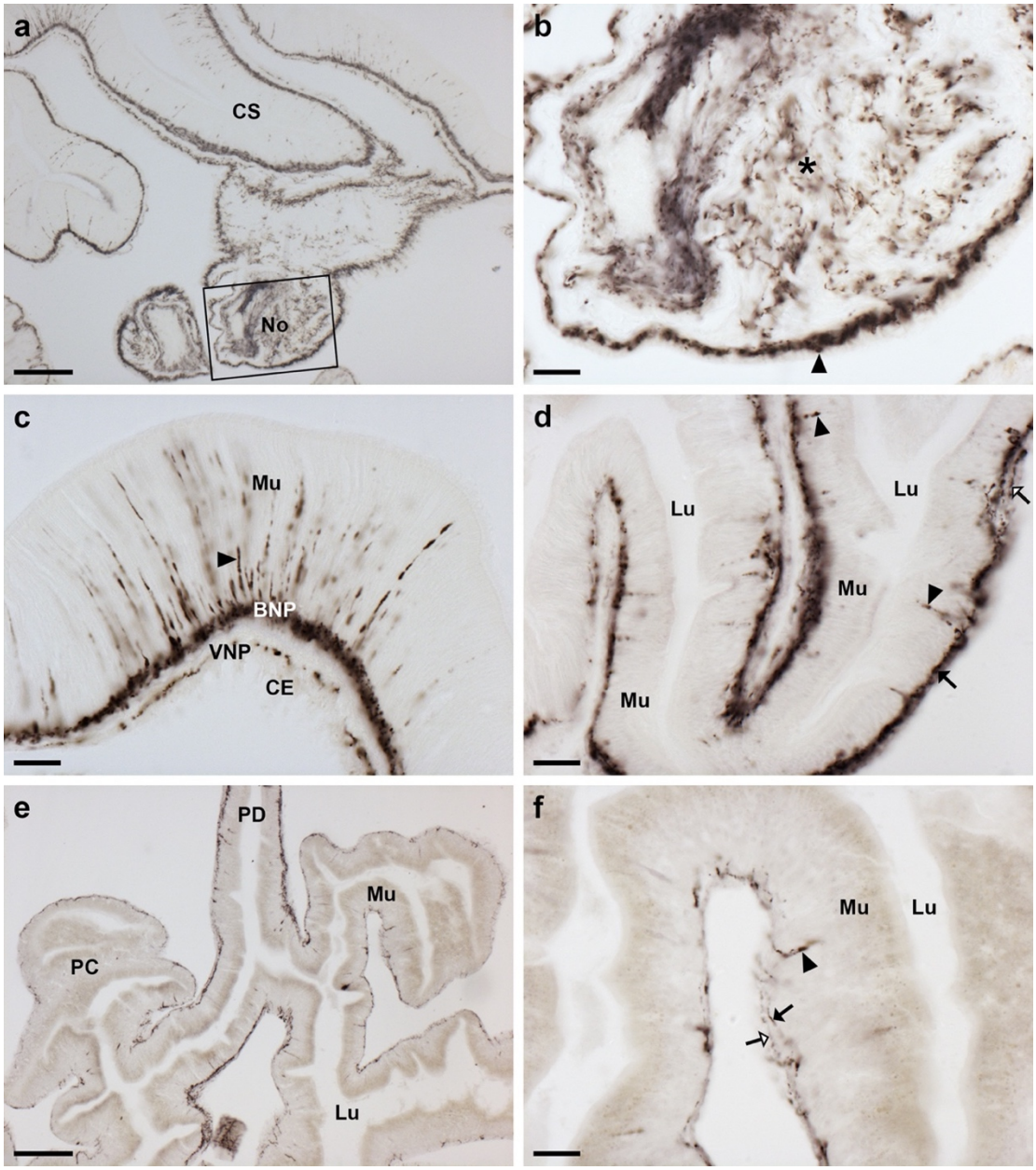

Figure 4.18 Localization of ArPPLN2h immunoreactivity in the cardiac stomach, pyloric stomach, pyloric ducts and pyloric caeca of *A. rubens*.
(a) Immunostaining in the cardiac stomach and in the nodule that links the cardiac stomach to extrinsic retractor strands; a high-magnification image of the boxed area is shown in (b). (b) Immunostained processes can be seen in the basiepithelial plexus beneath the coelomic lining of the nodule (arrowhead) and in the core of the nodule (asterisk). (c) High magnification image of a cardiac stomach showing immunostained cells in the mucosa (arrowhead) and immunostained processes in the basiepithelial nerve plexus beneath the mucosa and in the visceral nerve plexus beneath the coelomic epithelium. (d) High magnification image of the pyloric stomach showing immunostained cells in the mucosa (arrowheads) and immunostained processes in the basiepithelial nerve plexus (black arrow) and visceral nerve plexus (white arrow). (e) Immunostaining in a horizontal section of a pyloric duct and pyloric caecum. (f) High magnification image of a pyloric caecum showing immunostaining in mucosal cell bodies (arrowhead), in the basiepithelial nerve plexus (black arrow) and in the visceral nerve plexus (white arrow). BNP, basiepithelial nerve plexus; CE, coelomic epithelium;

CS, cardiac stomach; Lu, lumen; Mu, mucosa; No, nodule; PC, pyloric caeca; PD, pyloric duct; VNP, visceral nerve plexus. Scale bars: 100 μm in (a), (e); 20 μm in (b), (c), (d), (f). Refer to Figure 1.7 (page 38) and 1.8 (page 39) for details of starfish anatomy.

4.3.4.2.5 Body wall and body wall-associated appendages

ArPPLNP2h-immunoreactive fibers were observed in the coelomic lining of the body wall (Figure 4.19a). Thus, stained fibers are present in the coelomic basiepithelial nerve plexus that is located beneath the coelomic epithelium and which is closely associated with a longitudinally orientated muscle layer (Figure 4.19a, b). Furthermore, immunostained fibers were also observed within the circularly orientated muscle layer of the coelomic lining (Figure 4.19a, b). Immunostaining of nerve fibers was also observed in the sub-epidermal plexus of the body wall (Figure 4.19a, c, d, e). This staining also extends into papulae, hollow finger-shaped organs located above voids in the calcite skeleton that enable gas exchange between the external seawater and the coelomic fluid. Another type of body wall appendage in starfish are pedicellariae, pincer-like organs that keep the body surface clear of encrusting material. In pedicellariae immunostaining was observed in processes associated with the adductor muscles (Figure 4.19f).

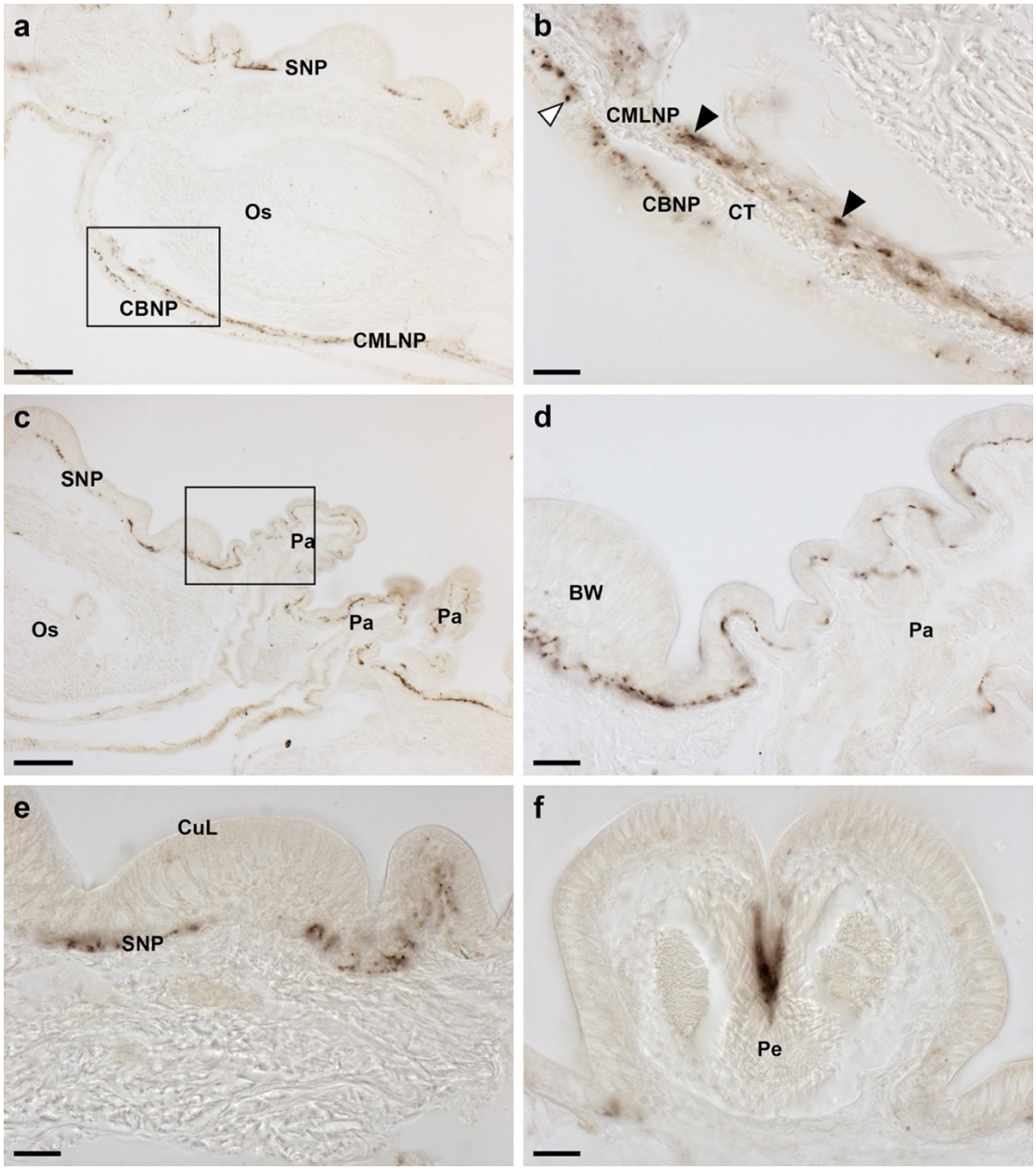

Figure 4.19 Localization of ArPPLN2h immunoreactivity in the body wall and body wall appendages of *A. rubens*.
(a) Transverse section of aboral body wall showing immunostaining in the sub-epidermal nerve plexus, the coelomic basiepithelial nerve plexus and circular muscle layer nerve plexus. The boxed area is shown at high magnification in (b). (b) High magnification image of the coelomic lining of the body wall showing stained processes in the coelomic basiepithelial nerve plexus (white arrowhead) in the nerve plexus associated with the circular muscle layer (black arrowheads). (c) Immunostaining in the sub-epidermal nerve plexus of the body wall and in papulae. The boxed area is shown at higher magnification in (d). (d) High magnification image showing immunostaining in the sup-epidermal nerve plexus of a papula and adjacent body wall. (e) High magnification of the body wall external epithelium showing immunostaining in the sub-epidermal nerve plexus. (f) High magnification image showing immunostained processes in a pedicellaria. BW, body wall; CBNP, coelomic basiepithelial nerve plexus; CMLNP, circular muscle layer nerve plexus; CT, collagenous tissue; CuL, cuticle layer; Os, ossicle; Pa, papulae; Pe, pedicellaria; SNP, sub-epidermal nerve plexus. Scale bars:

100 μm in (a), (c); 20 μm in (b), (d), (e), (f). Refer to Figure 1.7 (page 38) and 1.8 (page 39) for details of starfish anatomy.

4.3.4.2.6 Interossicular muscles

Immunostained fibers were revealed in association with interossicular muscles that link adjacent ossicles of the body wall endoskeleton. In Figure 4.20a these stained fibers can be seen at low magnification in a transverse section through the ambulacral region of the body wall. High magnification images show the profiles of immunostained fibers in the longitudinal supra-ambulabral muscle (Figure 4.20b) and in beaded immunostained fibers running along the length of muscle fibers in the transverse infra-ambulacral muscle (Figure 4.20c) and in the transverse supra-ambulacral muscle (Figure 4.20d). The immunostained processes can also be seen to extend into the ossicles (Figure 4.20c, d), where muscle fibers form loop-shaped straps around struts of the ossicular stereom. A similar pattern of immunostained fibers in association with interadambulacral muscles is shown in Figure 4.20 e and f.

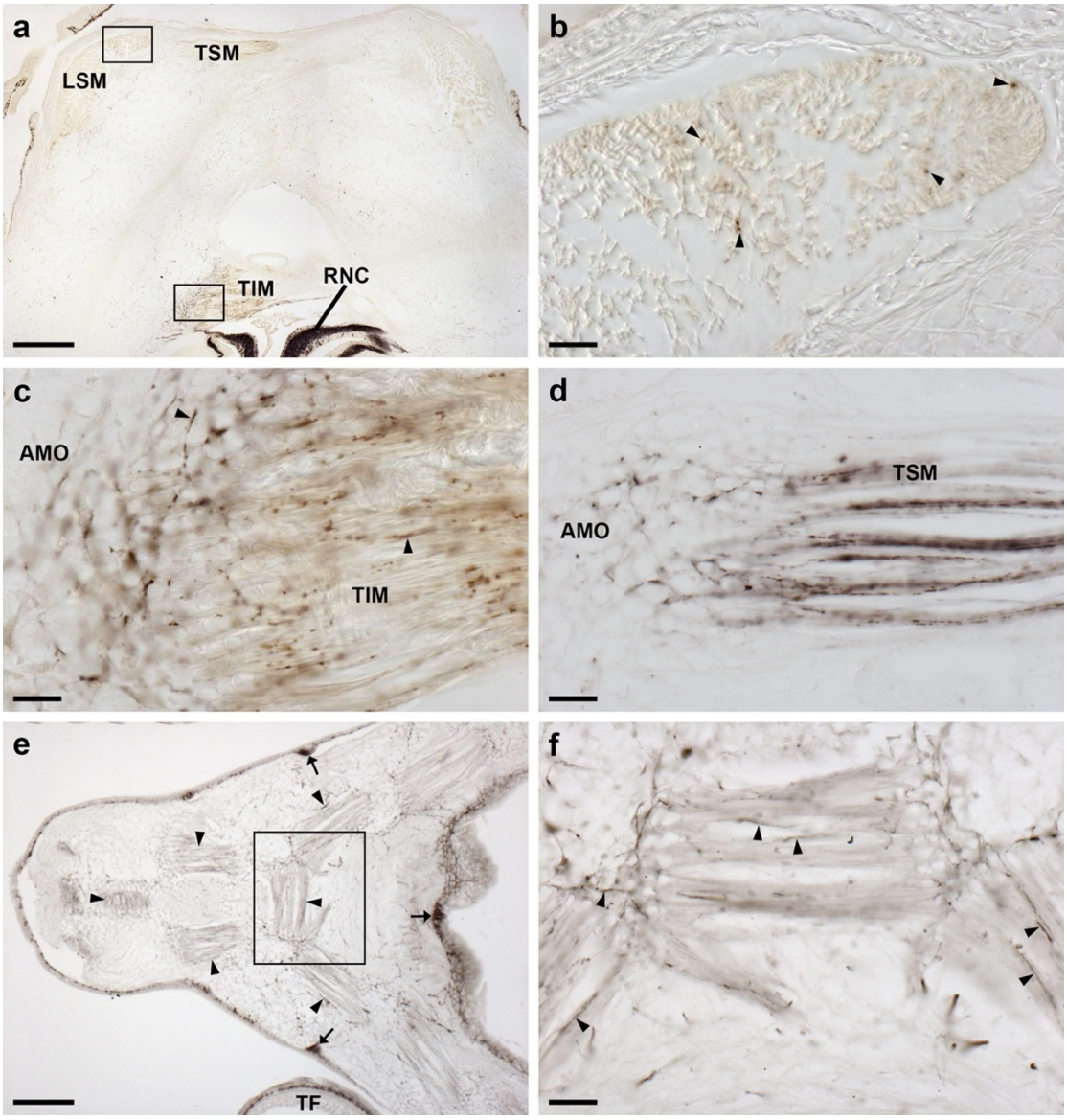

Figure 4.20 Localization of ArPPLN2h immunoreactivity in the innervation of interossicular muscles in *A. rubens*.

(a) Transverse section of the ambulacrum showing immunostaining associated with muscles linking the ambulacral ossicles, which include the TSM, TIM and LSM. The intensely stained radial nerve cord can also be seen in this image. The boxed regions are shown at higher magnification in panels (b) and (c). (b) High magnification image immunostained profiles of processes (arrowheads) in the LSM. (c) High magnification image of showing immunostained processes (arrowheads) in the TIM and at the TIM-AMO interface (d) High magnification image showing immunostained processes in the TSM and at the TIM-AMO interface. (e, f) Immunostaining in the body wall at the junction between two arms in a juvenile starfish. Immunostained fibers can be seen associated with muscles that link adambulacral ossicles (arrowheads). Stained fibers are also evident in thickenings of the sub-epithelial nerve plexus of the body wall (arrows) and in the tube feet. A high magnification image of the boxed region is shown in (f). (f) Immunostained processes (arrowheads) in muscles that link adambulacral ossicles. AMO, ambulacral ossicle; LSM, longitudinal supra-ambulacral muscle; RNC, radial nerve cord; TIM, transverse infra-ambulacral muscle; TSM, transverse supra-ambulacral muscle. Scale bars: 200 μm in (a); 20 μm in (b), (c), (d), (f); 100 μm in (e). Refer to Figure 1.7 (page 38) and 1.8 (page 39) for details of starfish anatomy.

4.3.5 Bioactivity of ArPPLN2h in *A. rubens*

4.3.5.1 ArPPLN2h has no effect on *in vitro* preparations of apical muscle and tube feet from *A. rubens* but is a potent relaxant of cardiac stomach preparations

ArPPLN2h (GRTSLSGSSGLTHLSSGFH) was tested at a high concentration (10^{-6} M) on three *in vitro* preparations from *A. rubens*: apical muscle, tube feet and cardiac stomach. No effects on the contractile state of apical muscle and tube foot preparations were observed, whereas ArPPLN2h caused relaxation of cardiac stomach preparations. ArPPLN2h caused dose-dependent relaxation of cardiac stomach preparations and comparison of the effects of ArPPLN2h with the SALMFamide neuropeptide S2 (SGPYSFNSGLTF-NH_2) revealed that the potency and efficacy of ArPPLN2h was very similar to that of S2 (Figure 4.21). Thus, relaxing effects were observed with ArPPLN2h and S2 in the concentration range 10^{-8} and 10^{-6} M and the maximum effect (E_{max}) observed at 10^{-6} M was $40.05 \pm 5.07\%$ and $48.03 \pm 8.17\%$ reversal of KCl-induced contraction for ArPPLN2h and S2, respectively.

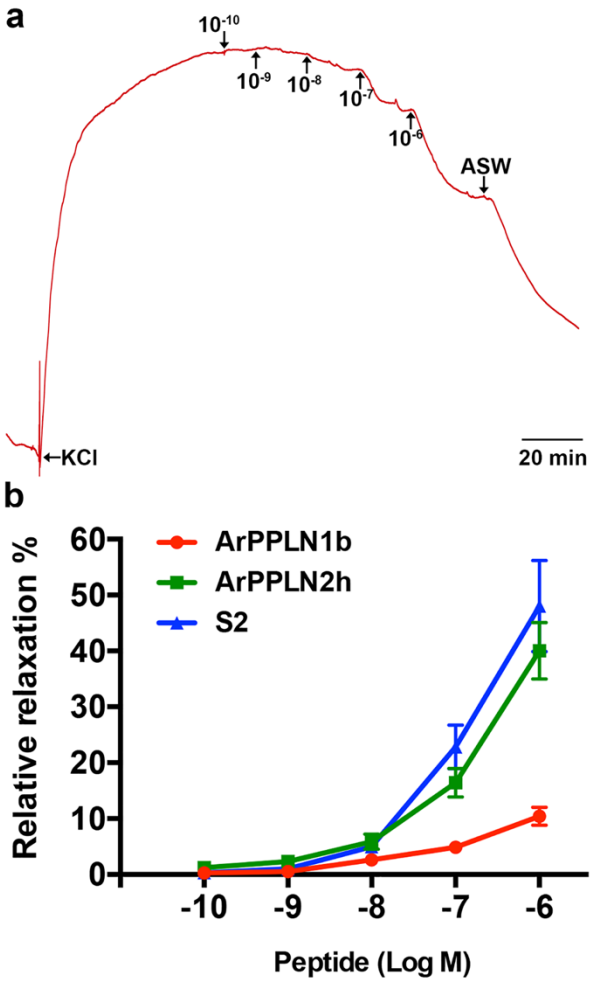

Figure 4.21 ArPPLN2h (GRTSLSGSSGLTHLSSGFH) causes dose-dependent relaxation of *in vitro* preparations of the cardiac stomach from *A. rubens*.
(a) Representative recording showing the dose-dependent relaxing effect of ArPPLN2h (10^{-10} - 10^{-6} M) on a cardiac stomach preparation pre-contracted with artificial seawater containing 30 mM added KCl (leftward arrow). Following tests with ArPPLN2h, the preparation was washed with artificial seawater (downward arrow). (b) Graph showing concentration-dependent relaxing effect of ArPPLN2h (green) on cardiac stomach preparations. Each point represents the mean ± SEM from at least four separate experiments, with the effect calculated as the percentage reversal of contraction induced by KCl. The effectiveness of ArPPLN2h as a cardiac stomach relaxant is much greater than that of the ArPPLN1b (red) but similar to the SALMFamide neuropeptide S2 (SGPYSFNSGLTF-NH_2) (blue).

4.3.5.2 ArPPLN2h does not induce cardiac stomach eversion

Previous studies revealed that the SALMFamide S2 causes cardiac stomach *in vitro* and induces cardiac stomach eversion when injected *in vivo* (Melarange et al., 1999). Here ArPPLN2h and S2 were found to cause cardiac stomach relaxation *in vitro* with similar potency and efficiency. Therefore, the effects of ArPPLN2h and S2 *in vivo*

were compared, with 100 µl of peptide at a concentration of 1 mM injected at two or three sites in the aboral body wall of the arms proximal to the junctions with the central disk region. Cardiac stomach eversion was observed within 5 min of injection in seven out of ten starfish injected with S2 but stomach eversion was not observed in any of ten animals injected with ArPPLN2h.

4.4 Discussion

In chapter 3 the structural, anatomical and functional characterization of neuropeptides derived from pedal peptide-like neuropeptide precursor 1 in the starfish *A. rubens* was reported. Here the structural, anatomical and functional characterization of neuropeptides derived from *A. rubens* pedal peptide-like neuropeptide precursor 2 (ArPPLNP2) has been reported.

A partial sequence of ArPPLNP2 was determined previously by analysis of transcriptome sequence data (Semmens et al., 2016), whilst here a cDNA comprising the entire open reading frame has been sequenced. ArPPLNP2 comprises thirteen copies of eleven PP/OK-type peptides (ArPPLN2a-k), with three copies of ArPPLN2h (GRTSLSGSSGLTHLSSGFH) and one copy each of the other ten peptides. The predicted structures of ArPPLN2a-k were confirmed here by mass spectroscopic analysis of *A. rubens* radial nerve cord extracts. All of the PP/OK-type peptides derived from ArPPLNP2 comprise nineteen residues and share a high level of sequence similarity with each other (Figure 4.2a). Furthermore, alignment of ArPPLNP2-derived peptides with other PP/OK-type neuropeptides in starfish (ArPPLNP1-derived peptides), other echinoderms and other invertebrates reveals conserved structural characteristics (Figure 4.2b). Thus, the hydrophobic residues (Phe, Leu, Met) at positions 5, 14 and 18 in ArPPLNP2-derived peptides appear to be characteristic of PP/OK-type neuropeptides, although the number of intervening residues is variable. Other residues in ArPPLNP2-derived peptides that also occur in at least some PP/OK-type peptides in other echinoderms and in protostomes include the glycine residues at positions 10 and 17. The functional significance of the conserved residues remains to be determined for starfish PP/OK-type peptides. However, it is noteworthy that a structure-activity study

on the prototypical crustacean orcokinin peptide revealed that N-terminal truncation to the position where residue 2 in orcokinin (phenylalanine) removed results in a complete loss of bioactivity. Furthermore, C-terminal truncation to the point where residue 12 in orcokinin (phenylalanine) is removed results in a 50% loss of bioactivity, whilst C-terminal truncation to the point where residue 10 in orcokinin (phenylalanine) is removed results in a complete loss of bioactivity (Bungart et al., 1995). Thus, these N- and C-terminal phenylalanine residues appear to be critically important for the bioactivity of orcokinin, consistent with the evolutionary conservation of hydrophobic residues at these positions in PP/OK-type peptides from other protostomian invertebrates and from echinoderms (e.g. starfish) (Figure 4.2b).

4.4.1 Functional interpretation of the expression patterns and actions ArPPLN2-type peptides in *A. rubens*

The main aim of this study was to obtain the first insights into the physiological roles of PPLN2-type peptides in *A. rubens*. To accomplish this, the objectives were to investigate the expression of ArPPLNP2 and neuropeptides derived from this precursor using mRNA *in situ* hybridization and immunohistochemistry and to investigate the *in vitro/in vivo* pharmacological actions of ArPPLN2h in *A. rubens* as a representative neuropeptide derived from ArPPLNP2. In the text below, the findings are discussed by focusing one-by-one on groups of anatomically and/or functionally related systems in *A. rubens*.

4.4.1.1 Radial nerve cords, circumoral nerve ring, marginal nerves, lateral motor nerves and innervation of interossicular muscles

Cells expressing ArPPLNP2 transcripts were detected in both the ectoneural and hyponeural regions of the radial nerve cords and circumoral nerve ring in *A. rubens*.

The distribution of cells in the radial nerve cords and circumoral nerve ring that were immunolabeled by antibodies to ArPPLN2h was consistent with the pattern of ArPPLNP2 mRNA expression. Furthermore, immunohistochemistry revealed dense networks of immunolabelled fibers in the ectoneural neuropile of the radial nerve cords and circumoral nerve ring. ArPPLN2h-expressing cells and fibers are also present in the marginal nerves, which are ectoneural thickenings of the basiepithelial nerve plexus located lateral to the outer row of tube feet in each arm. Collectively, these findings indicate that neuropeptides derived from ArPPLNP2 have a widespread role in mediating neuronal signaling in the ectoneural division of the starfish nervous system. However, little is known about the functional organization of the ectoneural nervous system in starfish (or echinoderms), although it is thought to comprise sensory neurons, interneurons and motor neurons (Cobb, 1970; Cobb, 1987; Mashanov et al., 2016). On the other hand, the hyponeural division of the nervous system is recognized as having a purely motor function, based on both anatomical and functional studies (Cobb, 1970; Cobb, 1987; Mashanov et al., 2016). Therefore, the presence of ArPPLNP2 transcripts and ArPPLN2h immunoreactivity in hyponeural cell bodies can be interpreted as evidence of a role for ArPPLNP2-derived neuropeptides in motoneuronal function in starfish. The processes of the ArPPLN2h-immunoreactive monopolar hyponeural cells are also immunoreactive and in some instances these can be traced beyond the hyponeural region of the radial nerve cords or circumoral nerve ring. For example, in sections of the arms stained processes can be seen projecting towards the transverse infra-ambulacral muscle, which is located just above the hyponeural system, indicating a potential role in neuromuscular signaling in starfish. Consistent with this notion, ArPPLN2h-immunoreactive processes are also present in the lateral motor nerve, which innervates interossicular muscles in the starfish body wall (Smith, 1937; 1950).

Accordingly, the widespread occurrence of ArPPLN2h-immunoreactive processes in interossicular muscles and other muscles in *A. rubens* is indicative of a general role for ArPPLNP2-derived neuropeptides in neuromuscular signaling.

4.4.1.2 Tube feet, terminal tentacle and associated structures

The presence of ArPPLNP2-expressing cells and ArPPLN2h-immunoreactive processes in the basiepithelial nerve plexus of tube feet in *A. rubens* suggested a potential role for ArPPLN2-derived neuropeptides in regulation of the contractility of these motile and muscular organs and therefore ArPPLN2h was tested for myoactivity on *in vitro* preparations of tube feet. Interestingly, ArPPLN2h had no effect on tube foot preparations. This contrasts with previous findings with the ArPPLNP1-derived neuropeptide ArPPLN1b, which has a pattern of expression in tube feet that is very similar to that of ArPPLN2h but which causes dose-dependent relaxation of tube foot preparations (Chapter 3). These findings are indicative of differences in the physiological roles of ArPPLNP1-derived and ArPPLNP2-derived neuropeptides in *A. rubens,* which may be explained by differences in the expression patterns of the as yet uncharacterized receptors that mediate effects of ArPPLN1b and ArPPLN2h. Both ArPPLN1b and ArPPLN2h are also present in the tube foot basal nerve ring and in processes that innervate the adhesive tube foot sucker and, as discussed previously in chapter 3, this could be indicative of roles in regulation of the secretion of proteins that mediate tube adhesion or detachment (Santos et al., 2005; Hennebert et al., 2012; Hennebert et al., 2013).

Each tube foot stem is linked via a tubular canal that extends through the body wall to a bulb-shaped muscular ampulla, which is located in the perivisceral coelom. Contraction of the ampulla facilitates tube foot extension, whereas relaxation of the

ampulla enables accommodation of fluid from the lumen of the stem when a tube foot contracts (Santos et al., 2005; Hennebert et al., 2012; Hennebert et al., 2013). Both ArPPLN1b-immunoreactive (Chapter 3) and ArPPLN2h-immunoreactive (this study) fibers are present in ampullae and are located in close proximity to the muscle layer. Previous studies have reported that the ampullae are innervated by hyponeural neurons (Smith, 1950) and therefore it is likely that ArPPLN1b- and ArPPLN2h-immunoreactive fibers in the ampulla originate from ArPPLNP1- and ArPPLNP2-expressing hyponeural motoneurons.

The terminal tentacle is a tube foot-like sensory organ located at the tip of each arm in *A. rubens* and in other starfish. ArPPLN2h-immunoreactive cells and fibers are present in the wall of the fluid-filled terminal tentacles, consistent with the pattern of expression seen in tube feet (see above). ArPPLN2h-immunoreactive cells and fibers are also present in the body wall epithelium and in lateral lappets that surround the terminal tentacle. The physiological roles of the lateral lappets (Smith, 1937) are not known, although a possible function would be to act as chemosensory organs, with detection of chemicals facilitated by their large surface area to volume ratio. Turning to a different sensory modality, located at the base of the terminal tentacle is a pigmented photosensory organ known as the optic cushion and here ArPPLNP2-expressing cells are present in the photoreceptor cell layer, located in-between pigmented cells. Interestingly, orcokinin appears to have a physiological role in mediating light entrainment of circadian activity in insects (Hofer and Homberg, 2006) and therefore it is possible that PP/OK-type peptides may have a similar role in starfish and other echinoderms.

4.4.1.3 Digestive system

Cells expressing ArPPLNP2 transcripts were detected in the coelomic epithelial layer in many regions of the digestive system, including the cardiac stomach, the extrinsic retractor strands of the cardiac stomach, the pyloric stomach, the pyloric ducts and the pyloric caeca. In accordance with this pattern of precursor expression, antibodies to ArPPLN2h labeled processes located in the visceral nerve plexus underlying the coelomic epithelium in all of these regions of the digestive system and in the peristomial membrane and esophagus. An abundance of immunoreactive fibers in the extrinsic retractor strand nodule of the cardiac stomach was particularly striking and consistent with the abundance of coelomic epithelial cells lining the nodule that express ArPPLNP2 transcripts. Furthermore, immunostained cells and processes were also revealed in the mucosal layer and the basiepithelial nerve plexus of the cardiac stomach, respectively. Consistent with the extensive expression of ArPPLN2-type neuropeptides in the cardiac stomach and other regions of the digestive system, it has been found that ArPPLN2h caused dose-dependent relaxation of *in vitro* cardiac stomach preparations here. The expression of ArPPLNP1 and neuropeptides derived from this precursor in the cardiac stomach of *A. rubens* has been reported and found that ArPPLN1b, like ArPPLN2h, causes relaxation of *in vitro* preparations of the cardiac stomach (Chapter 3). Here the bioactivity of ArPPLN1b and ArPPLN2h as cardiac stomach relaxants has been compared and found that ArPPLN2h is much more effective than ArPPLN1b. This difference in the bioactivity of the two peptides may be associated with differences in the patterns of expression of ArPPLNP1- and ArPPLNP2-derived peptides in the cardiac stomach. Both types of peptides are expressed by mucosal cells and their processes in the basiepithelial plexus, but only ArPPLNP2-derived peptide (ArPPLN2h) expression was detected in the visceral nerve plexus that underlies the coelomic

epithelium of the cardiac stomach. This is significant because the visceral nerve plexus is closely associated with the visceral muscle layer of the cardiac stomach, whereas the basiepithelial nerve plexus is separated from the visceral muscle layer by a layer of collagenous tissue. It is speculated that, therefore, ArPPLN2-type peptides derived from processes in the visceral nerve plexus act directly on the muscle layer to cause relaxation, whereas ArPPLN1-type and ArPPLN2-type peptides derived from processes in the basiepithelial nerve plexus may act indirectly by triggering local release of diffusible signaling molecules that act as muscle relaxants (e.g. nitric oxide; (Melarange and Elphick, 2003)).

Previous studies have revealed that the SALMFamide neuropeptides S1 and S2 cause relaxation of *in vitro* cardiac stomach preparations from *A. rubens*, but with S2 ten times more potent than S1 (Melarange et al., 1999). Therefore, here the bioactivity of ArPPLN2h with S2 has been compared and found that the potency/efficacy of ArPPLN2h is very similar to that of S2 *in vitro*. *In vivo* pharmacological tests with S2 have revealed that injection of this peptide into the perivisceral coelom of *A. rubens* triggers eversion of the cardiac stomach, indicating that S2 may be involved in physiological mechanisms that mediate control of stomach eversion when starfish feed extraorally on prey (e.g. mussels) (Melarange et al., 1999). Therefore, it was of interest to investigate if ArPPLN2h also triggers cardiac stomach eversion in *A. rubens*. Interestingly, it was found that whilst cardiac stomach eversion was observed within five minutes of injection in seven out of ten animals injected with S2, cardiac stomach eversion was not observed in any of ten animals injected with ArPPLN2h. Thus, whilst S2 and ArPPLN2h exhibit similar cardiac stomach relaxing activity *in vitro*, this does not necessary translate into the same bioactivity *in vivo*. This difference in *in vivo*

bioactivity may reflect differences in regions of the cardiac stomach musculature that are regulated by S2 and ArPPLN2h as muscle relaxants.

4.4.1.4 Hemal system and Tiedemann's bodies

The functional significance of ArPPLN2-type neuropeptide expression in the hemal system and the water vascular system associated Tiedemann's bodies of *A. rubens* is unknown. It is noteworthy, however, that ArPPLN1-type neuropeptide expression was also detected in these structures in *A. rubens* (Chapter 3). A common functional characteristic of the hemal system and Tiedemann's bodies are roles in the transport around the starfish body of fluids and circulating cells (Ferguson, 1984). It is noteworthy that previous studies on mollusks have revealed that PP/OK-type peptides regulate ciliary activity (Gaston, 1998) and therefore PPLN1-type and PPLN2-type peptides may have a similar role in the starfish hemal system and water vascular system. Furthermore, such a role could extend to other systems; for example, in ciliary-mediated movement of food materials through the digestive system, as discussed previously for ArPPLNP1-derived peptides in chapter 3.

4.4.2 Comparison of the expression and bioactivity of ArPPLN1-type and ArPPLN2-type peptides in *A. rubens*

Comparison of the expression patterns of ArPPLN1-type and ArPPLN2-type precursors/neuropeptides reveals some general similarities. Both neuropeptide types are widely expressed in *A. rubens* with, for example, prominent expression in the ectoneural and hyponeural regions of the radial nerve cords and circumoral nerve ring, tube feet, digestive system and innervation of interossicular muscles. By way of comparison, the precursor of relaxin-like gonad stimulating peptide in *A. rubens* (AruRGPP) has a much more restricted pattern of expression, including a small and sparsely distributed

population of cells in the ectoneural region of the radial nerve cords and circumoral nerve ring and in the tube feet. In fact, only region where AruRGPP expression is prominent in *A. rubens* is in the arm tip epithelium surrounding the terminal tentacle (chapter 2).

The similarities in the expression patterns of ArPPLN1-type and ArPPLN2-type precursors/neuropeptides presumably reflect a common evolutionary origin as PP/OK-type precursors/neuropeptides, as discussed in more detail below. However, there are also distinct differences in the expression patterns and bioactivity of ArPPLN1-type and ArPPLN2-type precursors/neuropeptides. Some of these differences have already been discussed above and here others have been highlighted. The prototype of PPLN1-type peptides in starfish is starfish myorelaxant peptide (SMP), which was discovered on account of its relaxing effect on the apical muscle of *P. pectinifera* (Kim et al., 2016) and accordingly ArPPLN1b causes dose-dependent relaxation of apical muscle preparations from *A. rubens* (Chapter 3). Furthermore, consistent with the bioactivity of ArPPLN1b, antibodies to ArPPLN1b reveal that this peptide is present in axonal processes that ramify amongst the muscle fibers of the apical muscle (Chapter 3). It is interesting, therefore, that in this study no ArPPLN2h-immunoreactivity was detected in the apical muscle of *A. rubens* and in accordance with this finding ArPPLN2h does not affect the contractile state of the apical muscle *in vitro*. Thus, whilst both PPLN1-type and PPLN2-type peptides act as muscle relaxants in starfish, it appears that they are specialized with respect to the muscle systems that they regulate. Thus, PPLN1-type peptides act as relaxants of the apical muscle and tube feet, whereas PPLN2-type peptides do not cause relaxation of these muscle preparations *in vitro*. Conversely, PPLN2-type peptides cause relaxation of cardiac stomach preparations with an efficacy and potency comparable to that of the SALMFamide neuropeptide S2, whilst PPLN1-

type peptides are much less efficacious as cardiac stomach relaxants. Indeed, it is possible that the relaxing effect of ArPPLN1b on the cardiac stomach *in vitro* (Chapter 3) reflects agonist cross-reactivity with receptors that are naturally activated by ArPPLN2-type peptides. Addressing this issue will require molecular identification of the receptors that mediate the effects of PP/OK-type peptides in starfish, although this is an objective that has yet to be accomplished for any animal species.

5 General discussion

Neuropeptides are signaling molecules that modulate neural circuits to regulate behavior and physiological processes throughout the animal kingdom. Research on neuropeptides in echinoderms, which occupy an "intermediate" position in animal phylogeny between the protostomes and the vertebrates, can provide new insights into the evolution of neuropeptide signaling systems. In the experimental work reported in this thesis, neuropeptides belonging to two different neuropeptide families, relaxin-type and pedal peptide/orcokinin-type, have been characterised in the starfish *A. rubens*.

5.1 General summary

Investigation of the expression of AruRGPP in *A. rubens* using mRNA *in situ* hybridization revealed expression by cells in the radial nerve cords, circumoral nerve ring and tube feet. Furthermore, a band of AruRGPP-expressing cells was also identified in the body wall epithelium lining the cavity that surrounds the sensory terminal tentacle and optic cushion at the tips of the arms, where AruRLPP2 is also expressed. *In vitro* tests revealed that AruRGP induces spawning of ovarian fragments from *A. rubens*. Collectively, these findings suggest that AruRGP may be released by cells in the arm tips to trigger spawning in starfish in response to environmental cues.

Analysis of the expression of ArPPLNP1, ArPPLNP2 and peptides derived from these precursors in *A. rubens* using mRNA *in situ* hybridization and immunohistochemistry revealed a widespread distribution, including expression in radial nerve cords, circumoral nerve ring, digestive system, tube feet and innervation of interossicular muscles. Consistent with this pattern of expression, peptides derived from

ArPPLNP1 and ArPPLNP2 act as muscle relaxants in starfish. A summary of the results obtained in this project can be found at the end of this section in Table 5.1.

5.2 Relaxin-type neuropeptides in starfish

5.2.1 An evolutionary perspective on relaxin-type neuropeptides in starfish

Two relaxin-type neuropeptide precursors from the starfish *A. rubens* have been cloned and analyzed. Based on sequence analysis and phylogenetic relationships in the relaxin/insulin/IGF neuropeptide family, AruRGPP and AruRLPP2 are closer to relaxin/insulin-like peptide precursors than insulin/IGF-type peptide precursors (Figure 2.4). Protostome insulin-like peptide precursors are more likely to belong to the insulin/IGF subfamily and there are no reports of relaxin-type neuropeptide identification in protostomes. This suggests that relaxin-type neuropeptides may be unique to deuterostomes.

RGPs from different types of starfish share more similarities with each other than with AruRLPP2 (Figure 2.3). Thus, AruRLP2 is a relaxin-type peptide but not an RGP-type neuropeptide. Analysis of genome and transcriptome sequences of other starfish species may enable discovery of orthologues of AruRLPP2. When it comes to the RGPs, AruRGP is identical (100%) to AamRGP from *A. amurensis* but shares less sequence identity with AjaRGP from *Aphelasterias japonica* (Order Forcipulatida; Family Asteriidae) (87%) and with PpeRGP from *P. pectinifera* (Figure 2.2C) (Order Valvatida; Family Asterinidae) (65%), which is consistent with the different genera they belong to. In this study, the gene structure of some members of the relaxin/insulin/IGF neuropeptide family were compared (Figure 2.5), which provided further evidence that the two starfish relaxin-like neuropeptides belong to the relaxin/insulin-like peptide subfamily.

It can be concluded that the RGPs and RLP2 are members of the relaxin/insulin-like peptide family. Furthermore, the A chains of starfish RGPs and RLP2 all harbour the cysteine motif (CCxxxCxxxxxxxxC), but none of the B chains possess the distinct and well-conserved vertebrate relaxin-specific receptor-binding motif RxxxRxx(I/V) (Bathgate et al., 2002). Receptors that mediate effects of relaxin-type peptides in starfish are not known.

5.2.2 Future directions for research on relaxin-type neuropeptides in starfish

The receptors of the relaxin-type subfamily of peptides in vertebrates have been identified and the structures and properties of the four vertebrate relaxin-type receptors (RXFP1 - 4, four highly conserved family A GPCRs) have been characterized (Bathgate et al., 2013). Therefore, these receptors may provide a basis for identification of relaxin-type receptors in starfish. Potential starfish relaxin-type peptide receptors could be identified by BLAST analysis of genome and transcriptome data and/or by analyzing the location of related genes on chromosomes/scaffolds. Paralogous genes that emerged through local duplication of an ancestral gene prior to and during the emergence of vertebrates tend to be located in the same vicinity on vertebrate ancestral chromosomes linkage groups (Kim et al., 2014). By comparing the vertebrate rhodopsin-like neuropeptide GPCRs with nonvertebrate chordate and protostomian GPCRs, it has been suggested that local duplication prior to the emergence of vertebrates produced the current diversity of neuropeptide and GPCR superfamilies (Yun et al., 2015). The localization of neuropeptide precursor and receptor genes on starfish genomic scaffolds or chromosomes could be helpful to predict potential receptors for relaxin-type peptides in starfish. Then candidate receptors could be tested by pharmacological

characterization when heterologously expressed in cells, as demonstrated previously for starfish GnRH-type receptors (Tian et al., 2016).

For the two starfish relaxin-type neuropeptides, only the localization of cells expressing AruRGPP/AruRLPP2 mRNA has been investigated (chapter 2). To gain further insights into the expression of the neuropeptides derived from these precursors, immunohistochemical methods need to be employed. Currently, antibodies to AruRGP and AruRLP2 have not been produced. However, Masatoshi Mita and colleagues have successfully generated antibodies to PpeRGP (Katayama and Mita, 2016; Yamamoto et al., 2016). A novel method for conjugate preparation was developed to produce specific antibodies against disulfide-rich heterodimeric peptide-KLH conjugates. However, the antibodies to PpeRGP are so specific that AamRGP, which is identical AruRGP, is not detected. Nevertheless, the strategy used to generate PpeRGP antibodies could be applied to AruRGP in the future. By producing antibodies to AruRGP it may be possible to determine the release sites of AruRGPP-expressing cells, which would provide new insights into how the levels of RGP in the coelom are elevated in starfish prior to spawning.

Previous reports showed that RGP/GSS is expressed in the radial nerve cords (Mita et al., 2009a; Mita et al., 2009b), while in this study a cluster of RGP-expressing cells in the arm tips of starfish have been discovered. Further investigation of RGP expression patterns in other starfish species would determine if arm tip expression of RGP is a general characteristic of starfish and would provide further insights into whether arm tip RGP-expressing cells could be the physiological source of RGP that triggers spawning. Furthermore, several experiments could be performed to test this hypothesis. There is evidence that at least in some starfish species spawning of one

starfish can induce spawning of other starfish nearby with a concentration of about 2 eggs ml^{-1} or 1 x 10^4 sperm ml^{-1} (Beach et al., 1975; Caballes and Pratchett, 2017). Spawning incidence of males are higher than that of females. Particularly, sperm seems more likely to increase the spawning rates (more incidence and less response time) of males compared to eggs (Caballes and Pratchett, 2017). Therefore, it would be interesting to perform experiments where cells expressing RGP in the arm tips are removed by cutting off the arm tips and then investigating if this prevents spawning-induced spawning. Also the effect of arm tip ablation on the concentration of RGP in the coelomic fluid could be investigated in starfish during the spawning season.

Another approach for analysis of the physiological roles of relaxin-type peptides in starfish would be to use gene knockdown/deletion methods; for example, using zinc-finger nucleases (ZFNs), transcription activator-like effector nucleases (TALENs) or clustered regularly interspaced short palindromic repeats (CRISPR). If RGPP gene expression in the radial nerve cords or the arm tips could be manipulated separately, then the source of RGP as a regulator of starfish reproduction could be determined.

If the arm tips are the actual source of RGP responsible for triggering spawning in starfish, then RGP synthesized in the radial nerve cord and tube feet may have other roles. Pharmacological tests similar to those used for PP/OK-type neuropeptides (chapter 3, 4) could be used to check whether RGP causes relaxation or contraction of the tube feet, the effects that would be indicative of roles in regulation of the locomotor activity and/or feeding behavior of starfish. Before the purification of RGP, the shedding substance obtained from the radial nerve extracts of starfish was reported to cause considerable contraction of the intact ovaries (Chaet, 1964b). A similar effect has been reported for NGIWYamide purified from sea cucumber, *Apostichopus japonicus*.

This neuropeptide can induce oocyte maturation and gamete spawning (Kato et al., 2009), but it can also cause contraction of radial longitudinal muscle, intestine and tentacle of sea cucumber and lead to stiffness of collagenous tissue in the body wall dermis of sea cucumber (Iwakoshi, 1995; Birenheide et al., 1998; Inoue et al., 1999; Ohtani et al., 1999). Likewise, because AruRGP mRNA is also transcribed in tube feet of *A. rubens* it would be of interest to test the effects of AruRGP on other parts of *A. rubens* besides the gonad, including tube feet. It was not possible to do these experiments in this study because only very limited amounts of AruRGP were available for the *in vitro* tests reported in chapter 2.

The *in vitro* and *in vivo* effects of RGP on spawning have been investigated extensively (Mita, 2016), whereas RLP2 is a new discovery and nothing is known about its physiological roles. Because AruRLPP2 expression was only detected in the starfish arm tips using mRNA *in situ* hybridization, this may explain why AruRLP2 was not detected in the radial nerve cord extracts using mass spectrometry. If AruRLP2 could be synthesized it would be interesting to investigate if it also triggers spawning, like AruRGP, or it has other physiological roles in starfish.

The expression of ArRGPP and ArRLP2 during starfish larval development has not been investigated. A previous study has investigated the expression of other neuropeptide precursors in *A. rubens* larvae (Mayorova et al., 2016) and therefore it would be interesting to extend this to AruRGPP and AruRLP2 to obtain insights into potential roles of relaxin-type peptides in larval starfish.

5.3 PP/OK-type neuropeptides

5.3.1 Evolution and comparative physiology of PP/OK-type neuropeptide signaling in the Bilateria

PP/OK-type neuropeptides were first discovered in protostomian invertebrates (mollusks, arthropods) and the identification PP/OK-type neuropeptide precursors in echinoderms established that the evolution of PP/OK-type neuropeptides can be traced back to the common ancestor of protostomes and deuterostomes (Rowe and Elphick, 2012). The functional characterization of PP/OK-type neuropeptides in starfish has provided the first opportunity to compare the physiological roles of PP/OK-type neuropeptides in protostomian and deuterostomian invertebrates, thereby gaining insights into the evolution of PP/OK-type signaling.

The discovery of a PP/OK-type neuropeptide (SMP) that acts as a muscle relaxant in the starfish *P. pectinifera* provided the first insight into the physiological roles of PP/OK-type neuropeptides in a deuterostome (Kim et al., 2016). Here characterisation ArPPLNP1, ArPPLNP2 and peptides derived from these precursors in *A. rubens* has provided the first insights into the anatomy of PP/OK-type neuropeptide signaling in a deuterostome. Collectively, the data obtained from *P. pectinifera* and *A. rubens* indicate that SMP/PPLN-type neuropeptides have a general and widespread role as inhibitory neuromuscular transmitters in starfish.

This study is the first detailed analysis of the anatomical expression patterns and actions of PP/OK-type neuropeptides in an echinoderm. In the future, it would be interesting to perform similar investigations in other echinoderms. For example, do PP/OK-type neuropeptides act as muscle relaxants in all echinoderms? Addressing this issue is feasible because precursors of PP/OK-type neuropeptides have been identified in other echinoderms, including two precursors in the sea urchin *S. purpuratus* (SpPPLNP1 and SpPPLNP2; (Rowe and Elphick, 2012)), one precursor in the sea cucumber *A. japonicus* (Rowe et al., 2014) and one or more precursors in several brittle

star species (Zandawala et al., 2017). The existence of multiple PP/OK-type neuropeptide precursors in echinoderm species must be a consequence of one or more duplications of a gene or genes encoding a common ancestral precursor protein(s), but the timing of these gene duplications is not known. Thus, it is not clear whether the existence of two PP/OK-type precursors in sea urchins and in starfish is a consequence of duplication of an ancestral precursor in a common ancestor of both sea urchins and starfish or whether it reflects independent duplication events in the echinoid (sea urchin) and asteroid (starfish) lineages. Further insights into this issue may emerge when complete genome sequences are available for species belonging to each of the five extant echinoderm classes.

As discussed in detail in chapter 3, comparative analysis of the physiological roles of PP/OK-type neuropeptides in the Bilateria is limited in as much as the echinoderms are the only deuterostomian phylum in which PP/OK-type neuropeptides have been identified. Thus, the functional characterization of PP/OK-type neuropeptides in starfish reported here and in previous paper (Kim et al., 2016) represents the totality of our knowledge of physiological roles of PP/OK-type neuropeptides in deuterostomes. This contrasts with a much more extensive series of studies on PP-type neuropeptides in mollusks and OK-type neuropeptides in arthropods. It is clear from these studies that PP/OK-type neuropeptides have a wide variety of physiological roles in protostomes, including regulation of muscle and ciliary activity associated with locomotor activity in mollusks (Hall and Lloyd, 1990) and regulation of both frequency and amplitude of hindgut contraction in arthropods (Stangier et al., 1992). A unifying theme amongst the pharmacological actions of PP/OK-type neuropeptides in protostomes are stimulatory effects, with the effector tissues often being muscular in nature. Thus, this contrasts with the relaxing effects of PP/OK-type neuropeptides on starfish muscle reported here

(Chapter 3, 4) and previously ((Kim et al., 2016). This may reflect an excitatory-inhibitory transition in the roles of PP/OK-type neuropeptides as regulators of muscle activity that accompanied the divergence of protostomes and deuterostomes. To address this issue, investigation of the occurrence and physiological roles of PP/OK-type neuropeptides in a variety of deuterostomian and protostomian taxa is now needed. Furthermore, discovery of the receptors that mediate the effects of PP/OK-type neuropeptides will be necessary to gain a deeper understanding of the evolution PP/OK-type neuropeptide signaling in the Bilateria.

One of the challenges associated with investigation of the evolution of PP/OK-type neuropeptide signaling is that receptors for this family of neuropeptides have as yet not been identified in any species. Investigation of the evolution of other neuropeptide signaling systems has revealed that in some cases the ligands for orthologous neuropeptide receptors can diverge to such an extent over large evolutionary timescales that they are not recognizable as orthologous neuropeptides based on sequence similarity. A good example of this would be neuropeptide-S (NPS) in vertebrates and crustacean-cardioactive peptide (CCAP)-type neuropeptides in protostomes, which exhibit very little sequence similarity in spite of being ligands for orthologous receptors (Mirabeau and Joly, 2013; Semmens et al., 2015). Likewise, the possibility remains that orthologs of the protostome/echinoderm PP/OK-type neuropeptides exist in hemichordates and/or chordates, but have not been identified thus far due to sequence divergence. For this reason, discovery of receptors for PP/OK-type neuropeptides are essential for reconstruction of the evolution of this signaling system in the animal kingdom. Intriguingly, there is some evidence that the evolutionary origin of PP/OK-type neuropeptide signaling may extend beyond the Bilateria to other metazoans because the SITFamide precursor in the placozoan *Trichoplax adhaerens* comprises

multiple copies of peptides that share some sequence similarity with PP/OK-type neuropeptides (Nikitin, 2015). This similarity may, of course, simply reflect convergence. Nevertheless, it highlights the need for further characterization of PP/OK-type neuropeptide signaling in a range of phyla and discovery of the receptors that mediate the effects of these neuropeptides.

5.3.2 Future directions for research on PP/OK-type peptides in starfish and other echinoderms

It is currently difficult to identify PP/OK-type peptide receptors in starfish because PP/OK-type receptors have yet to be identified in any animal species. However, there are co-evolutionary relationships between the peptides and receptors (Mirabeau and Joly, 2013) and the genomic locations of genes encoding neuropeptide precursors or receptors can provide insights into evolutionary relationships. The genome of *A. rubens* has yet to be sequenced but the genome sequences of other starfish species have been obtained, including the crown-of-thorns starfish *A. planci* (Hall et al., 2017) and *P. miniata* (http://www.echinobase.org/Echinobase/pm). Identification of other genes that are located near to the PP/OK-type precursor genes in these species may provide insights into relationships of PP/OK-type peptides with other neuropeptides. In this way, candidate receptors could be identified.

Discovery of the effects of ArPPLN1-type and ArPPLN2-type peptides in causing muscle relaxation in starfish has provided the first insight into the physiological roles of PP/OK-type neuropeptides in echinoderms, but it would be simplistic to conclude that the sole function of these neuropeptides in starfish is to act as inhibitory neuromuscular transmitters. For example, the abundance of ArPPLN1-type and ArPPLN2-type peptide expression in the radial nerve cords and circumoral nerve ring

may be indicative of roles in communication between neurons within these major components of the starfish nervous system. Furthermore, as discussed in chapter 3, the presence of ArPPLN1 and ArPPLN2 type peptides in regions of the digestive system involved in ciliary-mediated transit of food material may be indicative of roles in neural control of ciliary activity, which would be consistent with the effects that PP-type peptides have in causing an increase in ciliary beating frequency in mollusks (Hall and Lloyd, 1990). Software such as ciliaFA has been reported to allow automated, high throughput measurement of respiratory and ependymal ciliary beat frequency (ranging from 3 to 52 Hz) (Smith et al., 2012) and therefore this could be useful to investigate the effects of ArPPLNs on ciliary activity in the starfish digestive system.

From a developmental perspective, localization of the expression several neuropeptide precursors in the larvae of *A. rubens* was reported recently using mRNA *in situ* hybridization (Mayorova et al., 2016). However, at the time when this study was completed in the Elphick group, probes/antibodies for localization of the expression of ArPPLN1/2-type neuropeptides were not available. With the generation of the ArPPLN1/2-specific probes/antibodies reported here, there now exists an opportunity to extend analysis of expression of ArPPLN1/2-type neuropeptides to the larval stages of *A. rubens*.

Another interesting avenue for future research on PP/OK-type neuropeptides would be to compare the neuroanatomy of these signaling systems in different types of starfish, sampling species based on phylogenetic relationships. Such comparisons could reveal whether or not PPLN-type neuropeptides act as mediators of inhibitory neuromuscular transmission in all extant starfish species. Furthermore, comparison of species according to differences in ecological adaptations (e.g. burrowing versus non-

burrowing species; (Santos et al., 2005)) might reveal how the physiology and anatomy of a neuropeptide signaling system in starfish has been adapted for life in different niches.

Extending the comparative approach further, precursors of PP/OK-type neuropeptides have been identified in three of the four other extant echinoderm classes: echinoids (e.g. the sea urchin *S. purpuratus*; (Rowe and Elphick, 2012)), holothurians (e.g. the sea cucumber *A. japonicus*; (Rowe et al., 2014)) and ophiuroids (e.g. the brittle star *Ophionotus victoriae*; (Zandawala et al., 2017)). However, nothing is known about the physiological roles of PP/OK-type neuropeptides in other echinoderms. For example, it would be interesting to determine if PP/OK-type neuropeptides act as inhibitory neuromuscular transmitters in all echinoderms.

5.4 Importance of this study

The expression pattern of four neuropeptide precursors (AruRGPP, AruRLPP2, ArPPLNP1 and ArPPLNP2) have been systematically investigated in the starfish *A. rubens*. This is the first comprehensive analysis of the expression of these neuropeptide precursor types in an echinoderm. AruRGPP and AruRLPP2 are highly expressed in the starfish arm tips, where the sensory organs of starfish (terminal tentacle and optic cushion) are located. This novel finding provides new insights into the physiological source of AruRGP and AruRLP2 to regulate starfish reproduction affected by environmental cues.

The wide expression of ArPPLNP1, ArPPLNP2 and corresponding peptides detected via *in situ* hybridization and immunohistochemistry imply multiple functions of the pedal peptide/orcokinin-type neuropeptides in starfish besides acting as muscle relaxants, which was demonstrated by *in vitro* tests on apical muscle, tube feet and

stomach preparations in this study. With the development of other bioassays, other functions of these neuropeptides may be revealed; for example, analysis of effects on ciliary beat frequency in the pyloric duct and analysis of effects on body wall stiffness. In summary, this study has enriched the limited knowledge of starfish neuroanatomy.

Table 5.1 Results summary of this project.

Neuropeptide precursor	**Abb.**	**Accession number**	***In situ* hybridization**	**Peptides identified by mass spectrometry**	**Immunohistochemistry**	**Function**
Asterias rubens relaxin-like gonad-stimulating peptide precursor	AruRGPP	KT601728	radial nerve cord (ectoneural), circumoral nerve ring (ectoneural); tube feet, arm tip epithelium, terminal tentacle.	A chain, B chais, one inter disulfide bridge	N/A	Causes spawning of *A. rubens* ovarian fragments
Asterias rubens relaxin-like peptide precursor 2	AruRLPP2	KT601729	arm tip epithelium	N/A	N/A	N/A
Asterias rubens pedal peptide-like neuropeptide precursor 1	ArPPLNP1	KT870153	radial nerve cord (ectoneural, hyponeural), circumoral nerve ring (ectoneural, hyponeural); tube feet, arm tip epithelium, terminal tentacle, lateral lappet; peristomial membrane, esophagus, cardiac stomach, pyloric stomach, pyloric duct, pyloric caeca; apical muscle, coelomic epithelium.	ArPPLN1a, ArPPLN1b, ArPPLN1c, ArPPLN1d, ArPPLN1e	radial nerve cords, circumoral nerve ring, marginal nerve cords, lateral motor nerves; hemal system, tiedemann's bodies; tube feet, terminal tentacle, lateral lappet, optic cushion; peristomial membrane, esophagus, cardiac stomach, pyloric stomach, pyloric duct, pyloric caeca; apical muscle, coelomic epithelium, papulae, spine; interossicular muscles.	Causes relaxation of *in vitro* apical muscle, tube foot, cardiac stomach preparations from *A. rubens*
Asterias rubens pedal peptide-like neuropeptide precursor 2	ArPPLNP2	KT601720	radial nerve cord (ectoneural, hyponeural), circumoral nerve ring (ectoneural, hyponeural); tube feet, arm tip epithelium, terminal tentacle, optic cushion; nodule, cardiac stomach, pyloric stomach, pyloric duct, pyloric caeca.	ArPPLN2a, ArPPLN2b, ArPPLN2d, ArPPLN2e, ArPPLN2f, ArPPLN2g-partial, ArPPLN2h, ArPPLN2i, ArPPLN2j, ArPPLN2k,	radial nerve cords, circumoral nerve ring, marginal nerve cords, lateral motor nerves; hemal system, tiedemann's bodies; tube feet, terminal tentacle, lateral lappet, optic cushion; peristomial membrane, esophagus, nodule, cardiac stomach, pyloric stomach, pyloric duct, pyloric caeca; apical muscle, coelomic epithelium, papulae, spine; interossicular muscles.	Causes relaxation of *in vitro* cardiac stomach preparations from *A. rubens*

6 Acknowledgements

I would like to first and foremost thank my supervisor Prof. Maurice Elphick for giving me the opportunity to do my PhD in his lab, his excellent guidance and support throughout my PhD study, including the application of a joint scholarship between China Scholarship Council and QUML to support my study.

I would also like to thank…

my co-supervisor Dr. Angelika Stollewerk and panel member Dr. Caroline Brennan for constructive comments on my ongoing work.

Professor Lindy Holden-Dye and Dr QueeLim Ch'ng for kindly agreeing to examine my PhD thesis.

Dr. Michaela Egertova for teaching me the technique of *in situ* hybridization and immunocytochemistry.

Dr. Elisa Piccaro for her kind help and support when I had trouble with my primary project.

all other members of the Elphick group (Matthew L. Rowe, Meet Zandawala, Jerome Delroisse, Dean Semmens, Anton Barreiro-Iglesias, Ana Belen Tinoco Perez, Liisa Blowes, Tian Shi, Esther Odekunle, Weigang Cai, Luis Yanez Guerra, Xingxing Zhong, Ya Zhang) for their support.

Marleen Klann and Petra Ungerer for their help in the first year of my PhD project.

people who in my office and school of biological and chemical sciences for a good time.

my friends who always had an “open ear” for the worries of a PhD student.

my family who supported me throughout the last four years.

7 References

Adham IM, Burkhardt E, Benahmed M, Engel W. 1993. Cloning of a cDNA for a novel insulin-like peptide of the testicular Leydig cells. J Biol Chem 268(35):26668-26672.

Agüera A, Trommelen M, Burrows F, Jansen JM, Schellekens T, Smaal A. 2012. Winter feeding activity of the common starfish (Asterias rubens L.): The role of temperature and shading. J Sea Res 72:106-112.

Anderson JM. 1953. Structure and function in the pyloric caeca of Asterias forbesi. Biol Bull 105(1):47-61.

Anderson JM. 1954. Studies on the cardiac stomach of the starfish, Asterias forbesi. Biol Bull 107(2):157-173.

Atwood DG, Simon JL. Correlation of gamete shedding with presence of neurosecretory granules in Echinaster and Patiria (Echinodermata; Asteroidea); 1971. AMER SOC ZOOLOGISTS 1041 NEW HAMPSHIRE ST, LAWRENCE, KS 66044. p 701-&.

Balvers M, Spiess AN, Domagalski R, Hunt N, Kilic E, Mukhopadhyay AK, Hanks E, Charlton HM, Ivell R. 1998. Relaxin-like factor expression as a marker of differentiation in the mouse testis and ovary. Endocrinology 139(6):2960-2970.

Bamberger AM, Ivell R, Balvers M, Kelp B, Bamberger CM, Riethdorf L, Loning T. 1999. Relaxin-like factor (RLF): a new specific marker for Leydig cells in the ovary. Int J Gynecol Pathol 18(2):163-168.

Bargmann CI. 1998. Neurobiology of the Caenorhabditis elegans genome. Science 282(5396):2028-2033.

Barker MF, Nichols D. 1983. Reproduction, recruitment and juvenile ecology of the starfish, Asterias rubens and Marthasterias glacialis. J Mar Biol Assoc U K 63(04):745-765.

Barnes H, Powell H. 1951. The growth-rate of juvenile Asterias rubens L. J Mar Biol Assoc U K 30(02):381-385.

Bathgate RA, Halls ML, van der Westhuizen ET, Callander GE, Kocan M, Summers RJ. 2013. Relaxin family peptides and their receptors. Physiol Rev 93(1):405-480.

Bathgate RA, Samuel CS, Burazin TC, Layfield S, Claasz AA, Reytomas IG, Dawson NF, Zhao C, Bond C, Summers RJ, Parry LJ, Wade JD, Tregear GW. 2002. Human relaxin gene 3 (H3) and the equivalent mouse relaxin (M3) gene Novel members of the relaxin peptide family. J Biol Chem 277(2):1148-1157.

Bathgate RAD, Hsueh AJW, Sherwood OD. 2006. Physiology and Molecular Biology of the Relaxin Peptide Family. In: Neill JD, ed. Physiology of Reproduction. New York: Academic.

Beach DH, Hanscomb NJ, Ormond RF. 1975. Spawning pheromone in crown-of-thorns starfish. Nature 254(5496):135-136.

Beck JC, Cooper MS, Willows AO. 2000. Immunocytochemical localization of pedal peptide in the central nervous system of the gastropod mollusc Tritonia diomedea. J Comp Neurol 425(1):1-9.

Beijnink FB, Voogt PA. 1986. The aboral haemal system of the sea star, Asterias rubens (Echinodermata, Asteroidea): An ultrastructural and histochemical study. Zoomorphology 106(1):49-60.

Beisswanger R, Corbeil D, Vannier C, Thiele C, Dohrmann U, Kellner R, Ashman K, Niehrs C, Huttner WB. 1998. Existence of distinct tyrosylprotein

sulfotransferase genes: molecular characterization of tyrosylprotein sulfotransferase-2. Proc Natl Acad Sci U S A 95(19):11134-11139.
Bendena WG, Campbell J, Zara L, Tobe SS, Chin-Sang ID. 2012. Select Neuropeptides and their G-Protein Coupled Receptors in Caenorhabditis Elegans and Drosophila Melanogaster. Front Endocrinol (Lausanne) 3:93.
Birenheide R, Tamori M, Motokawa T, Ohtani M, Iwakoshi E, Muneoka Y, Fujita T, Minakata H, Nomoto K. 1998. Peptides controlling stiffness of connective tissue in sea cucumbers. Biol Bull 194(3):253-259.
Blowes LM, Egertova M, Liu Y, Davis GR, Terrill NJ, Gupta HS, Elphick MR. 2017. Body wall structure in the starfish Asterias rubens. Journal of anatomy 231(3):325-341.
Bond CP, Parry LJ, Samuel CS, Gehring HM, Lederman FL, Rogers PA, Summers RJ. 2004. Increased expression of the relaxin receptor (LGR7) in human endometrium during the secretory phase of the menstrual cycle. J Clin Endocrinol Metab 89(7):3477-3485.
Bondy CA, Gainer H, Russell JT. 1987. Effects of stimulus frequency and potassium channel blockade on the secretion of vasopressin and oxytocin from the neurohypophysis. Neuroendocrinology 46(3):258-267.
Braun BC, Muller K, Jewgenow K. 2015. Expression profiles of relaxin family peptides and their receptors indicate their influence on spermatogenesis in the domestic cat (Felis catus). Domest Anim Endocrinol 52:25-34.
Broeck JV. 2001. Insect G protein-coupled receptors and signal transduction. Arch Insect Biochem Physiol 48(1):1-12.
Broertjes JJS, Posthuma G. 1978. Direct visualization of the haemal system in starfish by a staining procedure. Experientia 34(9):1243-1245.
Brogiolo W, Stocker H, Ikeya T, Rintelen F, Fernandez R, Hafen E. 2001. An evolutionarily conserved function of the Drosophila insulin receptor and insulin-like peptides in growth control. Curr Biol 11(4):213-221.
Bryant-Greenwood GD, Schwabe C. 1994. Human relaxins: chemistry and biology. Endocr Rev 15(1):5-26.
Bullesbach EE, Schwabe C. 2000. The relaxin receptor-binding site geometry suggests a novel gripping mode of interaction. J Biol Chem 275(45):35276-35280.
Bungart D, Kegel G, Burdzik S, Keller R. 1995. Structure-activity relationships of the crustacean myotropic neuropeptide orcokinin. Peptides 16(2):199-204.
Burger LL, Sherwood OD. 1995. Evidence that cellular proliferation contributes to relaxin-induced growth of both the vagina and the cervix in the pregnant rat. Endocrinology 136(11):4820-4826.
Burke RD, Osborne L, Wang D, Murabe N, Yaguchi S, Nakajima Y. 2006. Neuron-specific expression of a synaptotagmin gene in the sea urchin Strongylocentrotus purpuratus. J Comp Neurol 496(2):244-251.
Burkhardt E, Adham IM, Brosig B, Gastmann A, Mattei MG, Engel W. 1994a. Structural organization of the porcine and human genes coding for a Leydig cell-specific insulin-like peptide (LEY I-L) and chromosomal localization of the human gene (INSL3). Genomics 20(1):13-19.
Burkhardt E, Adham IM, Hobohm U, Murphy D, Sander C, Engel W. 1994b. A human cDNA coding for the Leydig insulin-like peptide (Ley I-L). Hum Genet 94(1):91-94.
Byrne M, Morrice MG, Wolf B. 1997. Introduction of the northern Pacific asteroid Asterias amurensis to Tasmania: reproduction and current distribution. Mar Biol 127(4):673-685.

Caballes CF, Pratchett MS. 2017. Environmental and biological cues for spawning in the crown-of-thorns starfish. PLoS One 12(3):e0173964.
Callander GE, Bathgate RA. 2010. Relaxin family peptide systems and the central nervous system. Cell Mol Life Sci 67(14):2327-2341.
Chaet AB. 1964a. Calcium and the Shedding Substance of Patiria Miniata. Am Zool 4:407.
Chaet AB. 1964b. A mechanism for obtaining mature gametes from starfish. Biol Bull 126(1):8-13.
Chaet AB. 1964c. Shedding Substance Activity of Starfish Nerves. Tex Rep Biol Med 22:204.
Chaet AB. 1966a. The gamete-shedding substances of starfishes: a physiological-biochemical study. Am Zool 6(2):263-271.
Chaet AB. 1966b. Neurochemical control of gamete release in starfish. Biol Bull 130(1):43-58.
Chaet AB. Gamete release and shedding substance of sea-stars; 1967; Symp. Zool. Soc. Lond. p 13-24.
Chaet AB, McConnaughy R. 1959. Physiologic activity of nerve extracts. Biol Bull 117:407-408.
Chaet AB, Smith RH. 1962. Role of gamete-shedding substance from starfish nerves. Am Zool 2:511.
Chang MM, Leeman SE, Niall HD. 1971. Amino-acid sequence of substance P. Nat New Biol 232(29):86-87.
Chassin D, Laurent A, Janneau JL, Berger R, Bellet D. 1995. Cloning of a new member of the insulin gene superfamily (INSL4) expressed in human placenta. Genomics 29(2):465-470.
Christie AE. 2008. In silico analyses of peptide paracrines/hormones in Aphidoidea. Gen Comp Endocrinol 159(1):67-79.
Christie AE, Lundquist CT, Nassel DR, Nusbaum MP. 1997. Two novel tachykinin-related peptides from the nervous system of the crab Cancer borealis. J Exp Biol 200(Pt 17):2279-2294.
Christie AE, Nolan DH, Garcia ZA, McCoole MD, Harmon SM, Congdon-Jones B, Ohno P, Hartline N, Congdon CB, Baer KN, Lenz PH. 2011. Bioinformatic prediction of arthropod/nematode-like peptides in non-arthropod, non-nematode members of the Ecdysozoa. Gen Comp Endocrinol 170(3):480-486.
Clynen E, Reumer A, Baggerman G, Mertens I, Schoofs L. 2010. Neuropeptide biology in Drosophila. Advances in experimental medicine and biology 692:192-210.
Cobb JL. 1970. The significance of the radial nerve cords in asteroids and echinoids. Z Zellforsch Mikrosk Anat 108(4):457-474.
Cobb JL. 1978. An ultrastructural study of the dermal papulae of the starfish, Asterias rubens, with special reference to innervation of the muscles. Cell Tissue Res 187(3):515-523.
Cobb JLS. 1987. Neurobiology of the Echinodermata. Nervous systems in invertebrates: Springer. p 483-525.
Conklin D, Lofton-Day CE, Haldeman BA, Ching A, Whitmore TE, Lok S, Jaspers S. 1999. Identification of INSL5, a new member of the insulin superfamily. Genomics 60(1):50-56.
Consortium TCeS. 1998. Genome sequence of the nematode C. elegans: a platform for investigating biology. Science 282(5396):2012-2018.

Dare PJ. 1982. Notes on the swarming behaviour and population density of Asterias rubens L.(Echinodermata: Asteroidea) feeding on the mussel, Mytilus edulis L. ICES J Mar Sci 40(2):112-118.
De Lange RP, van Golen FA, van Minnen J. 1997. Diversity in cell specific co-expression of four neuropeptide genes involved in control of male copulation behaviour in Lymnaea stagnalis. Neuroscience 78(1):289-299.
Dircksen H, Burdzik S, Sauter A, Keller R. 2000. Two orcokinins and the novel octapeptide orcomyotropin in the hindgut of the crayfish Orconectes limosus: identified myostimulatory neuropeptides originating together in neurones of the terminal abdominal ganglion. J Exp Biol 203(Pt 18):2807-2818.
Dolmer P. 1998. The interactions between bed structure of Mytilus edulis L. and the predator Asterias rubens L. J Exp Mar Biol Ecol 228(1):137-150.
Dubois P, Ameye L. 2001. Regeneration of spines and pedicellariae in echinoderms: a review. Microsc Res Tech 55(6):427-437.
Duboule D. 1995. Guidebook to the homeobox genes: Oxford Univ. Press.
Eigenbrot C, Randal M, Quan C, Burnier J, O'Connell L, Rinderknecht E, Kossiakoff AA. 1991. X-ray structure of human relaxin at 1.5 A. Comparison to insulin and implications for receptor binding determinants. J Mol Biol 221(1):15-21.
Elkhawagah AR, Longobardi V, Neglia G, Salzano A, Zullo G, Sosa GA, Campanile G, Gasparrini B. 2015. Effect of Relaxin on Fertility Parameters of Frozen-Thawed Buffalo (Bubalus bubalis) Sperm. Reprod Domest Anim 50(5):756-762.
Elphick MR, Emson RH, Thorndyke MC. 1989. FMRFamide-like immunoreactivity in the nervous system of the starfish Asterias rubens. Biol Bull 177(1):141-145.
Elphick MR, Newman SJ, Thorndyke MC. 1995. Distribution and action of SALMFamide neuropeptides in the starfish Asterias rubens. J Exp Biol 198(Pt 12):2519-2525.
Elphick MR, Price DA, Lee TD, Thorndyke MC. 1991a. The SALMFamides: a new family of neuropeptides isolated from an echinoderm. Proceedings Biological sciences 243(1307):121-127.
Elphick MR, Reeve JR, Jr., Burke RD, Thorndyke MC. 1991b. Isolation of the neuropeptide SALMFamide-1 from starfish using a new antiserum. Peptides 12(3):455-459.
Elphick MR, Semmens DC, Blowes LM, Levine J, Lowe CJ, Arnone MI, Clark MS. 2015. Reconstructing SALMFamide Neuropeptide Precursor Evolution in the Phylum Echinodermata: Ophiuroid and Crinoid Sequence Data Provide New Insights. Front Endocrinol (Lausanne) 6:2.
Euler USv, Gaddum JH. 1931. An unidentified depressor substance in certain tissue extracts. J Physiol 72(1):74-87.
Evans BA, John M, Fowler KJ, Summers RJ, Cronk M, Shine J, Tregear GW. 1993. The mouse relaxin gene: nucleotide sequence and expression. J Mol Endocrinol 10(1):15-23.
Felsenstein J. 1985. Confidence limits on phylogenies: an approach using the bootstrap. Evolution:783-791.
Ferguson JC. 1984. Translocative functions of the enigmatic organs of starfish—the axial organ, hemal vessels, Tiedemann's bodies, and rectal caeca: An autoradiographic study. Biol Bull 166(1):140-155.
Ferlin A, De Toni L, Sandri M, Foresta C. 2016. Relaxin and INSL3 in the muscolo-skeletal system: from bench to bedside. Br J Pharmacol.
Fevold HL, Hisaw FL, Meyer RK. 1930. The relaxative hormone of the corpusluteum. Its purification and concentration. J Am Chem Soc 52(8):3340-3348.

Fredriksson R, Lagerstrom MC, Lundin LG, Schioth HB. 2003. The G-protein-coupled receptors in the human genome form five main families. Phylogenetic analysis, paralogon groups, and fingerprints. Molecular pharmacology 63(6):1256-1272.
Fricker LD. Neuropeptides and other bioactive peptides: from discovery to function; 2012. Morgan & Claypool Life Sciences. p 1-122.
Frooninckx L, Van Rompay L, Temmerman L, Van Sinay E, Beets I, Janssen T, Husson SJ, Schoofs L. 2012. Neuropeptide GPCRs in C. elegans. Front Endocrinol (Lausanne) 3:167.
Garm A, Nilsson DE. 2014. Visual navigation in starfish: first evidence for the use of vision and eyes in starfish. Proceedings Biological sciences 281(1777):20133011.
Gaston MR. 1998. Neuropeptide TPep action on salivary duct ciliary beating rate in the nudibranch mollusc Tritonia diomedea. Invert Neurosci 3(4):327-333.
Georgescu D, Sears RM, Hommel JD, Barrot M, Bolanos CA, Marsh DJ, Bednarek MA, Bibb JA, Maratos-Flier E, Nestler EJ, DiLeone RJ. 2005. The hypothalamic neuropeptide melanin-concentrating hormone acts in the nucleus accumbens to modulate feeding behavior and forced-swim performance. J Neurosci 25(11):2933-2940.
Gnessi L, Basciani S, Mariani S, Arizzi M, Spera G, Wang C, Bondjers C, Karlsson L, Betsholtz C. 2000. Leydig cell loss and spermatogenic arrest in platelet-derived growth factor (PDGF)-A-deficient mice. J Cell Biol 149(5):1019-1026.
Gomes I, Wardman JH, Stockton Jr SD, Devi LA. Neuropeptide Receptors; 2013. Morgan & Claypool Life Sciences. p 1-167.
Good-Avila SV, Yegorov S, Harron S, Bogerd J, Glen P, Ozon J, Wilson BC. 2009. Relaxin gene family in teleosts: phylogeny, syntenic mapping, selective constraint, and expression analysis. BMC Evol Biol 9(1):293.
Gotze M, Pettelkau J, Schaks S, Bosse K, Ihling CH, Krauth F, Fritzsche R, Kuhn U, Sinz A. 2012. StavroX--a software for analyzing crosslinked products in protein interaction studies. J Am Soc Mass Spectrom 23(1):76-87.
Gray TS, Morley JE. 1986. Neuropeptide Y: anatomical distribution and possible function in mammalian nervous system. Life Sci 38(5):389-401.
Gronke S, Clarke DF, Broughton S, Andrews TD, Partridge L. 2010. Molecular evolution and functional characterization of Drosophila insulin-like peptides. PLoS Genet 6(2):e1000857.
Gunnersen JM, Crawford RJ, Tregear GW. 1995. Expression of the relaxin gene in rat tissues. Mol Cell Endocrinol 110(1-2):55-64.
Halanych KM. 2004. The new view of animal phylogeny. Annu Rev Ecol Evol Syst 35:229-256.
Hall JD, Lloyd PE. 1990. Involvement of pedal peptide in locomotion in Aplysia: modulation of foot muscle contractions. J Neurobiol 21(6):858-868.
Hall K. 1960. Modification by relaxin of the response of the reproductive tract of mice to oestradiol and progesterone. J Endocrinol 20:355-364.
Hall MN, Gabay J, Schwartz M. 1983. Evidence for a coupling of synthesis and export of an outer membrane protein in Escherichia coli. Embo j 2(1):15-19.
Hamel J-F, Mercier A. 1995. Prespawning behavior, spawning, and development of the brooding starfish Leptasterias polaris. Biol Bull 188(1):32-45.
Hansell DJ, Bryant-Greenwood GD, Greenwood FC. 1991. Expression of the human relaxin H1 gene in the decidua, trophoblast, and prostate. J Clin Endocrinol Metab 72(4):899-904.

Haraguchi S, Ikeda N, Abe M, Tsutsui K, Mita M. 2016. Nucleotide sequence and expression of relaxin-like gonad-stimulating peptide gene in starfish Asterina pectinifera. Gen Comp Endocrinol 227:115-119.
Hartman HB, Chaet AB. 1962. Gamete shedding with radial nerve extracts. Fed Amer Soc Exp Biol 21:363.
Hennebert E. 2010. Adhesion mechanisms developed by sea stars: A review of the ultrastructure and composition of tube feet and their secretion. Biological Adhesive Systems: Springer. p 99-109.
Hennebert E, Jangoux M, Flammang P. 2013. Functional biology of asteroid tube feet. In: Lawrence J, ed. Starfish: Biology and ecology of the Asteroidea: Baltimore, MD: Johns Hopkins University Press. p 24-36.
Hennebert E, Wattiez R, Waite JH, Flammang P. 2012. Characterization of the protein fraction of the temporary adhesive secreted by the tube feet of the sea star Asterias rubens. Biofouling 28(3):289-303.
Hewes RS, Taghert PH. 2001. Neuropeptides and neuropeptide receptors in the Drosophila melanogaster genome. Genome Res 11(6):1126-1142.
Hisaw FL. 1926. Experimental relaxation of the pubic ligament of the guinea pig. Exp Biol Med 23(8):661-663.
Hofer S, Dircksen H, Tollback P, Homberg U. 2005. Novel insect orcokinins: characterization and neuronal distribution in the brains of selected dicondylian insects. J Comp Neurol 490(1):57-71.
Hofer S, Homberg U. 2006. Evidence for a role of orcokinin-related peptides in the circadian clock controlling locomotor activity of the cockroach Leucophaea maderae. J Exp Biol 209(Pt 14):2794-2803.
Hoffmann FG, Opazo JC. 2011. Evolution of the relaxin/insulin-like gene family in placental mammals: implications for its early evolution. J Mol Evol 72(1):72-79.
Hökfelt T, Broberger C, Xu ZD, Sergeyev V, Ubink R, Diez M. 2000. Neuropeptides—an overview. Neuropharmacol 39(8):1337-1356.
Holland LZ, Albalat R, Azumi K, Benito-Gutierrez E, Blow MJ, Bronner-Fraser M, Brunet F, Butts T, Candiani S, Dishaw LJ, Ferrier DE, Garcia-Fernandez J, Gibson-Brown JJ, Gissi C, Godzik A, Hallbook F, Hirose D, Hosomichi K, Ikuta T, Inoko H, Kasahara M, Kasamatsu J, Kawashima T, Kimura A, Kobayashi M, Kozmik Z, Kubokawa K, Laudet V, Litman GW, McHardy AC, Meulemans D, Nonaka M, Olinski RP, Pancer Z, Pennacchio LA, Pestarino M, Rast JP, Rigoutsos I, Robinson-Rechavi M, Roch G, Saiga H, Sasakura Y, Satake M, Satou Y, Schubert M, Sherwood N, Shiina T, Takatori N, Tello J, Vopalensky P, Wada S, Xu A, Ye Y, Yoshida K, Yoshizaki F, Yu JK, Zhang Q, Zmasek CM, de Jong PJ, Osoegawa K, Putnam NH, Rokhsar DS, Satoh N, Holland PW. 2008. The amphioxus genome illuminates vertebrate origins and cephalochordate biology. Genome Res 18(7):1100-1111.
Holman GM, Nachman RJ, Schoofs L, Hayes TK, Wright MS, De Loof A. 1991. The Leucophaea maderae hindgut preparation: a rapid and sensitive bioassay tool for the isolation of insect myotropins of other insect species. Insect Biochem 21(1):107-112.
Hoshino A, Lindberg I. Peptide biosynthesis: prohormone convertases 1/3 and 2; 2012. Morgan & Claypool Life Sciences. p 1-112.
Hsu SY. 1999. Cloning of two novel mammalian paralogs of relaxin/insulin family proteins and their expression in testis and kidney. Mol Endocrinol 13(12):2163-2174.

Hudson P, Haley J, Cronk M, Shine J, Niall H. 1981. Molecular cloning and characterization of cDNA sequences coding for rat relaxin. Nature 291(5811):127-131.
Hudson P, John M, Crawford R, Haralambidis J, Scanlon D, Gorman J, Tregear G, Shine J, Niall H. 1984. Relaxin gene expression in human ovaries and the predicted structure of a human preprorelaxin by analysis of cDNA clones. Embo j 3(10):2333-2339.
Ikegami S. 1976. Role of asterosaponin A in starfish spawning induced by gonad-stimulating substance and 1-methyladenine. J exp Zool 198(3):359-366.
Ikegami S, Tamura S, Kanatani H. 1967. Starfish gonad: action and chemical identification of spawning inhibitor. Science 158(3804):1052-1053.
Imlay MJ, Chaet AB. 1967. Microscopic observations of gamete-shedding substance in starfish radial nerves. Trans Am Microsc Soc 86:120-126.
Inoue M, Birenheide R, Koizumi O, Kobayakawa Y, Muneoka Y, Motokawa T. 1999. Localization of the neuropeptide NGIWYamide in the holothurian nervous system and its effects on muscular contraction. Proc R Soc B 266(1423):993-1000.
Irving L. 1924. Ciliary currents in starfish. J Exp Zool Part A: Ecol Gen Phys 41(1):115-124.
Ivell R, Balvers M, Domagalski R, Ungefroren H, Hunt N, Schulze W. 1997. Relaxin-like factor: a highly specific and constitutive new marker for Leydig cells in the human testis. Mol Hum Reprod 3(6):459-466.
Iwakoshi E. 1995. Comparative aspects of structure and action of bioactive peptides isolated from the seacucumber Stichopus japonicus. Peptide chemistry:261-264.
Jackson MB, Konnerth A, Augustine GJ. 1991. Action potential broadening and frequency-dependent facilitation of calcium signals in pituitary nerve terminals. Proc Natl Acad Sci U S A 88(2):380-384.
Jangoux M. 1982. 2. ETUDE STRUCTURELLE ET FONCTIONNELLE DU TUBE DIGESTIF D'ASTERIAS RUBENS L.(ECHINODERMATA: ASTEROIDEA). Aust Mus Mem 16:17-38.
Janies D. 2001. Phylogenetic relationships of extant echinoderm classes. Can J Zool 79(7):1232-1250.
Jekely G. 2013. Global view of the evolution and diversity of metazoan neuropeptide signaling. Proc Natl Acad Sci U S A 110(21):8702-8707.
Jiang H, Kim HG, Park Y. 2015. Alternatively spliced orcokinin isoforms and their functions in Tribolium castaneum. Insect Biochem Mol Biol 65:1-9.
John MJ, Borjesson BW, Walsh JR, Niall HD. 1981. Limited sequence homology between porcine and rat relaxins: implications for physiological studies. Endocrinology 108(2):726-729.
Johnson EC, Bohn LM, Barak LS, Birse RT, Nassel DR, Caron MG, Taghert PH. 2003. Identification of Drosophila neuropeptide receptors by G protein-coupled receptors-beta-arrestin2 interactions. The Journal of biological chemistry 278(52):52172-52178.
Kanatani H. 1964. Spawning of Starfish: Action of Gamete-Shedding Substance Obtained from Radial Nerves. Science 146(3648):1177-1179.
Kanatani H. 1973. Maturation-inducing substance in starfishes. Int Rev Cytol 35:253-298.
Kanatani H. 1979. Hormones in echinoderms. In: Barrington E, ed. Hormones and Evolution. Vol 1: London: Academic Press. p 273-307.

Kanatani H. 1983. Nature and action of the mediators inducing maturation of the starfish oocyte. Ciba Foundation symposium 98:159-170.
Kanatani H, Noumura T. 1962. On the nature of active principles responsible for gamete-shedding in the radial nerves of starfishes. J Fac Sci Univ Tokyo, Ser IV 9:403-416.
Kanatani H, Ohguri M. 1966. Mechanism of starfish spawning. I. Distribution of active substance responsible for maturation of oocytes and shedding of gametes. Biol Bull 131(1):104-114.
Kanatani H, Shirai H. 1967. In vitro production of meiosis inducing substance by nerve extract in ovary of starfish. Nature 216:284-286.
Kanatani H, Shirai H. 1969. Mechanism of starfish spawning. II. Some aspects of action of a neural substance obtained from radial nerve. Biol Bull 137(2):297-311.
Kanatani H, Shirai H. 1970. Mechanism of starfish spawning. III. Properties and action of meiosis-inducing substance produced in gonad under influence of gonad-stimulating substance. Dev Growth Differ 12(2):119-140.
Kanatani H, Shirai H. 1971. Chemical structural requirements for induction of oocyte maturation and spawning in starfishes. Dev Growth Differ 13(1):53-64.
Kasik J, Muglia L, Stephan DA, Menon RK. 2000. Identification, chromosomal mapping, and partial characterization of mouse InsI6: a new member of the insulin family. Endocrinology 141(1):458-461.
Katayama H, Mita M. 2016. A sulfanyl-PEG derivative of relaxin-like peptide utilizable for the conjugation with KLH and the antibody production. Bioorg Med Chem 24(16):3596-3602.
Kato S, Tsurumaru S, Taga M, Yamane T, Shibata Y, Ohno K, Fujiwara A, Yamano K, Yoshikuni M. 2009. Neuronal peptides induce oocyte maturation and gamete spawning of sea cucumber, Apostichopus japonicus. Dev Biol 326(1):169-176.
Kawauchi H, Kawazoe I, Tsubokawa M, Kishida M, Baker BI. 1983. Characterization of melanin-concentrating hormone in chum salmon pituitaries. Nature 305(5932):321-323.
Kern A, Hubbard D, Amano A, Bryant-Greenwood GD. 2008. Cloning, expression, and functional characterization of relaxin receptor (leucine-rich repeat-containing g protein-coupled receptor 7) splice variants from human fetal membranes. Endocrinology 149(3):1277-1294.
Kessner D, Chambers M, Burke R, Agus D, Mallick P. 2008. ProteoWizard: open source software for rapid proteomics tools development. Bioinformatics (Oxford, England) 24(21):2534-2536.
Kim CH, Kim EJ, Go HJ, Oh HY, Lin M, Elphick MR, Park NG. 2016. Identification of a novel starfish neuropeptide that acts as a muscle relaxant. J Neurochem 137(1):33-45.
Kim DK, Yun S, Son GH, Hwang JI, Park CR, Kim JI, Kim K, Vaudry H, Seong JY. 2014. Coevolution of the spexin/galanin/kisspeptin family: Spexin activates galanin receptor type II and III. Endocrinology 155(5):1864-1873.
Klein C. 2016. The role of relaxin in mare reproductive physiology: A comparative review with other species. Theriogenology 86(1):451-456.
Klonisch T, Hombach-Klonisch S, Buchmann J, Fischer B, Bergmann M, Steger K. 1999. Relaxin-like factor expression in a human ovarian Sertoli-Leydig cell tumor. Fertil Steril 72(3):546-548.
Koman A, Cazaubon S, Couraud PO, Ullrich A, Strosberg AD. 1996. Molecular characterization and in vitro biological activity of placentin, a new member of the insulin gene family. J Biol Chem 271(34):20238-20241.

Krantz JC, Jr., Bryant HH, Carr CJ. 1950. The action of aqueous corpus luteum extract upon uterine activity. Surg Gynecol Obstet 90(3):372-375.
Kumar S, Stecher G, Tamura K. 2016. MEGA7: Molecular Evolutionary Genetics Analysis Version 7.0 for Bigger Datasets. Mol Biol Evol 33(7):1870-1874.
Laurent A, Rouillac C, Delezoide AL, Giovangrandi Y, Vekemans M, Bellet D, Abitbol M, Vidaud M. 1998. Insulin-like 4 (INSL4) gene expression in human embryonic and trophoblastic tissues. Mol Reprod Dev 51(2):123-129.
Lawrence JM. 2013. Starfish: biology and ecology of the Asteroidea: JHU Press.
Lecroisey C, Le Petillon Y, Escriva H, Lammert E, Laudet V. 2015. Identification, evolution and expression of an insulin-like peptide in the cephalochordate Branchiostoma lanceolatum. PLoS One 10(3):e0119461.
Lee CM, Su MT, Lee HJ. 2009. Pigment dispersing factor: an output regulator of the circadian clock in the German cockroach. J Biol Rhythms 24(1):35-43.
Li C, K K. 2008. Neuropeptides. WormBook. .
Li C, Kim K, Nelson LS. 1999. FMRFamide-related neuropeptide gene family in Caenorhabditis elegans. Brain research 848(1-2):26-34.
Li L, Pulver SR, Kelley WP, Thirumalai V, Sweedler JV, Marder E. 2002. Orcokinin peptides in developing and adult crustacean stomatogastric nervous systems and pericardial organs. J Comp Neurol 444(3):227-244.
Liu C, Chen J, Sutton S, Roland B, Kuei C, Farmer N, Sillard R, Lovenberg TW. 2003. Identification of relaxin-3/INSL7 as a ligand for GPCR142. J Biol Chem 278(50):50765-50770.
Liu C, Kuei C, Sutton S, Chen J, Bonaventure P, Wu J, Nepomuceno D, Kamme F, Tran DT, Zhu J, Wilkinson T, Bathgate R, Eriste E, Sillard R, Lovenberg TW. 2005. INSL5 is a high affinity specific agonist for GPCR142 (GPR100). J Biol Chem 280(1):292-300.
Liu F, Baggerman G, D'Hertog W, Verleyen P, Schoofs L, Wets G. 2006. In silico identification of new secretory peptide genes in Drosophila melanogaster. Mol Cell Proteomics 5(3):510-522.
Lloyd PE, Connolly CM. 1989. Sequence of pedal peptide: a novel neuropeptide from the central nervous system of Aplysia. J Neurosci 9(1):312-317.
Lloyd PE, Phares GA, Phillips NE, Willows AO. 1996. Purification and sequencing of neuropeptides from identified neurons in the marine mollusc, Tritonia. Peptides 17(1):17-23.
Lok S, Johnston DS, Conklin D, Lofton-Day CE, Adams RL, Jelmberg AC, Whitmore TE, Schrader S, Griswold MD, Jaspers SR. 2000. Identification of INSL6, a new member of the insulin family that is expressed in the testis of the human and rat. Biol Reprod 62(6):1593-1599.
Lowe CJ, Wray GA. 1997. Radical alterations in the roles of homeobox genes during echinoderm evolution. Nature 389(6652):718-721.
Lu C, Lam HN, Menon RK. 2005. New members of the insulin family: regulators of metabolism, growth and now ... reproduction. Pediatr Res 57(5 Pt 2):70r-73r.
Lu C, Walker WH, Sun J, Weisz OA, Gibbs RB, Witchel SF, Sperling MA, Menon RK. 2006. Insulin-like peptide 6: characterization of secretory status and posttranslational modifications. Endocrinology 147(12):5611-5623.
Ma S, Gundlach AL. 2007. Relaxin-family peptide and receptor systems in brain: insights from recent anatomical and functional studies. Adv Exp Med Biol 612:119-137.
Ma S, Olucha-Bordonau FE, Hossain MA, Lin F, Kuei C, Liu C, Wade JD, Sutton SW, Nunez A, Gundlach AL. 2009. Modulation of hippocampal theta oscillations

and spatial memory by relaxin-3 neurons of the nucleus incertus. Learn Mem 16(11):730-742.
Magnesen T, Redmond KJ. 2012. Potential predation rates by the sea stars Asterias rubens and Marthasterias glacialis, on juvenile scallops, Pecten maximus, ready for sea ranching. Aquacult Int 20(1):189-199.
Malenka R. 2010. Intercellular communication in the nervous system: Academic Press.
Mashanov V, Zueva O, Rubilar T, Epherra L, Garcia-Arraras JE. 2016. Echinodermata. Structure and Evolution of Invertebrate Nervous Systems Editors Schmidt-Rhaesa A, Harzsch S, Purschke G Oxford University Press:665-688.
Mayorova TD, Tian S, Cai W, Semmens DC, Odekunle EA, Zandawala M, Badi Y, Rowe ML, Egertova M, Elphick MR. 2016. Localization of Neuropeptide Gene Expression in Larvae of an Echinoderm, the Starfish Asterias rubens. Front Neurosci 10:553.
McGowan BM, Stanley SA, Smith KL, White NE, Connolly MM, Thompson EL, Gardiner JV, Murphy KG, Ghatei MA, Bloom SR. 2005. Central relaxin-3 administration causes hyperphagia in male Wistar rats. Endocrinology 146(8):3295-3300.
Melarange R, Elphick MR. 2003. Comparative analysis of nitric oxide and SALMFamide neuropeptides as general muscle relaxants in starfish. J Exp Biol 206(Pt 5):893-899.
Melarange R, Potton DJ, Thorndyke MC, Elphick MR. 1999. SALMFamide neuropeptides cause relaxation and eversion of the cardiac stomach in starfish. Proc R Soc Lond B Biol Sci 266(1430):1785-1789.
Menschaert G, Vandekerckhove TT, Baggerman G, Landuyt B, Sweedler JV, Schoofs L, Luyten W, Van Criekinge W. 2010. A hybrid, de novo based, genome-wide database search approach applied to the sea urchin neuropeptidome. J Proteome Res 9(2):990-996.
Mercier A, Hamel J-F. 2013. Reproduction in Asteroidea. In: Lawrence J, ed. Starfish: Biology and Ecology of the Asteroidea: Baltimore: The Johns Hopkins University Press. p 37-50.
Mirabeau O, Joly JS. 2013. Molecular evolution of peptidergic signaling systems in bilaterians. Proc Natl Acad Sci U S A 110(22):E2028-2037.
Mita M. 2013. Relaxin-like gonad-stimulating substance in an echinoderm, the starfish: A novel relaxin system in reproduction of invertebrates. Gen Comp Endocrinol 181:241-245.
Mita M. 2016. Starfish gonadotropic hormone: Relaxin-like gonad-stimulating peptides. Gen Comp Endocrinol 230-231:166-169.
Mita M, Daiya M, Haraguchi S, Tsutsui K, Nagahama Y. 2015. A new relaxin-like gonad-stimulating peptide identified in the starfish Asterias amurensis. Gen Comp Endocrinol 222:144-149.
Mita M, Ito C, Kubota E, Nagahama Y, Shibata Y. 2009a. Expression and Distribution of Gonad-stimulating Substance in Various Organs of the Starfish Asterina pectinifera. Ann N Y Acad Sci 1163(1):472-474.
Mita M, Katayama H. 2016. A relaxin-like gonad-stimulating peptide from the starfish Aphelasterias japonica. Gen Comp Endocrinol 229:56-61.
Mita M, Yoshikuni M, Ohno K, Shibata Y, Paul-Prasanth B, Pitchayawasin S, Isobe M, Nagahama Y. 2009b. A relaxin-like peptide purified from radial nerves induces oocyte maturation and ovulation in the starfish, Asterina pectinifera. Proc Natl Acad Sci U S A 106(23):9507-9512.

Mo J, Prevost SF, Blowes LM, Egertova M, Terrill NJ, Wang W, Elphick MR, Gupta HS. 2016. Interfibrillar stiffening of echinoderm mutable collagenous tissue demonstrated at the nanoscale. Proc Natl Acad Sci U S A 113(42):E6362-e6371.
Mock P, Frydman R, Bellet D, Diawara DA, Lavaissiere L, Troalen F, Bidart JM. 1999. Pro-EPIL forms are present in amniotic fluid and maternal serum during normal pregnancy. J Clin Endocrinol Metab 84(6):2253-2256.
Moore SJ, Thorndyke MC. 1993. Immunocytochemical mapping of the novel echinoderm neuropeptide SALMFamide 1 (S1) in the starfish Asterias rubens. Cell Tissue Res 274(3):605-618.
Moroz LL, Edwards JR, Puthanveettil SV, Kohn AB, Ha T, Heyland A, Knudsen B, Sahni A, Yu F, Liu L, Jezzini S, Lovell P, Iannucculli W, Chen M, Nguyen T, Sheng H, Shaw R, Kalachikov S, Panchin YV, Farmerie W, Russo JJ, Ju J, Kandel ER. 2006. Neuronal transcriptome of Aplysia: neuronal compartments and circuitry. Cell 127(7):1453-1467.
Muda M, He C, Martini PG, Ferraro T, Layfield S, Taylor D, Chevrier C, Schweickhardt R, Kelton C, Ryan PL, Bathgate RA. 2005. Splice variants of the relaxin and INSL3 receptors reveal unanticipated molecular complexity. Mol Hum Reprod 11(8):591-600.
Muschol M, Salzberg BM. 2000. Dependence of transient and residual calcium dynamics on action-potential patterning during neuropeptide secretion. J Neurosci 20(18):6773-6780.
Nakayama K. 1997. Furin: a mammalian subtilisin/Kex2p-like endoprotease involved in processing of a wide variety of precursor proteins. Biochem J 327 (Pt 3):625-635.
Nathoo AN, Moeller RA, Westlund BA, Hart AC. 2001. Identification of neuropeptide-like protein gene families in Caenorhabditiselegans and other species. Proc Natl Acad Sci U S A 98(24):14000-14005.
Nesvizhskii AI, Keller A, Kolker E, Aebersold R. 2003. A statistical model for identifying proteins by tandem mass spectrometry. Anal Chem 75(17):4646-4658.
Newman SJ, Elphick MR, Thorndyke MC. 1995a. Tissue Distribution of the SALMF Amide Neuropeptides S1 and S2 in the Starfish Asterias rubens Using Novel Monoclonal and Polyclonal Antibodies. II. Digestive System. Proc R Soc Lond B Biol Sci 261(1361):187-192.
Newman SJ, Elphick MR, Thorndyke MC. 1995b. Tissue distribution of the SALMFamide neuropeptides S1 and S2 in the starfish Asterias rubens using novel monoclonal and polyclonal antibodies. I. Nervous and locomotory systems. Proceedings Biological sciences 261(1360):139-145.
Nikitin M. 2015. Bioinformatic prediction of Trichoplax adhaerens regulatory peptides. Gen Comp Endocrinol 212:145-155.
O'Connor WB, Cain GD, Zarrow MX. 1966. Elongation of the interpubic ligament in the little brown bat (Myotis lucifugus). Proc Soc Exp Biol Med 123(3):935-937.
O'Shea M, Schaffer M. 1985. Neuropeptide function: the invertebrate contribution. Annu Rev Neurosci 8(1):171-198.
Ohtani M, Iwakoshi E, Muneoka Y, Minakata H, Nomoto K. 1999. Isolation and characterization of bioactive peptides from the sea cucumber, Stichopus japonicus. Peptide Science—Present and Future: Springer. p 419-420.
Pascual N, Castresana J, Valero ML, Andreu D, Belles X. 2004. Orcokinins in insects and other invertebrates. Insect Biochem Mol Biol 34(11):1141-1146.

Paust HJ, Wessels J, Ivell R, Mukhopadhyay AK. 2002. The expression of the RLF/INSL3 gene is reduced in Leydig cells of the aging rat testis. Exp Gerontol 37(12):1461-1467.
Pearse JS, Eernisse DJ, Pearse VB, Beauchamp KA. 1986. Photoperiodic regulation of gametogenesis in sea stars, with evidence for an annual calendar independent of fixed daylength. Am Zool 26(2):417-431.
Pearson WL, Lloyd PE. 1989. Immunocytological localization of pedal peptide in the central nervous system and periphery of Aplysia. J Neurosci 9(1):318-325.
Penn P, Alexander C. 1980. Fine structure of the optic cusion in the asteroid Nepanthia belcheri. Mar Biol 58(4):251-256.
Peterson KJ, Eernisse DJ. 2016. The phylogeny, evolutionary developmental biology, and paleobiology of the Deuterostomia: 25 years of new techniques, new discoveries, and new ideas. Org Divers Evol 16(2):401-408.
Pierce SB, Costa M, Wisotzkey R, Devadhar S, Homburger SA, Buchman AR, Ferguson KC, Heller J, Platt DM, Pasquinelli AA, Liu LX, Doberstein SK, Ruvkun G. 2001. Regulation of DAF-2 receptor signaling by human insulin and ins-1, a member of the unusually large and diverse C. elegans insulin gene family. Genes & development 15(6):672-686.
Pitia AM, Minagawa I, Uera N, Hamano K, Sugawara Y, Nagura Y, Hasegawa Y, Oyamada T, Sasada H, Kohsaka T. 2015. Expression of insulin-like factor 3 hormone-receptor system in the reproductive organs of male goats. Cell Tissue Res 362(2):407-420.
Price DA, Greenberg MJ. 1977. Structure of a molluscan cardioexcitatory neuropeptide. Science 197(4304):670-671.
Pusch W, Balvers M, Ivell R. 1996. Molecular cloning and expression of the relaxin-like factor from the mouse testis. Endocrinology 137(7):3009-3013.
Reich A, Dunn C, Akasaka K, Wessel G. 2015. Phylogenomic analyses of Echinodermata support the sister groups of Asterozoa and Echinozoa. PLoS One 10(3):e0119627.
Rholam M, Brakch N, Germain D, Thomas DY, Fahy C, Boussetta H, Boileau G, Cohen P. 1995. Role of amino acid sequences flanking dibasic cleavage sites in precursor proteolytic processing. The importance of the first residue C-terminal of the cleavage site. Eur J Biochem 227(3):707-714.
Rouille Y, Duguay SJ, Lund K, Furuta M, Gong Q, Lipkind G, Oliva AA, Jr., Chan SJ, Steiner DF. 1995. Proteolytic processing mechanisms in the biosynthesis of neuroendocrine peptides: the subtilisin-like proprotein convertases. Front Neuroendocrinol 16(4):322-361.
Rowe ML, Achhala S, Elphick MR. 2014. Neuropeptides and polypeptide hormones in echinoderms: new insights from analysis of the transcriptome of the sea cucumber Apostichopus japonicus. Gen Comp Endocrinol 197:43-55.
Rowe ML, Elphick MR. 2012. The neuropeptide transcriptome of a model echinoderm, the sea urchin Strongylocentrotus purpuratus. Gen Comp Endocrinol 179(3):331-344.
Ruppert EE, Fox RS, Barnes RD. 2004. Invertebrate Zoology. Belmont, CA: Thomson, Brooks/Cole.
Saha AK, Tamori M, Inoue M, Nakajima Y, Motokawa T. 2006. NGIWYamide-induced contraction of tube feet and distribution of NGIWYamide-like immunoreactivity in nerves of the starfish Asterina pectinifera. Zoolog Sci 23(7):627-632.

Saitou N, Nei M. 1987. The neighbor-joining method: a new method for reconstructing phylogenetic trees. Mol Biol Evol 4(4):406-425.
Samuel CS, Lekgabe ED, Mookerjee I. 2007. The effects of relaxin on extracellular matrix remodeling in health and fibrotic disease. Adv Exp Med Biol 612:88-103.
Samuel CS, Royce SG, Hewitson TD, Denton KM, Cooney TE, Bennett RG. 2016. Anti-fibrotic actions of relaxin. Br J Pharmacol.
Santos R, Haesaerts D, Jangoux M, Flammang P. 2005. Comparative histological and immunohistochemical study of sea star tube feet (Echinodermata, Asteroidea). J Morphol 263(3):259-269.
Schink W, Struck H. 1968. Relaxin in the Allen-Doisy test. Zentralbl Gynakol 90(20):675-678.
Schuetz AW. 1969. Chemical properties and physiological actions of a starfish radial nerve factor and ovarian factor. Gen Comp Endocrinol 12(2):209-221.
Schwabe C, McDonald JK. 1977a. Primary structure of the B-chain of porcine relaxin. Biochem Biophys Res Commun 75(2):503-510.
Schwabe C, McDonald JK. 1977b. Relaxin: a disulfide homolog of insulin. Science 197(4306):914-915.
Schwabe C, McDonald JK, Steinetz BG. 1976. Primary structure of the A chain of porcine relaxin. Biochem Biophys Res Commun 70(2):397-405.
Schwarz F, Aebi M. 2011. Mechanisms and principles of N-linked protein glycosylation. Curr Opin Struct Biol 21(5):576-582.
Scott DJ, Layfield S, Yan Y, Sudo S, Hsueh AJ, Tregear GW, Bathgate RA. 2006. Characterization of novel splice variants of LGR7 and LGR8 reveals that receptor signaling is mediated by their unique low density lipoprotein class A modules. J Biol Chem 281(46):34942-34954.
Scott DJ, Tregear GW, Bathgate RA. 2005. LGR7-truncate is a splice variant of the relaxin receptor LGR7 and is a relaxin antagonist in vitro. Ann N Y Acad Sci 1041:22-26.
Seidah NG. 2011. The proprotein convertases, 20 years later. Methods Mol Biol 768:23-57.
Semmens DC, Beets I, Rowe ML, Blowes LM, Oliveri P, Elphick MR. 2015. Discovery of sea urchin NGFFFamide receptor unites a bilaterian neuropeptide family. Open Biol 5(4):150030.
Semmens DC, Elphick MR. 2017. The evolution of neuropeptide signalling: insights from echinoderms. Brief Funct Genomics.
Semmens DC, Mirabeau O, Moghul I, Pancholi MR, Wurm Y, Elphick MR. 2016. Transcriptomic identification of starfish neuropeptide precursors yields new insights into neuropeptide evolution. Open Biol 6(2):150224.
Shabanpoor F, Separovic F, Wade JD. 2009. The human insulin superfamily of polypeptide hormones. Vitam Horm 80:1-31.
Sherwood OD. 2004. Relaxin's physiological roles and other diverse actions. Endocr Rev 25(2):205-234.
Shirahase T, Aoki M, Watanabe R, Watanabe Y, Tanaka M. 2016. Increased alcohol consumption in relaxin-3 deficient male mice. Neurosci Lett 612:155-160.
Shirai H. 1986. Gonad-stimulating and maturation-inducing substance. Methods in cell biology 27:73-88.
Shuai XX, Meng YD, Lu YX, Su GH, Tao XF, Han J, Xu SD, Luo P. 2016. Relaxin-2 improves diastolic function of pressure-overloaded rats via phospholamban by activating Akt. Int J Cardiol 218:305-311.

Skiebe P, Dreger M, Meseke M, Evers JF, Hucho F. 2002. Identification of orcokinins in single neurons in the stomatogastric nervous system of the crayfish, Cherax destructor. J Comp Neurol 444(3):245-259.
Smith CM, Djakow J, Free RC, Djakow P, Lonnen R, Williams G, Pohunek P, Hirst RA, Easton AJ, Andrew PW, O'Callaghan C. 2012. ciliaFA: a research tool for automated, high-throughput measurement of ciliary beat frequency using freely available software. Cilia 1:14.
Smith JE. 1937. On the nervous system of the starfish Marthasterias glacialis (L.). Phil Trans R Soc B 227(542):111-173.
Smith JE. 1950. The motor nervous system of the starfish, Astropecten irregularis (Pennant), with special reference to the innervation of the tube feet and ampullae. Philos Trans R Soc Lond B Biol Sci 234(618):521-558.
Sossin WS, Fisher JM, Scheller RH. 1989. Cellular and molecular biology of neuropeptide processing and packaging. Neuron 2(5):1407-1417.
Southey BR, Amare A, Zimmerman TA, Rodriguez-Zas SL, Sweedler JV. 2006. NeuroPred: a tool to predict cleavage sites in neuropeptide precursors and provide the masses of the resulting peptides. Nucleic Acids Res 34(Web Server issue):W267-272.
Squecco R, Garella R, Idrizaj E, Nistri S, Francini F, Baccari MC. 2015. Relaxin Affects Smooth Muscle Biophysical Properties and Mechanical Activity of the Female Mouse Colon. Endocrinology 156(12):4398-4410.
Stangier J, Hilbich C, Burdzik S, Keller R. 1992. Orcokinin: a novel myotropic peptide from the nervous system of the crayfish, Orconectes limosus. Peptides 13(5):859-864.
Steiner DF. 1998. The proprotein convertases. Curr Opin Chem Biol 2(1):31-39.
Steiner DF, Chan SJ, Welsh JM, Kwok SC. 1985. Structure and evolution of the insulin gene. Annu Rev Genet 19:463-484.
Steinetz BG, Beach VL, Blye RP, Kroc RL. 1957. Changes in the composition of the rat uterus following a single injection of relaxin. Endocrinology 61(3):287-292.
Steinetz BG, Horton L, Lasano S. 2009. The source and secretion of immunoactive relaxin in rat milk. Exp Biol Med (Maywood) 234(5):562-565.
Steinetz BG, O'Byrne EM, Butler MC, Hickman LB. 1983. Hormonal regulation of the connective tissue of the symphysis pubis. Biology of Relaxin and its Role in the Human:71-92.
Sterkel M, Oliveira PL, Urlaub H, Hernandez-Martinez S, Rivera-Pomar R, Ons S. 2012. OKB, a novel family of brain-gut neuropeptides from insects. Insect Biochem Mol Biol 42(7):466-473.
Tallent MK. 2008. Presynaptic inhibition of glutamate release by neuropeptides: use-dependent synaptic modification. Results Probl Cell Differ 44:177-200.
Tashima LS, Hieber AD, Greenwood FC, Bryant-Greenwood GD. 1995. The human Leydig insulin-like (hLEY I-L) gene is expressed in the corpus luteum and trophoblast. J Clin Endocrinol Metab 80(2):707-710.
Teerds KJ, de Boer-Brouwer M, Dorrington JH, Balvers M, Ivell R. 1999. Identification of markers for precursor and leydig cell differentiation in the adult rat testis following ethane dimethyl sulphonate administration. Biol Reprod 60(6):1437-1445.
Thomas G. 2002. Furin at the cutting edge: from protein traffic to embryogenesis and disease. Nat Rev Mol Cell Biol 3(10):753-766.
Thompson JD, Higgins DG, Gibson TJ. 1994. CLUSTAL W: improving the sensitivity of progressive multiple sequence alignment through sequence weighting,

position-specific gap penalties and weight matrix choice. Nucleic Acids Res 22(22):4673-4680.
Tian S, Zandawala M, Beets I, Baytemur E, Slade SE, Scrivens JH, Elphick MR. 2016. Urbilaterian origin of paralogous GnRH and corazonin neuropeptide signalling pathways. Sci Rep 6:28788.
Trigg TE, Wright PJ, Armour AF, Williamson PE, Junaidi A, Martin GB, Doyle AG, Walsh J. 2001. Use of a GnRH analogue implant to produce reversible long-term suppression of reproductive function in male and female domestic dogs. J Reprod Fertil Suppl 57:255-261.
Turbeville JM, Schulz JR, Raff RA. 1994. Deuterostome phylogeny and the sister group of the chordates: evidence from molecules and morphology. Mol Biol Evol 11(4):648-655.
Unger H. 1962. Experimentelle und histologische Untersuchungen über Wirkfaktoren aus dem Nervensystem von Asterias Marthasterias glacialis; Asteroidea; Echinodermata. Zool Jb Abt Allg Zool Physiol Tiere 69:481-536.
Uthicke S, Doyle J, Duggan S, Yasuda N, McKinnon AD. 2015. Outbreak of coral-eating Crown-of-Thorns creates continuous cloud of larvae over 320 km of the Great Barrier Reef. Sci Rep 5:16885.
van den Pol AN. 2012. Neuropeptide transmission in brain circuits. Neuron 76(1):98-115.
Veenstra JA. 2000. Mono- and dibasic proteolytic cleavage sites in insect neuroendocrine peptide precursors. Arch Insect Biochem Physiol 43(2):49-63.
Veenstra JA. 2010. Neurohormones and neuropeptides encoded by the genome of Lottia gigantea, with reference to other mollusks and insects. Gen Comp Endocrinol 167(1):86-103.
Veenstra JA. 2011. Neuropeptide evolution: neurohormones and neuropeptides predicted from the genomes of Capitella teleta and Helobdella robusta. Gen Comp Endocrinol 171(2):160-175.
Veenstra JA, Ida T. 2014. More Drosophila enteroendocrine peptides: Orcokinin B and the CCHamides 1 and 2. Cell Tissue Res 357(3):607-621.
Vlasuk GP, Inouye S, Ito H, Itakura K, Inouye M. 1983. Effects of the complete removal of basic amino acid residues from the signal peptide on secretion of lipoprotein in Escherichia coli. J Biol Chem 258(11):7141-7148.
von Heijne G. 1984. How signal sequences maintain cleavage specificity. J Mol Biol 173(2):243-251.
von Heijne G. 1985. Signal sequences: the limits of variation. J Mol Biol 184(1):99-105.
Wang Y, Wang M, Yin S, Jang R, Wang J, Xue Z, Xu T. 2015. NeuroPep: a comprehensive resource of neuropeptides. Database : the journal of biological databases and curation 2015:bav038.
Wei Z, Baggerman G, R JN, Goldsworthy G, Verhaert P, De Loof A, Schoofs L. 2000. Sulfakinins reduce food intake in the desert locust, Schistocerca gregaria. J Insect Physiol 46(9):1259-1265.
Weiss G. 1989. Relaxin in the male. Biol Reprod 40(2):197-200.
Wilkinson TN, Speed TP, Tregear GW, Bathgate RA. 2005. Evolution of the relaxin-like peptide family. BMC Evol Biol 5:14.
Willie JT, Sinton CM, Maratos-Flier E, Yanagisawa M. 2008. Abnormal response of melanin-concentrating hormone deficient mice to fasting: hyperactivity and rapid eye movement sleep suppression. Neuroscience 156(4):819-829.

Willows AO, Pavlova GA, Phillips NE. 1997. Modulation of ciliary beat frequency by neuropeptides from identified molluscan neurons. J Exp Biol 200(10):1433-1439.
Wulff JP, Sierra I, Sterkel M, Holtof M, Van Wielendaele P, Francini F, Broeck JV, Ons S. 2017. Orcokinin neuropeptides regulate ecdysis in the hemimetabolous insect Rhodnius prolixus. Insect Biochem Mol Biol 81:91-102.
Yamamoto K, Kiyomoto M, Katayama H, Mita M. 2016. Radioimmunoassay of relaxin-like gonad-stimulating peptide in the starfish Patiria (=Asterina) pectinifera. Gen Comp Endocrinol 243:84-88.
Yasuda-Kamatani Y, Yasuda A. 2000. Identification of orcokinin gene-related peptides in the brain of the crayfish Procambarus clarkii by the combination of MALDI-TOF and on-line capillary HPLC/Q-Tof mass spectrometries and molecular cloning. Gen Comp Endocrinol 118(1):161-172.
Yegorov S, Good S. 2012. Using paleogenomics to study the evolution of gene families: origin and duplication history of the relaxin family hormones and their receptors. PLoS One 7(3):e32923.
Yki-Jarvinen H, Wahlstrom T, Seppala M. 1983. Immunohistochemical demonstration of relaxin in the genital tract of pregnant and nonpregnant women. J Clin Endocrinol Metab 57(3):451-454.
Yun S, Furlong M, Sim M, Cho M, Park S, Cho EB, Reyes-Alcaraz A, Hwang JI, Kim J, Seong JY. 2015. Prevertebrate Local Gene Duplication Facilitated Expansion of the Neuropeptide GPCR Superfamily. Mol Biol Evol 32(11):2803-2817.
Zandawala M, Moghul I, Yanez Guerra LA, Delroisse J, Abylkassimova N, Hugall AF, O'Hara TD, Elphick MR. 2017. Discovery of novel representatives of bilaterian neuropeptide families and reconstruction of neuropeptide precursor evolution in ophiuroid echinoderms. Open Biol 7(9).
Zhao S, Fields PA, Sherwood OD. 2001. Evidence that relaxin inhibits apoptosis in the cervix and the vagina during the second half of pregnancy in the rat. Endocrinology 142(6):2221-2229.
Zhao S, Kuenzi MJ, Sherwood OD. 1996. Monoclonal antibodies specific for rat relaxin. IX. Evidence that endogenous relaxin promotes growth of the vagina during the second half of pregnancy in rats. Endocrinology 137(2):425-430.
Zimmermann S, Steding G, Emmen JM, Brinkmann AO, Nayernia K, Holstein AF, Engel W, Adham IM. 1999. Targeted disruption of the Insl3 gene causes bilateral cryptorchidism. Mol Endocrinol 13(5):681-691.
Zuckerkandl E, Pauling L. 1965. Evolutionary divergence and convergence in proteins. Evolving genes and proteins 97:97-166.

8 Supplement

A

```
1    atgacaagcaacaaccgccatctcttccaggcaacttgcctagttctcctccttctacac
      M  T  S  N  N  R  H  L  F  Q  A  T  C  L  V  L  L  L  L  H    20
61   gctgccttccacggtggagccctcggtgagaagtactgcgatgacgatttccacatggcg
      A  A  F  H  G  G  A  L  G  E  K  Y  C  D  D  D  F  H  M  A    40
121  gtgttccggacgtgcgcggtcagcaagcggagccagccggggatgagccttagcgacgtg
      V  F  R  T  C  A  V  S  K  R  S  Q  P  G  M  S  L  S  D  V    60
181  ttgaccatgaaccgctttcgaggtcacaacattaaacgaagcatcgacagcacacttgaa
      L  T  M  N  R  F  R  G  H  N  I  K  R  S  I  D  S  T  L  E    80
241  gacaacgccttttttcatgagcggtttggagaagagatctgaatacactggcatcgcctcg
      D  N  A  F  F  M  S  G  L  E  K  R  S  E  Y  T  G  I  A  S   100
301  tactgttgccttcacggatgcacgcccagtgaattatccgtcgtctgctaa
      Y  C  C  L  H  G  C  T  P  S  E  L  S  V  V  C  *             116
```

B

```
1    atggccaacaacctccgtcgtcgtttccaagcaacatgcctggttctcctcatattacaa
      M  A  N  N  L  R  R  R  F  Q  A  T  C  L  V  L  L  I  L  Q    20
61   gcaaccatcaacacgggagccgtcggtgaaaagttctgcgacaacgacttccacttggcc
      A  T  I  N  T  G  A  V  G  E  K  F  C  D  N  D  F  H  L  A    40
121  gtctatcagacctgttcaacccacaagcggggtgatggtgagccggtgcttagcctgaaa
      V  Y  Q  T  C  S  T  H  K  R  G  D  G  E  P  V  L  S  L  K    60
181  gacgtattgacagggagccgcttgcgaggtaatatcaaacggagcttcggatctacattg
      D  V  L  T  G  S  R  L  R  G  N  I  K  R  S  F  G  S  T  L    80
241  gaggacgaagccttttcgcgagcagactggtgaagaggtctgaatacgatggcattgcc
      E  D  E  A  F  F  A  S  R  L  V  K  R  S  E  Y  D  G  I  A   100
301  tcttattgttgcatacacggatgtacaccgagcgagttggctgtcgtctgctaa
      S  Y  C  C  I  H  G  C  T  P  S  E  L  A  V  V  C  *          117
```

C

```
1    atggcatcacagtgccgcctaatcctagcctcaatctcagccgtctgtttggttatcacc
      M  A  S  Q  C  R  L  I  L  A  S  I  S  A  V  C  L  V  I  T    20
61   tctttgatgtgtctaccagccgtgcaagccactgaaacgaccaacaggcattgcggggca
      S  L  M  C  L  P  A  V  Q  A  T  E  T  T  N  R  H  C  G  A    40
121  gcttttcccgactttgtattggcggcttgttcaatggctaagcgatccatcagatcatca
      A  F  P  D  F  V  L  A  A  C  S  M  A  K  R  S  I  R  S  S    60
181  ccgtcactgcatgacttgctccaagcttttaaatcagatgaataccaggcaaaccgttac
      P  S  L  H  D  L  L  Q  A  F  K  S  D  E  Y  Q  A  N  R  Y    80
241  acctcacccattcatctgcgcaagcgcgaagaatacatgacaatagccgactattgctgt
      T  S  P  I  H  L  R  K  R  E  E  Y  M  T  I  A  D  Y  C  C   100
301  tctgttggatgttctccaagcgacctcgttgcttcaggaatttgttaa
      S  V  G  C  S  P  S  D  L  V  A  S  G  I  C  *                115
```

D

```
1    atgacatccaagtaccgcctaatcctcgcctcggtacctgccgttgttttcgtaatcgcc
      M  T  S  K  Y  R  L  I  L  A  S  V  P  A  V  V  F  V  I  A    20
61   actctgagtttgtcgatggtacaagccgattcgagcagtaagcactgcgggtcagctttc
      T  L  S  L  S  M  V  Q  A  D  S  S  S  K  H  C  G  S  A  F    40
121  ccccagtttgtatggacggcttgctcaatggctaagagatccaacagatccccacgctcg
      P  Q  F  V  W  T  A  C  S  M  A  K  R  S  N  R  S  P  R  S    60
181  ctggatgacttgctggaaacgtttaaatcagctagacacctcgatatcagttacaggaca
      L  D  D  L  L  E  T  F  K  S  A  R  H  L  D  I  S  Y  R  T    80
241  cccatccgtctgagcaagcgccaggattacgatggaatggccgattactgttgtatcatt
      P  I  R  L  S  K  R  Q  D  Y  D  G  M  A  D  Y  C  C  I  I   100
301  ggatgctccaccaatgaacttatcgcctcaggaatttgctaa
      G  C  S  T  N  E  L  I  A  S  G  I  C  *                      113
```

Supplementary figure 8.1 relaxin-like gonad-stimulating peptide precursor (RGPP) and relaxin-like peptide precursor 2 RLPP2) identified from other starfish species. **A:** The PmiRGPP cDNA sequence (lowercase, 351 bases; AKZP01031377.1) encoding the PmiRGP precursor protein (uppercase, 116 amino acid residues) is shown. **B:** The AplRGPP cDNA sequence (lowercase, 354 bases; gbr_scaffold8) encoding the AplRGP precursor protein (uppercase, 117 amino acid residues) is shown. **C:** The PmiRLPP2 cDNA sequence (lowercase, 348 bases; AKZP01053386.1) encoding the PmiRLP2 precursor protein (uppercase, 115 amino acid residues) is shown. **D:** The AplRLPP2 cDNA sequence (lowercase, 342 bases; gbr_scaffold3) encoding the AplRLP2 precursor protein (uppercase, 113 amino acid residues) is shown. The predicted signal peptide is shown in blue and predicted dibasic cleavage sites are shown in green. Relaxin-type peptides (with cysteine [C] residues underlined) are shown in red, with the A and B chains highlighted in green and blue, respectively. The asterisk shows the position of the stop codon.

9 Appendices

9.1 Preparation of extracts of *A. rubens* radial nerve cords for mass spectrometry

(1) Radial nerve cords were dissected from the arms of *A. rubens* using the method described by Chaet (1964);
(2) The radial nerve cords were transferred into 90% methanol/9% acetic acid with or without the addition of protease inhibitors (pepstatin A (0.01 mM); phenylmethylsulfonyl fluoride (PMSF; 0.1 mM));
(3) Tissue was lysed and homogenized by sonication (two 2 minutes pulses with 15 s intervals);
(4) The extract was centrifuged at 13,000 rpm in a benchtop microcentrifuge for 5 minutes at 4°C and the supernatant was transferred to a glass vial;
(5) The solvent was bubbled off using nitrogen gas and the remaining extract was then stored at -20°C;
(6) 10 µl of the extract obtained in step (5) was diluted with 50 µl of 1 mM ammonium bicarbonate (Sigma Aldrich) to neutralize the high concentration of acetic acid used for extraction;
(7) To break disuphide bridges and then chemically modify (alkylate) cysteine residues, 5 µl 100 mM dithiothreritol (Sigma Aldrich) was added to the extract at 60°C for 15 minutes and then 5 µl of 200 mM iodoacetamide (Sigma Aldrich) was added in the dark at room temperature for 30 minutes;
(8) Samples of both the reduced/alkylated and non-reduced/non-alkylated material were treated with trypsin (Promega) solution (0.5 µg) incubating overnight at 37^{o}C;
(9) The trypsin digestion was arrested by adding 10 µl of 10% formic acid (J T Baker).

9.2 Mass spectrometry procedure

NanoLC-ESI-MS/MS was used to analyze samples of radial nerve extracts. A 3 µl aliquot of each sample separated by reversed phase chromatography prior to mass spectrometric analysis was used. The procedures are shown below:
(1) Prepare two columns, an Acclaim PepMap µ-pre-column cartridge (300 µm i.d. x 5 mm 5 µm 100 Å) and an Acclaim PepMap RSLC (75 µm x 25 cm 2 µm 100 Å)

(Thermo Scientific), installed on an Ultimate 3000 RSLCnano system (Dionex, Sunnyvale, CA);

(2) Make mobile phase buffer A (0.1% formic acid in water) and B (0.1 % formic acid in acetonitrile);

(3) Load the samples onto the μ-pre-column equilibrated in 2% aqueous acetonitrile containing 0.1% trifluoroacetic acid for 8 minutes at 10 μl min^{-1};

(4) Elute the peptides onto the analytical column at 300 nl min^{-1} by increasing the mobile phase B concentration from 4% to 25% for 90 minutes then to 35% for 10 minutes and 90% for 5 minutes followed by 15 minutes' re-equilibration at 4% buffer B;

(5) Inject the peptides into a Thermo Orbitrap Fusion (Q-OT-qIT, Thermo Scientific) mass spectrometer directly (300 μl min^{-1}) via a Triversa Nanomate nanospray source (Advion Biosciences, NY);

(6) Perform the survey scans of peptide precursors from 400 to 1600 m/z at 120K resolution (at 200 m/z) with automatic gain control (AGC) 5 x 10^5;

(7) Isolate the precursor ions with charge states 2-6 at 1.2Th in the quadrupole and HCD fragments with standardized collision energy of 35;

(8) Analyze the Tandem Mass Spectrometry (MS / MS) data using Orbitrap 30K Resolution with AGC set to 5.4 x 10^4 and the maximum injection time of 200 ms;

(9) The dynamic rejection duration is set to 60 seconds, with a tolerance of 10 ppm around the selected precursor and its isotopes;

(10) Turn on the Monoisotopic precursor selection running in the highest speed mode with a 2-second cycle.

9.3 Preparation of RNA probes

The RNA probes were synthesized by using a PCR method:

(1) Linearised plasmids containing the right cDNAs were used in combination with M13 primers (Forward: 5'-GTAAAACGACGGCCAGTG-3'; Reverse: 5'-GGAAACAGCTATGACCATG-3'). *Taq* DNA polymerase (*Taq* DNA Polymerase with Thermopol Buffer, New England Biolabs) was used as recommended in the manufacturer's instructions under conditions for a routine PCR (initial denaturation at 95 ^oC for 30 seconds; 30 cycles of 95 ^oC for 30 seconds, annealing at 50 ^oC for 30 seconds, elongation at 68 ^oC for 1-2 minute; final extension at 68 ^oC for 5 minutes; hold at 4 ^oC) with two reaction volume of 50 μl including 5 μl 10x Thermo-pol buffer, 5 μL 2

mM dNTPs (Sigma-Aldrich); 2.5 µl 10 mM forward primer (Sigma-Aldrich), 2.5 µl 10 mM reverse primer (Sigma-Aldrich), 1 µl plasmid DNA, 0.5 µl 2.5 units Taq-polymerase (New England Biolabs) and 33.5 µl ddH_2O;

(2) 5 µl PCR product and 1.5% gel electrophoresis was performed to check the size of the fragment after finishing the reactions;

(3) Purify the remaining PCR product using PCR Product Purification Kit (High Pure PCR Product Purification Kit, Roche), when a PCR product of right size is obtained;

(4) Prepare a mixture of the labeling reaction including 10µl linearized plasmid DNA (~1µg), 2µl 10 x DIG RNA labeling mixture (Roche), 2µl 10x transcription buffer (Roche), 2µl T3 or T7 RNA polymerase (Roche) for antisense or sense probe, respectively, and 4µl sterile DEPC treated water;

(5) After mixing and centrifuging the mixture briefly, incubate the reaction for 2.5 hours at 37 ^{o}C;

(6) Add RNase-free DNase (Roche) to the labelling mixture and digest the template DNA for 30 minutes at 37 ^{o}C;

(7) Stop the reaction by adding 2µl 0.2M EDTA (pH 8.0) and add 2µl 4M LiCl and 50µl pre-chilled (-20 ^{o}C) ethanol to the reaction;

(8) Mix mixture well and leave for at least 30 minutes at -80 ^{o}C;

(9) Centrifuge the reaction at 13000 rpm for 15 minutes at 4 ^{o}C, and then decant the ethanol;

(10) Wash the pellet with pre-chilled 70% ethanol and centrifuge again at 13000 rpm for 5 minutes at 4 ^{o}C;

(11) Decant the ethanol and dry the pellet on a hot plate at 45 ^{o}C for approximately 15 minutes;

(12) Dissolve the pellet in 50µl sterile DEPC-treated water and add 1µl RNase inhibitor (Roche);

(13) Check the quality of the probes using 1% gel electrophoresis and measure the concentration;

(14) Adjust the probe concentration to about 100 ng/µl with 25% formaldehyde (FA) / 2x saline-sodium citrate (SSC) for long-term storage at -20 ^{o}C.

9.4 Tissue fixation for *in situ* hybridization

Small-sized adult *A. rubens* (diameter 4 - 6 cm) were fixed in 4% paraformaldehyde (PFA) in phosphate-buffered saline (PBS, pH 7.4) overnight at 4 ^{o}C. Then different protocols were followed to make paraffin-embedded and frozen sections.

For paraffin-embedded sections:

(1) 4% PFA/PBS fixed starfish were dissected into arms and central disk and washed in autoclaved PBS for 10 minutes;

(2) to decalcify the tissue, arms and central disk were placed in Morse's solution (10 % sodium citrate; 20 % formic acid in autoclaved water) for approximately 3 or 8 hours, respectively, changing the solution every hour;

(3) the tissues were washed in dH_2O 10 minutes;

(4) place arm or central disk in 50% ethanol, 70% ethanol, 90% ethanol and 3 x 100% ethanol sequentially for 30 minutes each;

(5) place arms or central disk in xylene solution for 1 x 5 minutes, and then 1 x 8 minutes;

(6) the tissues were washed in melted filtered wax for 3 x 1 hours in oven;

(7) finally, add filtered wax into a rectangle formed by two L-shape metal, and place the tissues into the wax.

To enable visualization of the pigmented eye spot located at the tips of the starfish arms, frozen sections of arm tips were also prepared because the pigment is lost with the wax embedding method.

For frozen sections (mainly used for the arm tips):

(1) arm tips were dissected and washed in PBS for 3 x 5 minutes;

(2) place the tips in 10% sucrose/PBS and 20% sucrose/PBS, 30% sucrose/PBS sequentially for 3 hours each at room temperature;

(3) dry the tips by using paper tissue and place the tips into RA Lamb OCT embedding cryoembedding Matrix (Fischer Scientific) for 5 minutes;

(4) add embedding matrix into a rectangle formed by two L-shape metal molds;

(5) place the tips into the embedding matrix and freeze it immediately with dry ice for dissection.

9.5 Probe hybridization and immunodetection

For probe hybridisation and immunodetection of *in situ* hybridization, there is only slight difference in the tissue rehydration at the beginning and slide mounting at the end for paraffin-embedded and frozen sections. Paraffin-embedded slides were placed in an oven at 65 ^{o}C for 45 minutes followed by 15 minutes to cool down at room temperature. Then slides were processed according to the procedure below:

(1) Place slides into xylene for 3 x 7 minutes to get rid of the wax;

(2) Rehydrate the tissue through a graded series of ethanol (2 x 7 minutes 100% ethanol, 1 x 7 minutes 90% ethanol, 1 x 7 minutes 70% ethanol, 1 x 7 minutes 50% ethanol, 1 x 7 minutes 30% ethanol, 2 x 7 minutes PBS);

(3) Post-fix the slides in 4% PFA/PBS for 20 minutes at room temperature;

(4) Wash slides with PBS/Tween 0.1% for 3 x 5 minutes;

(5) Digest the tissue with Proteinase K (final concentration 10μg/mL) (QIAgen)/Protein K buffer (50 mM Tris-HCl [pH 7.5]; 6.25 mM EDTA in dH_2O) at 37 ^{o}C for 12 minutes;

(6) Post-fix slides again with 4% PFA/PBS used in step (3) for 5 minutes at room temperature;

(7) Wash slides with PBS/Tween 0.1% for 3 x 5 minutes;

(8) Acetylate slides with 1.325 % triethanolamine (pH 7-8), 0.25% acetic anhydride and 0.175% acetic acid in dH_2O with stirring for 10 minutes;

(9) Wash slides with PBS/Tween 0.1% for 2 x 5 minutes and 5 x SSC for 5 minutes at RT;

(10) Dry and pre-hybridise slides with hybridisation buffer (50% formamide; 5 x SSC; 500 μg/ml yeast; 50 μg/ml heparin; 0.1 % Tween-20 in dH_2O) in humidified chamber made by 5 x SSC for approximately 2 hours;

(11) Denature DIG-labeled mRNA probes (800 ng/ml) at 85 ^{o}C for 2 minutes and add the probe-hybridization buffer mixture to the prehybridised slides;

(12) Seal the slides with parafilm and keep them in humidified chamber at 65 ^{o}C overnight for hybridisation;

(13) Remove the parafilm by using 5x SSC with slight shaking and wash slides with 0.2x SSC 2 x 40 minutes at 65 ^{o}C to get rid of the excess probes;

(14) Wash slides with 0.2x SSC 10 minutes and equilibrated in buffer B1 (10 mM Tris-HCl [pH 7.5]; 150 mM NaCl in autoclaved water) for 10 minutes at room temperature;

(15) Dry slides on blotting paper and incubate slides with 5% goat serum/B1 in humidified chamber for approximately 2 hours;
(16) Add alkaline phosphatase (AP)-conjugated anti-DIG antibody (Roche) at 1:3000 dilution in 2.5% goat serum/B1 and incubate slides in humidified chamber overnight at 4 ^{o}C;
(17) Wash slides with buffer B1 (3 x 5 minutes) and equilibrate slides with buffer B3 (100 mM Tris-HCl [pH 9.5]; 100 mM NaCl; 50 mM $MgCl_2$ in dH_2O) for 10 minutes at room temperature;
(18) Dry slides on blotting paper and add staining buffer (nitro-blue tetrazolium chloride [NBT, 75 mg/ml in dimethylformamide] and 5-bromo-4-chloro-3'-indolyphosphate p-toluidine salt substrate solution [BCIP, 50 mg/ml BCIP in dH_2O]) to slides in humidified chamber until desired signal was achieved;
(19) Stop the reaction when the desired staining intensity is achieved by rinsing the slides in dH_2O for 3 x 5 minutes;
(20) Dry slides on hotplate for about 45 minutes until totally dry;
(21) Wash slides with 100% ethanol for 2 x 10 seconds and histoclear (Natural Diagnostics) for 2 x 7 minutes;
(22) Add histomount (Natural Diagnostics) and put a cover slip gently on the slides;
(23) Leave the slides in the fume for 2-3 days until they are dry to be stored in a dark box for photography.

For frozen sections:
(1) Dry slides over night at room temperature;
(2) Wash slides with PBS 2 x 7 minutes;
(3) Do exactly the same as the paraffin-embedded sections until step (19);
(20) Add hydromount (Natural Diagnostics) and put a cover slip gently on the slides;
(21) Leave the slides at room temperature for 1 - 2 hours until a little dry for photography or keep at 4 ^{o}C for storage.

9.6 Immunohistochemistry using monoclonal antibody 1E11

This experiment was performed following the steps below:
(1) Fix the starfish arm tips lightly (up to 30 minutes in 4% paraformaldehyde/PBS; pH 7.4) because immunostaining with the 1E11 antibody is fixation sensitive (R.D. Burke, personal communication);

(2) Dissect the fixed arm tips according to the procedure for frozen sections described in 9.4;
(3) Wash the slides in PBS (2 x 10 minutes) and then incubate for 20 minutes in PBS containing 1% hydrogen peroxide to quench endogenous peroxidases;
(4) Wash the slides again with PBST (2 x 10 minutes) and block the tissues with 5% goat serum/PBST for 2 hour at room temperature;
(5) Add antibody 1E11 (diluted 1: 3 with 5% goat serum/PBST) and incubate the slides overnight at 4°C;
(6) After washing the slides with PBST (3 x 5 minutes) to remove the antibody, add goat anti-mouse horseradish peroxidase conjugated secondary antibodies immunoglobulins (Jackson Immuno Research) diluted 1: 500 in PBST containing 2% goat serum and incubate for 3 hour at room temperature;
(7) Wash the slides with PBST 3 x 5 minutes to remove the secondary antibodies;
(8) Add staining buffer (0.05% diaminobenzidine, 0.05% nickel chloride, 0.015% hydrogen peroxide in PBS) to each slide until desired staining is observed (about 5 minutes);
(9) Wash the slides sequentially in PBS and autoclaved water, 10 minutes each;
(10) Add coverslips to mount the slides using Hydromount (Natural Diagnostics).

9.7 Masson's Trichrome staining

To identify which kind of *A. rubens* tissues, Masson's Trichrome staining was used to differentiates collagenous (blue) from non-collagenous (red) tissue in adjacent slide of the one fixed by Bouin's solution for immunocytochemistry. The protocol is described below.
(1) De-paraffinise using xylene (2 x 10 min) and rehydrate slides through different percent ethanols (100%, 100%, 90%, 70%, 50%; 10 min for each);
(2) Washing the slides in distilled water (2 x 10 min), and rinse it in warm running tap water for 10 min;
(3) Then washing the slides again in distilled water (2 x 10 min) followed by staining in Biebrich scarlet-acid fuchsin solution (0.9% Biebrich scarlet, 0.1% Acid fuchsin, 0.01% glacial Acetic acid) for 10 - 15 min;
(4) Wash the slides in distilled water (3 x 5 min) to get rid of the Biebrich scarlet-acid fuchsin solution;

(5) Differentiate the slides in phosphomolybdic-phosphotungstic acid solution (2.5% Phosphomolybdic acid, 2.5% Phosphotungstic acid) for 10 - 15 min;
(6) Transfer the slides directly (without rinse) to aniline blue solution (2.5% Aniline blue, 2% glacial Acetic acid, in Distilled water) and stain for 5 - 10 min;
(7) rinse briefly in distilled water and differentiate in 1% acetic acid solution for 2 min and wash in distilled water (3 x 5 min);
(8) dehydrate through 95% ethanol and two changes of 100% ethanol quickly to keep the Biebrich scarlet-acid fuchsin staining to xylene (2 x 10 min) and mount in DPX.

9.8 Publication 1

RESEARCH ARTICLE

Cellular Localization of Relaxin-Like Gonad-Stimulating Peptide Expression in *Asterias rubens*: New Insights Into Neurohormonal Control of Spawning in Starfish

Ming Lin,[1] Masatoshi Mita,[2] Michaela Egertová,[1] Cleidiane G. Zampronio,[3] Alexandra M. Jones,[3] and Maurice R. Elphick[1]*

[1]Queen Mary University of London, School of Biological & Chemical Sciences, London, UK
[2]Department of Biology, Faculty of Education, Tokyo Gakugei University, Tokyo, Japan
[3]School of Life Sciences and Proteomics Research Technology Platform, University of Warwick, Coventry, UK

ABSTRACT

Gamete maturation and spawning in starfish is triggered by a gonad-stimulating substance (GSS), which is present in extracts of the radial nerve cords. Purification of GSS from the starfish *Patiria pectinifera* identified GSS as a relaxin-like polypeptide, which is now known as relaxin-like gonad-stimulating peptide (RGP). Cells expressing RGP in the radial nerve cord of *P. pectinifera* have been visualized, but the presence of RGP-expressing cells in other parts of the starfish body has not been investigated. Here we addressed this issue in the starfish *Asterias rubens*. An *A. rubens* RGP (AruRGP) precursor cDNA was sequenced and the A chain and B chain that form AruRGP were detected in *A. rubens* radial nerve cord extracts using mass spectrometry. Comparison of the bioactivity of AruRGP and *P. pectinifera* RGP (PpeRGP) revealed that both polypeptides induce oocyte maturation and ovulation in *A. rubens* ovarian fragments, but AruRGP is more potent than PpeRGP. Analysis of the expression of AruRGP in *A. rubens* using mRNA in situ hybridization revealed cells expressing RGP in the radial nerve cords, circumoral nerve ring, and tube feet. Furthermore, a band of RGP-expressing cells was identified in the body wall epithelium lining the cavity that surrounds the sensory terminal tentacle and optic cushion at the tips of the arms. Discovery of these RGP-expressing cells closely associated with sensory organs in the arm tips is an important finding because these cells are candidate physiological mediators for hormonal control of starfish spawning in response to environmental cues. J. Comp. Neurol. 525:1599–1617, 2017.

INDEXING TERMS: echinoderm; neuropeptide; gonadotropin; gamete; spawning; ovary; mRNA in situ hybridization; RRID AB_2617214

Control of reproductive maturation and function in animals is regulated by a variety of polypeptide hormones. In vertebrates, hypothalamic gonadotropin-releasing hormone (GnRH) acts on the pituitary gland to stimulate release of follicle-stimulating hormone (FSH) and luteinizing hormone (LH), which then act synergistically to promote gamete maturation and gonadal function (Pierce and Parsons, 1981). Gonadotropic hormones identified in invertebrates include egg-laying hormone (ELH) in molluscs, which is related to vertebrate corticotropin-releasing

The first two authors contributed equally to this work.

Grant sponsor: China Scholarship Council studentship (awarded to M.L.); Grant sponsor: BBSRC; Grant numbers: BB/M001644/1 (awarded to M.R.E.), BB/M001032/1 (awarded to A.M.J.), JSPS KAKENHI 16K07417 (awarded to M.M.).

*CORRESPONDENCE TO: Prof. Maurice Elphick, School of Biological & Chemical Sciences, Queen Mary University of London, London E1 4NS, UK. E-mail: m.r.elphick@qmul.ac.uk

Received July 12, 2016; Revised October 25, 2016;
Accepted October 26, 2016.
DOI 10.1002/cne.24141
Published online November 21, 2016 in Wiley Online Library (wileyonlinelibrary.com)

hormone (CRH) (Chiu et al., 1979; Conn and Kaczmarek, 1989), and an insulin-like peptide that regulates egg maturation in the mosquito *Aedes aegypti* (Brown et al., 2008).

The first report of a gonadotropic substance in an invertebrate was the observation that extracts of radial nerve cords from the starfish *Asterias forbesi* induce shedding of gametes when injected in this species (Chaet and McConnaughy, 1959). The active substance was named gonad-stimulating substance (GSS) and was characterized biochemically as a peptide hormone (Kanatani, 1979). Furthermore, antibodies to GSS were generated and used to localize its expression in the starfish *Pycnopodia helianthoides*, with immunostaining observed in the radial hemal sinus located above the radial nerve cords (Caine and Burke, 1985). However, the molecular identity of GSS was not determined until 2009, 50 years after its activity was first reported (Mita et al., 2009a). Using the Japanese starfish species *Patiria pectinifera* as an experimental system, GSS was purified and identified as a heterodimer comprising two polypeptides: A and B chains. The A and B chains are linked by two disulfide bridges, with the A chain also having a single intramolecular disulfide bridge. Furthermore, the A chain contains a cysteine motif CCxxxCxxxxxxxxC, which is a signature sequence of the insulin/insulin-like growth factor (IGF)/relaxin superfamily (Mita et al., 2009a). More specifically, phylogenetic sequence analysis revealed that *P. pectinifera* GSS is a member of the relaxin-type peptide family. Therefore, the GSS identified in *P. pectinifera* has been designated as relaxin-like gonad-stimulating peptide or RGP (Haraguchi et al., 2016). Subsequently, orthologs of *P. pectinifera* RGP (PpeRGP) have been identified in other starfish species, including *Asterias amurensis, Asterias rubens*, and *Aphelasterias japonica* (Mita et al., 2015; Mita and Katayama, 2016; Semmens et al., 2016).

The hormone relaxin was first discovered based on the observation that injection of serum from pregnant guinea pigs or rabbits caused relaxation of the pubic ligament of virgin guinea pigs (Hisaw, 1926). The ovarian corpus luteum and other parts of the reproductive tract were identified as sources of relaxin and its physiological role as a hormonal regulator of processes associated with preparation for parturition in mammals was established (Sherwood, 2004). Determination of the structure of relaxin revealed that it is an insulin-like dimeric peptide comprising an A and B chain that are linked by disulfide bridges (Schwabe and McDonald, 1977). Subsequently, it was discovered that the prototypical ovarian relaxin belongs to a family of relaxin/insulin-like peptides, which also occur in nonmammalian vertebrates (Bathgate et al., 2002; Hsu et al., 2005). Furthermore, investigation of the expression and functions of these peptides has revealed roles that extend beyond reproductive physiology. For example, relaxin-3 is a neuropeptide expressed by neurons located in the nucleus incertus of the brain stem that project to many other regions of the brain. Accordingly, relaxin-3 regulates a variety of processes, including arousal, stress, feeding, metabolism, and memory (Smith et al., 2011).

Starfish RGP was the first relaxin-type peptide to be functionally characterized in an invertebrate (Mita et al., 2009a). Furthermore, its role as a gonadotropic peptide in starfish is interesting because it suggests that the prepartum actions of relaxin in mammals may reflect an evolutionarily ancient role in regulation of reproductive processes. The discovery of RGP has enabled investigation of its expression profile in *P. pectinifera*. Quantitative polymerase chain reaction (PCR) revealed expression in the radial nerve cords, consistent with the original discovery of GSS/RGP in this tissue. However, expression was also detected, albeit at much lower levels, in the cardiac stomach and tube feet (Mita et al., 2009a), which suggests that RGP may have nonreproductive functions in starfish. Analysis of RGP expression in *P. pectinifera* at the cellular level, using mRNA in situ hybridization techniques, has revealed that it is expressed by a population of cells located in the ectoneural epithelium of the radial nerve cords (Mita et al., 2009a). However, a wider analysis of RGP

ABBREVIATIONS

Aam RGP	*Asterias amurensis* relaxin-like gonad-stimulating peptide
Aja RGP	*Aphelasterias japonica* relaxin-like gonad-stimulating peptide
AP	Alkaline phosphatase
AruRGP	*Asterias rubens* relaxin-like gonad-stimulating peptide
AruRLP2	*Asterias rubens* relaxin-type precursor
ASW	Artificial seawater
BCIP	5-bromo-4-chloro-3′-indolyphosphate p-toluidine
CL	Connective tissue layer
CONR	Circumoral nerve ring
CRH	Corticotropin-releasing hormone
DIG	Digoxygenin
Ec	Ectoneural region
EC_{50}	Median effective concentration
ELH	Egg laying hormone
Ep	Epithelial layer
FSH	Follicle-stimulating hormone
GnRH	Gonadotropin-releasing hormone
GSS	Gonad-stimulating substance
Hy	Hyponeural region
IGF	Insulin-like growth factor
LH	Luteinizing hormone
ML	Muscle layer
MS	Mass spectrometry
NBT	Nitro-blue tetrazolium
OC	Optic cushion
PBS	Phosphate-buffered saline
PBST	PBS / 0.1% Tween-20
PCR	Polymerase chain reaction
PFA	Paraformaldehyde
PMSF	Phenylmethylsulfonyl fluoride
Ppe	RGP *Patiria pectinifera* relaxin-like gonad-stimulating peptide
RG	Prelaxin-like gonad-stimulating peptide
Sp	Spine
SSC	Saline-sodium citrate
Su	Sucker
TF	Tube foot
TT	Terminal tentacle

expression in the starfish body using mRNA in situ hybridization techniques has, as yet, not been conducted. This is of interest because it is not known if the radial nerve cord is the physiological source of RGP that triggers gamete maturation and release in starfish.

Recently, analysis of radial nerve cord transcriptome sequence data obtained from the common European starfish *A. rubens* enabled identification of a transcript encoding an RGP-type precursor protein in this species (Semmens et al., 2016). Here we cloned and sequenced a cDNA encoding the *A. rubens* RGP (AruRGP) precursor, confirmed the presence of AruRGP in extracts of *A. rubens* radial nerve cords using mass spectrometry, and demonstrated the bioactivity of synthetic AruRGP in triggering oocyte maturation and ovulation. Furthermore, we used mRNA in situ hybridization to analyze the expression of AruRGP throughout the body of *A. rubens*, which has enabled visualization of cells expressing RGP in the radial nerve cords and in other parts of the body. Our findings provide important new insights into how RGP may mediate hormonal control of gamete maturation and release in starfish.

MATERIALS AND METHODS

Animals

Starfish (*A. rubens*) were collected at low tide from the Thanet coast (Kent, UK) or were obtained from a fisherman based at Whitstable (Kent, UK). The animals were maintained in a circulating seawater aquarium at ~12°C in the School of Biological & Chemical Sciences at Queen Mary, University of London, and were fed on mussels (*Mytilus edulis*).

cDNA cloning and sequencing and sequence analysis

BLAST analysis of *A. rubens* neural transcriptome sequence data using the PpeRGP precursor as a query identified a 2,915 base contig (1122961) encoding a 109 residue RGP-type precursor protein (GenBank: KT601728) (Semmens et al., 2016). To confirm this contig sequence, which was obtained by assembly of Illumina HiSeq reads, and to obtain a template for probe synthesis, a cDNA encoding the *A. rubens* RGP (AruRGP) precursor was cloned and sequenced.

Total RNA was extracted from radial nerves of *A. rubens* using the SV Total RNA Isolation System (Promega, Madison, WI) and cDNA was synthesized using the QuantiTect Rev. Transcription Kit (Qiagen, Chatsworth, CA). A cDNA including the entire coding region of the AruRGP precursor transcript was amplified by PCR using Phusion high-fidelity PCR master mix (New England Biolabs, Beverly, MA) with the oligonucleotide primers 5′-ATGGCAAACTACCGTCTCAT-3′ and 5′-GCCACCCATGAAATAGTCAA-3′ (custom synthesized by Sigma-Aldrich, St. Louis, MO). The PCR product was gel-extracted and purified using a QIAquick gel extraction kit (Qiagen). Then the AruRGP cDNA was cloned into pBluescript SKII (+) vector (Agilent Technologies, Palo Alto, CA), which was cut with the EcoRV-HF restriction endonuclease (New England Biolabs) for sequencing.

The ExPASy translate tool (http://web.expasy.org/translate/) was used to determine the protein sequence of the AruRGP precursor and SignalP 4.1 (http://www.cbs.dtu.dk/services/SignalP/) was used to predict the signal peptide. Comparison of the sequence of the AruRGP precursor protein with RGP-type precursors identified previously in other species (Mita et al., 2009a,; Mita and Katayama, 2016) was performed using ClustalW (Thompson et al., 1994). Phylogenetic analysis of the relationship of AruRGP with other relaxin-like peptides was investigated using the neighbor-joining method (Zuckerkandl and Pauling, 1965; Felsenstein, 1985; Saitou and Nei, 1987) with MEGA 7.0.14 (Kumar et al., 2016).

Preparation of extracts of *A. rubens* radial nerve cords for mass spectrometry

Extracts of *A. rubens* radial nerve cords were prepared to enable use of mass spectrometry to investigate the presence and structure of AruRGP in this tissue. Radial nerve cords were dissected from specimens of *A. rubens* as described previously (Chaet, 1964) and then transferred into 90% methanol / 9% acetic acid with or without the addition of protease inhibitors (pepstatin A [0.01 mM]; phenylmethylsulfonyl fluoride [PMSF; 0.1 mM]). The tissue was sonicated (two 2-min pulses with 15-sec intervals) and homogenized to lyse cells. The extract was centrifuged (10,000*g* for 5 min at 4°C) and the supernatant transferred to a glass vial. Finally, the solvent was bubbled off using nitrogen gas before being stored at −20°C.

Aliquots of 10 µl of radial nerve extract were diluted using 50 µl of 1 mM ammonium bicarbonate (Sigma Aldrich) to neutralize the high concentration of acetic acid used for extraction. Some aliquots were also subject to reduction to break disulfide bridges followed by alkylation of cysteine residues. For reduction, samples were treated with 5 µl of 100 mM dithiothreritol (Sigma Aldrich) and heated at 60°C for 15 minutes. Alkylation was performed by adding 5 µl of 200 mM iodoacetamide (Sigma Aldrich) and incubated in the dark at room temperature for 30 minutes. Samples of both reduced/alkylated and nonreduced/nonalkylated material were also digested using

0.5 μg trypsin (Promega) solution and incubated overnight at 37°C, with the digest arrested by addition of 10 μl of 10% formic acid (J.T. Baker, Phillipsburg, NJ).

Mass spectrometry

NanoLC-ESI-MS/MS was used to analyze samples of radial nerve extracts, with a 3 μl aliquot of each sample separated by reversed phase chromatography prior to mass spectrometric analysis. Two columns were utilized, an Acclaim PepMap μ-pre-column cartridge (300 μm i.d. × 5 mm 5 μm 100 Å) and an Acclaim PepMap RSLC (75 μm × 25 cm 2 μm 100 Å) (Thermo Scientific), installed on an Ultimate 3000 RSLCnano system (Dionex, Sunnyvale, CA). Mobile phase buffer A was 0.1% formic acid in water and mobile phase B was 0.1% formic acid in acetonitrile. Samples were loaded onto the μ-pre-column equilibrated in 2% aqueous acetonitrile containing 0.1% trifluoroacetic acid for 8 minutes at 10 μl min^{-1}, after which peptides were eluted onto the analytical column at 300 nl min^{-1} by increasing the mobile phase B concentration from 4% B to 25% over 90 minutes then to 35% B over 10 minutes and 90% B over 5 minutes, followed by a 15-minute re-equilibration at 4% B. Peptides were injected directly from the LC (300 nl min^{-1}) via a Triversa Nanomate nanospray source (Advion Biosciences, NY) into a Thermo Orbitrap Fusion (Q-OT-qIT, Thermo Scientific, Pittsburgh, PA) mass spectrometer. Survey scans of peptide precursors from 400 to 1600 *m/z* were performed at 120K resolution (at 200 *m/z*) with automatic gain control (AGC) 5 × 10^5. Precursor ions with charge state 2–6 were isolated (isolation at 1.2 Th in the quadrupole) and subjected to HCD fragmentation with normalized collision energy of 35. Tandem mass spectrometry (MS/MS) data were analyzed using the Orbitrap at 30K resolution, AGC was set to 5.4 × 10^4, and the max injection time was 200 ms. Dynamic exclusion duration was set to 60 seconds with a 10 ppm tolerance around the selected precursor and its isotopes. Monoisotopic precursor selection was turned on. The instrument was run in top speed mode with 2-second cycles.

Analysis of mass spectrometry data

Raw data were converted to mascot generic format using MSConvert in ProteoWizard Toolkit (v. 3.0.5759) (Kessner et al., 2008). MS spectra were searched with Mascot engine (Matrix Science, v. 2.4.1) (Nesvizhskii et al., 2003) against a database comprising 40 *A. rubens* neuropeptide precursor proteins (Semmens et al., 2016), all proteins in GenBank from species belonging to the family Asteriidae and the common Repository of Adventitious Proteins Database (http://www.thegpm.org/cRAP/index.html). Theoretical peptides were generated from a tryptic digestion allowing up to two missed cleavages and variable modifications; carbamidomethyl on cysteine, oxidation on methionine, amidation (by modification of C-terminal glycines), and pyroglutamate (by modification of N-terminal glutamines). A no-enzyme search was performed for samples not treated with trypsin. Precursor mass tolerance was 10 ppm and product ions were searched at 0.05 Da tolerances. Scaffold (v. Scaffold_4.6.1, Proteome Software) was used to validate MS/MS-based peptide and protein identifications. Peptide identifications were accepted if they could be established at greater than 95.0% probability by the Scaffold Local FDR algorithm. Protein identifications were accepted if they could be established at greater than 95.0% probability and contained at least two identified peptides. Protein probabilities were assigned by the Protein Prophet algorithm (Nesvizhskii et al., 2003). Proteins that contained similar peptides and could not be differentiated based on MS/MS analysis alone were grouped to satisfy the principles of parsimony. Proteins sharing significant peptide evidence were grouped into clusters. The program Stavrox (v. 3.6.0) was used to search for crosslinked spectra (Gotze et al., 2012). Default settings were used except that semitryptic digestion was permitted, disulfide bonds were specified as the crosslinker, and high mass accuracy data were used with precursor mass tolerance of 5 ppm and fragment mass tolerance of 15 ppm. The full-length AruRGP precursor was used as the reference sequence.

Comparison of the effects of synthetic AruRGP and PpeRGP on *A. rubens* ovarian fragments

Asterias rubens RGP (AruRGP) and *P. pectinifera* RGP (PpeRGP) were synthesized commercially by the Peptide Institute (Osaka, Japan) and their bioactivity was assayed using ovarian fragments from *A. rubens*, as described previously (Shirai, 1986). Modified van't Hoff's artificial seawater (ASW) adjusted to pH 8.2 with 0.02 M borate buffer was prepared (Kanatani and Shirai, 1970) and the ovaries of mature female starfish were excised and cut using scissors into small fragments containing only a few lobes. The ovarian fragments were then incubated in ASW containing synthetic AruRGP or PpeRGP at a range of concentrations (5 × 10^{-8} to 4 × 10^{-10} M) for 1 hour. The samples were examined to determine whether or not spawning had occurred and were scored (Shirai, 1986) as follows: (+++) spawning occurred and most of the oocytes were matured; (++) about 50% of the oocytes were matured; (+) a few oocytes were matured; and (–) no spawning occurred. The scores were converted to

numerical values (+++ = 100; + + = 67; + = 33; − = 0) so that the median effective concentration (EC_{50}) could be determined graphically. Means ± SEM were determined from five separate assays using ovaries from different animals.

Synthesis of digoxygenin-labeled RNA probes for AruRGP precursor transcripts

A pBluescript SKII (+) vector containing the cloned and sequenced AruRGP precursor cDNA was used to synthesize RNA probes. First, a routine PCR was performed using *Taq* DNA polymerase (*Taq* DNA Polymerase with Thermopol Buffer, New England Biolabs) and standard M13 primers (Forward: 5′-GTAAAACGACGGCCAGTG-3′, Reverse: 5′-GGAAACAGCTATGACCATG-3′, custom-synthesized by Sigma-Aldrich) to linearize the plasmid and amplify the insert. The PCR product, which included the AruRGP precursor cDNA sequence and T3 and T7 RNA polymerase sites, was purified using a QIAquick gel extraction kit (Qiagen).

RNA probes were synthesized from the PCR product using a digoxygenin (DIG)-labeled nucleotide triphosphate mix (Roche, Nutley, NJ) supplemented with dithiothreitol (Promega), a placental RNase inhibitor (Promega), and RNA polymerases (New England Biolabs), according to the manufacturer's instructions. T3 or T7 RNA polymerase was used for synthesis of the antisense or sense probes, respectively. Reaction products were digested with RNase free DNase (New England Biolabs) to remove template DNA and then stored at −20°C in 25% formamide made up in 2× saline-sodium citrate (SSC) buffer.

Fixation and sectioning of starfish

Specimens of *A. rubens* (diameter 4–6 cm) were fixed in 4% paraformaldehyde (PFA) in phosphate-buffered saline (PBS, pH 7.4) overnight at 4°C. Different protocols were used to prepare paraffin-embedded sections or frozen sections of fixed tissue.

To prepare specimens for embedding in paraffin wax, fixed starfish were cut with scissors to separate the five arms from the central disk region. Tissues were washed in autoclaved PBS for 10 minutes and then transferred to Morse's solution (10% sodium citrate; 20% formic acid in autoclaved water) for decalcification (typically 3 hours for arms and 8 hours for central disk). Then tissues were washed in distilled water for 10 minutes and dehydrated through a graded series of ethanol (50%, 70%, 90%, 3 × 100%; 30 minutes for each step). After clearing in xylene (1 × 5 minutes and 1 × 8 minutes; VWR Chemicals, Chicago, IL), the tissue was incubated in molten paraffin wax (3 × 1 hour) in an oven at ∼58°C. The tissue was embedded in wax using L-shaped brass molds and stored at room temperature. Sections (12 μm) were cut using a Leica RM2145 microtome and collected on poly-L-lysine-coated slides (Polysine; VWR).

To enable visualization of the pigmented optic cushion located at the tips of the starfish arms, frozen sections of arm tips were also prepared because the pigment is lost with the wax-embedding method. After fixation, arm tips were washed in PBS (3 × 5 minutes) and then cryoprotected by incubation in sucrose solutions of ascending concentration (10%, 20%, 30% sucrose for 3 hours each step, at room temperature). The arm tips were embedded in RA Lamb OCT embedding cryoembedding Matrix (Fischer Scientific) and immediately frozen on dry ice. Sections (12 μm) were cut using a Leica CM3050 S cryomicrotome and collected on poly-L-lysine-coated slides (Polysine; VWR) and then stored at −20°C.

Localization of AruRGP transcripts using mRNA in situ hybridization

To increase adherence of sections, slides with paraffin wax-embedded sections were placed in an oven at 65°C for 45 minutes followed by 15 minutes at room temperature to cool down. Slides were then incubated in xylene (3 × 7 min; VWR Chemicals) to remove the wax and rehydrated through a descending ethanol series (2 × 7 minutes 100%, 1 × 7 minutes 90%, 1 × 7 minutes 70%, 1 × 7 minutes 50%, 1 × 7 minutes 30%). The slides were then washed in PBS (2 × 7 minutes) and postfixed in 4% PFA/PBS for 20 minutes at room temperature. Following washes in PBS/0.1% Tween-20 (National Diagnostics, Manville, NJ) (PBST; 3 × 5 minutes), sections were incubated at 37°C for 12 minutes in Proteinase K (Qiagen) solution at a concentration of 10 μg/ml in a buffer containing 50 mM Tris-HCl (pH 7.5) and 6.25 mM EDTA. Sections were postfixed in 4% PFA/PBS for 5 minutes at room temperature and washed in PBST (3 × 5 minutes). Sections were then acetylated for 10 minutes in 1.325% triethanolamine (pH 7–8) (VWR Chemicals), 0.25% acetic anhydride (VWR Chemicals), and 0.175% acetic acid (VWR Chemicals) made up in distilled water, with continuous stirring. After washes in PBST (2 × 5 minutes) and 5× SSC (5 minutes) at room temperature, slides were prehybridized in hybridization buffer (50% formamide (Amresco, Solon, OH); 5× SSC; 500 μg/ml yeast total RNA (Sigma-Aldrich); 50 μg/ml heparin (Sigma-Aldrich); 0.1% Tween-20 in distilled water) in a humid chamber for 2 hours. Hybridization was performed overnight in a humid chamber at 65°C by incubation of slides in

hybridization buffer containing 800 ng/ml of denatured DIG-labeled mRNA antisense or sense probes (100 µl per slide) with a coverslip made of Parafilm (Bemis, Terre Haute, IN).

The following day the slides were incubated in 5× SSC with slight shaking until the parafilm coverslip had floated off. Then slides were washed in 0.2× SSC (2 × 40 minutes at 65°C followed by 10 minutes at room temperature) followed by buffer B1 (10 mM Tris-HCl, pH 7.5; 150 mM NaCl in autoclaved water) for 10 minutes at room temperature. After blocking slides with 5% goat serum (Sigma-Aldrich)/B1 buffer in a humid chamber for 2 hours at room temperature, slides were incubated with alkaline phosphatase (AP)-conjugated anti-DIG antibody (Roche) at 1:3,000 dilution in 2.5% goat serum/B1 buffer in a humid chamber overnight at 4°C.

On the third day, slides were washed in B1 buffer (3 × 5 minutes at room temperature) followed by buffer B3 (100 mM Tris-HCl, pH 9.5; 100 mM NaCl; 50 mM $MgCl_2$ in distilled water) for 10 minutes at room temperature. AP substrate was prepared in buffer B3 by adding 4.5 µl/ml of nitro-blue tetrazolium chloride (NBT) (Amresco) stock solution (75 mg/ml) in 70% dimethylformamide (Avantor, formerly Mallinkrodt Baker, St. Louis, MO) and 3.5 µl/ml of 5-bromo-4-chloro-3′-indolyphosphate p-toluidine (BCIP) (Panreac AppliChem) stock solution (50 mg/ml in 70% dimethylformamide) and applied to slides (500 µl per slide). Slides were then incubated in a humid chamber and checked regularly. Once strong staining was observed, the reaction was terminated by washing slides in distilled water (3 × 5 minutes). Slides were then dried on a hotplate and then incubated in 100% ethanol (2 × 10 sec) followed by clearing in Histo-Clear (National Diagnostics) for 2 × 7 minutes. Finally, slides were mounted with HistoMount (National Diagnostics) and coverslipped.

The method used for mRNA in situ hybridization on sections of frozen tissue was the same as described above but with the following modifications. The initial oven-drying, dewaxing, and hydration steps were not necessary, so these steps were omitted and instead slides were dried at room temperature prior to washing in PBS (2 × 7 minutes). Following staining of sections, slides were mounted with an aqueous mounting medium (Hydromount; National Diagnostics) and coverslipped. Mounted slides were left at room temperature to dry for 1–2 hours and then stored at 4°C.

Photographs of sections were captured with a QIClick CCD Camera (01-QICLICK-R-F-CLR-12; QImaging) linked to a DMRA2 light microscope (Leica), using Volocity v.6.3.1 image analysis software (Perkin-Elmer, Boston, MA) running on an iMac computer (27-inch with OS X Yosemite, v. 10.10). Images were compiled into montages and labeled using Photoshop CC (2015.0.0; Adobe Systems, San Jose, CA), including use of cropping and contrast adjustment tools, running on a MacBook Pro computer (13-inch, with OS X El Capitan).

Immunohistochemistry using monoclonal antibody 1E11

To facilitate interpretation of the expression pattern of AruRGP transcripts in starfish arm tips revealed using mRNA in situ hybridization methods, adjacent frozen sections were processed for immunohistochemical analysis using monoclonal antibody 1E11, which was generously provided by Dr. Robert D. Burke (University of Victoria, Canada; RRID AB_2617214). 1E11 is a neuron-specific antibody to synaptotagmin B and is a marker of neural structures in echinoderms, including starfish (Burke et al., 2006; Saha et al., 2006). Importantly, the specificity of 1E11 for synaptotagmin B has been demonstrated by western blot analysis of radial nerve extracts from the sea urchin *Strongylocentrotus purpuratus* and comparison of immunostaining patterns observed with 1E11 and with antibodies to *S. purpuratus* synaptotagmin B. Further evidence of the specificity of 1E11 has been obtained by comparison of the distribution of 1E11 immunoreactivity with the distribution of synaptotagmin B mRNA in sea urchin revealed using mRNA in situ hybridization methods (Burke et al., 2006).

For immunohistochemistry with monoclonal antibody 1E11, starfish arm tips were lightly fixed (up to 30 minutes in 4% PFA/PBS; pH 7.4) because immunostaining with the 1E11 antibody is fixation-sensitive (R.D. Burke, pers. commun.). Frozen sections of starfish arm tips mounted on slides were washed in PBS and then incubated for 20 minutes in PBS containing 1% hydrogen peroxide to quench endogenous peroxidases. Following washing with PBST, slides were blocked with 5% goat serum/PBST for 2 hours at room temperature. The slides were then incubated overnight at 4°C with the 1E11 antibody, diluted 1:3 with 5% goat serum/PBST. After washing with PBST, slides were then incubated for 3 hours at room temperature with goat antimouse horseradish peroxidase conjugated secondary antibodies immunoglobulins (Jackson ImmunoResearch, West Grove, PA) diluted 1:500 in PBST containing 2% goat serum. After washing in PBST, staining buffer (0.05% diaminobenzidine, 0.05% nickel chloride, 0.015% hydrogen peroxide in PBS) was applied to each slide until staining was observed. Slides were washed sequentially in PBS and autoclaved water and then

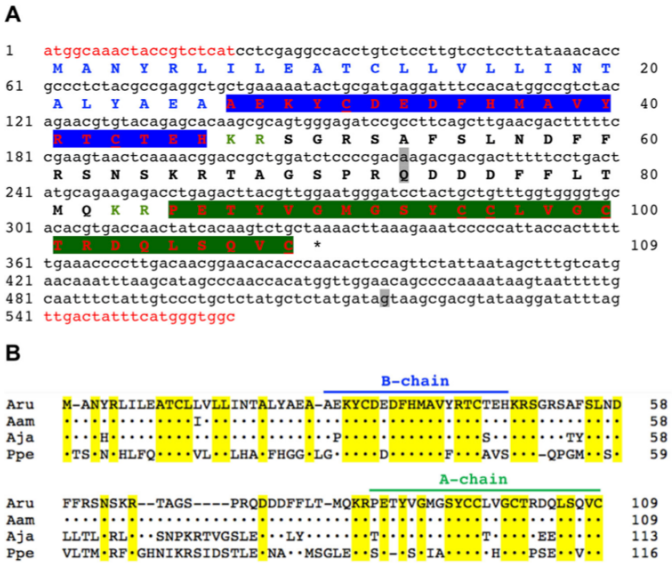

Figure 1. *A. rubens* relaxin-like gonad-stimulating peptide (AruRGP) precursor and comparison with RGP precursors from other starfish species. **A**: The cDNA sequence (lowercase, 560 bases) encoding the AruRGP precursor protein (uppercase, 109 amino acid residues) is shown. The predicted signal peptide is shown in blue and predicted dibasic cleavage sites are shown in green. Relaxin-type peptides (with cysteine [C] residues underlined) are shown in red, with the A and B chains highlighted in green and blue, respectively. Nucleotides and amino acids that differ from the previously reported AruRGP precursor cDNA and protein sequence that was assembled from transcriptome sequence data (GenBank accession number KT601728; Semmens et al., 2016) are highlighted in gray. Nucleotide sequences that were used as primers for cDNA cloning are shown in red and the asterisk shows the position of the stop codon. **B**: Alignment of the AruRGP precursor with RGP precursors from *A. amurensis* (AamRGP, GenBank accession number LC040882), *A. japonica* (AjaRGP, GenBank accession number LC104980), and *P. pectinifera* (PpeRGP, GenBank accession number AB496611). Regions of the precursors corresponding to the A and B chains are labeled (green and blue, respectively) and amino acid residues that are identical in all four precursors are highlighted in yellow.

coverslips were mounted using Hydromount (Natural Diagnostics). Photographs of immunostained sections and adjacent sections processed for AruRGP mRNA in situ hybridization were obtained as described above.

RESULTS

Cloning and sequencing of a cDNA encoding the *A. rubens* RGP precursor

A 560-base cDNA encoding the AruRGP precursor was cloned and sequenced, which is shown in Figure 1A together with the encoded 109 amino acid AruRGP precursor sequence. The AruRGP precursor has a predicted 26 amino acid signal peptide followed by the B chain (20 amino acids) (Fig. 1A). The A chain (25 amino acids) is located at the C terminus of the precursor and the intermediate 38 amino acid C peptide, which includes three putative dibasic proteolytic sites (KR; Fig. 1A), is sandwiched between the A and B chains.

An alignment of the amino acid sequence of the AruRGP precursor with the sequences of RGP precursors from *A. amurensis* (AamRGP), *A. japonica* (AjaRGP), and *P. pectinifera* (PpeRGP) (Mita et al., 2009a,; Mita and Katayama, 2016) is shown in Figure 1B. The amino acid sequence of the AruRGP precursor is very similar to that of the AamRGP precursor (99% identity) but it shares lower levels of similarity with the AjaRGP precursor (75% identity) and the PpeRGP precursor (45% identity) (Fig. 1B; Table 1). More specifically, comparison of the amino acid sequences of the A and B chains that form RGP reveals that AruRGP is identical to AamRGP. In contrast, the A and B chain of AruRGP share 84% and 90% identity, respectively, with the A and B chains

TABLE 1.

Table showing the % amino acid identity that AruRGP and regions of the AruRGP precursor share with RGP and regions of RGP precursors from *A. amurensis*, *A. japonica* and *P. pectinifera*. The values in parentheses are number of amino acids

	% identity (number of amino acid residues)					
		RGP precursor				
Species	RGP	Signal peptide	A chain	B chain	C peptide	Total
Asterias amurensis	100 (45)	96 (26)	100 (25)	100 (20)	100 (38)	99 (109)
Aphelasterias japonica	87 (45)	96 (26)	84 (25)	90 (20)	43 (42)	75 (113)
Patiria pectinifera	65 (43)	38 (29)	58 (24)	73 (19)	23 (44)	45 (116)

of AjaRGP, and 53% and 73% identity, respectively, with the A and B chains of PpeRGP (Table 1).

Phylogenetic analysis of the relationship of the precursors of AruRGP and other starfish RGPs with related precursor proteins from vertebrates and invertebrates revealed that starfish RGPs cluster in a clade comprising precursors of relaxin/insulin-like peptides, which is distinct from a clade comprising insulin/insulin-like growth factor (IGF)-type precursors (Fig. 2). Interestingly, a second relaxin-type precursor (AruRLP2) that was recently identified in *A. rubens* (Semmens et al., 2016) is also positioned within the branch of relaxin/insulin-like peptide precursors that contains the starfish RGP precursors (Fig. 2).

Mass spectrometric detection of AruRGP in *A. rubens* radial nerve extracts

To determine if the AruRGP precursor (Fig. 1) is processed to form mature AruRGP in a manner consistent with other relaxin-type peptides (Fig. 3A) (Schwabe and McDonald, 1977; Sherwood, 2004), we analyzed *A. rubens* radial nerve extracts with and without reduction/alkylation and with and without trypsin digestion. In samples subjected to reduction and alkylation, the A chain and B chain were identified by LC-MS/MS, while in the absence of reduction these peptides were not detected, indicating that the A and B chains are linked by disulfide bridges. The A chain (PETYVGMGSYCCLVGCTRDQLSQVC) was observed as 3 + ions (980.75 *m/z*; Fig. 3B) and the B chain (AEKYCDEDFHMAVYRTCTEH) was observed as 3 + ions (860.02 *m/z;* Fig. 3C) and 4 + ions, with and without oxidized methionine. Although these long and highly charged peptides had significant Mascot scores (Fig. 3B,C), they fragmented poorly. Therefore, to obtain further confirmation of the sequences of A chain and B chain peptides we analyzed radial nerve extract samples incubated with trypsin, which cleaves after lysine and arginine residues to yield peptides that could be completely sequenced using MS/MS. Trypsin was used with or without prior reduction of the peptides and therefore in principle masses and spectra for both disulfide bridge crosslinked and unlinked peptides could be detected under the relevant conditions. In samples subjected to reduction followed by trypsin treatment, the expected fragments of the A chain (PETYVGMGSYCCLVGCTR [2 + 1055.44; Fig. 3D]) and B chain (YCDEDFHMAVYR [2 + 541.22; Fig. 3E]) were detected and sequenced, respectively.

Treatment of nonreduced samples of radial nerve extracts with trypsin would be expected, based on the predicted structure of AruRGP (Fig. 3A), to produce two dimeric peptides linked by single disulfide bridges. We were unable to detect the larger of these predicted peptides comprising the N-terminal region of the A chain (PETYVGMGSYCCLVGCTR) linked to the central region of the B chain (YCDEDFHMAVYR). However, we were able to detect the smaller dimeric peptide comprising the C-terminal regions of the A chain (DQLSQVC) and B chain (TCTEH) in two charge states (690.28, 2 + and 460.52 3+) (Fig. 4).

Comparison of the effects of AruRGP and PpeRGP on ovarian fragments from *A. rubens*

Previous studies have shown that AamRGP does not induce spawning of ovaries from *P. pectinifera*, whereas PpeRGP triggers spawning of ovaries from *A. amurensis* (Mita et al., 2015). Here the effects of AruRGP and PpeRGP on oocyte maturation and ovulation was examined in the isolated ovary of *A. rubens* (Fig. 5A). Synthetic AruRGP induced oocyte maturation and ovulation in ovarian fragments from *A. rubens* within 30 minutes (Fig. 5B). Both AruRGP and PpeRGP caused dose-dependent induction of spawning of *A. rubens* ovarian fragments (Fig. 5C). However, the EC_{50} of AruRGP required to induce spawning (1.33 ± 0.09 nM) is approximately 10-fold lower than for PpeRGP (14 ± 1 nM), consistent with differences in the sequences of AruRGP and PpeRGP (Fig. 1B; Table 1).

Cellular localization of AruRGP precursor transcripts in *A. rubens*

Analysis of AruRGP precursor expression in *A. rubens* using mRNA in situ hybridization with antisense probes

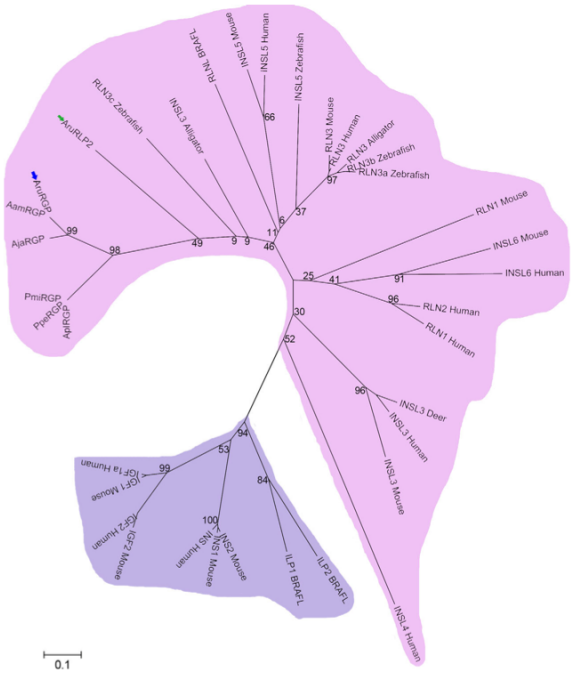

Figure 2. Neighbor joining tree showing the relationships of starfish relaxin-like gonad-stimulating peptide precursors with precursors of other members of the relaxin/insulin/insulin-like growth factor (IGF) peptide family. The *A. rubens* RGP (AruRGP) precursor (blue arrow) and other starfish RGP precursors form a distinct clade within the relaxin/insulin-like precursor family, which is highlighted in pink to distinguish it from the insulin/IGF precursor family that is highlighted in purple. A second *A. rubens* relaxin-type precursor (AruRLP2; green arrow) is a paralog of the AruRGP precursor that is also positioned within the relaxin/insulin-like clade of precursors. The full names and accession numbers of the 36 protein sequences included in the tree are as follows: AruRGP, relaxin-like gonad-stimulating peptide (ALJ99970.1, *Asterias rubens*); AamRGP, relaxin-like gonad-stimulating peptide precursor (BAR40315.1, *Asterias amurensis*); AjaRGP, relaxin-like gonad-stimulating peptide precursor (BAU20369.1, *Aphelasterias japonica*); PpeRGP, relaxin-like gonad-stimulating peptide precursor (BAI44654.1, *Patiria pectinifera*); AruRLP2, relaxin-like peptide precursor 2 (ALJ99971.1, *Asterias rubens*); AplRGP, relaxin-like gonad-stimulating peptide precursor (LC033566.1, *Acanthaster planci*); PmiRGP, relaxin-like gonad-stimulating peptide precursor (LC057656.1, *Patiria miniata*); RLN1 Human, relaxin 1 precursor (NP_008842.1, *Homo sapiens*); RLN2 Human, relaxin 2 precursor (NP_604390.1, *Homo sapiens*); RLN3 Human, relaxin 3 precursor (NP_543140.1, *Homo sapiens*); RLN1 Mouse, relaxin 1 precursor (NP_035402.2, *Mus musculus*); RLN3 Mouse, relaxin 3 precursor (NP_775276.1, *Mus musculus*); RLN3 Alligator, relaxin 3 precursor (XP_006023546.1, *Alligator sinensis*); INSL3 Alligator, insulin-like 3 (XP_006017481.1, *Alligator sinensis*); RLN3a Zebrafish, relaxin 3a precursor (NP_001032892.1, *Danio rerio*); RLN3b Zebrafish, relaxin 3b precursor (NP_001108535.1, *Danio rerio*); RLN3c Zebrafish, relaxin 3c precursor (NP_001108525.2, *Danio rerio*); INS Human, insulin precursor (NP_000198.1, *Homo sapiens*); INSL3 Human, insulin-like peptide 3 precursor, (NP_005534.2, *Homo sapiens*); INSL4 Human, insulin-like peptide 4 precursor (NP_002186.1, *Homo sapiens*); INSL5 Human, insulin-like peptide 5 precursor (NP_005469.2, *Homo sapiens*); INSL6 Human, insulin-like peptide 6 precursor (NP_009110.2, *Homo sapiens*); INSL3 Mouse, insulin-like 3 precursor (NP_038592.3, *Mus musculus*); INSL5 Mouse, insulin-like peptide precursor (NP_035961.1, *Mus musculus*); INSL6 Mouse, insulin-like peptide precursor (NP_038782.1, *Mus musculus*); INSL5 Zebrafish, insulin-like 5 precursor (NP_001122028.1, *Danio rerio*); INSL3 Deer, relaxin-like peptide (AAR25542.1, *Capreolus capreolus*); IGF1a Human, insulin-like growth factor 1 precursor (NP_000609.1, *Homo sapiens*); IGF2 Human, insulin-like growth factor 2 precursor (NP_000603.1, *Homo sapiens*); IGF1 Mouse, insulin-like growth factor 1 precursor (NP_001104745.1, *Mus musculus*); IGF2 Mouse, insulin-like growth factor 2 precursor (NP_034644.2, *Mus musculus*); INS1 Mouse, insulin-1 precursor (NP_032412.3, *Mus musculus*); INS2 Mouse, insulin-2 precursor (NP_032413.1, *Mus musculus*); RLNL BRAFL, relaxin-like peptide (EEA41967.1, *Branchiostoma floridae*); ILP1 BRAFL, insulin-like peptide 1 precursor ((Mita et al., 2009b), *Branchiostoma floridae*); ILP2 BRAFL, insulin-like peptide 2 precursor ((Mita et al., 2009b), *Branchiostoma floridae*). Bootstrap values for selected nodes are shown.

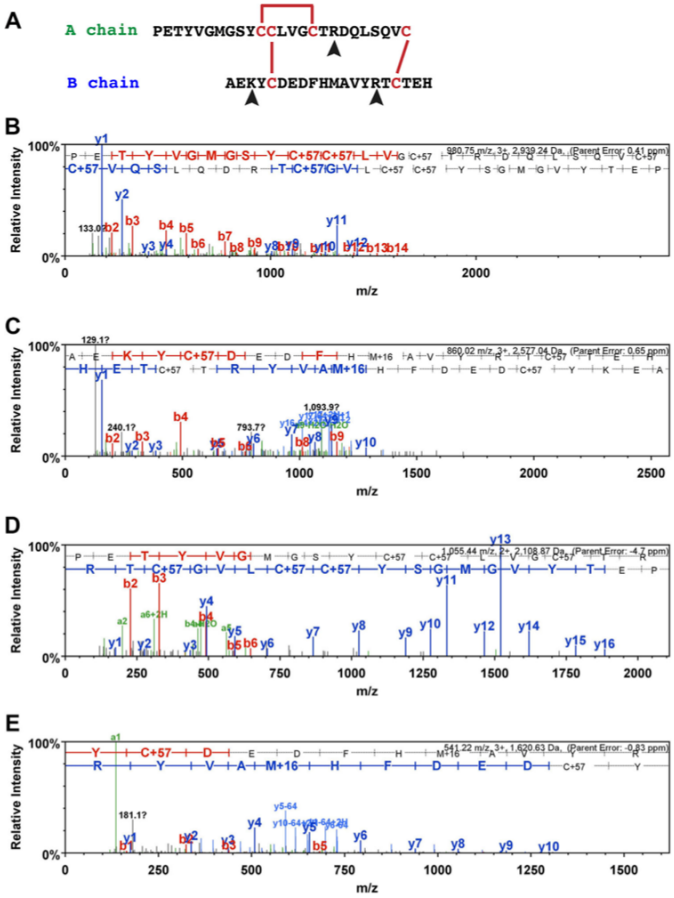

Figure 3. Mass spectrometric identification of AruRGP A chain and B chain in extracts of *A. rubens* radial nerve cords. **A**: Predicted dimeric structure of AruRGP, showing the sequences of the A chain and B chain. The positions of disulfide bridges are shown with red lines and tryptic cleavage sites are marked with arrowheads. **B,C**: MS/MS data for the A chain and B chain, respectively, from reduced and alkylated samples of radial nerve extract without tryptic digestion. The b series of peptide fragment ions are shown in red, the y series in blue and additional identified peptide fragment ions in green. The amino acid sequence identified in the mass spectrum is highlighted at the top of the figures. C+57 represents cysteine modified by carbamidomethylation and M+16 represents oxidized methionine. The observed *m/z* of the precursor ion for the A chain (PETYVGMGSYCCLVGCTRDQLSQVC; B) is 980.75 with a charge state 3+ and an error of 0.41 ppm between the experimentally determined and predicted values (Mascot score = 57). The observed *m/z* of the precursor ion for the B chain (AEKYCDEDFHMAVYRTCTEH; C) is 860.02 with a charge state of 3+ and an error of 0.65 ppm between the experimentally determined and predicted values (Mascot score = 31). **D,E**: MS/MS data for the complete sequences of fragments of the A chain and B chains, respectively, derived from reduced and alkylated samples of radial nerve extract subjected to tryptic digestion, with annotations in the same format as in B and C. The observed *m/z* of the precursor ion for the A chain fragment (PETYVGMGSYCCLVGCTR; D) is 1055.44 with a charge state of 2+ and an error of −4.7 ppm between the experimentally determined and predicted values (Mascot score = 98). The observed *m/z* of the precursor ion for the B chain fragment (YCDEDFHMAVYR; E) is 541.22 with a charge state of 3+ and an error of −0.83 ppm between the experimentally determined value and predicted value (Mascot score = 45).

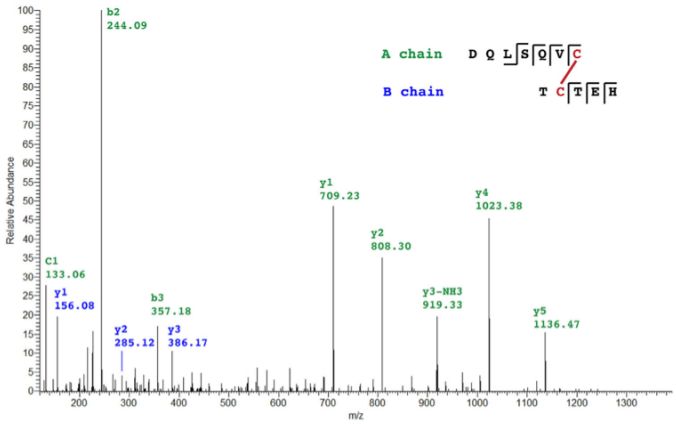

Figure 4. Mass spectrometric identification of a dimeric fragment of AruRGP in an extract of *A. rubens* radial nerve cords. The mass spectrum of a disulfide bridge linked dimeric peptide comprising DQLSQVC from the AruRGP A chain and TCTEH from the AruRGP B chain is shown. This dimeric peptide was detected in samples of radial nerve extract that were subjected to tryptic digestion without reduction. Peptide fragments from the A chain are shown in green and peptide fragments from the B chain are shown in blue. The observed *m/z* of the precursor ion is 690.28 with a charge state 2 + and an error of −0.73 ppm between the experimentally determined value and predicted value (Stavrox score = 145).

revealed stained cells in the radial nerve cords (Fig. 6A–D), in accordance with cloning of the AruRGP precursor cDNA from this tissue (see above) and previous studies on GSS/RGP in starfish. The specificity of this staining was confirmed by control experiments using sense probes, where no stained cells were observed (Fig. 6A, inset). The cells expressing AruRGP transcripts are located in the epithelium of the ectoneural region of the radial nerve cords (Fig. 6A–D). These cells are relatively few in number, with a bilaterally symmetrical group of two or three cells present on both sides of the V-shaped radial nerve cord when viewed in transverse sections of the starfish arm (Fig. 6A,B). Analysis of longitudinal sections revealed that these groups of cells occur along the length of the radial nerve cord, separated by gaps of 20–80 μm (Fig. 6C,D). The radial nerve cords are linked by a circumoral nerve ring that is located in the central disk region of starfish (Pentreath and Cobb, 1972) and AruRGP-expressing cells were also detected in the ectoneural epithelium of the nerve ring (Fig. 6E,F). The radial nerve cords and circumoral nerve ring control the coordinated activity of adjacent rows of tube feet located along the underside of each arm and around the mouth (Pentreath and Cobb, 1972). Cells expressing AruRGP transcripts were revealed in the tube feet in a subepithelial location along the length of the podium (Fig. 7A,B), at the base of the tube feet (Fig. 7C), and as a cluster of cells near to the tube foot sucker (Fig. 7D,E).

The most striking expression of AruRGP transcripts was revealed in the tip regions of the arms (Fig. 8). To facilitate interpretation of the staining shown in Figure 8, a labeled photograph of the arm tip region of a live specimen of *A. rubens* is shown in Figure 8A. The most prominent feature of the arm tip is the pigmented optic cushion, which is located at base of a tube foot-like organ specialized for sensory functions that is known as the terminal tentacle (Fig. 8A,B). Consistent with expression of AruRGP in tube feet (Fig. 7), cells expressing AruRGP transcripts were also revealed in the terminal tentacle (Fig. 8C,D). However, more extensive expression of AruRGP is present in the body wall epithelium that lines the cavity containing the terminal tentacle and optic cushion. Here AruRGP-expressing cells are located in the epithelium forming the "ceiling" (Fig. 8B) and "walls" (Fig. 8C) of the cavity, extending right up to distal tip of the arm (Fig. 8E). The staining observed in these cells is not observed in sections of arm tips incubated with sense probes, demonstrating the specificity of the labeling (Fig. 8E, inset). Observation of clusters of AruRGP-expressing cells in the arm tip body wall epithelium at high magnification revealed a meshwork of stained processes, suggesting that these cells are neurons (Fig. 8F).

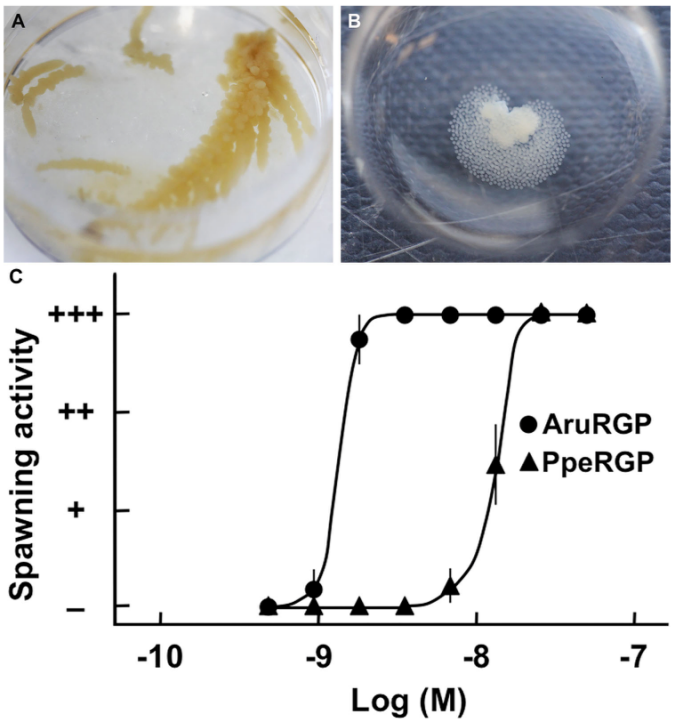

Figure 5. Comparison of the in vitro bioactivity of AruRGP and PpeRGP as inducers of spawning in *A. rubens*. **A**: Isolated ovary from *A. rubens*. **B**: AruRGP-induced spawning of an ovary fragment from *A. rubens*. **C**: Graph showing the dose-dependent effects of AruRGP (●) and PpeRGP (▲) in causing spawning of ovarian fragments. + + + denotes spawning occurred and most of oocytes were matured, + + denotes about 50% oocytes were matured, + denotes a few oocytes were matured, and – denotes no spawning occurred. Means ± SEM for five separate assays using ovarian tissue from different animals are shown. The median effective concentration (EC_{50}) of AruRGP required to induce spawning (1.33 ± 0.09 nM) is approximately 10-fold lower than for PpeRGP (14 ± 1 nM).

To more specifically investigate if the AruRGP-expressing cells in the arm tip body wall epithelium are neurons, both transverse and longitudinal sections of arm tips were analyzed at high magnification. This revealed examples of solitary cells or pairs of cells that clearly have stained processes emanating basally from an intraepithelial cell body (Fig. 9A,B). Furthermore, double-labeling experiments using the neural-specific antibody 1E11 revealed a layer of immunostained neural processes immediately beneath the layer of AruRGP-expressing cell bodies in arm tip epithelium (Fig. 9C–F). Therefore, collectively these observations indicate that AruRGP-expressing cells in the arm tip epithelium are neurons.

DISCUSSION

We report here the identification and functional characterization of relaxin-like gonad-stimulating peptide in the starfish *A. rubens* (AruRGP). Analysis of the sequence of AruRGP revealed that it is similar to RGP from other starfish species. AruRGP is identical to RGP from another species in the genus *Asterias*—*A. amurensis*—but, as would be expected, AruRGP shares lower levels of similarity with RGP from more distant species. Thus, AruRGP shares 87% sequence identity with RGP from *Aphelasterias japonica*, which belongs to the same order and family as *Asterias* (Order Forcipulatida; Family Asteriidae), and only 65% sequence identity with RGP from *P. pectinifera* (PpeRGP), which belongs to a different order of starfish (Order Valvatida; Family Asterinidae). All of the starfish RGPs, including AruRGP, belong to a family of relaxin/insulin-like peptides, which are distinct from insulin/IGF-type peptides.

The dimeric structure PpeRGP comprising an A chain and B chain has been demonstrated previously (Mita et al., 2009a), with the positions of intrachain and interchain disulfide bridges inferred from vertebrate relaxins (Schwabe and McDonald, 1977; Sherwood, 2004). Accordingly, monomeric PpeRGP A chain or PpeRGP B chain when tested individually or as a mixture lack

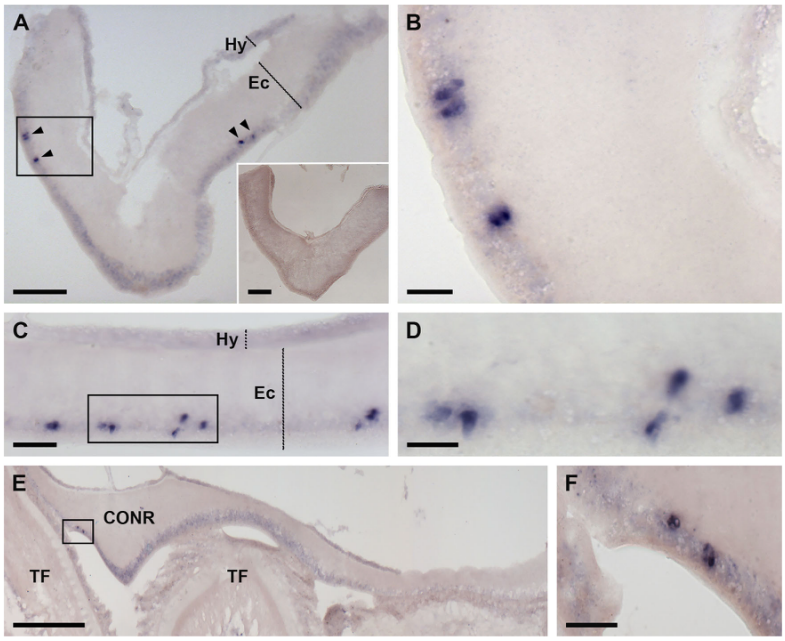

Figure 6. Localization of AruRGP precursor mRNA in the radial nerve cord and circumoral nerve ring of *A. rubens* using in situ hybridization. **A,B**: Transverse sections of radial nerve cord incubated with antisense probes (main panels of A and B) showing a bilaterally symmetrical group of 2–3 stained cells (arrowheads) in the epithelium of the ectoneural region of the nerve cord. Panel B shows a high-magnification view of the rectangular region highlighted in panel A. The inset of panel A shows the absence of staining in a transverse section of radial nerve cord incubated with sense probes, demonstrating the specificity of staining observed with antisense probes. **C,D**: Longitudinal parasagittal sections of the radial nerve cords incubated with antisense probes showing groups of cells interspersed along the length of the nerve cord in the ectoneural epithelium. Panel D shows a high-magnification view of the rectangular region highlighted in panel C. **E,F**: Transverse section of the disk region in *A. rubens* incubated with antisense probes, showing the circumoral nerve ring and tube feet. Stained cells can be seen in the ectoneural epithelium of the nerve cord, highlighted by the rectangle in E and shown at higher magnification in F. CONR, circumoral nerve ring; Ec, ectoneural region of radial nerve cord; Hy, hyponeural region of radial nerve cord; TF, tube foot. Scale bars = 50 μm in A and A inset; 10 μm in B,D; 25 μm in C; 200 μm in E; 20 μm in F.

gonadotropic activity, whereas synthetic dimeric PpeRGP comprising the A and B chains with disulfide bridges in the same positions as in vertebrate relaxin exhibits gonadotropic activity that is indistinguishable from RGP purified from radial nerve extracts (Mita et al., 2009a). Here we used mass spectrometry to confirm the presence and sequences of both the A chain and B chain of AruRGP in *A. rubens* radial nerve extracts. Furthermore, we demonstrated the presence of one of the two disulfide bridges that link the A chain and B chain. Informed by these findings and the conserved structure of relaxin-type peptides (Schwabe and McDonald, 1977; Sherwood, 2004), we had dimeric AruRGP synthesized with the structure shown in Figure 3A. The bioactivity of this synthetic AruRGP as a potent stimulator of spawning from *A. rubens* ovarian fragments was demonstrated here. Furthermore, as was found in a previous study on *A. amurensis* (Mita et al., 2015), AruRGP is 10-fold more potent than PpeRGP, consistent with the differences in the sequences of AruRGP and PpeRGP.

The main novel objective of this study was to comprehensively analyze the expression of AruRGP in *A. rubens* using mRNA in situ hybridization. Consistent with the original discovery of GSS/RGP in extracts of radial nerve cords (Chaet and McConnaughy, 1959), cells expressing AruRGP transcripts were revealed in the epithelium of the ectoneural region of the radial

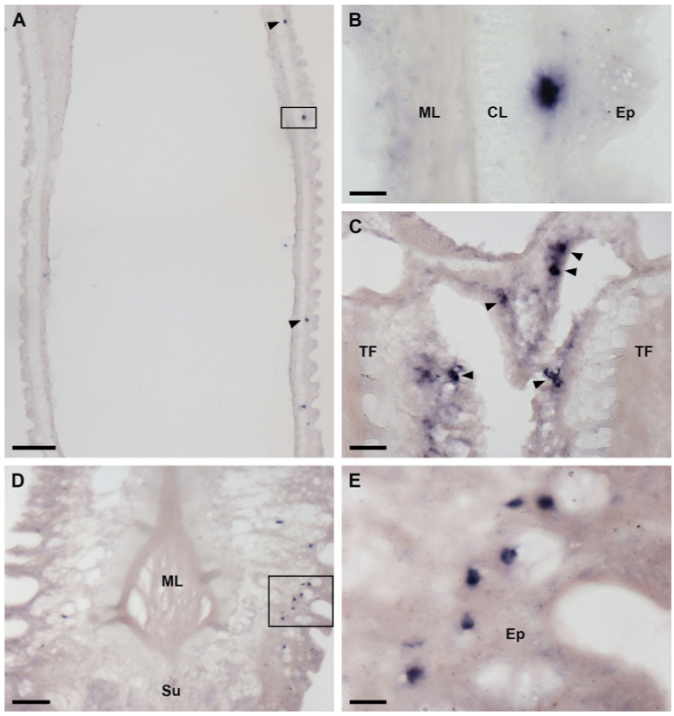

Figure 7. Localization of AruRGP precursor mRNA in tube feet of *A. rubens* using in situ hybridization. **A**: Longitudinal section of a tube foot showing three stained cells (arrowheads and rectangle) in the subepithelial layer of the podium. **B**: The region highlighted with a rectangle in A is shown here at higher magnification, with a stained cell located between the external epithelium and connective tissue layer. **C**: Stained cells (arrowheads) located in the subepithelial layer near to the base of adjacent tube feet. **D**: A group of stained cells (see rectangle) in the tube foot subepithelial layer just above the sucker. **E**: The region highlighted with a rectangle in D is shown here at higher magnification. CL, connective tissue layer; Ep, epithelium; ML, muscle layer; Su, sucker TF: tube foot. Scale bars = 100 μm in A; 10 μm in B; 25 μm in C; 50 μm in D; 10 μm in E.

nerve cords. These cells occur in bilaterally symmetrical groups of two or three cells along the length of the V-shaped radial nerve cord separated by gaps. The relative abundance of these cells in the radial nerve cords of *A. rubens* is similar to findings from *P. pectinifera*, where bilaterally symmetrical groups of four or five stained cells were observed in transverse sections of the radial nerve cord (Mita et al., 2009a). However, the exact location of the RGP-expressing cells in the radial nerve cord is different in *P. pectinifera* and *A. rubens*. In *P. pectinifera* the cells are located at the apex of the V-shaped nerve cord, whereas in *A. rubens* the cells are located more laterally, about half way up the left and right sides of the V-shaped nerve cord. The functional significance of these interspecies differences in the location RGP-expressing cells in the radial nerve cord is not known. AruRGP-expressing cells were also detected in the ectoneural epithelium of the circumoral nerve ring, which links the radial nerve cords in the central disk region of starfish.

Previous studies have revealed that GSS/RGP expression/activity is also detected in the cardiac stomach and tube feet of *P. pectinifera*, albeit at much lower levels than in the radial nerve cords (Mita et al., 2009a). Our analysis of AruRGP expression in *A. rubens* using mRNA in situ hybridization did not reveal expression in the cardiac stomach, which may reflect expression at levels below the threshold for detection with the

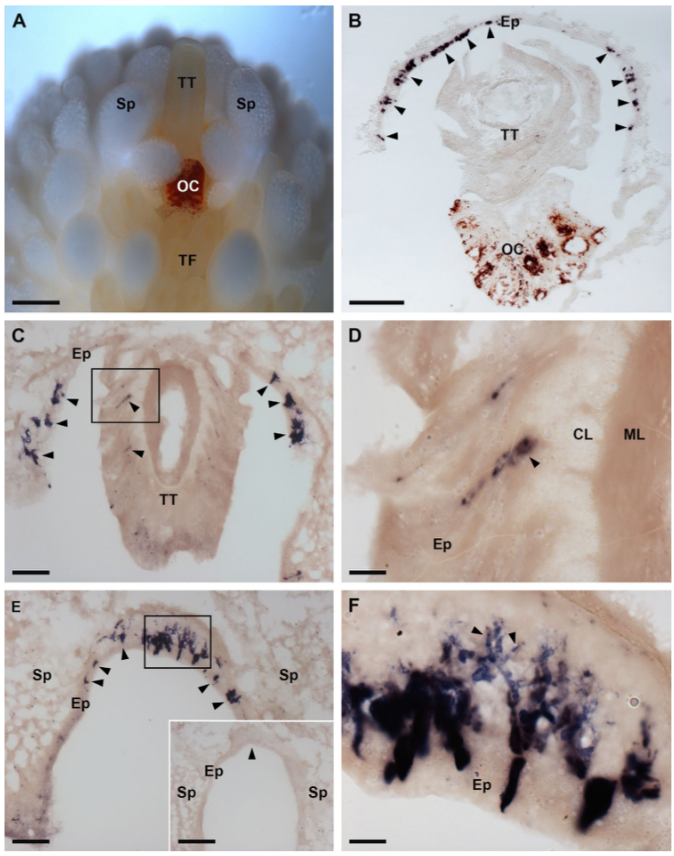

Figure 8. Localization of AruRGP precursor mRNA in the arm tips of *A. rubens* using in situ hybridization. **A**: Photograph of a living specimen of *A. rubens* showing the arm tip region viewed from the underside (oral) of the animal, taken using a Leica DFC420 C camera linked to a Leica S8 APO microscope. The most prominent feature is the pigmented optic cushion, which is located at the base of the terminal tentacle. The terminal tentacle and optic cushion are bounded on each side by spines and rows of tube feet can be seen adjacent to the optic cushion. **B**: Section of the arm tip showing the pigmented optic cushion and terminal tentacle. Stained cells expressing AruRGP precursor transcripts (arrowheads) can be seen in the body wall epithelium lining a cavity that surrounds the terminal tentacle and optic cushion. **C**: Section of an arm tip showing the terminal tentacle cut obliquely. Stained cells can be seen in the terminal tentacle (rectangle and arrowheads) and in the body wall epithelium at the base of the spines that surround the terminal tentacle (arrowheads). **D**: Detail of the region highlighted with a rectangle in panel C, showing stained cells (arrowhead) in the subepithelial layer of the terminal tentacle. **E**: Section through the distal region of the arm tip beyond the terminal tentacle, showing stained cells (arrowheads and rectangle) in the body wall epithelium at the base of two adjacent spines; the region highlighted with a rectangle is shown in panel F. The inset shows absence of staining (arrowhead) in a section of the arm tip adjacent to the section shown in the main panel and which was incubated with sense probes instead of the antisense probes used in the main panel E. **F**: Detail of the region highlighted with a rectangle in panel E, showing stained cells with processes (arrowheads) at high magnification. CL, connective tissue layer of terminal tentacle; Ep, epithelium of body wall; ML, muscle layer of terminal tentacle; OC, optic cushion; TF, tube foot; Sp, spine; TT, terminal tentacle. Scale bars = 400 μm in A; 100 μm in B, E inset; 50 μm in C,E; 10 μm in D,F.

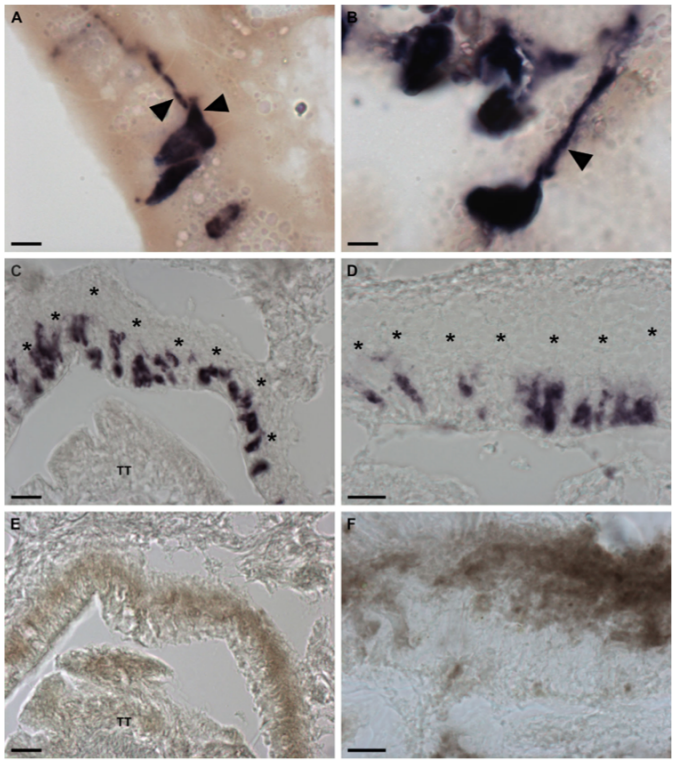

Figure 9. Neuron-like characteristics of cells expressing AruRGP in the arm tips of *A. rubens*. **A**: Transverse section of *A. rubens* arm tip showing two cells in the body wall epithelium that express the AruRGP precursor, as revealed by mRNA in situ hybridization, and that have stained axon-like processes (arrowheads). **B**: Longitudinal section of *A. rubens* arm tip showing a cell in the body wall epithelium that expresses the AruRGP precursor, as revealed by mRNA in situ hybridization, and that has a stained axon-like process (arrowhead). **C,D**: Transverse sections of *A. rubens* arm tip showing cells expressing AruRGP precursor transcripts, as revealed by mRNA in situ hybridization, in the body wall epithelium lining the cavity that contains the terminal tentacle (TT). **E,F**: Transverse sections of *A. rubens* arm tip adjacent to the sections shown in panels C and D, respectively, showing that the unstained region in panels C and D underlying the AruRGP expressing cells (see asterisks in panels C and D) is immunoreactive with monoclonal antibodies (1E11) to the axonal protein synaptotagmin B. This provides supporting evidence that the AruRGP expressing cells in the arm tip epithelium are neurons. Scale bars = 5 μm in A,B; 20 μm in C,E; 10 μm in D,F.

methods used or an interspecies difference in the expression patterns of RGP. However, consistent with the detection of GSS/RGP in *P. pectinifera* tube feet (Mita et al., 2009a), we did reveal the expression of AruRGP by cells in the tube feet of *A. rubens*. Thus, groups of AruRGP-expressing cells were observed at the base of the podia, interspersed along its length and concentrated in a cluster near to the tube foot sucker.

Because GSS/RGP was originally extracted from the radial nerve cords of starfish (Chaet and McConnaughy, 1959; Mita et al., 2009a), there has been an assumption that this tissue is the physiological source of GSS/RGP that then acts as a hormone to trigger gamete maturation and release (Chaet, 1966; Kanatani, 1979; Mita, 2013). Furthermore, prior to the identification of GSS as RGP, it was proposed that GSS is synthesized by supporting cells (Kanatani, 1979), which are radial glia-like cells located in the epithelial layer of the ectoneural region of the nerve cord and that have processes (fibers) that extend across the

ectoneural neuropile. It was postulated that secretory granules containing GSS are transported along the supporting cell fibers and their contents are released as hormones from the inner surface of the radial nerve cords (Unger, 1962). However, a difficulty with this hypothesis is that histochemical analysis of the radial nerve cords reveals that the supporting cell fibers terminate at the connective tissue boundary between the ectoneural and hyponeural regions of the radial nerve cords and do not reach as far as the inner surface (Mashanov et al., 2016). Furthermore, the number of cells expressing RGP in *P. pectinifera* (Mita et al., 2009a) and in *A. rubens* (this study) does not match with the number of supporting cells, which are present throughout entire ectoneural region of the radial nerve cords (Mashanov et al., 2016). It is possible that a subpopulation of the supporting cells express RGP, but it seems more likely that the cells expressing RGP in radial nerve cords are neurons. But as with supporting cells, the processes of neuronal cell bodies located in the ectoneural epithelium are confined to neuropile of the ectoneural region (Moore and Thorndyke, 1993; Mashanov et al., 2016), and therefore it is not clear how ectoneural neurons in the radial nerve cords expressing RGP could release RGP to act as a hormone. Furthermore, the overall pattern of RGP expression in the ambulacrum, with RGP-expressing cells or groups of cells located along the length of the nerve cords and in the tube feet, is perhaps more consistent with a role in coordination of tube foot activity as opposed to being a source of RGP as a reproductive hormone. Thus, RGP-expressing cells located in the radial nerve cords could be considered as functionally equivalent to neurons expressing relaxin-3 that are located in the brainstem of mammals (Sherwood, 2004).

Further evidence that the radial nerve cords may not be the physiological source of GSS/RGP as a hormonal regulator of spawning is the observation that the concentration/expression of GSS/RGP in the radial nerve cords remains constant throughout the year (Chaet, 1966; Mita, 2013). This contrasts with the concentration of GSS/RGP in the coelomic fluid, which increases just prior to spawning (Kanatani and Ohguri, 1966; Kanatani and Shirai, 1969), providing the key evidence that GSS/RGP acts as a hormonal regulator of gamete maturation and release physiologically. If the radial nerve cords are not the physiological source of GSS/RGP as a gonadotropic hormone in starfish, then what is the source?

Here we report the novel discovery of RGP-expressing cells located at the tips of each arm in *A. rubens*. A specialized anatomical feature of the arm tip is the terminal tentacle, which is similar in structure to the locomotory tube feet but has nonlocomotory sensory functions (Hennebert et al., 2013). At the base of the terminal tentacle is the pigmented optic cushion, which contains photoreceptive cells and functions as a simple eye enabling visual orientation (Penn and Alexander, 1980; Garm and Nilsson, 2014). AruRGP-expressing cells were not observed in the optic cushion but, consistent with the expression of AruRGP in the podia of the locomotory tube feet, AruRGP-expressing cells were evident in the terminal tentacle. Moreover, intense expression of AruRGP was observed in a band of cells located in the body wall epithelium that forms the "ceiling" and "walls" of a cavity surrounding the terminal tentacle and optic cushion. The discovery of these AruRGP-expressing cells is fascinating because their location in the arm tips, in close association with sensory systems, make them good candidates as a physiological source of RGP for regulation of gamete release in response to environmental cues. Observation of these cells at high magnification reveals that they are neuron-like, with stained processes emanating from stained cell bodies. Furthermore, consistent with a neuronal cell type, the AruRGP-expressing cells in arm tip epithelium are underlain by a layer that is immunoreactive with antibodies to the neural-specific protein synaptotagmin B. However, it remains to be determined where the processes of AruRGP-expressing cells in the arm tip epithelium project to. To address this issue it may be necessary to generate antibodies to AruRGP so that the peptide itself, rather the just the mRNA encoding it, can visualized throughout the entirety of cells expressing AruRGP.

If the RGP-expressing cells in the arm tips are the physiological source of RGP as a gonadotropic hormone, how in principle could the release of RGP from these cells into the coelomic fluid be triggered? A variety of environmental factors are thought to be important in triggering spawning in starfish (Mercier and Hamel, 2013), including increasing day length (Pearse et al., 1986; Byrne et al., 1997), changes in water temperature (Pearse and Walker, 1986), and the release of gametes by conspecifics (Hamel and Mercier, 1995). The RGP-expressing cells in the arm tips are ideally positioned to detect and integrate such environmental cues, located as they are in the arm tip body wall epithelium and in close proximity to the sensory terminal tentacle and optic cushion. Identification of these cells provides a basis for experimental studies in which their role as putative sources of RGP as a gonadotropic hormone in starfish could be investigated.

ACKNOWLEDGMENTS

We thank Angelika Stollewerk for acting as Ming Lin's co-supervisor during his PhD studies and for provision of

the photomicroscope used to take the photograph shown in Figure 8A. We also thank Phil Edwards for help with obtaining starfish, Paul Fletcher for maintaining our seawater aquarium, Weigang Cai, Antón Barreiro-Iglesias, and Dean Semmens for help with preparation of the starfish radial nerve cord extracts, Jérôme Delroisse and Antón Barreiro-Iglesias for help with photography, and Dean Semmens for helpful comments on the article. Finally, we thank Dr. Robert Burke (University of Victoria, Canada) for the generous gift of the 1E11 monoclonal antibodies.

CONFLICT OF INTEREST

The authors declare that they have no conflicts of interest.

ROLES OF AUTHORS

All authors had full access to all the data in the study and take responsibility for the integrity of the data and the accuracy of the data analysis. Study concept and design: ML, MM, and MRE. Acquisition of data: ML (cDNA cloning and generation of probes for AruRGP precursor; preparation of sections of starfish; mRNA in situ hybridization, MM (testing bioactivity of AruRGP and PpeRGP), ME (development of methodology for mRNA in situ hybridisation in starfish), CGZ and AMJ (mass spectrometry). Analysis and interpretation of data: ML, MM, CGZ, AMJ, and MRE. Drafting of the article: ML, MM, CGZ, AMJ, and MRE. Obtained funding: MRE, MM, and AMJ. Technical and material support: ME. Study supervision: MRE.

LITERATURE CITED

Bathgate RA, Samuel CS, Burazin TC, Layfield S, Claasz AA, Reytomas IG, Dawson NF, Zhao C, Bond C, Summers RJ, Parry LJ, Wade JD, Tregear GW. 2002. Human relaxin gene 3 (H3) and the equivalent mouse relaxin (M3) gene. Novel members of the relaxin peptide family. J Biol Chem 277:1148–1157.

Brown MR, Clark KD, Gulia M, Zhao Z, Garczynski SF, Crim JW, Suderman RJ, Strand MR. 2008. An insulin-like peptide regulates egg maturation and metabolism in the mosquito *Aedes aegypti*. Proc Natl Acad Sci U S A 105: 5716–5721.

Burke RD, Osborne L, Wang D, Murabe N, Yaguchi S, Nakajima Y. 2006. Neuron-specific expression of a synaptotagmin gene in the sea urchin *Strongylocentrotus purpuratus*. J Comp Neurol 496:244–251.

Byrne M, Morrice M, Wolf B. 1997. Introduction of the northern Pacific asteroid *Asterias amurensis* to Tasmania: reproduction and current distribution. Mar Biol 127:673–685.

Caine GD, Burke RD. 1985. Immunohistochemical localisation of gonad stimulating substance in the seastar *Pycnopodia helianthoides*. In: Keegan BF, O'Connor BDS, eds. Proceedings of the Fifth international Echinoderm Conference. Galway, Ireland: Balkema, Rotterdam. p 495–498.

Chaet AB. 1964. A mechanism for obtaining mature gametes from starfish. Biol Bull 126:8–13.

Chaet AB 1966. The gamete-shedding substances of starfishes: a physiological-biochemical study. Am Zool 6: 263–271.

Chaet A, McConnaughy R. 1959. Physiologic activity of nerve extracts. Biol Bull 117:407–408.

Chiu AY, Hunkapiller MW, Heller E, Stuart DK, Hood LE, Strumwasser F. 1979. Purification and primary structure of the neuropeptide egg-laying hormone of *Aplysia californica*. Proc Natl Acad Sci U S A 76:6656–6660.

Conn PJ, Kaczmarek LK. 1989. The bag cell neurons of *Aplysia*. Mol Neurobiol 3:237–273.

Felsenstein J. 1985. Confidence limits on phylogenies: an approach using the bootstrap. Evolution 783–791.

Garm A, Nilsson DE. 2014. Visual navigation in starfish: first evidence for the use of vision and eyes in starfish. Proc Biol Sci 281:20133011.

Gotze M, Pettelkau J, Schaks S, Bosse K, Ihling CH, Krauth F, Fritzsche R, Kuhn U, Sinz A. 2012. StavroX–a software for analyzing crosslinked products in protein interaction studies. J Am Soc Mass Spectrom 23:76–87.

Hamel J-F, Mercier A. 1995. Prespawning behavior, spawning, and development of the brooding starfish *Leptasterias polaris*. Biol Bull 188:32–45.

Haraguchi S, Ikeda N, Abe M, Tsutsui K, Mita M. 2016. Nucleotide sequence and expression of relaxin-like gonad-stimulating peptide gene in starfish *Asterina pectinifera*. Gen Comp Endocrinol 227:115–119.

Hennebert E, Jangoux M, Flammang P. 2013. Functional biology of asteroid tube feet. In: Lawrence J, ed. Starfish: Biology and ecology of the Asteroidea. Baltimore, MD: Johns Hopkins University Press. p 24–36.

Hisaw FL. 1926. Experimental relaxation of the pubic ligament of the guinea pig. Exp Biol Med 23:661–663.

Hsu SY, Semyonov J, Park JI, Chang CL. 2005. Evolution of the signaling system in relaxin-family peptides. Ann N Y Acad Sci 1041:520–529.

Kanatani H. 1979. Hormones in echinoderms. In: Barrington E, ed. Hormones and evolution. Vol 1. London: Academic Press. p 273–307.

Kanatani H, Ohguri M. 1966. Mechanism of starfish spawning. I. Distribution of active substance responsible for maturation of oocytes and shedding of gametes. Biol Bull 131:104–114.

Kanatani H, Shirai H. 1969. Mechanism of starfish spawning. II. Some aspects of action of a neural substance obtained from radial nerve. Biol Bull 137:297–311.

Kanatani H, Shirai H. 1970. Mechanism of starfish spawning. 3. Properties and action of meiosis-inducing substance produced in gonad under influence of gonad-stimulating substance. Dev Growth Differ 12:119–140.

Kessner D, Chambers M, Burke R, Agus D, Mallick P. 2008. ProteoWizard: open source software for rapid proteomics tools development. Bioinformatics 24:2534–2536.

Kumar S, Stecher G, Tamura K. 2016. MEGA7: Molecular evolutionary genetics analysis version 7.0 for Bigger datasets. Mol Biol Evol 33:1870–1874.

Mashanov V, Zueva O, Rubilar T, Epherra L, García-Arrarás J. 2016. Echinodermata. In: Schmidt-Rhaesa A, Harzsch S, Purschke G, eds. Structure and evolution of invertebrate nervous systems. Oxford, UK: Oxford University Press. p 665–688.

Mercier A, Hamel J-F. 2013. Reproduction in Asteroidea. In: Lawrence J, ed. Starfish: Biology and ecology of the Asteroidea. Baltimore, MD: Johns Hopkins University Press. p 37–50.

Mita M. 2013. Relaxin-like gonad-stimulating substance in an echinoderm, the starfish: a novel relaxin system in reproduction of invertebrates. Gen Comp Endocrinol 181:241–245.

Mita M, Katayama H. 2016. A relaxin-like gonad-stimulating peptide from the starfish *Aphelasterias japonica*. Gen Comp Endocrinol 229:56–61.
Mita M, Ito C, Kubota E, Nagahama Y, Shibata Y. 2009a. Expression and distribution of gonad-stimulating substance in various organs of the starfish *Asterina pectinifera*. Ann N Y Acad Sci 1163:472–474.
Mita M, Yoshikuni M, Ohno K, Shibata Y, Paul-Prasanth B, Pitchayawasin S, Isobe M, Nagahama Y. 2009b. A relaxin-like peptide purified from radial nerves induces oocyte maturation and ovulation in the starfish, *Asterina pectinifera*. Proc Natl Acad Sci U S A 106:9507–9512.
Mita M, Daiya M, Haraguchi S, Tsutsui K, Nagahama Y. 2015. A new relaxin-like gonad-stimulating peptide identified in the starfish *Asterias amurensis*. Gen Comp Endocrinol 222:144–149.
Moore SJ, Thorndyke MC. 1993. Immunocytochemical mapping of the novel echinoderm neuropeptide SALMFamide 1 (S1) in the starfish *Asterias rubens*. Cell Tissue Res 274:605–618.
Nesvizhskii AI, Keller A, Kolker E, Aebersold R. 2003. A statistical model for identifying proteins by tandem mass spectrometry. Anal Chem 75:4646–4658.
Pearse JS, Walker CW. 1986. Photoperiodic regulation of gametogenesis in a North Atlantic sea star, *Asterias vulgaris*. Int J Invert Reprod Dev 9:71–77.
Pearse JS, Eernisse DJ, Pearse VB, Beauchamp KA. 1986. Photoperiodic regulation of gametogenesis in sea stars, with evidence for an annual calendar independent of fixed daylength. Am Zool 26:417–431.
Penn P, Alexander C. 1980. Fine structure of the optic cusion in the asteroid *Nepanthia belcheri*. Mar Biol 58:251–256.
Pentreath VW, Cobb JL. 1972. Neurobiology of echinodermata. Biol Rev Camb Philos Soc 47:363–392.
Pierce JG, Parsons TF. 1981. Glycoprotein hormones: structure and function. Annu Rev Biochem 50:465–495.
Saha AK, Tamori M, Inoue M, Nakajima Y, Motokawa T. 2006. NGIWYamide-induced contraction of tube feet and distribution of NGIWYamide-like immunoreactivity in nerves of the starfish *Asterina pectinifera*. Zoolog Sci 23:627–632.
Saitou N, Nei M. 1987. The neighbor-joining method: a new method for reconstructing phylogenetic trees. Mol Biol Evol 4:406–425.
Schwabe C, McDonald JK. 1977. Relaxin: a disulfide homolog of insulin. Science 197:914–915.
Semmens DC, Mirabeau O, Moghul I, Pancholi MR, Wurm Y, Elphick MR. 2016. Transcriptomic identification of starfish neuropeptide precursors yields new insights into neuropeptide evolution. Open Biol 6:150224.
Sherwood OD. 2004. Relaxin's physiological roles and other diverse actions. Endocr Rev 25:205–234.
Shirai H. 1986. Gonad-stimulating and maturation-inducing substance. Methods Cell Biol 27:73–88.
Smith CM, Ryan PJ, Hosken IT, Ma S, Gundlach AL. 2011. Relaxin-3 systems in the brain–the first 10 years. J Chem Neuroanat 42:262–275.
Thompson JD, Higgins DG, Gibson TJ. 1994. CLUSTAL W: improving the sensitivity of progressive multiple sequence alignment through sequence weighting, position-specific gap penalties and weight matrix choice. Nucl Acids Res 22:4673–4680.
Unger H. 1962. Experimentelle und histologische Untersuchungen über Wirkfaktoren aus dem Nervensystem von *Asterias (Marthasterias) glacialis* (Asteroidea; Echinodermata). Zool Jb Abt Allg Zool Physiol Tiere 69:481–536.
Zuckerkandl E, Pauling L. 1965. Evolutionary divergence and convergence in proteins. Evolv Genes Prot 97:97–166.

9.9 Publication 2

Journal of Neurochemistry JNC

JOURNAL OF NEUROCHEMISTRY | 2016 | 137 | 33–45 doi: 10.1111/jnc.13543

ORIGINAL ARTICLE

Identification of a novel starfish neuropeptide that acts as a muscle relaxant

Chan-Hee Kim,*,[1] Eun Jung Kim,*,[1,2] Hye-Jin Go,* Hye Young Oh,* Ming Lin,† Maurice R. Elphick† and Nam Gyu Park*

*Department of Biotechnology, College of Fisheries Sciences, Pukyong National University, Busan, Korea

†School of Biological and Chemical Sciences, Queen Mary University of London, London, UK

Abstract

Neuropeptides that act as muscle relaxants have been identified in chordates and protostomian invertebrates but little is known about the molecular identity of neuropeptides that act as muscle relaxants in deuterostomian invertebrates (e.g. echinoderms) that are 'evolutionary intermediates' of chordates and protostomes. Here, we have used the apical muscle of the starfish *Patiria pectinifera* to assay for myorelaxants in extracts of this species. A hexadecapeptide with the amino acid sequence Phe-Gly-Lys-Gly-Gly-Ala-Tyr-Asp-Pro-Leu-Ser-Ala-Gly-Phe-Thr-Asp was identified and designated starfish myorelaxant peptide (SMP). Cloning and sequencing of a cDNA encoding the SMP precursor protein revealed that it comprises 12 copies of SMP as well as 3 peptides (7 copies in total) that are structurally related to SMP. Analysis of the expression of SMP precursor transcripts in *P. pectinifera* using qPCR revealed the highest expression in the radial nerve cords and lower expression levels in a range of neuromuscular tissues, including the apical muscle, tube feet and cardiac stomach. Consistent with these findings, SMP also caused relaxation of tube foot and cardiac stomach preparations. Furthermore, SMP caused relaxation of apical muscle preparations from another starfish species – *Asterias amurensis*. Collectively, these data indicate that SMP has a general physiological role as a muscle relaxant in starfish. Interestingly, comparison of the sequence of the SMP precursor with known neuropeptide precursors revealed that SMP belongs to a bilaterian family of neuropeptides that include molluscan pedal peptides (PP) and arthropodan orcokinins (OK). This is the first study to determine the function of a PP/OK-type peptide in a deuterostome.

Keywords: muscle, neuropeptide, orcokinin, pedal peptide, relaxation, starfish.

J. Neurochem. (2016) **137**, 33–45.

A variety of neuropeptides that act as smooth muscle relaxants in vertebrates have been identified, including calcitoningene-related peptide (CGRP), adrenomedullin, corticotropin-releasing hormone (CRH), urocortin, vasoactive intestinal peptide (VIP), pituitary adenylyl cyclase-activating peptide (PACAP) and peptide histidine isoleucine (PHI) (Robberecht *et al.* 1982; Brain *et al.* 1985; Grider and Makhlouf 1986; Williams *et al.* 1987; Miyata *et al.* 1989; Kitamura *et al.* 1993; Schilling *et al.* 1998). Likewise, studies on protostomian invertebrates such as insects have identified a number of myoinhibitory neuropeptides; for example type-A allatostatins, type-B allatostatins or myoinhibitory peptides (MIPs) and myosuppressins (Holman *et al.* 1986; Blackburn *et al.* 1995; Bendena *et al.* 1997). In the context of our understanding of the evolutionary history and relationships of neuropeptides in the animal kingdom (Mirabeau and Joly 2013), it appears that neuropeptides belonging to different families have been recruited to act as muscle relaxants in vertebrates and

Received October 21, 2015; revised manuscript received December 22, 2015; accepted January 11, 2016.

Address correspondence and reprint requests to Nam Gyu Park, Department of Biotechnology, College of Fisheries Sciences, Pukyoung National University, 45 Youngso-ro, Nam-gu, Busan 608-737, Korea. E-mail: ngpark@pknu.ac.kr (or) Maurice R. Elphick, School of Biological & Chemical Sciences, Queen Mary University of London, London, E1 4NS, UK. E-mail: m.r.elphick@qmul.ac.uk

[1]These authors contributed equally to this work.

[2]Present address: Center for Food and Drug Analysis, Busan Regional Food and Drug Administration, Ministry of Food and Drug Safety, Busan, Korea.

Abbreviations used: ACh, acetylcholine; RP, reversed-phase; RT-qPCR, real-time quantitative polymerase chain reaction; SMP, starfish myorelaxant peptide; TFA, trifluoroacetic acid.

protostomes. It is of interest, therefore, to identify neuropeptides that act as muscle relaxants in animals that occupy an 'intermediate' position with respect to the vertebrates and protostomes in animal phylogeny – the deuterostomian invertebrates, which include two chordate subphyla that are closely related to vertebrates (Urochordata and Cephalochordata) and the Ambulacraria (Hemichordata and Echinodermata) (Adoutte *et al.* 2000).

Nothing is known about the molecular identity of neuropeptides that act as muscle relaxants in hemichordates but neuropeptides that act as muscle relaxants have been identified in echinoderms – the SALMFamides. The prototypes for this family of neuropeptides were both identified in the starfish *Asterias rubens* and *Asterias forbesi* – S1 (GFNSALMF-NH_2) and S2 (SGPYSFNSGLTF-NH_2) (Elphick *et al.* 1991a,b). *In vitro* pharmacological tests with S1 and S2 revealed that both peptides cause relaxation of neuromuscular preparations from *A. rubens* – the cardiac stomach, tube feet and apical muscle – but with S2 more potent/effective than S1 (Elphick *et al.* 1995; Melarange *et al.* 1999; Elphick and Melarange 2001; Melarange and Elphick 2003). Subsequently, other members of the SALMFamide neuropeptide family were identified in other echinoderms (e.g. sea cucumbers) and these peptides were also found to act as muscle relaxants (Diaz-Miranda and Garcia-Arraras 1995; Ohtani *et al.* 2002).

It is unlikely that SALMFamides are the only family of neuropeptides that act as muscle relaxants in echinoderms, given the multitude of neuropeptides that have been found to act as muscle relaxants in vertebrates and protostomian invertebrates (see above). Therefore, here we set out to employ use of an *in vitro* muscle bioassay to screen for muscle relaxants in an echinoderm. The starfish species *Patiria pectinifera* was selected as a model system because it is widely distributed in the northern Pacific Ocean, and can be easily collected and transported as it is found in shallow coastal waters. This species adapts well to artificial conditions in the laboratory and as a non-specialized predator and/or scavenger it can be fed on algae, detritus and small invertebrates. For these reasons, this species has been used in many scientific studies as a model organism for studying starfish physiology, and it is also of interest from both economic and environmental perspectives (Ikegami *et al.* 1967; Dan-Sohkawa *et al.* 1986; Davydov *et al.* 1990; Mita *et al.* 2009; Jo *et al.* 2013; Haraguchi *et al.* 2015). The apical muscle of *P. pectinifera* was selected as a bioassay because it can be easily dissected from the aboral body wall of the arms in this species. Furthermore, as highlighted above, previous studies have revealed that SALMFamides cause relaxation of the apical muscle from the starfish *A. rubens* (Melarange and Elphick 2003).

Here, we report the isolation of a novel neuropeptide from *P. pectinifera* that causes relaxation of the apical muscle from this species – starfish myorelaxant peptide (SMP). A cDNA encoding the SMP precursor protein was cloned and sequenced, enabling investigation of its expression pattern in *P. pectinifera* and investigation of relationships with neuropeptides that have been identified in other echinoderms and other phyla.

Methods

Animals

Live specimens of the starfish species *Patiria pectinifera* (Fig. 1a and b) and *Asterias amurensis* were collected at Cheongsapo of Busan, Korea, and maintained in a recirculating seawater system at 15°C until use. The animals were fed once every 3 days with live manila clam, *Ruditapes philippinarum*. Live specimens of the starfish species *Asterias rubens* were collected at low tide from the Thanet coast of Kent in the UK, and maintained in a recirculating seawater system at 12°C until use. The animals were fed weekly with live mussels (*Mytilus edulis*). Approval by the local institution/ethics committee was not required for this work because experimental work on starfish is not subject to regulation.

Peptide extraction

Starfish (*P. pectinifera*) were cut into pieces using scissors, soaked in 70% methanol and then heated in a double boiler for 5 min to denature proteins and inhibit proteolytic enzyme activity. The boiled sample was cooled on ice and then homogenized (PT10-35; Kinematica AG, Luzern, Switzerland), followed by addition of glacial acetic acid to yield a final concentration of 5% acetic acid. The homogenate was then centrifuged (10, 000 *g*, 40 min, 4°C). The pellet was re-extracted in 5% acetic acid with same extraction method. The supernatant was pooled and concentrated using a rotary evaporator. The concentrated solution was diluted with 10 volumes of ethanol and then the suspension was centrifuged (10, 000 *g*, 40 min, 4°C) to remove the precipitate. The supernatant was evaporated to 100 mL, and then 100 mL of ethanol with 1.1 g sodium chloride was added to it. After centrifugation to remove precipitate, the supernatant was concentrated by evaporation, and 0.1 volume of 1 N hydrochloric acid was added. The precipitate was removed again by centrifugation (20, 000 *g*, 50 min, 4°C) and the supernatant was applied to a C18 cartridge (Sep-pak C18; Waters Corp., Miford, Massachusetts, USA). The column was washed with 10% methanol/0.1% trifluoroacetic acid (TFA) and retained materials were then eluted with 60% methanol/0.1% TFA. The eluate was evaporated and its biological activity on the apical muscle of *P. pectinifera* was investigated, as described below in the methods section for *in vitro* bioassay and pharmacology.

Peptide purification

The 60% methanol eluate was applied to a cation-exchange column (CM-52, 2.5 × 30 cm; Whatman, Maidstone, UK), and eluted with a linear gradient of 0.02–1.5 M ammonium acetate (pH 5.0) for 6 h at a flow rate of 2.75 mL/min. Absorbance peaks were monitored at 254 nm (ISCO Model UA-6 detector; Lincoln, NE, USA) and fractions were collected every 4 min. The bioactive fractions, which eluted between fraction numbers 40–45, were pooled and then subjected to reversed phase (RP)-HPLC (Vydac 218TP510 Protein & Peptide C18, 9.2 × 250 mm; The Separation Group. Inc., Hesperia, CA, USA). Elution was performed with a

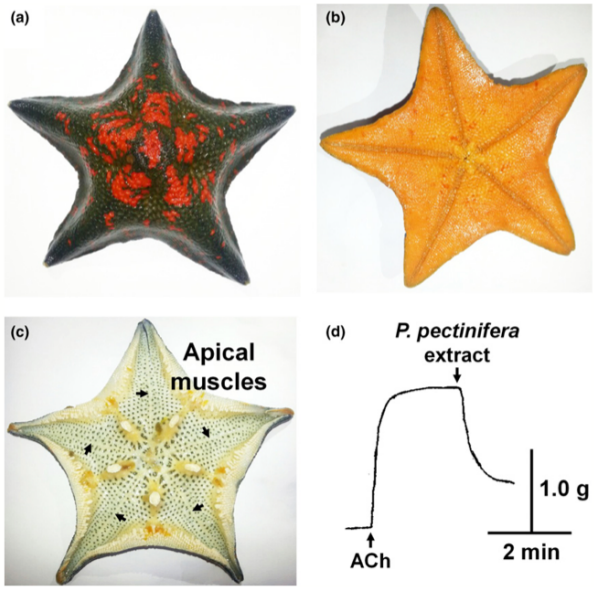

Fig. 1 The starfish *Patiria pectinifera*. The aboral side (a) and oral side (b) of an intact animal are illustrated. The position of the apical muscles on the inner surface of the aboral body wall of a dissected animal is shown in (c) marked by arrows. An extract of *P. pectinifera* containing peptidic materials relaxed apical muscle that was pre-contracted with 1 μM acetylcholine (ACh); up and down arrows represent application of ACh and the extract, respectively (d).

linear gradient of 0–60% acetonitrile/0.1% TFA at a flow rate of 3.0 mL/min for 120 min, and fractions were collected every 2 min.

Bioactive fractions eluted between 50 and 54 min with RP-HPLC and these were subjected to further purification steps using an anion-exchange column (TSKgel DEAE-5PW, 7.5 × 75 mm; Tosho Corp., Minato-ku, Tokyo, Japan) with a linear gradient of 0–0.5 M sodium chloride in 10 mM Tris-HCl (pH 9.2) at a flow rate of 0.5 mL/min for 100 min. A fraction that eluted with a concentration of about 0.1 M sodium chloride from the anion-exchange column caused relaxation of the apical muscle from *P. pectinifera*. This eluate was subjected to further RP-HPLC (Capcellpak C18, 4.6 × 250 mm; Shisheido CO. LTD., Chuo-ku, Tokyo, Japan). The absorbance peaks were recovered with a linear gradient of 15–30% acetonitrile/0.1% TFA at flow rate of 1 mL/min for 60 min. The bioactive peak was then subjected again to RP-HPLC using the same solvent gradient as in the previous RP-HPLC step but with a different column (Hypersil-BDS C18, 2 × 125 mm; HP, Waldbronn, Germany). Finally, the active peak was applied to the same column as in the previous step but with an isocratic elution of 20% acetonitrile/0.1% TFA at a flow rate of 0.5 mL/min.

Structure determination and synthesis of peptides

To determine the molecular mass and amino acid sequence of the purified SMP, it was analysed using an automated N-terminal amino acid gas-phase sequencer (PPSQ-1; Shimadzu Corp. Nakagyo-ku, Kyoto, Japan) and a MALDI-TOF mass spectrometer (Voyager-DE™ PRO spectrometer; Perseptive Biosystem, Framingham, MA, USA). On the basis of the structural determination results, two peptides, with or without the carboxyl-terminus amidated, were automatically synthesized by a conventional solid-phase method with Fmoc-protected amino acids and coupling reagents, 1-hydroxybenzotriazole and *N,N*-diisopropylcarbodimide, using a peptide synthesizer (PSSM-8; Shimadzu) as described previously (Kim *et al.* 2015). Other neuropeptides, S1 (GFNSALMFamide), S2 (SGPYSFNSGLTFamide), FMRFamide and FLRFamide were synthesized to enable comparison of their activities with that of the identified peptide.

In vitro bioassay and pharmacology

Three neuromuscular preparations, apical muscle, cardiac stomach and tube feet, were dissected from *P. pectinifera* for *in vitro* bioassay and pharmacology according to a slightly modified version of previously reported methods (Elphick *et al.* 1995; Melarange and Elphick 2003). Synthetic neuropeptides were also tested for bioactivity on apical muscle preparations from a different starfish species – *A. amurensis*. Briefly, the apical muscle was cut from the aboral body wall of an arm, where the apical muscle forms a thickening of longitudinally orientated muscle that runs along the mid-line of the inner side (Fig. 1c). A piece of cardiac stomach between the oral opening and extrinsic retractor strand was obtained by removing the aboral body wall from the central disc and the proximal region. An individual whole tube foot was dissected from the arm ambulacra but without the ampulla. All muscle preparations were cut to approximately 10 mm, and both ends of the muscle preparations were tied with cotton threads. The preparations were then suspended vertically in a 2 mL polypropylene chamber containing artificial seawater (ASW) with aeration, one end being connected to silver hook on the bottom of the chamber and the other to a force displacement

transducer (Type 45196A; NEC-Sanei Instrument Ltd., Tokyo, Japan). Output from the force displacement transducer was monitored by a recorder (WR7300; GRAPHTEC CORP., Yokohama, Japan) via an amplifier (AS1302; NEC-Sanei Instrument Ltd.), which recorded the mechanical responses of the device. Prior to testing, the muscle preparations were allowed to stabilize for about 90 min. The resting tension was then adjusted to 1.0 g for apical muscle and 0.5 g for cardiac stomach and tube foot. Muscles in the chamber were allowed to equilibrate for about 30 min in ASW, during which time the ASW in the chamber was freshly replaced every 15 min. Pre-contraction of apical muscle, cardiac stomach or tube foot preparations was induced by applying 1 μM acetylcholine (ACh), 10 μM carbachol or 30 mM high-potassium ASW respectively. Then immediately after equilibration, the muscles were treated with test samples to measure relaxation responses.

The bioassay system adopted for monitoring purification of the bioactive peptide was a system that measures relaxation of apical muscle from *P. pectinifera* pre-contracted for 2 min at 20 min intervals with 1 μM ACh. An aliquot of each test fraction was evaporated to dryness, dissolved with 50 μL of phosphate-buffered saline, and added into the chamber.

At least four separate experiments to test the pharmacological activities of synthetic SMP, C-terminally amidated SMP (SMPa-mide) and other neuropeptides were performed, using a concentration range of 10^{-10} M to 10^{-5} or 10^{-4} M at 25°C. EC_{50} values represent the concentration of peptide required to cause a response 50% of the maximum. The maximal response (E_{max}) was expressed as the percentage of the maximal relaxation induced by 10^{-4} or 10^{-5} M of each peptide compared to the maximal contraction of apical muscle by 1 μM ACh, of cardiac stomach by 10 μM carbacol or of tube foot by 30 mM high-potassium ASW. The relative activity was calculated as the ratio of the concentration of SMP or other peptides required to produce responses equivalent to a half-maximal response.

cDNA cloning and sequence analysis

Total RNA was extracted using RNeasy Mini kit (Qiagen, Valencia, CA, USA) from total tissues (except body wall) of *P. pectinifera*, and then mRNA was purified using Oligotex mRNA mini kit (Qiagen) following the manufacturer's instructions. The synthesis rapid amplification cDNA end (RACE)-ready cDNA template was performed with SMARTer™ RACE cDNA amplification Kit (Clontech, Mountain view, CA, USA) according to manufacturer's instructions.

Based on the amino acid sequence of the purified peptide, two degenerate primers were designed for 3′ RACE PCR, and then 5′ RACE PCRs were conducted with sequence-specific primers designed from the sequencing result of the 3′ RACE product. The sequences of primers used in RACE are listed in Table S1. The first PCR conditions for 3′ RACE included initial denaturation at 94°C for 3 min followed by: 5 cycles of 94°C for 1 min, 59°C for 1 min and 72°C for 1 min; 5 cycles of 94°C for 1 min, 57°C for 1 min and 72°C for 1 min; 20 cycles of 94°C for 1 min, 55°C for 1 min and 72°C for 1 min. Nested PCR for 3′RACE was performed with the same conditions as the first PCR. The first PCR product of 5′ RACE was obtained by the following thermal cycle profile: 5 cycles of 94°C for 30 s, 67°C for 30 s and 72°C for 1 min; 5 cycles of 94°C for 30 s, 65°C for 30 s and 72°C for 1 min; 25 cycles of 94°C for 30 s, 63°C for 30 s and 72°C for 1 min. Nested PCR for 5′ RACE was as follows: 5 cycles of 94°C for 30 s, 69°C for 30 s and 72°C for 1 min; 5 cycles of 94°C for 30 s, 67°C for 30 s and 72°C for 1 min; 25 cycles of 94°C for 30 s, 65°C for 30 s and 72°C for 1 min.

PCR products in the last step of 3′ and 5′ RACE were introduced into the pGEM-Teasy vector system (Promega, Madison, WI, USA) and sequenced. The full-length translated sequence of the SMP precursor, based on the cloned cDNA nucleotide sequence, was aligned by BLAST (http://blast.ncbi.nlm.nih.gov/blast.cgi) and the sequence was submitted to the GenBank database (Accession number: KT870152). Multiple sequence alignment of the full-length *P. pectinifera* SMP precursor and related proteins in other species was performed using Clustal Omega (http://www.ebi.ac.uk/Tools/msa/clustalo/).

Asterias rubens radial nerve cord transcriptome sequence data obtained by Illumina HiSeq sequencing, as reported previously (Semmens *et al.* 2013), were analysed using BLAST to identify a homologue of the *P. pectinifera* SMP precursor. Using the sequence of the *P. pectinifera* SMP precursor as a query, a 444 bp *A. rubens* contig (1025452) comprising a partial sequence corresponding to the 3′ region of the *P. pectinifera* SMP precursor cDNA was identified. Then ovarian transcriptome sequence data obtained from multiple echinoderm species [(Reich *et al.* 2015); http://www.echinobase.org/Echinobase/Blasts] was analysed and non-overlapping contigs encoding the 5′ region (GAUS01027726.1) and the 3′ region (GAUS01027727.1) of a SMP-type precursor transcript was identified from the starfish species *Asterias forbesi.* Combining these partial sequence data from *A. rubens* and *A. forbesi*, primers were designed to enable PCR amplification of the full-length SMP precursor coding sequence from *A. rubens*, as described below.

Total RNA was extracted from radial nerve cords of *A. rubens* using the SV Total RNA Isolation System according to the manufacturer's instructions (Promega). Then cDNA was synthesized using the QuantiTect Rev. Transcription Kit in accordance with the manufacturer's instructions (Qiagen). A cDNA containing the coding sequence of the *A. rubens* SMP-type precursor was amplified by PCR using Phusion high-fidelity PCR master mix (NEB, Ipswich, MA, USA) and the oligo primers 5′-ATGCGGCTCATCATGCAC-3′ and 5′-TACACACCAAGCAGTGACA-3′. The conditions for PCR included initial denaturation at 98°C for 2 min followed by: 30 cycles of 98°C for 10 s, 55°C for 30 s, 72°C for 1 min, 72°C for 8 min and hold at 4°C. 1% gel electrophoresis was performed to analyse the PCR products and then the PCR product was gel-extracted and purified using a QIAquick gel extraction kit (Qiagen). Zero Blunt TOPO PCR cloning kit (Invitrogen, Carlsbad, CA, USA) was used to ligate the PCR product into the pCR-Blunt II with TOPO vector for sequencing. The sequence obtained (GenBank accession number KT870153) was translated into protein sequence using ExPASy (http://web.expasy.org/translate/) and SignalP 4.1 (http://www.cbs.dtu.dk/services/SignalP/) was used to predict the signal peptide of the translated protein sequence.

Real-time quantitative PCR (RT-qPCR) analysis

To quantitatively analyse expression of SMP precursor transcripts in different starfish tissues/organs, RT-qPCR was employed using a LightCycler 480 Real-Time PCR System (Roche, Mannheim, Germany) with LightCycler 480 SYBR green master I (Roche). Total RNA extracted from the apical muscle, radial nerve cord, cardiac stomach, pyloric stomach, coelomic lining containing

transverse muscles, tube feet, pyloric caecae, testis and ovary were obtained from five specimens of *P. pectinifera*. cDNA was synthesized using the TOPscript cDNA synthesis Kit with oligo dT (dT18) (Enzynomics, Daejeon, Korea) according to the manufacturer's instructions. The primer pairs used for amplifying SMP precursor cDNA and elongation factor 1α (EF1α) cDNA as a control for normalization were SMP RT-F and SMP RT-R, and EF1α RT-F and EF1α RT-R respectively (see Table S1 for sequences). Based on the standard curves for both SMP and EF1α, the relative expression levels of SMP transcripts in each tissue were normalized against the level of the EF1α control using the following formula: relative expression = $[(1 + E_{SMP})^{CP\_SMP}]^{-1}/[(1 + E_{EF1\alpha})^{CP\_EF1\alpha}]^{-1}$, in which E is PCR efficiency ($E = 10^{-1/slope} - 1$) and CP is the threshold cycle number. Triplicate amplifications were carried out independently, and the relative quantification results were expressed as the fold levels of SMP precursor transcripts.

Statistical analysis

All data are presented as means ± standard deviation. The statistical analysis for pharmacological data were performed using two-way analysis of variance (ANOVA) supported by Bonferroni's multiple comparisons test when carrying out pair wise comparison between the same doses of different peptides. For RT-qPCR data, comparison between tissues was carried out by one-way ANOVA, followed by Duncan's Multiple Range test.

Statistical analyses were performed using SPSS 21 program (SPSS, Chicago, IL, USA) and graphs were generated using GraphPad Prism software version 6.0 for Windows (GraphPad Software, San Diego, CA, USA). p values with $p < 0.05$ were considered statistically significant.

Results

Purification of a novel hexadecapeptide that relaxes the apical muscle of *P. pectinifera*

A whole-body extract of *P. pectinifera* induced relaxation of apical muscle pre-contracted with ACh (Fig. 1d), indicating that it was an appropriate source to isolate myorelaxants. A single absorbance peak (peak A) containing a myorelaxant was successfully purified from the whole-body extract through six steps of column purification which sequentially were cation, repeated RP and anion HPLC. Finally, peak A was isocratically eluted with 20% acetonitrile/0.1% TFA at 16.1 min of the retention time (Fig. 2a). An aliquot of peak A relaxed the apical muscle of *P. pectinifera* that was pre-contracted by ACh (Fig. 2b). Purified peak A was identified as a sixteen-residue peptide with the sequence Phe-Gly-Lys-Gly-Gly-Ala-Tyr-Asp-Pro-Leu-Ser-Ala-Gly-Phe-Thr-Asp with a free carboxy terminus based on N-terminal amino acid sequencing and molecular mass analysis (Fig. 2c and Figure S1a). The purified hexadecapeptide was designated SMP. To confirm the primary structure and chemical properties of SMP under RP-HPLC, SMP with a free carboxy terminus (SMP) and SMP with an amidated carboxy terminus (SMPamide) were synthesized. The synthetic SMP and native SMP eluted with an identical retention time, and a mixture of the two peptides eluted as a single peak under RP-HPLC (Fig. 2d). Moreover, SMP and SMPamide did not have an identical retention time on RP-HPLC (Figure S1b). Collectively, the results demonstrate that the purified SMP is the hexdecapeptide Phe-Gly-Lys-Gly-Gly-Ala-Tyr-Asp-Pro-Leu-Ser-Ala-Gly-Phe-Thr-Asp-OH, with a free carboxy terminus and without any post-translational modifications.

SMP is a potent relaxant of *P. pectinifera* apical muscle *in vitro*

SMP and a C-terminally amidated analogue of SMP (SMPamide) both caused dose-dependent relaxation of *in vitro* apical muscle preparations from *P. pectinifera* (Fig. 2e). The threshold response, ED_{50} and E_{max} for SMP were 10^{-10} M, 6.0×10^{-8} M and 120.02 ± 7.00% and for SMPamide were 10^{-10} M and 4.0×10^{-8} M and 134.69 ± 9.57% respectively (Fig. 2e). These results corroborate the structural determination that SMP is not C-terminally amidated and does not require C-terminal modification for its bioactivity. Comparison of the bioactivity of SMP with the starfish SALMFamide neuropeptides S1 and S2 revealed that SMP was more potent/efficacious than these peptides as a relaxant of the apical muscle from *P. pectinifera* (Fig. 2e). Thus, the E_{max} for S1 and S2 at a concentration of 10^{-5} M were only 44.15 ± 2.41 and 29.72 ± 8.29 respectively. Furthermore, the molluscan neuropeptides FLRFamide and FMRFamide, which share some sequence similarity with SALMFamides, exhibited little or no bioactivity as relaxants of apical muscle preparations, even at concentrations as high as 10^{-5} M (Fig. 2e).

The *P. pectinifera* SMP precursor protein comprises twelve copies of SMP and seven copies of other SMP-like peptides

A cDNA encoding the *P. pectinifera* SMP precursor was cloned and sequenced (GenBank accession number: KT870152) and the nucleotide sequence and the deduced protein sequence are shown in Fig. 3. The cDNA sequence comprised 1682 bp, starting with a 5′ untranslated region of 148 bp, followed by an open reading frame of 1281 bp, a 3′ untranslated region of 253 bp including a poly-A tail. The open reading frame of the SMP precursor encodes a 426 amino acid residue protein that contains four regions: a signal peptide (Met^{1}-Ala^{19}), as predicted by SignalP 4.1 (http://www.cbs.dtu.dk/services/SignalP/), a N-terminal spacer peptide (Ser^{20}-Arg^{56}) containing several acidic amino acids, a region containing twelve copies of SMP and seven copies of SMP-like peptides with each peptide copy bounded by dibasic cleavage sites (Phe^{57}-Arg^{402}) and a C-terminal region (Thr^{403}-Arg^{426}).

SMP precursor transcripts are widely expressed in *P. pectinifera* and SMP causes *in vitro* relaxation of other muscle preparations from *P. pectinifera*

The relative expression levels of the SMP precursor mRNA in different tissues (apical muscle, radial nerve cord, cardiac

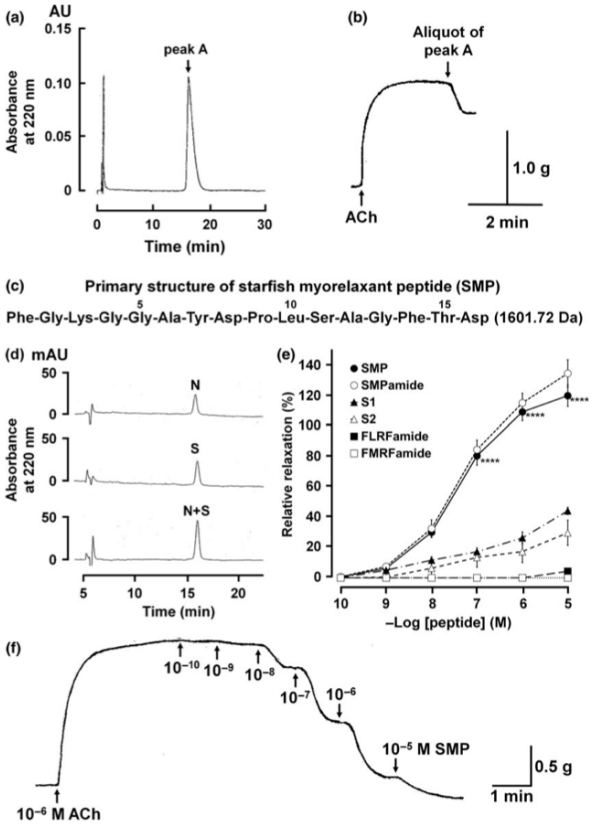

Fig. 2 Isolation, structure determination and pharmacology of purified myorelaxant peptide. Peak A was isocratically eluted with 20% acetonitrile/0.1% trifluoroacetic acid on RP-HPLC (a), and an aliquot of purified peak A caused relaxation of the apical muscle (b). Purified peak A was identified as a peptide comprised of sixteen amino acid residues with a molecular mass of 1601.72 Da, which we have named starfish myorelaxant peptide or SMP (c). Comparison of chromatographic properties of native SMP (N) and synthetic SMP (S) on RP-HPLC showed that native SMP and synthetic SMP with a free carboxy terminal have identical retention times on RP-HPLC (d). The concentration-dependent relaxing activity of SMP on the apical muscle of *P. pectinifera*. SMP with free carboxyl terminus and amidated carboxy terminus is SMP (●) and SMPamide (○), respectively. The effects of S1 (▲) and S2 (△) from the starfish *A. rubens* and the molluscan neuropeptides FLRFamide (■) and FMRFamide (□) are shown to compare their activity with SMP. Each point represents the mean ± standard deviation determined from four separate experiments. ****$p < 0.0001$ for SMP (●) compared with S1/S2. The percentage relaxing activity was calculated by comparing each relaxation effect to the maximal contraction of the apical muscle by 1 μM ACh (e). Representative recording of the concentration-dependent relaxing effect of SMP on *P. pectinifera* apical muscle pre-contracted with 1 μM ACh (f).

stomach, pyloric stomach, coelomic lining, tube feet, pyloric caecae, testis and ovary) were determined by RT-qPCR (Fig. 4a). The highest expression of SMP precursor transcripts was detected in radial nerve cords, which are the major components of the nervous system in starfish. In addition, relatively high expression levels of SMP precursor transcripts were observed, in descending order, in apical muscle, tube feet, coelomic lining, cardiac stomach, pyloric stomach and pyloric caecae. However, the expression of SMP precursor transcripts in reproductive organs (ovary and testis) was barely detectable. These findings indicate that SMP is a neuropeptide and suggest that SMP may have widespread roles as a regulator of muscle activity in *P. pectinifera*. To address this issue, SMP was tested *in vitro* on two other neuromuscular preparations in which SMP precursor transcripts are detected – cardiac stomach and tube feet. SMP caused dose-dependent relaxation of both preparations and, as with apical muscle preparations, SMP was more potent/effective as a muscle relaxant than the SALMFamides S1 and S2 (Fig. 4b and c).

SMP causes relaxation of apical muscle preparations from the starfish *Asterias amurensis* and identification of an SMP-type precursor in *Asterias rubens*

Having identified SMP as a muscle relaxant in *P. pectinifera*, we then investigated if this peptide also acts as a muscle relaxant in other starfish species. To address this issue we tested synthetic SMP on apical muscle preparations from *A. amurensis*. SMP caused dose-dependent relaxation and the E_{max} was 82.1 ± 1.94% at a concentration of 10^{-5} M (Fig. 5a). Previous studies have shown that the SALMFamide neuropeptides S1 and S2 cause relaxation of apical

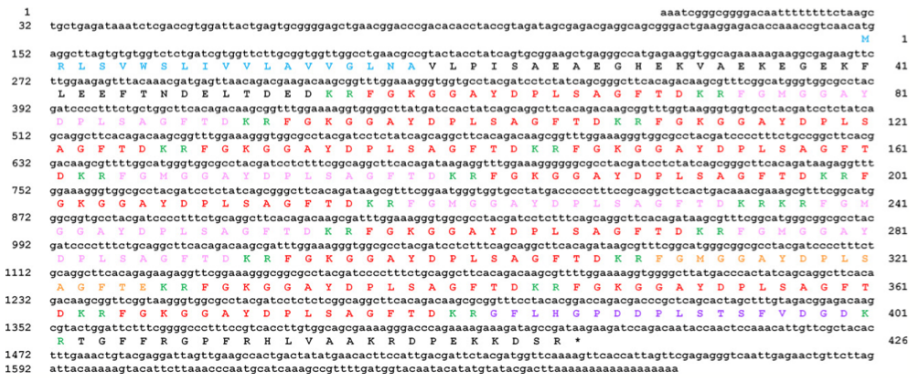

Fig. 3 Precursor of starfish myorelaxant peptide (SMP) in *Patiria pectinifera*. The DNA sequence of a transcript (lowercase, 1682 bases) encoding the *P. pectinifera* SMP precursor (uppercase, 426 amino acid residues) is shown. The predicted signal peptide, the purified mature SMP (SMP_a) and three other variants (SMP_b, [Met^3]-SMP_a; SMP_c, [Met^3, Glu^{16}]-SMP_a; SMP_d, SMP_a-related octadecapeptide) are shown in blue, red, pink, orange and purple, respectively, and putative dibasic cleavage sites (KR) are shown in green. The asterisk shows the position of the stop codon. The SMP precursor protein comprises twelve copies of SMP and seven copies of SMP-like peptides.

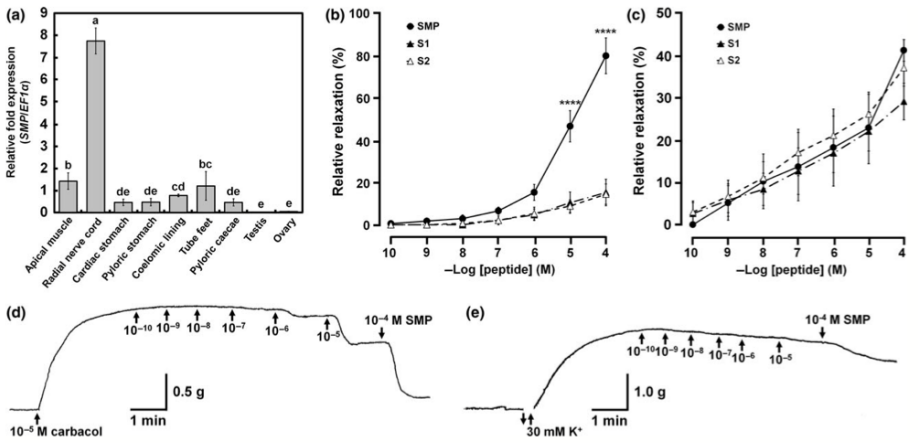

Fig. 4 The expression levels for the starfish myorelaxant peptide (SMP) precursor transcript in various organs/tissues from *P. pectinifera* and the pharmacological effects of SMP on cardiac stomach and tube foot from *P. pectinifera*. Relative expression levels of SMP transcripts in each organ/tissue were normalized against the level of the EF1α gene as an internal control. Mean ± standard deviation ($n = 3$) are shown. Means denoted by the same letter did not differ significantly ($p > 0.05$) whilst different letters (a, b, c, d, e) at the top of the bars indicate statistically significant differences ($p < 0.05$) between tissues determined by one-way ANOVA followed by Duncan's Multiple Range test (a). SMP caused concentration-dependent relaxation of the cardiac stomach (b) and tube foot (c) from *P. pectinifera*. The relaxing activity of SMP (●) was compared with S1 (▲) and S2 (△). Each point represents the mean ± standard deviation determined from four separate experiments. Statistically significant difference between SMP and S1/S2 represents with ****$p < 0.0001$. The percentage relaxing activity was calculated by comparing each relaxation effect to the maximal contraction of cardiac stomach caused by 10 μM carbacol and of tube foot caused by 30 mM high-potassium artificial seawater respectively. Representative recordings of the effects of SMP on cardiac stomach (d) and tube foot (e) preparations are shown.

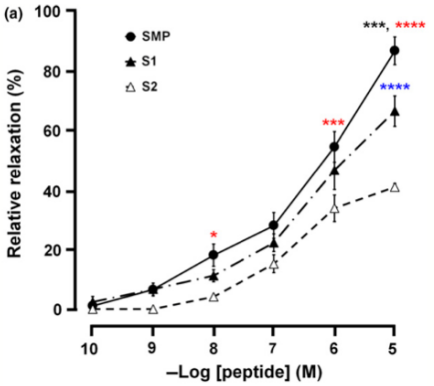

(b)

MRLIMHSVVLLLAVIGLSMALPASKDSEDKEKLTEKEKEE
IFEEFGEEDDGKRGFGMGAYDPLSAGFTDKRFGGKGAFDP
LSAGFTDKRFGGKGAFDPLSAGFTDKRFGGSRGAFDPLSA
GFTDKRFGGKGAFDPLSAGFTDKRFGGSRGAFDPLSAGFT
DKRFGGKGAFDPLSAGFTDKRSFVHGDFDPLSTGFVDGDK
RAGFMNGVFHPLVAKRVPEKKDRR

Fig. 5 Pharmacological effect of starfish myorelaxant peptide (SMP) on apical muscle from *Asterias amurensis* and identification of an SMP-type precursor in *Asterias rubens*. (a). The concentration-dependent relaxing activity of SMP (●) compared with S1 (▲) and S2 (△) on the apical muscle of *A. amurensis*. Each point represents the mean ± standard deviation determined from four separate experiments. Statistically significant differences between the effects of SMP and S1, SMP and S2, and S1 and S2 are represented by black, red and blue asterisks (*$p < 0.05$, ***$p < 0.001$ and ****$p < 0.0001$), respectively. The percentage relaxing activity was calculated by comparing each relaxation effect to the maximal contraction of apical muscle caused by 1 μM ACh. (b) Amino acid sequence of a 224-residue SMP-type precursor protein identified in *A. rubens*, which comprises a predicted 20-residue signal peptide (blue) and eight copies of putative SMP-like peptides (red) and putative dibasic cleavage sites (KR, green). The sequence of the cDNA encoding this protein is shown in Figure S2.

muscle preparations from *Asterias rubens*, which is closely related to *A. amurensis* (Melarange and Elphick 2003). Therefore, we compared the bioactivity of SMP with S1 and S2 and found that the E_{max} for S1 and S2 at a concentration of 10^{-5} M were less than for SMP, 62.3 ± 4.4 and 38.7 ± 1.21, respectively (Fig. 5a). However, by comparison with S1 and S2, SMP was less effective as a relaxant of the apical muscle from *A. amurensis* (Fig. 5a) than from *P. pectinifera* (Fig. 2e). These findings indicate that SMP or a related peptide(s) exists in *A. amurensis* and that SMP-type peptides are likely to act as muscle relaxants throughout the Asteroidea. Accordingly, a cDNA encoding an SMP-type precursor was identified in *A. rubens*, comprising a 224-residue protein with a predicted 20-residue signal peptide and eight copies of putative SMP-like peptides: four copies of the peptide FGGKGAFDPLSAGFTD, two copies of the peptide FGGSRGAFDPLSAGFTD and one copy each of GFGMGAYDPLSAGFTD and SFVHGDFDPLSTGFVD GD (Fig. 5b and Figure S2, GenBank Accession number: KT870153). It is noteworthy that the C-terminal region of three of these peptides (DPLSAGFTD) is identical to the corresponding region of *P. pectinifera* SMP.

Starfish SMP precursors are homologues of neuropeptide precursors that have been identified in other echinoderms

To investigate relationships with neuropeptide precursors that have been in other animals, the *P. pectinifera* and *A. rubens* SMP precursor proteins were submitted as queries against the GenBank nr database using BLAST. The top two hits (XP_785647.1 and XP_003727926) were identified as neuropeptide precursor proteins that have been described previously from the sea urchin *Strongylocentrotus purpuratus* and designated as Spnp6 and Spnp7, respectively (Rowe and Elphick 2012). In Fig. 6, we show a multiple sequence alignment of the *P. pectinifera* SMP precursor, the *A. rubens* SMP-type precursor, Spnp6, Spnp7 and a homologue of Spnp7 that has been identified in the sea cucumber *Apostichopus japonicus* [Ajnp7 (Rowe *et al.* 2014)]. Furthermore, alignment of the putative neuropeptides derived from the *P. pectinifera* SMP precursor, the *A. rubens* SMP-type precursor, Spnp6, Spnp7 and Ajnp7 (Fig. 7) reveals that the peptides have a number of features in common. These include two phenylalanine residues located at or near the N- and C-termini of the peptides as well as a conserved core region with the motif (D/E)-(P)-(L/M), structural characteristics that may be important for the bioactivity of these peptides.

Discussion

Here, we have isolated a novel hexadecapeptide (FGKGGAYDPLSAGFTD) from starfish that acts as a muscle relaxant and which we have designated as SMP. Previous studies have identified the SALMFamide neuropeptides S1 and S2 as muscle relaxants in starfish (Melarange *et al.* 1999; Melarange and Elphick 2003) and here the bioactivity of SMP, S1 and S2 as muscle relaxants were compared. When tested on three preparations from *P. pectinifera* (apical muscle, cardiac stomach and tube feet), SMP was more effective/potent than S1 or S2. This finding is likely to be physiologically relevant with respect to S1 because we know that S1 occurs in the closely related species *Patiria miniata*. However, *P. miniata* does not contain S2 and this species has instead an S2-like peptide (Elphick *et al.* 2013, 2015). Therefore, the inferior bioactivity of S2 as a myorelaxant in *P. pectinifera* may in part be attributable to

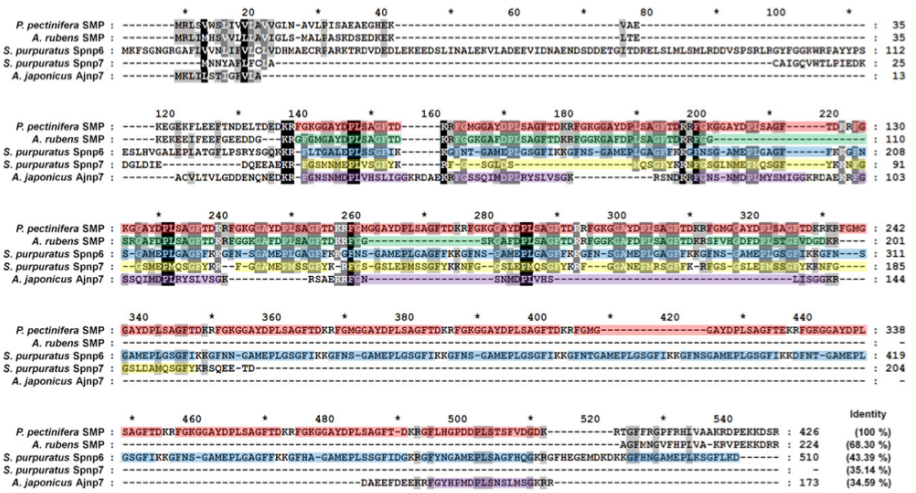

Fig. 6 Multiple sequence alignment of the *P. pectinifera* starfish myorelaxant peptide (SMP) precursor with related neuropeptide precursors in other echinoderms. Highlighted red, green, blue, yellow and purple boxes represent multiple copies of neuropeptides separated by putative cleavage sites (KR or KK). All of the precursors contain multiple copies of related peptides: *P. pectinifera* SMP precursor contains twelve copies of SMP and seven copies of SMP-like peptides; *A. rubens* SMP precursor contains eight copies of SMP-like peptides; *S. purpuratus* neuropeptide precursor 6 (Spnp6) contains twenty-one copies of nine SMP-like peptides; Spnp7 precursor contains ten copies of nine SMP-like peptides; *A. japonicus* neuropeptide precursor 7 (Ajnp7) contains six copies of five SMP-like peptides. The sequences of Spnp6, Spnp7 and Ajnp7 are from (Rowe and Elphick 2012; Rowe *et al.* 2014).

differences in peptide structure. Furthermore, analysis of the sequences of the two SALMFamide precursor proteins in *P. miniata* reveals that they comprise S1, the S2-like peptide and fourteen other SALMFamide-type peptides (Elphick *et al.* 2013, 2015). So comparison of the effects of SMP with S1 or S2 tested in isolation does not reflect the physiological occurrence of 'cocktails' of SALMFamides. Nevertheless, the superior bioactivity of SMP as a myorelaxant, compared to S1 and S2, in tests on muscle preparations from both *P. pectinifera* and *Asterias amurensis* clearly indicates that SMP is a physiologically important regulator of muscle relaxation in starfish.

Analysis of the distribution of the expression of the SMP precursor in *P. pectinifera* using qPCR revealed a widespread pattern of expression, including all three neuromuscular preparations that SMP causes relaxation of *in vitro* – the apical muscle, cardiac stomach and tube feet. Likewise, immunocytochemical- and radioimmunoassay-based analysis of the distribution of S1 and S2 in *A. rubens* reveals a widespread pattern of expression (Moore and Thorndyke 1993; Elphick *et al.* 1995; Newman *et al.* 1995a,b). Therefore, it is likely that SMP and SALMFamide neuropeptides act in concert as muscle relaxants to regulate a variety of physiological processes in starfish. For example, relaxing effects on the apical muscle *in vivo* may be associated with neural mechanisms that control changes in body posture, whereas relaxing effects on tube feet *in vivo* may be associated with locomotor activity. The relaxing action of SALMFamides on the cardiac stomach is thought be relevant to neural mechanisms controlling stomach eversion during feeding in starfish (Melarange *et al.* 1999) and this role may equally apply to the novel SMP neuropeptide identified here. Further insights into the physiological roles of SMP and other SMP-like peptides derived from the same precursor protein may be obtained by analysis of the distribution of these peptides at the cellular level. As highlighted above, detailed immunocytochemical analyses of the distribution of S1 and S2 in *A. rubens* have been reported previously (Moore and Thorndyke 1993; Elphick *et al.* 1995; Newman *et al.* 1995a,b) and it would be interesting to compare the distribution of SMP and SALMFamides using this approach.

Comparative analysis of the sequence of SMP and the SMP precursor with neuropeptides and neuropeptide precursors that have been identified in other animals reveals that SMP belongs to a bilaterian family of neuropeptides that includes molluscan pedal peptides (PP) and arthropodan orcokinins (OK) (Fig. 8, Figure S3 and Table S2). The occurrence of PP/OK-type peptides in echinoderms has been

Origin	Peptides	Sequence	No. residues	Identity	References
P. pectinifera	SMP_a	-FGK-GGAYDPLSAGFTD--	16		This study
	SMP_b	-FGM-GGAYDPLSAGFTD--	16	93.75	
	SMP_c	-FGM-GGAYDPLSAGFTE--	16	87.50	
	SMP_d	GFL--HGPDDPLSTSFVDGD	18	43.75	
A. rubens	$ArSMP_a$	GFGM--GAYDPLSAGFTD--	16	75.00	This study
	$ArSMP_b$	-FGG-KGAFDPLSAGFTD--	16	81.25	
	$ArSMP_c$	-FGGSRGAFDPLSAGFTD--	17	75.00	
	$ArSMP_d$	SFV--HGDFDPLSTGFVDGD	18	50.00	
S. purpuratus	$Spnp6_a$	RFLT-G-ALEPISSGFI---	15	46.67	Rowe & Elphick 2012
	$Spnp6_b$	GFNT-G-AMEPLGSGFI---	15	40.00	
	$Spnp6_c$	GFNS-G-AMEPLGAGFF---	15	46.67	
	$Spnp6_d$	GFNS-G-AMEPLGSGFI---	15	40.00	
	$Spnp6_e$	GFNN-G-AMEPLGSGFI---	15	40.00	
	$Spnp6_f$	DFNT-G-AMEPLGSGFI---	15	40.00	
	$Spnp6_g$	GFHA-G-AMEPLSSGFIDG-	17	50.00	
	$Spnp6_h$	GFYN-G-AMEPLSAGFHQG-	17	50.00	
	$Spnp6_i$	GFHN-G-AMEPLKSGFLKD-	17	37.50	
	$Spnp7_a$	-FGS-MN-MEPLVSGFY---	14	28.57	
	$Spnp7_b$	-FGS-G--LDSMQSGFY---	13	38.46	
	$Spnp7_c$	NFGS-GLNMEPMQSGFY---	16	40.00	
	$Spnp7_d$	NFGG-S--MEPMQSGFY---	14	46.15	
	$Spnp7_e$	-FGG-A--MEPMSSGFY---	13	61.54	
	$Spnp7_f$	-FGS-G-SLEPMSSGFY---	14	50.00	
	$Spnp7_g$	NFGG-S--LEPMQSGFY---	14	46.15	
	$Spnp7_h$	-FGG-A--NEPMRSGFF---	13	53.85	
	$Spnp7_i$	NFGG-S--LDAMQSGFY---	14	46.15	
A. japonicus	$Ajpnp7_a$	-FG--NSNMDPIVHSLIGG-	16	33.33	Rowe et al. 2014
	$Ajpnp7_b$	-FGS-SQIMDPLRYSLVSG-	17	31.25	
	$Ajpnp7_c$	-FG--NSNMDPIMYSMIGG-	16	33.33	
	$Ajpnp7_d$	-FG--NSNMDPIVHSLISGG	17	33.33	
	$Ajpnp7_e$	-FG--YHPMDPLSNSLMSG-	16	40.00	

Fig. 7 Alignment of starfish myorelaxant peptide (SMP_a) with putative SMP-like neuropeptides derived from echinoderm SMP-type precursors: the starfish *P. pectinifera* and *A. rubens*; sea urchin *S. purpuratus*; sea cucumber *A. japonicus*. Conserved residues are highlighted in black and grey.

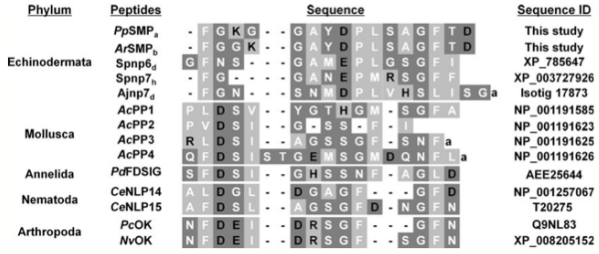

Fig. 8 Alignment of echinoderm starfish myorelaxant peptide (SMP)-type peptides with protostomian pedal peptide (PP)/orcokinin(OK)-type peptides. The basic amino acids Lys, Arg and His are shown in the black with light grey highlighting, and the acidic residues Glu and Asp are shown in black with dark grey highlighting. All other amino acids are classified as hydrophobic (white with light grey highlighting) or hydrophilic (white with dark grey highlighting). Lower case 'a' denotes a C-terminal amide group. Species abbreviations and references: Pp, *P. pectinifera;* Ar, *A. rubens*; Sp, *S. purpuratus* (Reich *et al.* 2015); Aj, *A. japonicus* (Du *et al.* 2012; Rowe and Elphick 2012); Ac, *Aplysia californica* (Moroz *et al.* 2006); Pd, *Platynereis dumerilii* (Conzelmann *et al.* 2011); Ce, *Caenorhabditis elegans* (Nathoo *et al.* 2001); Pc, *Procambrus clarkii* (Yasuda-Kamatani and Yasuda 2000); Nv, *Nasonia vitripennis* (Hauser *et al.* 2010).

reported previously based on analysis of genome/transcriptome sequence data (Rowe and Elphick 2012; Rowe *et al.* 2014) and in Figs 6 and 7, respectively, we show alignments of SMP and the SMP precursor with related PP/OK-type neuropeptides and precursor proteins that have been identified in the sea urchin *S. purpuratus* and the sea cucumber

A. japonicus. These alignments reveal conserved residues that may be important for the bioactivity of PP/OK-type peptides in echinoderms. In Fig. 8 we show an alignment of SMP and other representative echinoderm PP/OK-type peptides with molluscan pedal peptides and arthropodan orcokinins. What this reveals is the conservation of hydrophobic residues, which are typically phenylalanine, proximal to or at the N- and C-termini of the peptides. This suggests that these evolutionarily conserved structural features are important for the bioactivity of PP/OK-type peptides in the Bilateria. However, the motif (D/E)-(P)-(L/M) that is a conserved feature of the core of echinoderm PP/OK-type peptides, including SMP (Fig. 7), is not seen in molluscan and arthropodan PP/OK-type peptides and therefore this may be a unique characteristic of echinoderm representatives of this neuropeptide family. Investigation of the structure-activity relationships of orcokinin in *Orconectes limosus* has revealed that C-terminal amidation results in a reduction of bioactivity (Bungart *et al.* 1995), whereas here we found that C-terminal amidation of SMP neither reduces nor enhances its bioactivity. These findings contrast with neuropeptides that are naturally C-terminally amidated *in vivo*, where loss of the C-terminal amide typically results in a dramatic loss of bioactivity (Greenberg and Price 1979).

With the identification of SMP as a member of the PP/OK-type family of neuropeptides, it is of interest to consider what is known about the physiological roles of these neuropeptides in other phyla. PP was originally discovered in the mollusc *Aplysia californica* as a peptide that causes contraction of pedal muscles (Lloyd and Connolly 1989; Hall and Lloyd 1990); it also stimulates beating of cilia associated with the foot (Longley and Peterman 2013). OK was first isolated from neural extracts of the crayfish *Orconectus limosus* on account of its stimulatory effect on hindgut activity (Stangier *et al.* 1992). Subsequently, OK-type peptides have been identified in several arthropod species and found to have a variety of effects, including stimulation of the prothoracic gland and regulation of ecdysteroidogenesis in the silk moth *Bombyx mori* (Yamanaka *et al.* 2011) and regulation of circadian activity in the cockroach *Leucophaea maderae* (Hofer and Homberg 2006; Soehler *et al.* 2011; Wei and Stengl 2011). Thus, in both molluscs and arthropods, PP/OK-type neuropeptides have stimulatory effects on the activity of muscle and other tissues. This contrasts with the inhibitory effect that SMP has in causing relaxation of muscle in starfish, as reported here. It will be interesting, therefore, to investigate in future studies if PP/OK-type peptides also act as muscle relaxants in other echinoderms or if this is a unique characteristic of PP/OK-type peptides in starfish.

Thus far, PP/OK-type peptides have not been identified in other deuterostomian phyla such as hemichordates, which are a sister clade to the echinoderms, or chordates. One possibility is that PP/OK-type peptides have been lost in hemichordates and chordates and the echinoderms are unique amongst the deuterostomes in retaining peptides belonging to this bilaterian neuropeptide family. Alternatively, the possibility remains that members of this neuropeptide family exist in hemichordates and chordates but their relationship with PP/OK-type peptides has not been observed because of sequence divergence. Addressing this issue would be facilitated if the receptors that mediate the effects of PP/OK-type peptides in echinoderms or in protostomes were identified, and therefore this represents an important objective for future research on PP/OK-type peptides.

Acknowledgements and conflict of interest disclosure

This work was supported by Korea Ministry of Environment (MOE) as 'Eco-innovation Program (201300030002)', the China Scholarship Council (ML) and Queen Mary University of London (MRE). The authors declare that they have no conflicts of interest with the contents of this article.

All experiments were conducted in compliance with the ARRIVE guidelines.

Supporting information

Additional supporting information may be found in the online version of this article at the publisher's web-site:

Figure S1. MALDI-TOF mass spectrum of purified peak A (A). Comparison of the chromatographic properties of synthetic SMP with a free carboxyl terminus (SMP) and SMP with an amidated carboxyl terminus (SMPamide) on RP-HPLC reveals that the two peptides elute at different retention times with isocratic 20% acetonitrile/0.1% TFA (B).

Figure S2. Precursor of starfish myorelaxant peptide (SMP)-type neuropeptides in *Asterias rubens*.

Figure S3. Multiple sequence alignment showing that starfish SMP precursors share sequence similarity with other echinoderm pedal peptide-type precursors (Spnp6, Spnp7, Ajnp7) and with protostomian pedal peptide (PP)/orcokinin(OK)-type peptide precursors.

Table S1. Primers used for RACE and RT-qPCR analysis of SMP precursor expression in *P. Pectinifera*.

Table S2. Identity and similarity grid showing the identity/similarity percentages for the amino acid sequences of SMP precursors and PP/OK-type peptide precursors.

References

Adoutte A., Balavoine G., Lartillot N., Lespinet O., Prud'homme B. and de Rosa R. (2000) The new animal phylogeny: reliability and implications. *Proc. Natl Acad. Sci. USA* **97**, 4453–4456.

Bendena W. G., Garside C. S., Yu C. G. and Tobe S. S. (1997) Allatostatins: diversity in structure and function of an insect neuropeptide family. *Ann. N. Y. Acad. Sci.* **814**, 53–66.

Blackburn M. B., Wagner R. M., Kochansky J. P., Harrison D. J., Thomas-Laemont P. and Raina A. K. (1995) The identification of two myoinhibitory peptides, with sequence similarities to the

galanins, isolated from the ventral nerve cord of *Manduca sexta*. *Regul. Pept.* **57**, 213–219.
Brain S. D., Williams T. J., Tippins J. R., Morris H. R. and MacIntyre I. (1985) Calcitonin gene-related peptide is a potent vasodilator. *Nature* **313**, 54–56.
Bungart D., Kegel G., Burdzik S. and Keller R. (1995) Structure-activity relationships of the crustacean myotropic neuropeptide orkinin. *Peptides* **16**, 199–204.
Conzelmann M., Offenburger S. L., Asadulina A., Keller T., Munch T. A. and Jekely G. (2011) Neuropeptides regulate swimming depth of *Platynereis* larvae. *Proc. Natl Acad. Sci. USA* **108**, E1174–E1183.
Dan-Sohkawa M., Yamanaka H. and Watanabe K. (1986) Reconstruction of bipinnaria larvae from dissociated embryonic cells of the starfish, *Asterina pectinifera*. *J. Embryol. Exp. Morphol.* **94**, 47–60.
Davydov P. V., Shubravyi O. I. and Vassetzky S. G. (1990) The starfish *Asterina pectinifera*, in *Animal Species for Developmental Studies*, (Dettlaff T. A. and Vassetzky S. G., eds.), pp. 287–311. Springer, US.
Diaz-Miranda L. and Garcia-Arraras J. E. (1995) Pharmacological action of the heptapeptide GFSKLYFamide in the muscle of the sea cucumber *Holothuria glaberrima* (Echinodermata). *Comp. Biochem. Physiol. C* **110**, 171–176.
Du H., Bao Z., Hou R. *et al.* (2012) Transcriptome sequencing and characterization for the sea cucumber *Apostichopus japonicus* (Selenka, 1867). *PLoS ONE* **7**, e33311.
Elphick M. R. and Melarange R. (2001) Neural control of muscle relaxation in echinoderms. *J. Exp. Biol.* **204**, 875–885.
Elphick M. R., Price D. A., Lee T. D. and Thorndyke M. C. (1991a) The SALMFamides: a new family of neuropeptides isolated from an echinoderm. *Proc. Biol. Sci.* **243**, 121–127.
Elphick M. R., Reeve J. R., Jr, Burke R. D. and Thorndyke M. C. (1991b) Isolation of the neuropeptide SALMFamide-1 from starfish using a new antiserum. *Peptides* **12**, 455–459.
Elphick M. R., Newman S. J. and Thorndyke M. C. (1995) Distribution and action of SALMFamide neuropeptides in the starfish *Asterias rubens*. *J. Exp. Biol.* **198**, 2519–2525.
Elphick M. R., Achhala S. and Martynyuk N. (2013) The evolution and diversity of SALMFamide neuropeptides. *PLoS ONE* **8**, e59076.
Elphick M. R., Semmens D. C., Blowes L. M., Levine J., Lowe C. J., Arnone M. I. and Clark M. S. (2015) Reconstructing SALMFamide neuropeptide precursor evolution in the phylum echinodermata: ophiuroid and crinoid sequence data provide new insights. *Front. Endocrinol. (Lausanne)* **6**, 2.
Greenberg M. J. and Price D. A. (1979) FMRFamide, a cardioexcitatory neuropeptide of molluscs: an agent in search of a mission. *Am. Zool.* **19**, 163–174.
Grider J. R. and Makhlouf G. M. (1986) Colonic peristaltic reflex: identification of vasoactive intestinal peptide as mediator of descending relaxation. *Am. J. Physiol.* **251**, G40–G45.
Hall J. D. and Lloyd P. E. (1990) Involvement of pedal peptide in locomotion in *Aplysia*: modulation of foot muscle contractions. *J. Neurobiol.* **21**, 858–868.
Haraguchi S., Ikeda N., Abe M., Tsutsui K. and Mita M. (2015) Nucleotide sequence and expression of relaxin-like gonad-stimulating peptide gene in starfish *Asterina pectinifera*. *Gen. Comp. Endocrinol.* pii: S0016-6480(15)00185-9. doi: 10.1016/j.ygcen.2015.06.017. [Epub ahead of print].
Hauser H., Neupert S., Williamson M., Predel R., Tanaka Y. and Grimmelikhuijzen C. J. (2010) Genomics and peptidomics of neuropeptides and protein hormones present in the parasitic wasp Nasonia vitripennis. *J. Proteome Res.* **9**, 5296–5310.
Hofer S. and Homberg U. (2006) Evidence for a role of orcokinin-related peptides in the circadian clock controlling locomotor activity of the cockroach *Leucophaea maderae*. *J. Exp. Biol.* **209**, 2794–2803.
Holman G. M., Cook B. J. and Nachman R. J. (1986) Isolation, primary structure and synthesis of leucomyosuppressin, an insect neuropeptide that inhibits spontaneous contractions of the cockroach hindgut. *Comp. Biochem. Physiol. C* **85**, 329–333.
Ikegami S., Tamura S. and Kanatani H. (1967) Starfish gonad: action and chemical identification of spawning inhibitor. *Science* **158**, 1052–1053.
Jo Y. B., Park S. H., Jeon J. K., Ko C. H., Ryu C. and Park Y. K. (2013) Biodiesel production via the transesterification of soybean oil using waste starfish (*Asterina pectinifera*). *Appl. Biochem. Biotechnol.* **170**, 1426–1436.
Kim C. H., Go H. J. and Park N. G. (2015) Two myomodulins isolated from central nervous system of Northwest Pacific Sea Hare, *Aplysia kurodai*, and their activities on other mollusks. *Protein Pept. Lett.* **22**, 341–347.
Kitamura K., Kangawa K., Kawamoto M., Ichiki Y., Nakamura S., Matsuo H. and Eto T. (1993) Adrenomedullin: a novel hypotensive peptide isolated from human pheochromocytoma. *Biochem. Biophys. Res. Commun.* **192**, 553–560.
Lloyd P. E. and Connolly C. M. (1989) Sequence of pedal peptide: a novel neuropeptide from the central nervous system of *Aplysia*. *J. Neurosci.* **9**, 312–317.
Longley R. D. and Peterman M. (2013) Neuronal control of pedal sole cilia in the pond snail *Lymnaea stagnalis appressa*. *J. Comp. Physiol. A Neuroethol. Sens. Neural. Behav. Physiol.* **199**, 71–86.
Melarange R. and Elphick M. R. (2003) Comparative analysis of nitric oxide and SALMFamide neuropeptides as general muscle relaxants in starfish. *J. Exp. Biol.* **206**, 893–899.
Melarange R., Potton D. J., Thorndyke M. C. and Elphick M. R. (1999) SALMFamide neuropeptides cause relaxation and eversion of the cardiac stomach in starfish. *Proc. Biol. Sci.* **266**, 1785–1785.
Mirabeau O. and Joly J. S. (2013) Molecular evolution of peptidergic signaling systems in bilaterians. *Proc. Natl Acad. Sci. USA* **110**, E2028–E2037.
Mita M., Yoshikuni M., Ohno K., Shibata Y., Paul-Prasanth B., Pitchayawasin S., Isobe M. and Nagahama Y. (2009) A relaxin-like peptide purified from radial nerves induces oocyte maturation and ovulation in the starfish, *Asterina pectinifera*. *Proc. Natl Acad. Sci. USA* **106**, 9507–9512.
Miyata A., Arimura A., Dahl R. R., Minamino N., Uehara A., Jiang L., Culler M. D. and Coy D. H. (1989) Isolation of a novel 38 residue-hypothalamic polypeptide which stimulates adenylate cyclase in pituitary cells. *Biochem. Biophys. Res. Commun.* **164**, 567–574.
Moore S. J. and Thorndyke M. C. (1993) Immunocytochemical mapping of the novel echinoderm neuropeptide SALMFamide 1 (S1) in the starfish *Asterias rubens*. *Cell Tissue Res.* **274**, 605–618.
Moroz L. L., Edwards J. R., Puthanveettil S. V. *et al.* (2006) Neuronal transcriptome of *Aplysia*: neuronal compartments and circuitry. *Cell* **127**, 1453–1467.
Nathoo A. N., Moeller R. A., Westlund B. A. and Hart A. C. (2001) Identification of neuropeptide-like protein gene families in *Caenorhabditis elegans* and other species. *Proc. Natl Acad. Sci. USA* **98**, 14000–14005.
Newman S. J., Elphick M. R. and Thorndyke M. C. (1995a) Tissue distribution of the SALMF amide neuropeptides S1 and S2 in the starfish *Asterias rubens* using novel monoclonal and polyclonal antibodies. II. digestive system. *Proc. Biol. Sci.* **261**, 187–192.
Newman S. J., Elphick M. R. and Thorndyke M. C. (1995b) Tissue distribution of the SALMFamide neuropeptides S1 and S2 in the starfish *Asterias rubens* using novel monoclonal and polyclonal antibodies. I. Nervous and locomotory systems. *Proc. Biol. Sci.* **261**, 139–145.

Ohtani M., Iwakoshi E., Muneoka Y., Minakata H. and Nomoto K. (2002) Isolation and characterization of bioactive peptides from the sea cucumber, *Stichopus japonicus*, in *Peptide Science - Present and Future*, (Shimonishi Y., ed.), pp. 419–420. Springer, Netherlands.

Reich A., Dunn C., Akasaka K. and Wessel G. (2015) Phylogenomic analyses of Echinodermata support the sister groups of Asterozoa and Echinozoa. *PLoS ONE* **10**, e0119627.

Robberecht P., Tatemoto K., Chatelain P. *et al.* (1982) Effects of PHI on vasoactive intestinal peptide receptors and adenylate cyclase activity in lung membranes. A comparison in man, rat, mouse and guinea pig. *Regul. Pept.* **4**, 241–250.

Rowe M. L. and Elphick M. R. (2012) The neuropeptide transcriptome of a model echinoderm, the sea urchin *Strongylocentrotus purpuratus*. *Gen. Comp. Endocrinol.* **179**, 331–344.

Rowe M. L., Achhala S. and Elphick M. R. (2014) Neuropeptides and polypeptide hormones in echinoderms: new insights from analysis of the transcriptome of the sea cucumber *Apostichopus japonicus*. *Gen. Comp. Endocrinol.* **197**, 43–55.

Schilling L., Kanzler C., Schmiedek P. and Ehrenreich H. (1998) Characterization of the relaxant action of urocortin, a new peptide related to corticotropin-releasing factor in the rat isolated basilar artery. *Br. J. Pharmacol.* **125**, 1164–1171.

Semmens D. C., Dane R. E., Pancholi M. R., Slade S. E., Scrivens J. H. and Elphick M. R. (2013) Discovery of a novel neurophysin-associated neuropeptide that triggers cardiac stomach contraction and retraction in starfish. *J. Exp. Biol.* **216**, 4047–4053.

Soehler S., Stengl M. and Reischig T. (2011) Circadian pacemaker coupling by multi-peptidergic neurons in the cockroach *Leucophaea maderae*. *Cell Tissue Res.* **343**, 559–577.

Stangier J., Hilbich C., Burdzik S. and Keller R. (1992) Orcokinin: a novel myotropic peptide from the nervous system of the crayfish, *Orconectes limosus*. *Peptides* **13**, 859–864.

Wei H. and Stengl M. (2011) Light affects the branching pattern of peptidergic circadian pacemaker neurons in the brain of the cockroach *Leucophaea maderae*. *J. Biol. Rhythms* **26**, 507–517.

Williams C. L., Peterson J. M., Villar R. G. and Burks T. F. (1987) Corticotropin-releasing factor directly mediates colonic responses to stress. *Am. J. Physiol.* **253**, G582–G586.

Yamanaka N., Roller L., Zitnan D., Satake H., Mizoguchi A., Kataoka H. and Tanaka Y. (2011) Bombyx orcokinins are brain-gut peptides involved in the neuronal regulation of ecdysteroidogenesis. *J. Comp. Neurol.* **519**, 238–246.

Yasuda-Kamatani Y. and Yasuda A. (2000) Identification of orcokinin gene-related peptides in the brain of the crayfish *Procambarus clarkii* by the combination of MALDI-TOF and on-line capillary HPLC/Q-Tof mass spectrometries and molecular cloning. *Gen. Comp. Endocrinol.* **118**, 161–172.